Springer Tracts in Modern Physics
Volume 224

Springer Tracts in Modern Physics

Springer Tracts in Modern Physics provides comprehensive and critical reviews of topics of current interest in physics. The following fields are emphasized: elementary particle physics, solid-state physics, complex systems, and fundamental astrophysics.
Suitable reviews of other fields can also be accepted. The editors encourage prospective authors to correspond with them in advance of submitting an article. For reviews of topics belonging to the above mentioned fields, they should address the responsible editor, otherwise the managing editor.
See also springer.com

Joachim Ankerhold

Quantum Tunneling in Complex Systems

The Semiclassical Approach

With 62 Figures

Springer

Joachim Ankerhold

Physikalisches Institut
Universität Freiburg
Hermann Herder Str. 3
79104 Freiburg, Germany
E-mail: ankerhold@physik.uni-freiburg.de

Library of Congress Control Number: 2006938410

Physics and Astronomy Classification Scheme (PACS):
03.65 Sq, 05.60.Gg, 05.40.-a, 74.50.+r, 82.20.Db

ISSN print edition: 0081-3869
ISSN electronic edition: 1615-0430
ISBN-10 3-540-68074-8 Springer Berlin Heidelberg New York
ISBN-13 978-3-540-68074-1 Springer Berlin Heidelberg New York

Springer is a part of Springer Science+Business Media
springer.com

Typesetting: by the authors using a Springer LaTeX macro package
Cover production: WMXDesign GmbH, Heidelberg

Printed on acid-free paper SPIN: 10906101 56/techbooks 5 4 3 2 1 0

To E. and K. and E.

Preface

Tunneling is a genuine quantum effect, a direct consequence of the matter wave structure of quantum mechanics. Recent progress in engineering and manufacturing aggregates on the nanoscopic and mesoscopic scale have led to fascinating developments in directly influencing and controlling quantum properties in general, and tunneling in particular. In parallel, an exciting exchange of experimental techniques and theoretical concepts from fields such as atomic, molecular, and condensed matter physics has emerged. The aim of this book is to provide a survey of one of the most powerful theoretical tools to describe tunneling, namely, the semiclassical approximation, and to show that tunneling phenomena are central issues in this fast rising interdisciplinary field.

The literature about quantum tunneling is enormous, and that about semiclassics as well. The intention here is to discuss tunneling from a semiclassical perspective, which in turn means that this book does not address tunneling in general nor the general methodology of the semiclassical approximation. Tunneling probabilities for one dimensional anharmonic systems can be evaluated by means of semiclassical expansions whenever energy scales, on which the barrier penetration occurs, are large compared to some intrinsic quantum mechanical energy scales of the systems. This concept has been generalized to tunneling events in presence of dissipative environments, where rate constants characterize the time scale for transmission. For multi-dimensional systems, particularly for those with non-regular phase space structures, or for time dependent approaches to capture tunneling, however, general conditions are hard to formulate and may depend on specific features of the problem under consideration. In fact, in practical applications semiclassical calculations are often more accurate than expected from general estimates, which may be one reason for their widespread and successful use in physics and chemistry. In situations such as dissipative tunneling through high barriers, numerically exact treatments are either prohibitive or so demanding that semiclassical methods are basically the only tools for a proper description. In other cases, where exact results are available, semiclassical considerations often provide a better understanding for our physical intuition and serve as starting points for elegant approximate developments.

Complex quantum systems which allow for manipulations are inevitably embedded in some sort of surrounding. This can be either an external control field, static or time dependent, a small number of additional degrees of freedom generating non-regular dynamics, or a dissipative background leading to energy exchange and fluctuations. The tunneling degree of freedom itself can be even a collective degree of freedom consisting of a macroscopically large number of microscopic entities, which has led to fundamental questions like e.g. if and if yes, to what extent quantum mechanical properties could be realized on a macroscopic level. Phenomenologically, tunneling in these complex systems displays a rich variety of facets depending on macroscopic parameters such as temperature, spectral bath densities, driving amplitudes and frequencies, magnetic and electric fields.

In this book theoretical results are applied to and illustrated by explicit realizations ranging in length from the subatomic scale of a few fermi (fm) to the mesoscopic scale of a few microns (μm), thus covering systems over nine orders of magnitude and objects as diverse as nuclei, ensembles of atoms, molecular structures, and superconducting circuits. Owing to my own scientific background in condensed phase systems, these examples must reflect a personal viewpoint and only in this sense can be understood as representative. The same is true for the semiclassical approaches and formulations: I did not attempt to give a comprehensive account so that some of them may deserve a deeper presentation, others are addressed only briefly.

Science is a social event and so this book would not have been possible without intensive collaborations and discussions with many colleagues from different fields in physics and chemistry. Particularly, I benefited from and enjoyed to work with H. Grabert, F. Grossmann, P. Hänggi, G.-L. Ingold, P. Pechukas, E. Pollak, C. Rummel, D. Tannor, M. Thoss, and U. Weiss. I am indebted to the Quantronics group at the CEA Saclay, particularly D. Esteve, H. Pothier, C. Urbina, D. Vion, for wonderful collaborations and thank G. Buntkowsky, D. Haviland, A. Lupascu, J. Pekola, and W. Wernsdorfer for their help in understanding experimental details and providing some of the figures. I am grateful as well to my students M. Saltzer and M. Duckheim for their important contributions, critical questions, and ideas.

Some results discussed in this book have been obtained during extended stays and short time visits at other places: as a fellow of the Alexander von Humboldt Foundation at the Columbia University, New York; as a Heisenberg fellow of the German Science Foundation at the CEA Saclay, the Weizmann Institute of Science, the Technical University of Helsinki, and the University of Geneva. I have always enjoyed the warm hospitality of my host institutions.

Most importantly, I deeply thank my wife Evangelia and our children Katerina and Elias for their never ending patience and embracing love.

Freiburg, *Joachim Ankerhold*
October 2006

Contents

1

Introduction

A semiclassical description of tunneling in systems with complex dynamics requires an arsenal of theoretical techniques adapted to the problem under investigation. Conceptually, two types of processes are usually distinguished, namely, coherent and incoherent tunneling. The former one appears in bi- and multistable potentials and, more precisely, should be termed quantum coherence. It originates from the coherent overlap of wave functions located in individual domains, which are separated by energy or phase-space barriers. The latter one describes the situation, where in the language of scattering theory asymptotic states in the distant past do not overlap in the distant future with those that have penetrated a barrier. Accordingly, incoherent tunneling is seen in scattering processes between two reservoirs and in the decay of metastable states into a continuum. However, in presence of interaction with environmental degrees of freedom coherent tunneling dynamics can be destroyed leading to relaxation via incoherent decay as well.

1.1 Theoretical Concepts

The earliest approach to determine tunneling amplitudes is based on an approximate solution of the stationary Schrödinger equation in terms of an expansion in $\hbar$ for the energy dependent wave function. Technically, this WKB treatment necessitates a matching of semiclassical wave functions, which in general is quite a cumbersome task. Hence, modern semiclassical expansions are dominantly based on the path integral representation of quantum mechanics, in particular, of the time evolution operator, of the statistical operator for the thermal equilibrium, and, as a combination of both, of the nonequilibrium density matrix. The path integral naturally operates with trajectories which in a semiclassical approximation correspond to orbits minimizing the action. A further advantage is that this formulation allows for the inclusion of additional degrees of freedom, most importantly, of a thermal heat bath. We will not explain details of the path integral formulation here, especially

Joachim Ankerhold: *Quantum Tunneling in Complex Systems*
STMP **224**, 1–5 (2007)
DOI 10.1007/3-540-68076-4_1

their mathematical subtleties, and refer the reader to excellent books such as [1, 2, 3, 4, 5, 6]. The same is true for the semiclassical expansion, which has grown into a sub-field of theoretical physics, but is used in the sequel only with respect to tunneling. More information is provided by the extensive literature, e.g. in [7, 8, 9].

Tunneling, as quantum mechanics in general, has two perspectives: a time independent one in the energy domain and a dynamical one in the time domain (cf. also Fig. 1.1). For all conservative systems a description in the energy domain is feasible independent of whether they are pure or mixed according to an energy dependent distribution. Hence, approaches to calculate transmission probabilities (WKB) and energy averaged tunneling rates (thermodynamic methods) have been developed starting from microcanonical or canonical formulations. However, in case of external time dependent driving or dissipation a time dependent approach is necessary. Indeed, even in cases of wave packets penetrating barriers at fixed energies reveals a dynamical semiclassical picture aspects of the tunneling event that cannot be gained merely from transmission probabilities. In the last decade, intensive research to develop proper semiclassical propagation schemes has provided deeper insight into the failure of standard Gaussian semiclassics to capture deep tunneling. Eventually, the time evolution for systems out of equilibrium

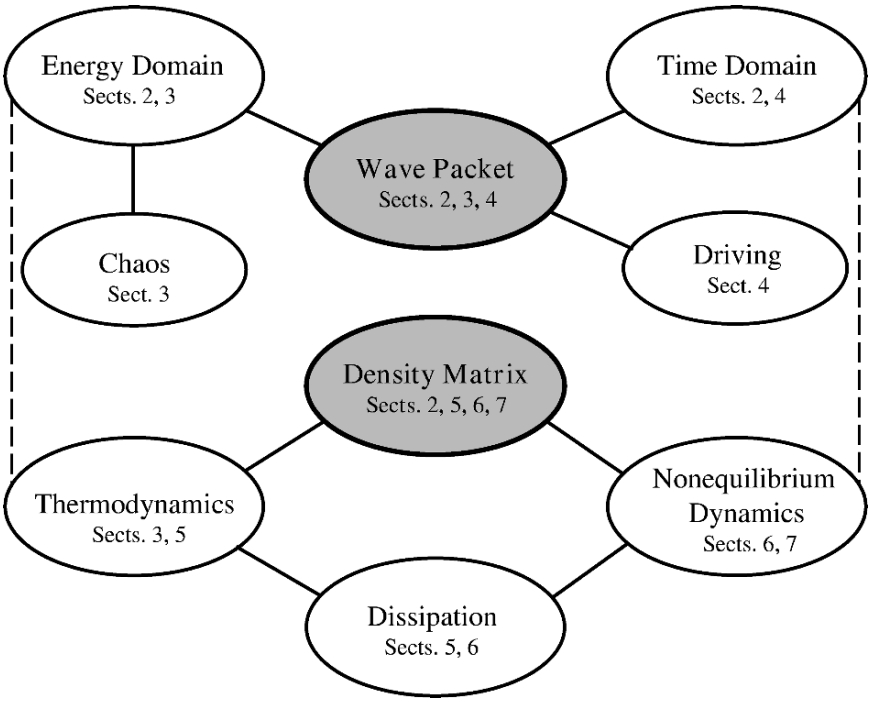

Fig. 1.1. Structure of this book.

in terms of reduced density matrices, described in the context of dissipative quantum systems, has turned out to be extremely challenging. A proper semiclassical approximation is highly desired since the formally exact path integral expressions can in general not be evaluated analytically and in the long time domain, where tunneling happens to occur, not even numerically.

For systems coupled to a heat bath, quantum mechanical tunneling dominates only at sufficiently low temperatures, while at high temperatures energy barriers are surmounted via classical thermal activation. Theories for tunneling thus merge with rate theories developed originally for chemical systems and indeed, many semiclassical concepts for tunneling have been derived in the 1970s in the community of physical chemistry. Physics joined these efforts essentially in the early 1980s, partially triggered by the experimental progress to fabricate electrical devices on the mesoscopic scale. The latter ones allowed for the first time to study tunneling processes under well controlled conditions and gave rise to the most accurate verifications of theoretical rate expressions. In this century experimentalists have been extending their technology to actually design, tailor and manipulate quantum matter on ever larger scales. Ensembles of atoms reach the size of mesoscopic devices and mesoscopic devices are used to implement artificial atoms. Theory is again the complementary part in this exciting adventure.

However, the semiclassical methodology for tunneling processes is not completely developed yet, there still exist more or less "white patches". Examples include tunneling in systems with mixed phase space and tunneling through multi-dimensional barriers, where substantial progress has not been achieved so far. Some of the fundamental subtleties which one encounters are addressed in this book. For a further reading on concepts for quantum tunneling we refer to the literature, for instance: Tunneling in general is reviewed in [10]; dissipative quantum systems and applications to tunneling are presented in [11, 12] and approaches for calculations of rate constants are outlined in [13].

1.2 Physical Systems

In this book we are primarily interested in complex systems, a notion which certainly needs some clarification. Roughly speaking, we call a tunneling system complex when its phenomenology exhibits qualitatively different aspects of tunneling while sweeping through the space of external and/or internal parameters. Typically, there is some relation to the underlying physical realization, which then is built up of more than one degree of freedom or influenced by additional external and/or intrinsic forces. A prominent example is the tunneling of the superconducting phase difference in Josephson junctions, where this phase is actually a collective coordinate of the superconducting condensates and as such its dynamics affects a physical system with macroscopically many degrees of freedom. Other examples of collective processes have been discovered in fission events of nuclear matter, collapse of Bose-Einstein condensates,

or tunneling of magnetization in molecular nanomagnets. As a direct consequence, the interaction with residual degrees of freedom, e.g. electromagnetic modes in a circuit, vibronic degrees of freedom in molecules, phonons in condensed phase, is inevitable. Barrier penetration in presence of dissipative environments includes changeovers from coherent to incoherent dynamics, from thermal activation to deep tunneling, and even to localization. Another facet of tunneling appears in two- or higher dimensional systems when the corresponding classical dynamics is non-regular with chaotic phase space structures leading to distributions of tunneling probabilities which may strongly oscillate as functions of energy. Complexity also arises due to the application of external time dependent fields during the barrier penetration. The absorption of photons typically influences transmission rates substantially leading e.g. in case of decay from a metastable well to intrawell excitations and resonant tunneling. A similar situation can be found for atoms in strong external laser fields, which drives valence electrons out of the Coulomb-well and re-scatters them when the phase of the field changes.

To illustrate this rich phenomenology, examples on length scales from nuclei to mesoscopic devices are discussed in this book. Specifically, we will discuss fission of nuclear matter, collapse of cold atomic gases with attractive interaction, nanomagnets in form of molecular complexes, rotational tunneling in dihydride-metal compounds, and macroscopic quantum phenomena in Josephson junction devices including tunneling of quantum bits. To concentrate on the essential features and not to overload this presentation a deeper analysis of the respective systems had to be excluded. More details are contained in e.g. [14] for systems on the molecular level, in [15] for Macroscopic Quantum Tunneling and in [16] for spin tunneling in nanomagnets; for the semiclassical approximation of transport phenomena in mesoscopic physics [17] provides a thorough overview.

1.3 Structure of the Book

The structure of the book closely follows the discussion of the theoretical concepts above and is sketched in Fig. 1.1. In the next Chap. 2 some basic results from the semiclassical theory are collected and the relevant notation is introduced. The remaining Sections deal with tunneling of individual wave packets on the one hand and with tunneling of ensembles described by density matrices on the other hand. The wave packet aspect is discussed in Chap. 3 in the energy domain, while in Chap. 4 dynamical approaches are outlined, particularly, for externally driven tunneling. In addition in Chap. 3 two powerful thermodynamic approaches for rate calculations are introduced, the bounce and the instanton method, however, without taking into account dissipation so that they can be regarded as effective means to perform thermal averages over tunneling rates of individual (quasi-)eigenstates. The basic structure of the corresponding semiclassical procedures becomes thus very transparent. The

generalization of these thermodynamic formulations to dissipative systems is then given in Chap. 5. The nonequilibrium dynamics of density matrices is the subject of Chaps. 6 and 7, where in the former one the temperature range above the so-called crossover temperature is addressed, while in the latter one a dynamical approach particularly for the low temperature range and covering coherent as well as incoherent tunneling processes is presented. This in turn allows to derive detailed conditions for the applicability of the thermodynamic methods and reveals the intimate relation between dynamics, dissipation, and tunneling. The book closes with some remarks about central issues, for which the semiclassical theory of tunneling needs further developments in the future.

References

1. R. P. Feynman and A. P. Hibbs. *Quantum Mechanics and Path Integrals*. McGraw-Hill, 1965.
2. B. Felsager. *Geometry, Particles, and Fields*. Odense University Press, 1981.
3. L.S. Schulman. *Techniques and Applications of Path Integrals*. Wiley, 1981.
4. M.S. Swanson. *Path Integrals and Quantum Processes*. Academic Press, 1992.
5. C. Grosche and F. Steiner. *Handbook of Feynman Path Integrals*. Springer, 1998.
6. H. Kleinert. *Path Integrals in Quantum Mechanics, Statistics, Polymer Physics, and Financial Markets*. World Scientific, 2002.
7. M.C. Gutzwiller. *Chaos in Classical and Quantum Mechanics*. Springer, 1990.
8. M. Brack and R.K. Bhaduri. *Semiclassical Physics*. Wesley, 1997.
9. D. Tannor. *Introduction to Quantum Mechanics, A Time Dependent Perspective*. University Science Books, 2003.
10. M. Razavy. *Quantum Theory of Tunneling*. World Scientific, 2003.
11. U. Weiss. *Quantum Dissipative Systems*. World Scientific, 1999.
12. T. Dittrich, P. Hänggi, G.-L. Ingold, B. Kramer, G. Schön, and W. Zwerger. *Quantum Transport and Dissipation*. Wiley-VCH, 1998.
13. P. Hänggi, P. Talkner, and M. Borkovec. *Rev. Mod. Phys.*, 62:251, 1990.
14. T. Miyazaki (Ed.). *Atom Tunneling Phenomena in Physics, Chemistry and Biology*. Springer, 2006.
15. S. Tagaki. *Macroscopic Quantum Tunneling*. Cambridge, 2002.
16. E. Chudnovsky and J. Tejada. *Macroscopic Quantum Tunneling of the Magnetic Moment*. Cambridge, 2005.
17. K. Richter. *Semiclassical Theory of Mesoscopic Quantum Systems*. STMP 161. Springer, 2000.

2

Semiclassical Approximation

In the early days of quantum mechanics – before the concept of matter waves had been introduced – the understanding of atomic spectra was based on classical mechanics combined with conditions for discreteness. The latter ones related the action of a classical orbit to multiples of $\hbar$. This seed grew, shortly after wave mechanics was cast into Schrödinger's equation, into a semiclassical scheme known today as WKB approximation [1, 2, 3], which allowed to obtain the wave function in terms of classical trajectories. It was in the late 1960 only that semiclassics turned into the focus of intensive scientific activities. Since then semiclassical approximations, mathematically embedded in the context of asymptotic series, have been derived for the time evolution operator, its Fourier transform, the resolvent, and the statistical operator and successfully applied in basically all fields of physics and physical chemistry. Semiclassics offers a way to quantize also classically nonintegrable systems based on periodic orbits and in the last years has provided powerful tools to capture the quantum dynamics of even high dimensional systems. One appealing feature of a semiclassical description is that it suggests an understanding of quantum phenomena in terms of classical entities. However, one has to be cautious: While such an interpretation may indeed be helpful in specific cases, in general and particularly for tunneling processes, it makes no sense to speak about the real existence of individual trajectories.

In this Chapter we collect some main results of semiclassical quantum mechanics, which will then be used in the remainder of this book. For transparency we restrict ourselves in many cases to one-dimensional systems, while generalizations to higher dimensions are mostly straightforward and well-described in the literature.

2.1 At the Very Beginning: The WKB Approach

Let us consider a quantum particle of mass M moving in one dimension under the influence of a potential field $V(q)$. The corresponding Hamiltonian reads

Joachim Ankerhold: *Quantum Tunneling in Complex Systems*
STMP **224**, 7–20 (2007)
DOI 10.1007/3-540-68076-4_2

$$\hat{H} = \frac{\hat{p}^2}{2M} + V(\hat{q}) \tag{2.1}$$

and its eigenbasis follows from the eigenstates of the time independent Schrödinger equation $\hat{H}|\psi\rangle = E|\psi\rangle$. In position representation we try for the solutions of

$$\frac{\mathrm{d}^2\psi(q)}{\mathrm{d}q^2} + \frac{2M}{\hbar^2}\left[E - V(q)\right]\psi(q) = 0 \tag{2.2}$$

an ansatz of the form

$$\psi(q) = \exp\left[\frac{\mathrm{i}}{\hbar}W(q)\right] \tag{2.3}$$

with an exponent determined by

$$W'(q)^2 - \mathrm{i}\hbar W''(q) - p(q)^2 = 0\,. \tag{2.4}$$

Here and in the sequel we use the abbreviation $W' = \mathrm{d}W/\mathrm{d}q$ and further introduced the classical momentum $p(q) = \sqrt{2M[E - V(q)]}$. The idea is to solve (2.4) by assuming that the momentum $p(q)$ shows only small variations over length scales of the order of the de Broglie wave length $\lambda_{\mathrm{B}}(q) = 2\pi\hbar/p(q)$. One then expands in a power series of $\hbar$ [4, 5, 6]

$$W = W_0 - \mathrm{i}\hbar W_1 - \hbar^2 W_2 - \ldots \tag{2.5}$$

and upon insertion into (2.4) and putting terms of equal powers in $\hbar$ to zero separately, one arrives at a set of iteratively coupled equations for the $W_k, k = 1, 2, 3, \ldots$. In lowest order ($\hbar^0$) one has $W_0'(q)^2 - p(q)^2 = 0$, which is immediately solved by the classical short action

$$W_0(q, q_0) = \int_{q_0}^{q} \mathrm{d}q'\, p(q')\,, \tag{2.6}$$

where q_0 defines an arbitrary, but fixed reference point. Now, for W_0 to be the leading contribution of a perturbative expansion one has to impose $\hbar|W_0''(q)| \ll |W_0'(q)^2|$ or equivalently

$$\hbar\left|\frac{p'(q)}{p(q)^2}\right| \ll 1\,. \tag{2.7}$$

This is the so-called WKB condition (Wentzel-Kramers-Brillouin) for matter waves and the analog to the eikonal condition in geometrical optics [7]. Apparently, the condition is violated at all points in the vicinity of $p(q) = 0$, i.e. near all turning points of the corresponding classical orbit. These give rise to caustics, a coalescence of classical orbits starting from the same initial position but with different momenta. Before we address this phenomenon in detail, we first proceed with the next order term in the expansion (2.5). From $W_1' = -W_0''/(2W_0')$ one has $W_1(q) = -\ln[p(q)]/2$ so that by neglecting higher order contributions the WKB wave function takes the form

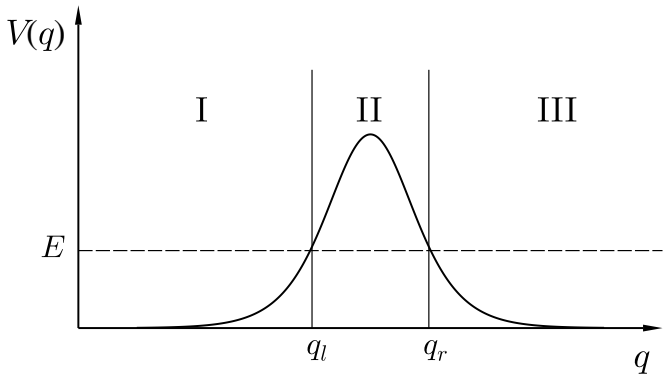

Fig. 2.1. Barrier potential with ranges I, II, and III for different semiclassical approximations, which must be matched according to the connection rules (2.9) and (2.10) at the turning points q_l and q_r defined by $E = V(q)$.

$$\psi_{\mathrm{WKB}}(q) = \frac{C_+}{\sqrt{p(q)}}\,\mathrm{e}^{\mathrm{i}W_0(q,q_0)/\hbar} + \frac{C_-}{\sqrt{p(q)}}\,\mathrm{e}^{-\mathrm{i}W_0(q,q_0)/\hbar} \tag{2.8}$$

with appropriate integration constants $C_\pm$. Of course, this result can be systematically improved by taking into account even higher order terms in the $\hbar$-expansion (2.5).

The regions around caustics require special care. There is no reason why the above expansion should not also hold in the range $E < V(q)$, i.e. in a range not accessible by a classical orbit, but sufficiently away from a turning point $E = V(q)$ (see e.g. Fig. 2.1). Accordingly, one puts $p(q) \to \mathrm{i}|p(q)|$ so that the oscillating wave function (2.8) develops exponentially decreasing and increasing contributions, thus reflecting the appearance of quantum tunneling. The matching between the WKB solutions in the classically allowed and the classically forbidden ranges is done e.g. by circumventing the turning point in the complex coordinate plane along a contour which ensures the validity of the WKB condition [4]. The result are connection rules which read for a transition from a classically accessible to a forbidden domain at a (left) turning point q_l

$$\begin{aligned}\frac{C_+}{\sqrt{p(q)}}\,\mathrm{e}^{\mathrm{i}W_0(q,q_\mathrm{l})/\hbar-\mathrm{i}\pi/4} + \frac{C_-}{\sqrt{p(q)}}\,\mathrm{e}^{-\mathrm{i}W_0(q,q_\mathrm{l})/\hbar+\mathrm{i}\pi/4} \;\longrightarrow\\ \frac{C_+}{\sqrt{|p(q)|}}\,\mathrm{e}^{-|W_0(q,q_\mathrm{l})|/\hbar}\,,\end{aligned} \tag{2.9}$$

where in the first line $q < q_\mathrm{l}$ and in the second one $q > q_\mathrm{l}$. In case of an outgoing matter wave to the right of a (right) turning point q_r, the transition from the range under the barrier is determined by

$$\frac{C_+}{\sqrt{|p(q)|}}\,\mathrm{e}^{|W_0(q,q_\mathrm{r})|/\hbar} \;\to\; \frac{C_+}{\sqrt{p(q)}}\,\mathrm{e}^{\mathrm{i}W_0(q,q_\mathrm{r})/\hbar+\mathrm{i}\pi/4} \tag{2.10}$$

with $q < q_\mathrm{r}$ on the right and $q > q_\mathrm{r}$ one the left hand side.

These rules allow for the evaluation of energy dependent transmission probabilities $T(E)$ through one-dimensional barrier potentials. As a first example, we consider a scattering barrier with asymptotically free states [4] as depicted in Fig. 2.1. Then, one has an incoming and a reflected WKB-wave on one side of the barrier (range I) and an outgoing WKB-wave on the other side (range III). The amplitude $t(E)$ of the latter is determined by connecting these partial waves via a proper WKB solution in the classical forbidden range (range II). This way one finds

$$T(E) \equiv |t(E)|^2 = \exp\left[-\frac{2}{\hbar}\left|\int_{q_\mathrm{l}(E)}^{q_\mathrm{r}(E)} \mathrm{d}qp(q)\right|\right] , \tag{2.11}$$

where the exponent contains twice the absolute of the short action $W(q_\mathrm{l}, q_\mathrm{r})$ between the turning points. It is thus identical to the short action of a *periodic orbit* at energy E in the *inverted* barrier potential.

In case of bounded one dimensional potentials with a single minimum, the above connection rules give rise to a quantization scheme known as the WKB or Bohr-Sommerfeld quantization, i.e.,

$$\frac{1}{2\pi\hbar}\oint \mathrm{d}qp = n + \frac{1}{2}\,. \tag{2.12}$$

Here the integral covers a full period of a classical orbit and n is a positive integer. The additional term $1/2$ on the right hand side accounts for the zero point fluctuations. This term, a direct consequence of the breakdown of the semiclassical approximation close to a turning point and associated with the appearance of additional phases in (2.9) and (2.10), was absent in the older version of this scheme. A multi-dimensional generalization of the WKB rule was first found by Einstein, later discovered independently again by Keller, and named EBK quantization (Einstein–Brillouin–Keller) [8, 9] in the literature [10]. It reads for a d-dimensional system

$$\frac{1}{2\pi\hbar}\oint_{C_i} \mathrm{d}\boldsymbol{qp} = n_i + \frac{\nu_i}{4}\ ,\ i = 1, \ldots, d\,, \tag{2.13}$$

where the C_i are d independent closed loops on a torus in d dimensions and ν_i are the corresponding Maslov indices counting the number of conjugate points along C_i.

From the above rules one derives quantized energy levels separated by a gap of order $\hbar$. However, in systems with classically degenerate ground states, e.g. double well potentials, an exact diagonalization of the corresponding Hamilton operator reveals that each such level consists actually of sublevels, the energies of which differ by terms exponentially small in $\hbar$. This fine structure due to quantum coherence between wells linked by barriers cannot be gained within the WKB/EBK schemes.

Uniform Approximation

There is an alternative way to glue together respective asymptotic WKB wave functions in the vicinity of a turning point. The idea is to linearize the barrier potential in a range around the turning point and to solve the corresponding Schrödinger equation exactly [4, 5]. Suppose the turning point is located at $q = q_0$, one then writes $V(q) \approx V(q_0) - F(q - q_0)$. The corresponding energy eigenfunctions are Airy-functions and by matching their asymptotics onto semiclassical solutions (2.8) one determines the free coefficients and obtains a uniform solution.

A similar strategy, namely to solve the Schrödinger equation for a reference potential exactly, is also used to remove the failure of the WKB-transmission probability (2.11) for energies close to the top of a smooth barrier potential [4, 5]. In this situation, left and right turning points, q_l and q_r, are not sufficiently separated from each other (of order λ_B or less) so that the above procedure based on the connection rules (2.9) and (2.10) does not apply. However, a smooth barrier potential can be approximated around its top by an inverted harmonic oscillator. The corresponding Schrödinger equation is again exactly solvable in terms of Weber functions. The asymptotic form of these functions is matched onto the asymptotic WKB wave functions, which eventually leads to the uniform semiclassical transmission probability

$$T_\mathrm{uni}(E) = \frac{1}{1 + \exp[2W(E)/\hbar]} \tag{2.14}$$

with $E = E(q_\mathrm{l}, q_\mathrm{r})$. For energies sufficiently below the barrier top this expression reduces to (2.11), while it reproduces the exact result for a purely parabolic barrier $V_\mathrm{pb}(q) = -M\omega^2 q^2/2$ for energies near the top, where $W_\mathrm{pb}(E) = \pi E/\omega$.

2.2 Real-time Propagator

The time dependent Schrödinger equation

$$\mathrm{i}\hbar \frac{\partial}{\partial t} |\psi(t)\rangle = \hat{H} |\psi(t)\rangle \tag{2.15}$$

can be formally integrated over a time period $t - t'$ to yield $|\psi(t)\rangle = \hat{G}(t - t')\,|\psi(t')\rangle$, where

$$\hat{G}(t) = \exp\left(-\frac{\mathrm{i}}{\hbar}\hat{H}t\right) \tag{2.16}$$

denotes the quantum mechanical real-time propagator. Its knowledge is completely equivalent to solving the Schrödinger equation itself and leads to an alternative formulation of quantum mechanics in terms of path integrals. First

pioneered by Feynman [11], the position representation of the real time propagator can be written as

$$G(q_{\rm f},t;q_{\rm i},0)\equiv\langle q_{\rm f}|\hat{G}(t)|q_{\rm i}\rangle=\int_{q(0)=q_{\rm i}}^{q(t)=q_{\rm f}}\mathcal{D}[q]\,{\rm e}^{{\rm i}S[q]/\hbar}\,. \tag{2.17}$$

Roughly speaking, the above integral sums over all paths running in time t from $q_{\rm i}$ to $q_{\rm f}$, where each paths is weighted by its action

$$S[q]=\int_0^t{\rm d}s\,\mathcal{L}[\dot{q}(s),q(s)] \tag{2.18}$$

with the classical Langrange-function $\mathcal{L}$ corresponding to the Hamiltonian $\mathcal{H}$. We do not discuss here the mathematical subtleties of path integrals – there is a vast body of literature, see e.g. [6, 12, 13, 14, 15, 16] – but rather consider it as a very powerful and elegant approach for a consistent semiclassical approximation. Before we do so, we mention an important property of the above propagator, namely,

$$G(q_{\rm f},t;q_{\rm i},0)=\int{\rm d}x\,G(q_{\rm f},t-s;x,s)\,G(x,s;q_{\rm i},0)\,, \tag{2.19}$$

which resembles the Chapman-Kolmogorov equation known from statistical mechanics [17] and reflects the half-group property of the propagator.

Now, a simple expectation is that the sum over paths is dominated by those orbits which extremalize the action, i.e. by those which obey the classical equation of motion $\delta S[q_{\rm cl}]=0$. In fact, the path integral (2.17) allows for a systematic asymptotic expansion in $\hbar$, which, to be more precise, is actually an expansion in a small parameter being the ratio of a quantum scale and a classical scale of the problem under consideration. By putting for an arbitrary path $q(s)=q_{\rm cl}+y(s)$ with $y(0)=y(t)=0$ one expands

$$S[q]=S[q_{\rm cl}]+\sum_{n\geq 2}\delta^n S[q_{\rm cl},y] \tag{2.20}$$

with the functional derivatives

$$\delta^n S[q_{\rm cl},y]=\frac{1}{n!}\int_0^t{\rm d}s_1\cdots{\rm d}s_n\,\left.\frac{\delta^n S[q]}{\delta q(s_1)\cdots\delta q(s_n)}\right|_{q=q_{\rm cl}}y(s_1)\cdots y(\sigma_2)\,. \tag{2.21}$$

This expansion is basically a series in the small parameter so that to leading order quantum corrections are captured by the second order term and higher order contributions are negligible. The corresponding approximation is called *Gaussian approximation* and contains the second order variational operator

$$\begin{aligned}L_2(s_1,s_2)&=\left.\frac{\delta^2 S[q]}{\delta q(s_1)\delta q(s_2)}\right|_{q=q_{\rm cl}}\\&=\delta(s_1-s_2)\left(M\frac{{\rm d}^2}{{\rm d}s_1^2}+\left.\frac{{\rm d}^2V(q)}{{\rm d}q^2}\right|_{q=q_{\rm cl}(s_1)}\right)\,.\end{aligned} \tag{2.22}$$

Gaussian fluctuations around the classical path thus live in a harmonic valley with a curvature given by the instantaneous position of the classical orbit. In case that there are several classical paths obeying the boundary conditions one has to perform such a local expansion around each of them. The underlying requirement is here that the classical paths are sufficiently separated from each other in function space. When this is not the case, large fluctuations may lead from one path to another one and the Gaussian approximation breaks down, a situations that typically appears around bifurcations when new classical paths pop up and one (or several) eigenvalues of L_2 pass through zero and become negative. Away from the bifurcation a Gaussian approximation is again valid with the negative eigenvalue giving rise to an additional phase (Maslov phase).

By solving the Gaussian path integral over the fluctuations one arrives at the well-known Van Vleck Gutzwiller propagator (VVG) [18, 19]

$$G_{\mathrm{VVG}}(q_{\mathrm{f}},t;q_{\mathrm{i}},0)=\frac{1}{\sqrt{2\pi\mathrm{i}\hbar}}\sum_{\alpha}\sqrt{|D_{\alpha}|}\,\exp\left[\frac{\mathrm{i}}{\hbar}S_{\mathrm{cl}}^{(\alpha)}(q_{\mathrm{f}},q_{\mathrm{i}},t)-\mathrm{i}\nu_{\alpha}\frac{\pi}{2}\right]. \quad (2.23)$$

Here, $S_{\mathrm{cl}}^{(\alpha)}\equiv S[q_{\mathrm{cl}}^{(\alpha)}]$ and the contributions of the harmonic fluctuations around the classical paths $q_{\mathrm{cl}}^{(\alpha)}$ are encoded in the prefactors D_{α}, which carry the stability informations about the respective paths [20, 21]. There are various ways to calculate them based on the eigenvalues of the operators $L_2^{(\alpha)}$, with the most compact expression being

$$D_{\alpha}=-\frac{\partial^2 S_{\mathrm{cl}}^{(\alpha)}(q_{\mathrm{i}},q_{\mathrm{f}},t)}{\partial q_{\mathrm{f}}\partial q_{\mathrm{i}}}\,. \quad (2.24)$$

The additional phase factors in (2.23) include the Maslov indices, which count the number of conjugate points (bifurcation points) along a certain path according to Morse theorem [22] and are physically related to caustics. Higher order corrections to the VVG have also been determined in [23, 24, 25].

In particular, for a harmonic potential the Gaussian semiclassical approximation gives the exact result

$$G_{\mathrm{harm}}(q_{\mathrm{f}},t;q_{\mathrm{i}},0)=\sqrt{\frac{M\omega}{2\pi\mathrm{i}\hbar|\sin(\omega t)|}}\,\mathrm{e}^{-\mathrm{i}\nu\pi/2}\times\exp\left\{\frac{\mathrm{i}M\omega}{2\hbar\sin(\omega t)}\left[(q_{\mathrm{i}}^2+q_{\mathrm{f}}^2)\cos(\omega t)-2q_{\mathrm{i}}q_{\mathrm{f}}\right]\right\}, \quad (2.25)$$

where ω is the frequency and M the mass of the oscillator. The Maslov phases for $t\geq t_{\nu}$ guarantee that at the caustics $\omega t_{\nu}=\nu\pi,\nu=1,2,\ldots$, where all classical paths starting at q_{i} with different momenta coalesce at $q_{\mathrm{f}}=(-1)^{\nu}q_{\mathrm{i}}$, the propagator reduces to

$$\lim_{t\to\nu\pi/\omega}G_{\mathrm{harm}}(q_{\mathrm{f}},t;q_{\mathrm{i}},0)=\mathrm{e}^{-\mathrm{i}\nu\pi/2}\,\delta\left[q_{\mathrm{f}}-(-1)^{\nu}q_{\mathrm{i}}\right]. \quad (2.26)$$

From the expression (2.25) one derives the propagator of a parabolic barrier by replacing ω by $\mathrm{i}\omega$ with $\nu = 0$ and that of a free particle for $\nu = 0$ by taking the limit $\omega \to 0$.

Even though the VVG propagator has been explicitly applied to the dynamics e.g. in a stadium billiard [26, 27], in a Coulomb potential [28], and for Rydberg atoms [29], in practical calculations it has one crucial deficiency: It requires to solve a boundary value problem for the classical paths which is notoriously very demanding, especially in higher dimensions. Hence, presently the most powerful semiclassical real-time propagators are based on a so-called initial value representation (IVR) (for recent reviews see [30, 31, 32]), where classical paths evolve in time starting with initial conditions, i.e. at a certain point in phase space. The best known IVR propagator is the Hermann-Kluk (HK) propagator [33, 34, 35]

$$\hat{G}_{\mathrm{HK}}(t) = \int \frac{\mathrm{d}^2\Omega}{2\pi\hbar} \, |\Omega(t), \gamma\rangle\langle\Omega, \gamma| \; R(\Omega, t) \, \mathrm{e}^{\mathrm{i}S(\Omega,t)\hbar} \,, \tag{2.27}$$

which includes paths starting at $s = 0$ at phase space points $\Omega = (p, q)$ and arriving at $s = t$ at $\Omega(t) = (p(t), q(t))$. The phase-space states are Gaussian wave-packets with width parameter γ reading in position representation

$$g_\gamma(p, q; Q) \equiv \langle Q|\Omega, \gamma\rangle = \left(\frac{\gamma}{\pi}\right)^{1/4} \exp\left[-\frac{\gamma}{2}(Q - q)^2 + \frac{\mathrm{i}}{\hbar} p(Q - q)\right] \tag{2.28}$$

and the prefactor is

$$R(p, q, t) = \det\left[\frac{1}{2}\left(m_{11} + m_{22} - \mathrm{i}\gamma m_{21} - \frac{1}{\mathrm{i}\gamma} m_{12}\right)\right]^{1/2} \tag{2.29}$$

containing the elements m_{ij} of the monodromy matrix

$$\mathsf{M}(t) = \begin{pmatrix} \frac{\partial p(t)}{\partial p} & \frac{\partial p(t)}{\partial q} \\ \frac{\partial q(t)}{\partial p} & \frac{\partial q(t)}{\partial q} \end{pmatrix} . \tag{2.30}$$

This matrix is conveniently calculated by solving for a system with classical Hamiltonian $\mathcal{H}$ the differential equation

$$\frac{\mathrm{d}\mathsf{M}}{\mathrm{d}t} = \begin{pmatrix} 0 & -\frac{\partial^2\mathcal{H}}{\partial q^2} \\ \frac{\partial^2\mathcal{H}}{\partial p^2} & 0 \end{pmatrix} \mathsf{M}(t) \tag{2.31}$$

with initial condition $\mathsf{M}(0) = \mathsf{1}$. Note that the HK propagator becomes exact as well for harmonic potentials and a free particle and reduces to the VVG expression when the phase space integration is carried out in stationary phase.

While the VVG-propagator is directly derived from the exact expression (2.17) as the leading term of an asymptotic series in $\hbar$, the situation for the HK-propagator is different. It has been used more as a practical

tool rather than a well defined result of a *bona fide* semiclassical expansion, even though some attempts in this directions have been pushed forward [36, 37, 38, 39, 40, 41, 42, 43], some of them [44, 45, 46] based on coherent states [47]. Accordingly, it originated merely from the constraint to reduce to the VVG-propagator in the stationary phase limit, which defines only a necessary but not a unique condition and thus gives rise to a whole class of equivalent initial value representations. Indeed, a variety of alternative IVR propagation schemes have been proposed [48, 49, 50, 51, 52, 53, 54], where some of them can be directly derived from the HK propagator by means of additional approximations [30]. After the practical utility of the HK propagator was demonstrated [36, 55], an increasing number of fascinating applications have been performed, see e.g. [56, 57, 58, 59, 60, 61, 62, 63, 64, 65, 66, 67] and for more details also the recent reviews [68, 69]. The mathematical basis for the HK-propagator has been formulated only very recently (see Sect. 4.3) and now allows also for systematic improvements beyond its standard form.

2.3 Energy-dependent Propagator

Complementary to the quantum propagator in the time domain (2.16) is its representation in the energy regime. In the spectral decomposition in terms of eigenfunctions $|\Phi_n\rangle$ of the Hamilton operator with eigenvalues E_n one has

$$G(q_\mathrm{f},t;q_\mathrm{i},0)=\sum_n \Phi_n(q_\mathrm{f})\Phi_n(q_\mathrm{i})^*\,\mathrm{e}^{-\mathrm{i}E_nt/\hbar}\,. \tag{2.32}$$

This can formally be Fourier transformed to read

$$\begin{aligned} K(q_\mathrm{f},q_\mathrm{i},E) &= \tfrac{1}{\mathrm{i}\hbar}\int_0^\infty \mathrm{d}t\; G(q_\mathrm{f},t;q_\mathrm{i},0)\mathrm{e}^{\mathrm{i}Et/\hbar} \\ &= \sum_n \frac{\Phi_n(q_\mathrm{f})\Phi_n(q_\mathrm{i})^*}{E-E_n+\mathrm{i}\epsilon} \end{aligned} \tag{2.33}$$

and is known as the energy dependent (retarded) propagator. Here, a small imaginary part $\epsilon>0$ ensures causality. By further taking the trace in position space one arrives at the resolvent

$$\mathcal{K}(E)=\sum_n \frac{1}{E-E_n+\mathrm{i}\epsilon}\,, \tag{2.34}$$

which plays the key role in generalizing the WKB quantization rule to systems with classically nonintegrable dynamics [70, 10]. Namely, it is related to the density of states

$$d(E)=\sum_n \delta(E-E_n) \tag{2.35}$$

via

$$d(E) = -\frac{1}{\pi}\mathrm{Im}\left\{\mathcal{K}(E)\right\} . \tag{2.36}$$

A semiclassical expansion of the propagator thus leads to a decomposition

$$d(E) = \bar{d}(E) + d_{\mathrm{osc}}(E) \tag{2.37}$$

in a smooth (classical) part and an oscillating part capturing quantum mechanical features. The corresponding semiclassical expression for classically chaotic systems, known as the Gutzwiller trace-formula [10, 70],

$$d_{\mathrm{osc}}(E) = \frac{1}{\pi\hbar}\sum_{\mathrm{p.o.}}\sum_{j=1}^{\infty}\frac{T_{\mathrm{po}}}{\left|\det(\mathsf{M}_{\mathrm{po}}^{j}-1)\right|^{1/2}}\cos\left[j\left(\frac{S_{\mathrm{po}}}{\hbar}-\mu_{\mathrm{po}}\frac{\pi}{2}\right)\right] \tag{2.38}$$

relates the quantum mechanical spectrum to purely classical information in terms of primitive periodic orbits (po) with period T_{po}, action S_{po}, and multiple traversals j. The monodromy matrix M_{po} contains the stability information of a specific po and μ_{po} denotes the Maslov index on the energy shell. Seminal applications of the trace formula include the quantization of the hydrogen atom in a uniform magnetic field [71], where the sum was performed by uniquely coding the periodic orbits, and the calculation of Rydberg series for the two electron system (Helium) [72].

2.4 Equilibrium Statistical Operator

An ensemble of quantum mechanical systems in thermal equilibrium is described by the statistical operator

$$\hat{\rho}_\beta = \frac{1}{Z}\,\mathrm{e}^{-\beta\hat{H}} \tag{2.39}$$

with the partition function $Z = \mathrm{Tr}\{\mathrm{e}^{-\beta\hat{H}}\}$. Formally it is related to the real-time propagator (2.16) via a Wick rotation $t \to -\mathrm{i}\hbar\beta$. Thus, its path integral representation in position space is easily gained from (2.17) as [6, 17]

$$\rho_\beta(q_{\mathrm{f}}, q_{\mathrm{i}}) = \frac{1}{Z}\int_{q(0)=q_{\mathrm{i}}}^{q(\hbar\beta)=q_{\mathrm{f}}}\mathcal{D}[q]\,\mathrm{e}^{-S_{\mathrm{E}}[q]/\hbar} . \tag{2.40}$$

Here, due to the Wick rotation one sums over paths connecting in Euclidian (*imaginary*) time $\hbar\beta$ the endpoints q_{i} and q_{f}, where the contribution of each paths is weighted with its Euclidian action

$$S_{\mathrm{E}}[q] = \int_0^{\hbar\beta}\mathrm{d}\sigma\mathcal{H}[p(\sigma), q(\sigma)] \tag{2.41}$$

containing the classical Hamiltonian $\mathcal{H}[p, q]$. Hence, for a particle of mass M moving in a potential field $V(q)$, i.e. $\mathcal{H}[p, q] = p^2/2M + V(q)$, the imaginary

time motion can be seen as a real-time dynamics in the inverted potential $-V(q)$. Further, in the partition function

$$Z = \oint \mathcal{D}[q]\, \mathrm{e}^{-S_{\mathrm{E}}[q]/\hbar} \tag{2.42}$$

all closed paths $q(0) = q(\hbar\beta)$ are summed up.

Despite these similarities there is a fundamental difference between the imaginary and the real-time propagators. Namely, the former one is always positive and real according to its physical role as a probability density. The immediate consequence is that ρ_β has, at least for all systems with well defined ground state, a well defined "long-time" limit being equivalent to the zero temperature limit: In position representation it projects onto the ground state with energy E_0, i.e.,

$$\lim_{\hbar\beta\to\infty} \rho_\beta(q,q) = |\Phi_0(q)|^2 \tag{2.43}$$

and gives thus direct access to the corresponding wave function. The above relation is also known as the Feynman-Kac formula [17, 6].

Another consequence is that the analog of the VVG-propagator (2.23), i.e. the Gaussian semiclassical expression for the statistical operator

$$\rho_\beta^{\mathrm{sc}}(q_{\mathrm{f}}, q_{\mathrm{i}}) = \frac{1}{Z_{\mathrm{sc}}\sqrt{2\pi}} \sum_\alpha \sqrt{D_\alpha^{\mathrm{E}}}\, \exp\left[-S_{\mathrm{E,min}}^{(\alpha)}(q_{\mathrm{f}}, q_{\mathrm{i}})\right] \tag{2.44}$$

with $S_{\mathrm{E,min}}^{(\alpha)}$ denoting the Euclidian action of the minimal action path $q_{\mathrm{min}}^{(\alpha)}$, does not contain Maslov phases. Namely, a simple analytic continuation of the expression

$$D_\alpha^{\mathrm{E}} = -\frac{\partial^2 S_{\mathrm{E,min}}^{(\alpha)}(q_{\mathrm{i}}, q_{\mathrm{f}})}{\partial q_{\mathrm{f}} \partial q_{\mathrm{i}}} \tag{2.45}$$

beyond the first conjugate point (one eigenvalue negative) is not possible as then the root in (2.44) would turn imaginary and the whole expression unphysical. In other words, unstable directions in function space cannot simply be accounted for by Maslov indices. Typically, conjugate points appear in presence of potential barriers [73] so that their appearance when lowering the temperature is directly related to tunneling through the classically forbidden range of the potential.

To illustrate this point let us consider a sufficiently smooth barrier potential that can be approximated around its top by a parabolic barrier of curvature ω_b. For high temperatures the density matrix for coordinates around the top is determined by local properties only and basically coincides with that of a pure parabolic barrier. At a critical temperature β_{c}, for $\rho_\beta(q,q)$ it is given by $\omega_{\mathrm{b}}\hbar\beta_{\mathrm{c}} = \pi$ according to a half an oscillation in $-V(q)$, a bifurcation occurs, new stable paths appear, and the Gaussian semiclassics breaks down [73]. For temperatures around β_{c} higher order terms in the expansion of the full action must be taken into account. Sufficiently above β_{c} the Gaussian approximation works again, however, now performed around the new stable orbits. The

latter ones fulfill excursions with large amplitudes in the inverted barrier so that even for coordinates near the parabolic barrier top the density matrix is determined by global properties of the potential. Physically, this describes the setting in of tunneling which causes the barrier to become transparent.

For systems without any barrier, the combination of the Feynman-Kac formula and the semiclassical expression (2.44) allows to successively extract energy eigenvalues and wave functions from purely classical information [74]. The idea is to successively apply the Feynman-Kac formula (2.43) to the semiclassical unnormalized density matrix $Z\,\rho_\beta(q,q)$. This way, one starts at a sufficiently low temperature β_0 to gain the ground state $|\Phi_0|^2$ together with its energy E_0; then, this ground state contribution is subtracted from $Z\,\rho_\beta(q,q)$ at a somewhat higher temperature $\beta_1 < \beta_0$ to extract the first excited state $|\Phi_1|^2$ with energy E_1 and so on state by state. Such a procedure leads to a sequence of density matrices $\rho_{k+1}, k \geq 0$ with the contributions of the first k states stripped off:

$$\rho_{k+1}(q,q) = Z\rho_\beta(q,q) - \sum_{l=0}^{k} |\Phi_l(q)|^2 \mathrm{e}^{-\beta_l E_l} \;,\; k \geq 0\,. \tag{2.46}$$

It was shown [74] that this procedure offers an alternative way of quantizing classically chaotic systems with the merit that due the positivity of the equilibrium density a substantially smaller number of classical orbits is required compared to the real-time scheme (2.38).

References

1. G. Wentzel. *Z. Phys.*, 38:518, 1926.
2. H.A. Kramers. *Z. Phys.*, 39:828, 1926.
3. L. Brillouin. *C.R. Acad. Sci. Paris*, 183:24, 1926.
4. L.D. Landau and E. Lifshitz. *Quantum Mechanics.* Pergamon, 1976.
5. M.V. Berry and K.E. Mount. *Rep. Prog. Phys.*, 35:315, 1972.
6. H. Kleinert. *Path Integrals in Quantum Mechanics, Statistics, Polymer Physics, and Financial Markets.* World Scientific, 2002.
7. H. Goldstein. *Classical Mechanics.* Addison-Wesley, 1980.
8. A. Einstein. *Verh. Dtsch. Phys. Ges.*, 19:82, 1917.
9. J.B. Keller. *Ann. Phys. (NY)*, 4:180, 1958.
10. M.C. Gutzwiller. *Chaos in Classical and Quantum Mechanics.* Springer, 1990.
11. R.P. Feynman. *Rev. Mod. Phys.*, 20:367, 1948.
12. R.P. Feynman and A.P. Hibbs. *Quantum Mechanics and Path Integrals.* McGraw-Hill, 1965.
13. B. Felsager. *Geometry, Particles, and Fields.* Odense University Press, 1981.
14. L.S. Schulman. *Techniques and Applications of Path Integrals.* Wiley, 1981.
15. M.S. Swanson. *Path Integrals and Quantum Processes.* Academic Press, 1992.
16. C. Grosche and F. Steiner. *Handbook of Feynman Path Integrals.* Springer, 1998.

17. R. P. Feynman. *Statistical Mechanics*. Benjamin, 1972.
18. J.H. Van Vleck. *Proc. Natl. Acad. Sci.*, 14:178, 1928.
19. M.C. Gutzwiller. *J. Math. Phys.*, 8:1979, 1967.
20. C. DeWitt-Morette. *Phys. Rev. E*, 81:848, 1951.
21. C. DeWitt-Morette. *Ann. Phys. (NY)*, 97:367, 1976.
22. M. Morse. *Variational Analysis*. John Wiley & Sons, 1973.
23. J.L. Dunham. *Phys. Rev.*, 41:713, 1932.
24. N. Fröman. *Phys. Rev. A*, 17:493, 1978.
25. A. Voros. *Phys. Rev. A*, 40:6814, 1989.
26. S. Tomsovic and E.J. Heller. *Phys. Rev. Lett.*, 67:664, 1991.
27. E.J. Heller and S. Tomsovic. *Physics Today*, 46:38, 1993.
28. I. Suárez Barnes, M. Nauenberg, M. Nockleby, and S. Tomsovic. *J. Phys. A*, 27:3299, 1994.
29. M. Mallalieu and C. Stroud. In D.H. Feng, J.R. Klauder, and M.R. Strayer, editors, *Coherent States: Past, Present, and Future*. World Scientific, 1994.
30. F. Grossmann. *Comments At. Mol. Phys.*, 34:41, 1999.
31. M. Baranger, M.A.M. de Aguiar, F. Keck, H.J. Korsch, and B. Schellhaaß. *J. Phys. A*, 34:7227, 2001.
32. W.H. Miller. *J. Phys. Chem. A*, 105:2942, 2001.
33. M.F. Herman and E. Kluk. *Chem. Phys.*, 91:27, 1984.
34. E. Kluk, M.F. Herman, and H.L. Davis. *J. Chem. Phys.*, 84:326, 1995.
35. M.F. Herman. *J. Chem. Phys.*, 85:2969, 1996.
36. K.G. Kay. *J. Chem. Phys.*, 100:4377, 1994.
37. M.F. Herman. *Annu. Rev. Phys. Chem.*, 45:83, 1994.
38. W.H. Miller. *Adv. Chem. Phys.*, 101:853, 1997.
39. W.H. Miller. *Faraday Discuss.*, 110:1, 1998.
40. W.H. Miller. *Mol. Phys.*, 100:397, 2002.
41. T. Yamamoto and W.H. Miller. *J. Chem. Phys.*, 118:2135, 2003.
42. B. Hu, Q. Jie, B. Li, and S. Wang. *Phys. Rev. A*, 63:044102, 2001.
43. S. Yoshida, F. Grossmann, E. Person, and J. Burgdörfer. *Phys. Rev. A*, 69:043410, 2004.
44. F. Grossmann and A.L. Xavier. *Phys. Lett. A*, 243:243, 1998.
45. M. Baranger, M.A.M. de Aguiar, F. Keck, H.J. Korsch, and B. Schellhaaß. *Phys. Rev. A*, 35:9493, 2002.
46. M. Baranger, M.A.M. de Aguiar, and H.J. Korsch. *J. Phys. A*, 36:9795, 2003.
47. J.R. Klauder and B.-S. Skagerstam. *Coherent States: Applications in Physics and Mathematical Physics*. World Scientific, 1985.
48. E.J. Heller. *J. Chem. Phys.*, 62:1544, 1975.
49. E.J. Heller. *J. Chem. Phys.*, 75:2923, 1981.
50. M.A. Sepulveda and E.J. Heller. *J. Chem. Phys.*, 101:8004, 1994.
51. M.A. Sepulveda and E.J. Heller. *J. Chem. Phys.*, 101:8016, 1994.
52. M.A. Alonso and G.W. Forbes. *J. Math. Phys.*, 40:1699, 1999.
53. M.A. Alonso and G.W. Forbes. *J. Opt. Soc. Am. A*, 18:1357, 2001.
54. E. Pollak and S. Miret-Artés. *J. Phys. A*, 37:9669, 2004.
55. K.G. Kay. *J. Chem. Phys.*, 100:4432, 1994.
56. S. Garashchuk and D. Tannor. *Chem. Phys. Lett.*, 262:477, 1996.
57. M.A. Sepulveda and F. Grossmann. *Adv. Chem. Phys.*, XCVI:191, 1996.
58. N. Makri and K. Thompson. *Chem. Phys. Lett.*, 291:101, 1998.
59. N. Makri and K. Thompson. *J. Chem. Phys.*, 110:1343, 1999.

60. K. Thompson and N. Makri. *Phys. Rev. E*, 59:4729(R), 1999.
61. K. Thompson and N. Makri. *J. Chem. Phys.*, 110:1343, 1999.
62. J. Shao and N. Makri. *J. Phys. Chem. A*, 103:7753, 1999.
63. R. Gelabert, X. Gimenéz, M. Thoss, H. Wang, and W.H. Miller. *J. Phys. Chem. A*, 104:10321, 1999.
64. X. Sun and W.H. Miller. *J. Chem. Phys.*, 110:6635, 1999.
65. D. Tannor and S. Garashchuk. *Annu. Rev. Phys. Chem.*, 51:553, 2000.
66. K.G. Kay. *Phys. Rev. Lett.*, 83:5190, 1999.
67. M. Thoss, H. Wang, and W.H. Miller. *J. Chem. Phys.*, 114:9220, 2001.
68. M. Thoss and H. Wang. *Annu. Rev. Phys. Chem.*, 55:299, 2004.
69. K.G. Kay. *Annu. Rev. Phys. Chem.*, 56:????, 2005.
70. M.C. Gutzwiller. *J. Math. Phys.*, 12:343, 1971.
71. D. Wintgen. *Phys. Rev. Lett.*, 61:1803, 1988.
72. G. Tanner and D. Wintgen. *Phys. Rev. Lett.*, 75:2928, 1995.
73. J. Ankerhold and H. Grabert. *Physica A*, 188:568, 1992.
74. F.J. Weiper, J. Ankerhold, H. Grabert, and E. Pollak. *Phys. Rev. Lett.*, 77:2662, 1996.

3

Tunneling in the Energy Domain

Tunneling processes which are not subject to time dependent forces can be described in the energy domain. In many cases though, individual energy dependent transmission probabilities are experimentally not accessible, but only their average over a distribution of energies. One then speaks of tunneling rates rather than probabilities. A general expression for the total rate is given by [1, 2]

$$\Gamma = \frac{1}{Z} \int_0^\infty \mathrm{d}E \; \Gamma(E)\, \rho(E)\, P(E) \tag{3.1}$$

with a proper normalization Z, the density of states $\rho(E)$, the (unnormalized) energy distribution $P(E)$, and where energy is measured from the base of the barrier. The microcanonical rate $\Gamma(E)$ is related to the transmission $T(E)$ via $\Gamma(E) = T(E)/[2\pi\hbar\rho(E)]$ and describes the flux through the barrier at energy E. Physically, its dimension is frequency so that the inverse of Γ is the typical time scale on which an initial population on one side of the barrier decays by barrier penetration. For systems where this population is given by a thermal ensemble, $P(E)$ is identical to a Boltzmann distribution. In principle, averaged rates can be calculated from (3.1) by means of the WKB technique introduced in Sect. 2.1. A much more convenient way, however, is based on the path integral representation of the partition function of the system and the fact that the imaginary part of the corresponding free energy ($\mathrm{Im}F$) is related to the temperature dependent decay rate [3]. At low temperatures the tunneling rate is determined by the so-called bounce orbit so that the $\mathrm{Im}F$ method is also referred to as the *bounce method*. The formulation is suited to treat tunneling through scattering barriers and from a metastable well into a continuum (incoherent tunneling).

Particularly in the latter case the situation is a bit more involved though. Namely, in principle the existence of a thermodynamic equilibrium in a metastable well requires at any finite temperatures the coupling to a heat bath which tends to restore this distribution after a particle has escaped. There are then three ways to proceed. One is to ignore the existence of the

Joachim Ankerhold: *Quantum Tunneling in Complex Systems*
STMP **224**, 21–60 (2007)
DOI 10.1007/3-540-68076-4_3

heat bath in an explicit calculation and to assume that a thermal distribution is always maintained. It turns out that this approximation, also termed quantum transition state theory (QTST) [1], provides rates which are upper bounds for the true ones. In this Chapter we will work with the ImF approach in this sense and especially demonstrate that it is then completely equivalent to WKB. A second way is to include environmental degrees of freedom (dissipation) in terms of a reduced description, where the heat bath is integrated out and one deals with an effective partition function. Since in this case the expression (3.1) is no longer meaningful, we discuss further details in Chap. 5. A full dynamical formulation of the nonequilibrium reduced density matrix will be outlined in Chap. 6 and gives detailed conditions for the validity of thermodynamic rate calculations. In a third way, one treats tunneling in presence of a heat bath as a process in a higher dimensional landscape with the total energy distributed between the tunneling degree of freedom and a collection of harmonic oscillators, thus generalizing the QTST to the multi-dimensional quantum transition state theory (MQTST). This will be presented in this Chapter in Sect. 3.3.1. Such an explicit multi-dimensional calculation has the merit of not only providing a deeper insight into tunneling in higher-dimensional topologies, but also confirming independently the results gained within the more elegant dissipative ImF approach.

Tunneling between classically degenerate energy minima occurs due to quantum coherence so that the energy ladder of a bistable potential with sufficiently high barrier consists for low lying states of energy doublets separated by an exponentially small tunnel splitting. When a wave packet is initially prepared in only one of the wells, it will coherently oscillate between the classical minima with a frequency given by this tunnel splitting. The method to calculate these splittings is similar to the ImF approach: It is also based on path integrals, but has to take care of the special types of minimal action paths, the so-called instantons, which provide the dominant contribution. The instanton approach was actually invented in high-energy physics [4]. For the sake of transparency, we discuss it here for vanishing dissipation and zero temperature and present generalized results in Chap. 5.

A calculation of tunneling rates for nonseparable multi-dimensional barrier degrees of freedom becomes very demanding. First, phase space allows for an increasing number of tunneling paths, a proliferation of orbits that in some cases is soothed by the exponential dependence of the tunneling probability on the lengths of the paths. Second, tunneling may be strongly influenced by more complex structures of classical phase space comprising regions of chaotic and those of regular motion. In the latter cases, a semiclassical description has been only partially developed so far, even though substantial progress has been achieved in the last years.

3.1 Quantum Decay Rate out of a Metastable Well

Tunneling from a metastable state into a continuum can be found almost everywhere in nature [2]. Historically, the radioactive decay of nuclei associated with the emission of α-particles was first explained by Gamow [5] and Gurney and Condon [6] by this type of potential barrier model (see Fig. 3.1). In the 1980s the tunneling of collective degrees of freedom consisting of macroscopically many degrees of freedom, then coined macroscopic quantum tunneling (MQT), has triggered a substantial amount of research [2]. The best known real systems in this respect are Josephson junction devices [7, 8], which allow for the most accurate measurements of tunneling probabilities. Meanwhile, MQT has been seen in a variety of other condensed phase systems such as for vortices, in nanomagnets and for Bose-Einstein-Condensates to name but a few.

Metastability is associated with a separation of time scales between the local dynamics in the well region and the escape process through the barrier. In a real system residing in thermal equilibrium in the well, this requires a sufficiently fast relaxation processes in the well compared to the escape which is fulfilled, when the barrier height V_b by far exceeds all other energy sales as e.g. coupling strength to a heat bath, temperature $k_{\rm B}T$ and ground state energy $\hbar\omega_0$. Since in this Chapter we restrict ourselves to the non-dissipative situation, let us briefly address some aspects in which way this picture is related to the full nonequilibrium dynamics and anticipate some results obtained in Chap. 6.

Imagine that a local thermal equilibrium is initially prepared in the well. Then, apart from a domain of very weak coupling to the bath, after an initial transient period of time a quasi-stationary state describing a constant flux across the barrier is approached, where nonequilibrium effects are restricted to a range around the barrier top. Accordingly, this flux state reduces inside the well (far from the barrier) indeed to a Boltzmann distribution and is related to a time independent escape rate. It turns out that under these circumstances a calculation of the tunneling rate based on a purely thermodynamic treatment like the ImF method is justified (for more details see Sect. 5.2.5). Corresponding rates are bounded from above by the non-dissipative rates gained in the sequel. Since an exact calculation of the partition function for an anharmonic system is prohibitive, in a semiclassical approximation to the path integral expression the dimensionless ratio $\max(k_{\rm B}T, \hbar\omega_0)/V_b$ serves as a small parameter. Note that for zero temperature the corresponding rate reduces to the ground state tunneling probability derived within the WKB approach from the time-independent Schrödinger equation.

We will start with the calculation of the total rate based on the transmissions $T(E)$ via the WKB approach and proceed with the presentation of the more powerful path integral methods.

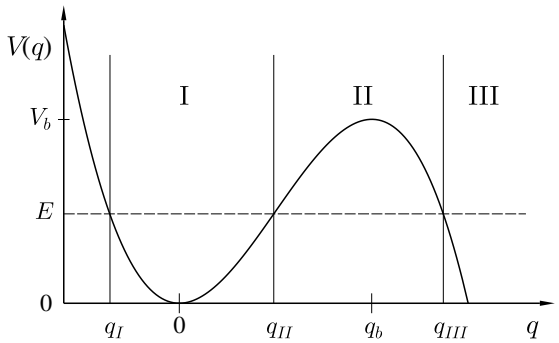

Fig. 3.1. Metastable well potential $V(q)$ with ranges I, II, and III, where for fixed energy E different semiclassical solutions apply. These solutions must be matched at q_{II} and q_{III}. See text for details.

3.1.1 WKB Treatment

To be specific, we consider a metastable well potential $V(q)$ as shown in Fig. 3.1 with a well located at $q = 0$ with $V(0) = 0$ and frequency $\omega_0 = \sqrt{V''(0)/M}$ and a barrier top located at $q = q_\mathrm{b}$ with $V_\mathrm{b} = V(q_\mathrm{b})$ and $\omega_\mathrm{b} = \sqrt{|V''(q_\mathrm{b})|/M}$. The standard WKB method based on the connection rules specified in Sect. 2.1 now works as follows. In the well region I, one has

$$\psi_I(q) = \frac{1}{\sqrt{p(q)}} \left(\mathrm{e}^{\mathrm{i}\int_{q_I}^{q} \mathrm{d}q' p(q')/\hbar - \mathrm{i}\pi/4} + \mathrm{e}^{-\mathrm{i}\int_{q_I}^{q} \mathrm{d}q' p(q')/\hbar + \mathrm{i}\pi/4} \right) . \tag{3.2}$$

In the classically forbidden range II, the wave function decays as

$$\psi_{II}(q) = \frac{1}{\sqrt{p(q)}} \mathrm{e}^{-\int_{q_{II}}^{q} \mathrm{d}q' |p(q')|/\hbar} , \tag{3.3}$$

where $E = p^2/2M + V(q)$. The outgoing wave function ψ_{III} in domain III is obtained from taking the right going component of ψ_I and continuing it via the connection rules and ψ_{II} to

$$\psi_{III}(q) = \mathrm{e}^{-2W(E)/\hbar} \; \frac{1}{\sqrt{p(q)}} \mathrm{e}^{\mathrm{i}\int_{q_{III}}^{q} \mathrm{d}q' p(q')/\hbar + \mathrm{i}\pi/4} . \tag{3.4}$$

Here, $2W(E)$ denotes the short action of the periodic orbit at energy E in the inverted barrier. The escape rate is then the outgoing current divided by the normalization of ψ_I in the well, i.e.,

$$\begin{aligned} \Gamma(E) &= \frac{\hbar}{M} \mathrm{Im} \left\{ \psi_{III}^* \frac{\partial \psi_{III}(q)}{\partial q} \right\} \left(\int_{q_I}^{q_{II}} \mathrm{d}q' |\psi_I(q')|^2 \right)^{-1} \\ &= \frac{1}{\tau_0(E)} \; \mathrm{e}^{-2W(E)/\hbar} \end{aligned} \tag{3.5}$$

with $\tau_0(E) = \oint \mathrm{d}q/\dot{q}$ being the period of a classical oscillation in the well.

The above result must be modified for low lying states with energies of order $\hbar\omega_0$ since then (3.2) no longer applies [9]. An improved result is gained by using the known eigenfunctions and energies $E_n = \hbar\omega_0(n + 1/2)$ of the harmonic oscillator near the well bottom in region I. This procedure yields

$$\Gamma_n \equiv \Gamma(E_n) = \frac{\omega_0}{\sqrt{\pi}} \frac{2^n}{n!} \left(\sqrt{\frac{M\omega_0}{\hbar}} C q_0 \right)^{2n+1} \mathrm{e}^{-S_\mathrm{B}/\hbar} \tag{3.6}$$

with a numerical factor C depending on the shape of the barrier potential, q_0 its classical exit point $V(q_0) = V(0)$, and $S_\mathrm{B} = 2W(0)$ the so-called bounce action. For instance, for the generic harmonic+cubic potential

$$V(q) = \frac{1}{2} M\omega_0^2 q^2 \left(1 - \frac{2q}{3q_\mathrm{b}} \right) \tag{3.7}$$

with a barrier at $q = q_\mathrm{b}$ and $q_0 = 3q_\mathrm{b}/2$, one finds $C = \sqrt{60}$ so that the ground state rate follows as [10, 11]

$$\Gamma_0 = \frac{\omega_0}{2\pi} \sqrt{\frac{V_\mathrm{b}}{\hbar\omega_0}} 12\sqrt{6\pi}\ \mathrm{e}^{-\frac{36}{5}\frac{V_\mathrm{b}}{\hbar\omega_0}}\,, \tag{3.8}$$

where $V_\mathrm{b} = 2M\omega_0^2 q_0^2/27$ is the barrier height. We note that these results require a sufficiently broad harmonic range around the well bottom, which is fulfilled when $V_\mathrm{b}/\hbar\omega_0 \gg 1$ meaning that tunneling is exponentially suppressed in accordance with the assumption of metastability.

Now, we assume a thermal distribution in the well of a metastable potential and treat the energy levels as a continuum with the density of states $\rho(E) = [1/\hbar\omega(E)]\theta(V_\mathrm{b} - E)$, where $\omega(E) = 2\pi/\tau_0(E)$ denotes the frequency for a classical oscillation in the well at energy E. Then, the result (3.5) is plugged into the expression (3.1) to yield

$$\Gamma_\beta = \frac{1}{Z} \int_0^{V_\mathrm{b}} \frac{\mathrm{d}E}{2\pi\hbar}\ \mathrm{e}^{-2W(E)/\hbar - \beta E}\,. \tag{3.9}$$

A steepest descent evaluation [12] leads to the condition $2\mathrm{d}W(E)/\mathrm{d}E = \hbar\beta$ meaning that the integral is dominated by the energy E_β of that periodic orbit in $-V(q)$ which has a period $\hbar\beta$. Accordingly, one arrives at

$$\Gamma_\beta = \frac{1}{Z} \frac{1}{\sqrt{2\pi\hbar|\tau'(E_\beta)|}}\ \mathrm{e}^{-2W(E_\beta) - \beta E_\beta} \tag{3.10}$$

with $\tau' = \mathrm{d}\tau/\mathrm{d}E$. Further, the normalization is taken as the partition function of the harmonic well $Z_0 = 1/[2\sinh(\omega_0\hbar\beta/2)]$. In principle, one must be careful in using the expression (3.5) also for energies where the level quantization must be accounted for according to (3.6). However, it turns out that in the relevant low temperature range $\omega_0\hbar\beta \gg 1$ a corresponding calculation leads to the same result as in (3.10) [13].

For high temperatures $\hbar\beta < 2\pi/\omega_\mathrm{b}$, the steepest descent condition in (3.9) cannot be fulfilled by an oscillating periodic orbit [12]. In this case the energy integral is dominated by energies around the barrier top, where the WKB result for the transmission, i.e. the exponential $\exp[-2W(E)]$, must be replaced by the exact expression for a parabolic barrier [see (2.14)]

$$T_\mathrm{pb}(E) = \frac{1}{1+\exp[2\pi(V_\mathrm{b}-E)/\hbar\omega_\mathrm{b}]} \tag{3.11}$$

so that one obtains

$$\Gamma = \frac{\omega_\mathrm{b}}{2\pi}\frac{\sinh(\omega_0\hbar\beta/2)}{\sin(\omega_\mathrm{b}\hbar\beta/2)}\,\mathrm{e}^{-\beta V_\mathrm{b}}\,. \tag{3.12}$$

At very high temperatures $\omega_0\hbar\beta \ll 1$, this rate reduces to

$$\Gamma_\mathrm{clTST} = \frac{\omega_0}{2\pi}\,\mathrm{e}^{-\beta V_\mathrm{b}}\,, \tag{3.13}$$

which coincides with the classical simple transition state theory result [2]. Apparently, when lowering the temperature the rate expression (3.12) diverges at the so-called crossover temperature

$$T_0 = \frac{\hbar\omega_\mathrm{b}}{2\pi k_\mathrm{B}}\,, \tag{3.14}$$

thus defining a lower bound in temperature for its validity. Physically, for $T > T_0$ escape is dominated by thermal activation over the barrier supplemented by quantum fluctuations, while for $T < T_0$ where (3.10) holds quantum tunneling prevails. In the classical regime the rate depends exponentially on temperature, whereas below the crossover it quickly saturates at a value corresponding to ground state tunneling (3.8). Experimentally, this crossover is a clear signature for the onset of deep quantum tunneling. There is a narrow layer around T_0 where the crossover between (3.10) and (3.12) happens to take place; the smaller the ratio $\hbar\omega_0/V_\mathrm{b}$ the sharper this transition. In this layer the integral (3.9) has to be evaluated beyond a Gaussian steepest descent approximation [12].

3.1.2 The ImF Method

The underlying idea of the ImF method is this: The finite lifetime of a metastable state can be understood as an imaginary part to the energy of that level. Equivalently, in a scattering experiment such states appear as resonances with finite widths, where their inverse is interpreted as a decay rate. Hence, putting $\epsilon_n = E_n + \mathrm{i}\hbar\Gamma_n/2$ with $E_n \gg \hbar\Gamma_n$, the partition function of the system is calculated as

$$Z = \sum_{n=0}^{\infty} \mathrm{e}^{-\beta\epsilon_n} \approx \sum_{n=0}^{\infty} \mathrm{e}^{-\beta E_n} - \mathrm{i}\frac{\hbar\beta}{2} \sum_{n=0} \Gamma_n \mathrm{e}^{-\beta E_n} \,. \tag{3.15}$$

Here, for energies near and above the barrier, the sum is taken as an integral. Obviously, the imaginary part in Z is proportional to the discrete version of the formula (3.1) and thus related to the total decay rate. Accordingly, one finds [12]

$$\Gamma = \frac{2}{\hbar}\mathrm{Im}F \tag{3.16}$$

with the free energy $F = -\ln Z/\beta$. The rate is determined by an exponentially small imaginary part of the partition function which in a semiclassical treatment can thus not be neglected against its dominating real part.

As we have seen in the previous Sect. 3.1.1, for sufficiently high temperatures tunneling no longer dominates and the continuum of energies around and above the barrier plays the crucial role. As a proper treatment shows (see [12]), the result (3.16) must then be replaced by the expression $\Gamma = (\omega_\mathrm{b}\beta/\pi)\mathrm{Im}F$. Both relations match at the crossover temperature T_0 (3.14) so that the final $\mathrm{Im}F$ formula reads

$$\Gamma = \begin{cases} (\omega_\mathrm{b}\beta/\pi)\ \mathrm{Im}F & \text{for } \ T \geq T_0 \\ \\ (2/\hbar)\ \mathrm{Im}F & \text{for } \ T \leq T_0 \end{cases} . \tag{3.17}$$

The most convenient way to apply the $\mathrm{Im}F$ method and to calculate the partition function of an unstable system, is to make use of its representation as a sum over paths in imaginary time (2.42) [14, 15, 11]. Since for these systems a true thermodynamic equilibrium does not exist, the calculation of Z must be performed by means of an analytic continuation pioneered by Langer [16]. In the semiclassical limit, i.e. for $V_\mathrm{b} \gg \hbar\omega_0$, the corresponding path integral (2.42) is dominated by all periodic minimal action paths $q_\mathrm{ma}^{(\alpha)}$ and Gaussian fluctuations around them so that one writes for an arbitrary paths $q(\sigma) = q_\mathrm{ma}^{(\alpha)}(\sigma) + y(\sigma)$ with $y(0) = y(\hbar\beta)$. In a metastable barrier potential of the type sketched in Fig. 3.1 there are always two trivial periodic orbits, namely, one at the well bottom $q_0(\sigma) = 0$ and one at the barrier top $q_\mathrm{b}(\sigma) = q_\mathrm{b}$. For temperatures $T > T_0$ when no oscillating orbit in $-V(q)$ exists (since $\hbar\beta < 2\pi/\omega_0$), these provide the dominating contributions to Z denoted by Z_0 and Z_b, respectively. It turns out that while around q_0 fluctuations $y(\sigma)$ are stable, around q_b there exists one unstable mode which induces translations in position around the barrier top. Due to an analytic continuation of the corresponding Gaussian integral [16, 12] these unstable fluctuations give rise to the imaginary contribution of the partition function, i.e. $Z = Z_0 + \mathrm{i}|Z_\mathrm{b}|$. Then, by writing $F = -(1/\beta)\ln(Z) \approx -(1/\beta)[\ln(Z_0) + \mathrm{i}|Z_\mathrm{b}|/Z_0]$ and using (3.17) one ends up with the expression (3.12).

For sufficiently low temperatures $T < T_0$ ($\hbar\beta > 2\pi/\omega_0$), a new type of periodic orbits appears which run in the time interval $\hbar\beta$ through the inverted

barrier potential $-V(q)$ with an arbitrary initial phase. These orbits, the so-called *bounces*, reflect the on-set of quantum tunneling. Langer's method has been put forward into this regime in [4, 17, 18, 19]. The bounce orbits $q_{\rm B}(\sigma)$ are determined explicitly by $\delta S_{\rm E}[q_{\rm B}] = 0$ and carry a corresponding minimal action $S_{\rm B}$. Again one puts $q(\sigma) = q_{\rm B}(\sigma) + y(\sigma)$ and expands the action functional up to second order $S_{\rm E}[q] \approx S_{\rm B} + \delta^2 S_{\rm E}[q_{\rm B}, y]$ with

$$\delta^2 S_{\rm E}[q_{\rm b}, y] = \frac{1}{2} \int_{-\hbar\beta/2}^{\hbar\beta/2} {\rm d}\sigma_1 {\rm d}\sigma_2 \, \frac{\delta^2 S[q]}{\delta q(\sigma_1)\delta q(\sigma_2)}\bigg|_{q=q_{\rm B}} y(\sigma_1) y(\sigma_2) \,. \tag{3.18}$$

Note that here for convenience the range of integration has been shifted due to the time translation invariance to lie symmetrically around $\sigma = 0$. The path integral over $q(\sigma)$ is thus transformed into a Gaussian path integral over the fluctuations $y(\sigma)$. This is most conveniently calculated by using the eigenfunctions to the second order variational operator contained in $\delta^2 S_{\rm E}$, i.e. $L_{\rm B}\phi_l = \Lambda_l^{({\rm B})}\phi_l$, with $\phi_l(-\hbar\beta/2) = \phi_l(\hbar\beta/2)$ and

$$\begin{aligned} L_{\rm B}(\sigma_1, \sigma_2) &= \frac{\delta^2 S_{\rm E}[q]}{\delta q(\sigma_1)\delta q(\sigma_2)}\bigg|_{q=q_{\rm B}} \\ &= \delta(\sigma_1 - \sigma_2) \left(-M \frac{{\rm d}^2}{{\rm d}\sigma_1^2} + \frac{{\rm d}^2 V(q)}{{\rm d}q^2}\bigg|_{q=q_{\rm B}(\sigma_1)} \right) . \end{aligned} \tag{3.19}$$

A straightforward evaluation along these lines encounters two subtleties though, which require special care. First, from the equation of motion one deduces that $\dot{q}_{\rm B}(\sigma)$ is proportional to the eigenfunction ϕ_1 with a vanishing eigenvalue. One further shows that $\dot{q}_{\rm B}$ generates infinitesimal changes in the phase of the bounce, while the total action is invariant even with respect to finite time translations. Hence, fluctuations in the direction of $\dot{q}_{\rm B}$ in function space cannot be treated in Gaussian or any higher approximation, but must be taken into account exactly. The procedure is to pick a representative out of the set of equivalent bounces and exploit that the integration over the phase is proportional to an integration over the total time interval. Second, since the bounce has one turning point, $\dot{q}_{\rm B}(\sigma)$ has one node, and consequently there must be one nodeless eigenfunction ϕ_0 with a smaller, i.e. negative, eigenvalue $\Lambda_0^{({\rm B})} < 0$. This unstable mode gives rise to an additional imaginary contribution to the partition function related to the bounce orbit $Z_{\rm B}$, which for temperatures sufficiently below T_0 dominates against the contribution $Z_{\rm b}$, so that $Z \approx Z_0 + {\rm i}|Z_{\rm B}|$. Eventually, the tunneling rate turns out to be

$$\Gamma = \sqrt{\frac{S_{\rm B}}{2\pi\hbar}} \sqrt{\frac{\det[L_0]}{\det'[L_{\rm B}]}} \, {\rm e}^{-S_{\rm B}/\hbar} \tag{3.20}$$

where L_0 is the second order variational operator around q_0 and in $\det'$ the zero eigenvalue is omitted. To calculate explicitly the prefactor, one uses an

approach developed by Coleman [19, 4] to evaluate ratios of functional determinants. For instance, in case of the metastable potential (3.7) the bounce at zero temperature $\hbar\beta \to \infty$ is explicitly obtained as

$$q_{\mathrm{B}}(\sigma) = \frac{3q_{\mathrm{b}}}{2}\frac{1}{\cosh(\omega_0\sigma/2)^2} \quad , \quad \sigma \in \left[-\frac{\hbar\beta}{2}, \frac{\hbar\beta}{2}\right] \tag{3.21}$$

and the corresponding rate coincides with (3.8).

Hence, for high as well as for low temperatures one gains the same rate expressions as within the WKB approach, which proves the equivalence of both methods [12]. However, the ImF-method enables us to calculate the decay rate of a metastable system by neither performing explicitly a thermal average (3.1), nor an explicit construction of wave functions. Further, it can be very conveniently also applied in presence of dissipation, see Chap. 5. We emphasize again that, as a purely thermodynamic approach, a prerequisite for its applicability is the existence of a local Boltzmann distribution inside the well region. In the non-dissipative case this is in a strict sense only guaranteed for sufficiently low temperatures, where tunneling occurs from the ground state.

While the ImF method is a non-dynamical method, it has nevertheless been used to derive in certain limits decay rates for barrier systems driven by external time dependent forces. One limit where it applies is the adiabatic limit of low frequency driving [20]. Then, an equilibrium distribution for each instantaneous phase of the external driving is approached and the total rate is an average over escape events in instantaneous barrier potentials. In the opposite case of very fast driving one may assume that the decay happens to occur in an averaged potential (averaged over one period of driving) so that again the problem reduces to a static rate calculation. For driving frequencies of the order of the well frequencies and/or for sufficiently strong driving a thermodynamic method must fail though.

3.1.3 Macroscopic Quantum Tunneling in Josephson Junctions

Josephson junctions (JJs) are one of the central building blocks for complex mesoscopic devices [7, 8]: two superconducting domains are separated by a thin insulating oxide barrier (Fig. 3.2). The tunneling of Cooper pairs through the device is, according to the Josephson relations, completely determined by the phase difference between the superconducting phases of left and right lead. JJs are easily fabricated and controllable and exhibit strongly nonlinear transport characteristics. Since the 1980s corresponding circuits have been designed to thoroughly test theoretical predictions for classical and quantum decay in various situations [21]. In the last years JJs have received considerable interest as elements to implement superconducting quantum bits [22, 23] and as extremely sensitive on-chip detectors [24, 25, 26, 27]. In the former case one exploits that the Josephson phase realizes an one-dimensional anharmonic potential well, in the latter one the exponential sensitivity of the

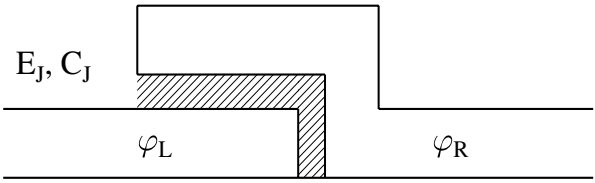

Fig. 3.2. Sketch of a cross section through a Josephson junction consisting of two overlapping superconducting domains with phases φ_{L} and φ_{R}, respectively, separated by a thin (typically a few Å) oxide layer (shaded area). The JJ is determined by the coupling energy E_{J}, the capacitance C_{J}, and the relative phase $\varphi = \varphi_{\mathrm{L}} - \varphi_{\mathrm{R}}$. For a picture of a real JJ see Fig. 3.5.

switching process out of the zero-voltage state with respect to the topology of the potential barrier and the surrounding noise is highly advantageous.

Dynamics of Josephson Junctions

In the basis of the charge eigenstates $\{|n\rangle, n \in \mathbf{Z}\}$ associated to the number of Cooper pairs having crossed the junction, the Hamiltonian of a JJ can be written as

$$H_{\mathrm{J}} = -\frac{1}{2} E_{\mathrm{J}} \sum_{n=-\infty}^{\infty} \left(|n\rangle\langle n+1| + |n+1\rangle\langle n| \right) . \tag{3.22}$$

Here, E_{J} denotes the Josephson coupling energy between left and right domain and is related to their superconducting gaps, cf. Fig. 3.2. The operator conjugate to the number operator $\hat{N}$, $\hat{N}|n\rangle = n|n\rangle$, is the phase operator $\hat{\varphi}$, i.e. $[\hat{N}, \hat{\varphi}] = \mathrm{i}$, related to the phase difference between the phases of the individual superconducting condensates. In the phase representation (3.22) reads

$$\hat{H}_{\mathrm{J}} = -E_{\mathrm{J}} \cos(\hat{\varphi}) . \tag{3.23}$$

For a complete description of a JJ also its capacitance C_{J} must be taken into account. The corresponding charging energy is $\hat{H}_C = \hat{Q}^2/(2C_{\mathrm{J}})$, where the charge $\hat{Q}$ is associated with $\hat{N}$ via $\hat{Q} = 2e\hat{N}$. Accordingly, when additionally an external bias current I_{b} is applied, the total Hamiltonian is

$$\hat{H} = \frac{\hat{Q}^2}{2C_{\mathrm{J}}} - E_{\mathrm{J}} \cos(\hat{\varphi}) - \phi_0 I_{\mathrm{b}} \hat{\varphi} \tag{3.24}$$

with the reduced flux quantum

$$\phi_0 = \frac{\hbar}{2e} . \tag{3.25}$$

The supercurrent flowing through the JJ is obtained from $\hat{I}_{\mathrm{S}} = 2e\dot{\hat{N}} = [\hat{N}, H_{\mathrm{J}}]/\mathrm{i}\phi_0$ as

$$\langle \hat{I}_{\mathrm{S}} \rangle = I_{\mathrm{c}} \langle \sin(\hat{\varphi}) \rangle \tag{3.26}$$

with the critical current $I_{\mathrm{c}} = E_{\mathrm{J}}/\phi_0$. Moreover, one gains from $\dot{\hat{\varphi}} = (\hbar/\mathrm{i})[\hat{\varphi}, H]$ that

$$\phi_0 \frac{\mathrm{d}\langle \hat{\varphi} \rangle}{\mathrm{d}t} = \frac{\langle \hat{Q} \rangle}{C_{\mathrm{J}}} = V \tag{3.27}$$

with the voltage V across the junction. In the classical limit these relations reduce to the known Josephson relations [7, 8]. When one formally identifies momentum $\hat{p} = \phi_0 \hat{Q}$ and mass $M = C_{\mathrm{J}} \phi_0^2$, the Hamiltonian (3.24) is equivalent to that of a fictitious particle moving in a tilted washboard potential

$$V_{\mathrm{J}}(\varphi) = -E_{\mathrm{J}} \cos(\varphi) - \phi_0 I_{\mathrm{b}} \varphi \,. \tag{3.28}$$

Note though that due to the discreteness of the eigenvalues of the charge operator, eigenstates to $\hat{H}$ must be periodic, i.e. $|\psi(\varphi)\rangle = |\psi(\varphi + 2\pi)\rangle$, when these states are physically indistinguishable [8] in contrast to those of a quantum particle in a spatially periodic potential, where this relation holds only up to a phase.

A realistic junction is embedded in an electrical circuit and also its resistance associated with quasi-particle transport must be taken into account. Classically, in the so-called RCSJ model (Resistively and Capacitively Shunted Junction) a real JJ is seen as an ideal JJ placed in parallel to a capacitor (C_{J}) and an ohmic resistor (R) [7], see Fig. 3.3. According to Kirchoff's law the total current through the junction is then given by

$$I_{\mathrm{b}} = I_{\mathrm{c}} \sin(\varphi) + \frac{V}{R} + C_{\mathrm{J}} \frac{\mathrm{d}V}{\mathrm{d}t} \,, \tag{3.29}$$

which due to (3.27) can be written in terms of φ. For a complete description also the current noise (Johnson-Nyquist noise) δI with $\langle \delta I \rangle = 0$ is included so

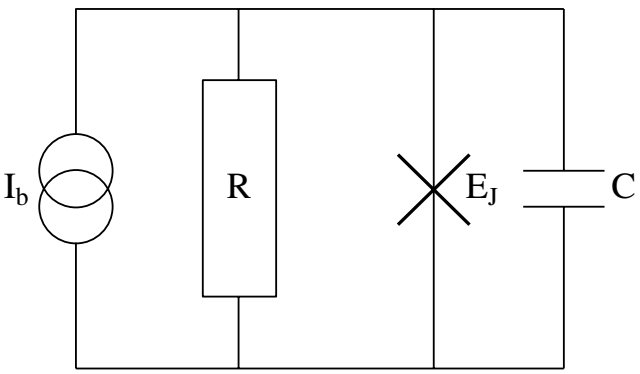

Fig. 3.3. Resistively and Capacitively Shunted Junction (RCSJ) model describing a JJ embedded in a circuit with total resistance R and total capacitance C biased by an external current I_{b}.

that the classical dynamics of a JJ obeys a Langevin equation of a fictitious particle, namely,

$$M\ddot{\varphi} + M\gamma\dot{\varphi} + \frac{\mathrm{d}V_{\mathrm{J}}(\varphi)}{\mathrm{d}\varphi} = \phi_0 \delta I\,. \tag{3.30}$$

The friction coefficient $\gamma = 1/RC$ (total capacitance C includes C_{J} and additional capacitances in the circuit) is related to the current noise via the dissipation fluctuation theorem

$$\langle \delta I(t)\delta I\rangle = 2k_{\mathrm{B}}T(M\gamma/\phi_0^2)\,\delta(t)\,. \tag{3.31}$$

The corresponding dissipative quantum system is obtained in the framework of a system+reservoir description, a subject treated in Chap. 5.

Tunneling Rates and Measurement

For a JJ biased by a current I_{b} sufficiently below the critical current I_{c}, the phase φ resides in one of the minima of the tilted washboard potential. When I_{b} tends towards I_{c}, the phase may escape from the metastable well and accumulates an average velocity related to a finite voltage across the junction, see (3.27). This switching out of the zero voltage state occurs in the high temperature domain by thermal activation, while below a certain crossover temperature quantum tunneling of the superconducting phase difference dominates, coined Macroscopic Quantum Tunneling (MQT). Experimental evidence for this latter process has been first obtained in [28, 29, 30, 31]. Since all parameters of such a circuit can be determined independently in the classical regime, a JJ allows for the most accurate comparison between experimental data and theoretical rate predictions in the tunneling domain [21, 32, 33, 34, 35, 36, 37].

The junction itself is completely characterized by its critical current I_{c} and its capacitance or equivalently its plasma frequency

$$\omega_0 = \omega_{00}(1-s^2)^{1/4} \tag{3.32}$$

for small oscillations around the well bottoms of the tilted washboard potential. Here, the plasma frequency at zero bias $s = I_{\mathrm{b}}/I_{\mathrm{c}} = 0$ reads $\omega_{00} = \sqrt{2E_{\mathrm{C}}E_{\mathrm{J}}}/\hbar$ with the charging energy $E_{\mathrm{C}} = 2e^2/C_{\mathrm{J}}$. These quantities are extracted by performing experiments at high temperatures, where the junction switches to its non zero-voltage state by thermal activation.

To determine the switching rate typically 10^4 to 10^5 switching events are collected. A bias current ramp $I_{\mathrm{b}}(t)$ is applied and the number of switching events at a certain bias current counted. From the switching probability

$$P(t) = 1 - \mathrm{e}^{-\int_0^t \mathrm{d}t'\,\Gamma(t')}\,, \tag{3.33}$$

one derives with $t = t(I_{\mathrm{b}})$ that $W(I_{\mathrm{b}}) \equiv \mathrm{d}P(I_{\mathrm{b}})/\mathrm{d}I_{\mathrm{b}} = \Gamma(I_{\mathrm{b}})[1-P(I_{\mathrm{b}})]/v_I$ with $v_I = \mathrm{d}I_{\mathrm{b}}(t)/\mathrm{d}t$ being the current ramp rate. This way, the histogram of switching events $W(I_{\mathrm{b}})$ is directly related to the rate (see e.g. [35])

$$\Gamma(I_\mathrm{b}) = v_I \frac{W(I_\mathrm{b})}{\int_{I_\mathrm{b}}^{I_\mathrm{c}} W(I_\mathrm{b})} \,. \tag{3.34}$$

Now, first the plasma frequency is determined by shining microwaves onto the JJ, which then acts as a classical anharmonic oscillator. By tuning the microwave frequency one observes a characteristic rate enhancement near the plasma frequency, a phenomenon called resonant activation [32, 35]. The width of the resonance corresponds to the Q-factor of the junction associated with its coupling strength to the electromagnetic environment. Next, the critical current I_c is extracted by exploiting the s dependence of the barrier height V_b, which separates a well from the continuum and determines the thermal activation factor in (3.13). Namely, for $(I_\mathrm{c} - I_\mathrm{b})/I_\mathrm{c} \ll 1$ one has

$$V_\mathrm{b} \approx 4E_\mathrm{J} \frac{\sqrt{2}}{3} (1-s)^{3/2} \tag{3.35}$$

so that at fixed temperature the function $B(s) = \ln(\omega_0/2\pi\Gamma(s))^{2/3}$ is basically a straight line proportional to $(1-s)$. Accordingly, lines taken at different temperatures are extrapolated to intersect at the same value $s = 1$, see Fig. 3.4.

When comparing decay rates for high and low temperatures, it is convenient to introduce an effective escape temperature by

$$\Gamma = \frac{\omega_0}{2\pi} \, \mathrm{e}^{-V_\mathrm{b}/k_\mathrm{B}T_\mathrm{esc}} \,. \tag{3.36}$$

Above the crossover temperature $T > T_0$ one has $T_\mathrm{esc} \propto T$ [see (3.13)], while for $T \ll T_0$ it approaches $T_\mathrm{esc} \propto 5\hbar\omega_0/36k_\mathrm{B}$ [see (3.8)]. Away from the purely

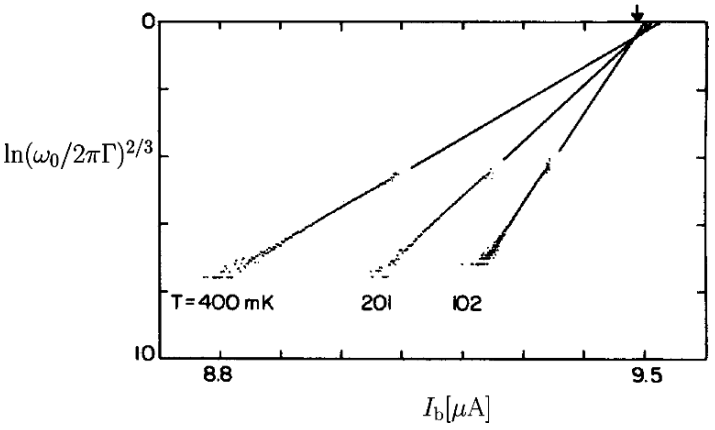

Fig. 3.4. $B(s) = \ln(\omega_0/2\pi\Gamma)^{2/3}$ as a function of the applied bias current $I_\mathrm{b} = sI_\mathrm{c}$ for various temperatures in the classical regime of thermal activation. Dots depict experimental data and straight lines are corresponding extrapolations intersecting at the critical current I_c (arrow). Courtesy of the Quantronics Group (SPEC), CEA Saclay.

classical limit, but still at $T > T_0$, quantum fluctuations lead to a rate enhancement [see (3.12)]. These theoretical predictions have been completely verified by the experimental data (see [21] for an overview). To obtain even a quantitative agreement one needs to take into account the influence of the dissipative environment on the rate expression, which will be done in Chap. 5.

3.1.4 Tunneling of Quantum Bits

The prospect to exploit features of quantum mechanics for information processing has triggered an enormous amount of research in the last years [38]. While first implementations of quantum mechanical two-state systems, called quantum bits or briefly qubits, have been realized in quantum optical systems and ensembles of molecules, in the last years the solid-state community has joined these efforts. So far the most successful solid state devices are based on superconducting qubits since superconductivity comes with a natural energy gap between the condensate and quasi-particles excitations so that decoherence due to these latter "perturbations" is strongly suppressed [22, 39].

The *Quantronium* [see Fig. 3.5] is a solid state based qubit setup consisting of a Cooper pair box (CPB) whose Josephson junction is split in two small junctions with Josephson energy E_J, delimiting an island with capacitance C and charging energy $E_\mathrm{C} = (2e)^2/2C$ [24, 40]. The two lowest lying states of the box with energies E_0 and E_1 encode a qubit and in the circuit give rise to loop currents of opposite direction. In parallel to the box is a third big Josephson junction (with $E'_\mathrm{J} \gg E_\mathrm{J}$ and $E'_\mathrm{C} \ll E_\mathrm{C}$) which serves as a detector. For the readout this big junction is biased by an external current pulse so that the total bias current it sees depends on the state of the qubit. The measurement consists of adiabatically driving the big junction into the regime where MQT sets in. Due to the exponential sensitivity of the tunneling rate on the total bias current, the two qubits states can efficiently be discriminated.

The analysis of the device becomes particularly transparent in the charging regime ($E_\mathrm{C} \gg E_\mathrm{J}$) where the two qubit states are determined by superpositions of zero or one excess Cooper pair on the island. Further, we consider the case of two symmetric JJs for the CPB, $d = 0$. To quantitatively describe the experimental data one has to take into account a finite d though [41]. Then, the Hamiltonian of the box-subsystem can be written in terms of Pauli matrices and by measuring all energies in units of E'_J the total dimensionless Hamiltonian of the circuit reads

$$H_\mathrm{QJ} = e_\mathrm{C}\,\sigma_z - e_\mathrm{J}\,\cos\left(\frac{\theta+\phi}{2}\right)\sigma_x + \frac{p_\theta^2}{2M} - \cos(\theta) - i_\mathrm{b}\theta \tag{3.37}$$

with the dimensionless parameters $e_\mathrm{C} = (E_\mathrm{C}/E'_\mathrm{J})(N_\mathrm{g} - 1/2)$ (reduced gate charge N_g), $e_\mathrm{J} = E_\mathrm{J}/(2E'_\mathrm{J})$, and $i_\mathrm{b} = \hbar I_\mathrm{b}/2eE'_\mathrm{J}$. Here, the first two terms describe the qubit and the remaining ones the read-out junction with $M =$

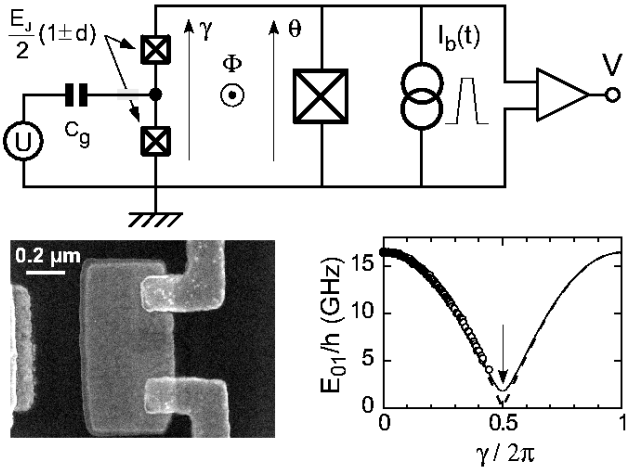

Fig. 3.5. Top: Quantronium circuit based on a split Cooper pair box (CPB) with charging energy E_C, Josephson energy E_J, and asymmetry d, which can be manipulated by a gate voltage U and a magnetic flux Φ. For the readout a larger JJ with phase θ is biased by a current pulse I_b to induce the switching to a finite voltage state. Bottom left: Scanning electron micrograph of the CPB with the two JJs. Bottom right: Measured energy splitting E_{01} of the two lowest energy eigenstates of the CPB (dots) at $N_\mathrm{g} = C_\mathrm{g}U/2e = 1/2$ as a function of $\gamma = \theta + 2e\Phi/h$. The dashed and solid lines are fits using $E_\mathrm{J} = 0.87 k_\mathrm{B}\mathrm{K}$ and $E_\mathrm{C} = 0.655 k_\mathrm{B}\mathrm{K}$ with $d = 0$ and $d = 0.1$, respectively. At $\gamma = \pi$ (arrow) a level crossing or small gap occurs depending on d. Courtesy of the Quantronics group (SPEC), CEA Saclay.

$C'E'_\mathrm{J}/4e^2$ being the scaled mass of a fictitious particle with corresponding momentum p_θ and conjugate phase θ. For further details we refer to [24, 42, 43]. Due to the coupling between the two subsystems, the qubit and the big junction, the dynamics of θ can be seen as that of a particle with two internal states.

Now, we consider the situation when the qubit is initially ($i_\mathrm{b} = 0$) prepared in its ground state. By rising the bias current $i_\mathrm{b} > 0$ adiabatically the phase θ can be seen as a classical variable with negligible kinetic energy due to the large mass (large capacitance C'). Depending on the spin state, the fictitious particle then evolves on adiabatic potential surfaces $\lambda_\pm(\theta)$ obtained by simply diagonalizing H_QJ in spin space for $M \to \infty$ [43]. When i_b is close to 1, however, the particle may tunnel out of the potential well and its kinetic energy cannot be neglected anymore. At finite bias the Hamiltonian H_QJ is most conveniently represented via a unitary transformation in the spin basis at the minimum θ_min of the lower adiabatic surface $\lambda_-(\theta)$, i.e.,

$$\tilde{H}_\mathrm{QJ} = \begin{pmatrix} \frac{p_\theta^2}{2M} + V_+(\theta) & \Delta(\theta) \\ \Delta(\theta) & \frac{p_\theta^2}{2M} + V_-(\theta) \end{pmatrix} . \tag{3.38}$$

Here, we introduced diabatic potential surfaces

$$V_{\pm} = -\cos(\theta) - i_{\rm b}\theta \pm \left(\sqrt{e_{\rm C}^2 + V_0^2} + \frac{V_0[V(\theta) - V_0]}{\sqrt{e_{\rm C}^2 + V_0^2}} \right) \tag{3.39}$$

and off-diagonal elements

$$\Delta(\theta) = \frac{e_{\rm C}[V_0 - V(\theta)]}{\sqrt{e_{\rm C}^2 + V_0^2}}\,, \tag{3.40}$$

where $V(\theta) = e_{\rm J}\cos(\frac{\theta+\phi}{2})$ and $V_0 = V(\theta_{\rm min})$. By construction, at $\theta = \theta_{\rm min}$ the off-diagonal elements vanish so that $V_-(\theta_-) = \lambda_-(\theta_-)$. Now, for the tunneling process one may approximate the diabatic surfaces in one well-barrier segment by a cubic expansion around $\theta_{\rm min}$ with $q = \theta - \theta_{\rm min}$ so that

$$V_{\pm}(q) = \frac{M\Omega_{\pm}^2}{2}\,(q - q_{\pm})^2[1 - (q - q_{\pm})/q_{0,\pm}] + \delta_{\pm,+} + \Delta V_{\rm min}\,, \tag{3.41}$$

where $\delta_{\mu,\nu}$ denotes the Kronecker symbol, and $\Delta V_{\rm min} = V_+(\theta_{\rm min}) - V_-(\theta_{\rm min})$.

As long as $V_{\pm}$ are sufficiently separated from each other everywhere in the barrier range, i.e. $|V_- - V_+| \gg \Delta$, the spin degree of freedom is essentially frozen and the particle escapes through $V_{\pm}$ via standard MQT. The corresponding escape rates $\Gamma_{\pm}$ can be directly inferred from (3.8).

There is an additional domain, however, which gives rise to an interesting new MQT phenomenon [43, 41]. Namely, when the two diabatic surfaces cross each other in the barrier range (see Fig. 3.6), the particle's spin, initially prepared in the gound state, may flip during the tunneling since this may enhance the probability for escape substantially (see Fig. 3.7 right). This process has some similarities to Landau-Zener transitions [44, 45] with the crucial difference though that while in this latter case real-time orbits pass a crossing region ballistically, here the transition occurs under the barrier while tunneling, i.e. for orbits in imaginary time including fluctuations around them. It was thus coined *Zener-flip tunneling* [41] and discussed also for other set-ups [46]. From another point of view, one may interpret the above phenomenon as tunneling of a particle with spin 1/2, the instantaneous position of which acts as a magnetic field. The crossing of the diabatic surfaces is then equivalent to a crossing of the Zeeman levels (see Fig. 3.7 left).

Hence, the standard ImF approach has to be extended to include spin flips so that the tunneling rate follows, in case of vanishing dissipation, from the imaginary part of the partition function

$$Z = \sum_{n=0}^{\infty} z_{2n} \tag{3.42}$$

with contributions z_{2n} consisting of $2n$ flips

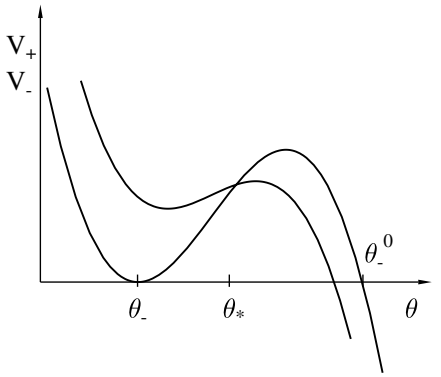

Fig. 3.6. Diabatic potential surfaces V_+ and V_- in the Zener flip range.

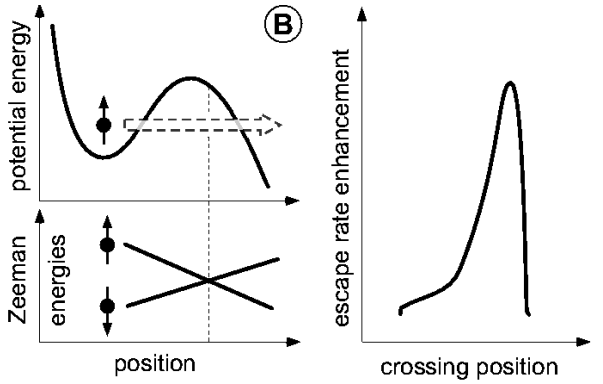

Fig. 3.7. Tunneling of a qubit out of a metastable well can be seen as tunneling of a fictitious particle with spin 1/2 such that its instantaneous position acts a magnetic field. When the corresponding Zeeman levels cross under the barrier, the escape rate is enhanced by spin flips (Zener-flip tunneling).

$$z_{2n} = \int \mathcal{D}q\, e^{-S_-[q]/\hbar} \int_{-\hbar\beta/2}^{\hbar\beta/2} d\tau_{2n} \Delta(q(\tau_{2n})) \cdots \int_{-\hbar\beta/2}^{\tau_2} d\tau_1 \Delta(q(\tau_1)) \times \exp\left[\sum_{k=1}^{n} \int_{\tau_{2k-1}}^{\tau_{2k}} d\tau (V_-(q) - V_+(q))/\hbar \right] , \quad (3.43)$$

where S_- denotes the bare action on the surface V_-. Semiclassically, the dominant contributions are provided by the corresponding minimal action paths. While for $n = 0$ these coincide with ordinary bounce paths on V_-, for $n > 1$ the flip-bounces switch to the V_+ surface on the way forth and again

onto V_- on the way back. One shows that these events happen most probably in a close vicinity of the intersection point. Eventually, the corresponding MQT rate can be cast into

$$\Gamma_{\rm Tot} = \Gamma_{\rm B} + f_{\rm flip}(\Delta_{\rm c}^2)\, \exp(-S_{\rm flip}/\hbar)\,, \tag{3.44}$$

where $\Gamma_{\rm B}$ denotes the standard MQT rate without spin flip, while the second term captures contributions due to flips. The prefactor $f_{\rm flip}$ of the flip contribution contains the coupling $\Delta_{\rm c}$ at the crossing point of $V_\pm$. For small couplings (non-adiabatic limit) one has $f_{\rm flip} \propto \Delta_{\rm c}^2/\Omega_1$ with the frequency Ω_1 being proportional to the second derivative of the flip-bounce action $S_{\rm flip}$ at the crossing [43]. The influence of low frequency environmental noise as a prevailing source of dephasing in the *Quantronium* [47] has been studied in [48].

The rate enhancement due to the Zener-flip phenomenon has been verified experimentally very recently [41], see Fig. 3.8. In these experiments the rate is not measured directly, but instead the bias current needed to detect a constant switching rate (feedback mode). Since effectively a rate enhancement corresponds to a weaker barrier, a spin flip while tunneling shows up in a sharp decrease of the switching current in the expected range of the magnetic flux. Note that in Fig. 3.8 a crossing of the diabatic surfaces at the readout only occurs in region B. In region A the switching happens to be by standard MQT from the lower surface, while in region C a crossing of the surfaces occurs in the well region while ramping adiabatically the bias current, which leads to a thermal population on the upper surface. Hence, at the readout one has tunneling from a thermal mixture of upper and lower surface, reminiscent of the Zener-flip tunneling at lower values of the magnetic flux. Zener-flip tunneling should also be observable in other superconducting qubit circuits, particularly, in the flux qubit based on SQUIDS [49]. A quite different realization could be spin dependent optical lattices as implemented e.g. in [50].

3.1.5 Collapse of Bose-Einstein Condensates with Attractive Interaction

In an ensemble of bosons an arbitrary number of particles can occupy the same microscopic state. At very low temperatures this leads to the phenomenon of Bose-Einstein condensation (BEC), where all bosons of the ensemble condensate in a zero momentum state and due to the overlaps of their wave functions form a collective quantum object. Predicted already during the heyday of quantum mechanics [51, 52, 53], BEC was actually realized and observed for dilute ultra-cold atomic clouds confined in magnetic traps a decade ago [54, 55]. Since then it has led to one of the most fascinating areas in contemporary physics with applications ranging from atomic and molecular to condensed matter systems [56, 57].

In a mean field description and at vanishing temperature the condensate wave function, which can also be interpreted as a classical order parameter

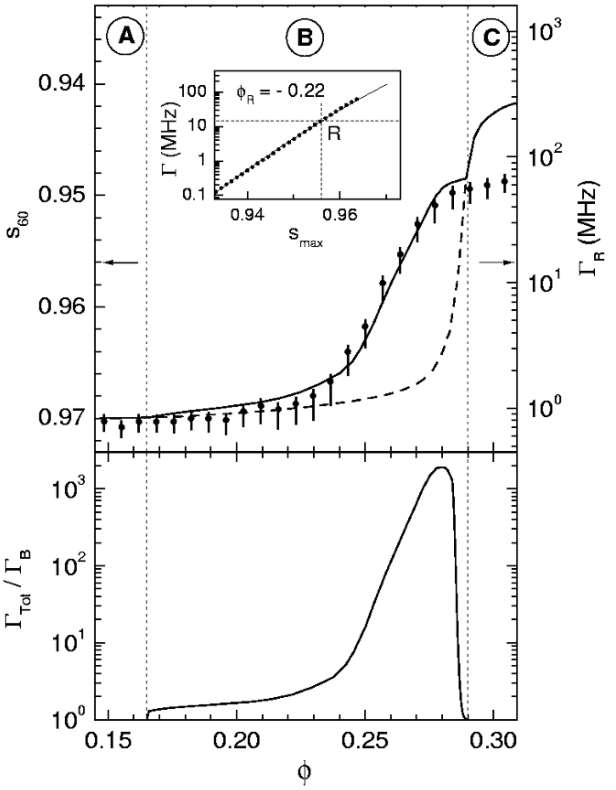

Fig. 3.8. Top panel: Experimental (dots) and calculated (lines) values of $s_{60} = I_{60}/I_c$ (I_{60} bias current with a switching probability of 60%) vs. the reduced magnetic flux $\phi = \Phi/(2\pi\phi_0)$ in the Zener region B, where the diabatic surfaces intersect. The curves are calculated with (solid) and without (dashed) Zener flips. The right vertical scale results from the conversion of s_{60} into a rate Γ_R according to the inset (see text). Arrows indicate the reference point R. Inset: Escape rate $\Gamma(s_{\max})$ measured (dots) and calculated (line) at $N_g = 1/2$ at the reference point R. Bottom panel: Escape rate enhancement calculated at constant rate $\Gamma_{Tot}(\phi, s_{60}) = \Gamma_{60}$ by dividing Γ_{60} by the rate Γ_B that would be observed at the same s_{60} in absence of Zener flips. See [41] for details.

field, is determined by the Gross-Pitaevskii (GP) equation

$$\mathrm{i}\hbar\frac{\partial\Psi(\boldsymbol{r},t)}{\partial t} = \left[-\frac{\hbar^2\nabla^2}{2M} + V_{\mathrm{ext}}(\boldsymbol{r}) + 2g|\Psi(\boldsymbol{r},t)|^2\right]\Psi(\boldsymbol{r},t)\,. \tag{3.45}$$

This nonlinear Schrödinger equation contains the atomic mass M, the external trapping potential V_{ext} and a self-interaction of strength g originating from two-body collisions assumed to be s-wave scattering processes. Hence, g is related to the corresponding s-wave scattering length a by $g = 2\pi\hbar^2 a/M$. The

confining potential $V_{\rm ext}$ is to a very good accuracy harmonic, not necessarily isotropic though.

BEC sets in below a so-called crossover temperature $T_{\rm c}$ which in the simplest case of an isotropic harmonic well with frequency ω_0 depends on the number of bosons N as $T_{\rm c} \propto \hbar\omega_0 N^{1/3}/k_{\rm B}$ [56]. Experimentally, ensembles of alkali atoms are used to approach the BEC regime as e.g. rubidium, sodium, and lithium. It turns out that a stable condensate only exists for a positive scattering length $a > 0$, i.e. repulsive atom-atom interaction. In the attractive case, realized for instance with ^{7}Li and ^{85}Rb, the condensate is metastable for a number of atoms $N < N_{\rm cr}$, where for typical parameters $N_{\rm cr}$ is of the order of one thousand. Experiments on ^{7}Li with a fixed scattering length have been reported in [58, 59, 60, 61, 62]. In more recent results on ^{85}Rb [63, 64] a Feshbach resonance has been used to tune the scattering length from positive (stable) to negative (unstable), which allows for a direct control of the collapse. The corresponding metastable state may decay by macroscopic quantum tunneling as analyzed in a number of studies [65, 66, 67]. Here we closely follow a description developed in [68, 69, 70].

A straightforward way to study an attractive condensate is to start with the energy functional corresponding to (3.45)

$$E[\Psi] = \int {\rm d}\boldsymbol{r}\Psi^*(\boldsymbol{r},t)\left[-\frac{\hbar^2\nabla^2}{2M} + V_{\rm ext}(\boldsymbol{r}) + g|\Psi(\boldsymbol{r},t)|^2\right]\Psi(\boldsymbol{r},t)\,. \tag{3.46}$$

For the simplest case of an isotropic trap (frequency ω_0), one assumes a Gaussian trial function

$$\Psi_{\rm G}(\boldsymbol{r}) = \sqrt{\frac{N}{\pi^{3/2}d^3}}{\rm e}^{-\boldsymbol{r}^2/2d^2} \tag{3.47}$$

with variational parameter d. Upon inserting this ansatz into the energy functional, one finds

$$v(r) \equiv \frac{4E[\Psi_{\rm G}(r)]}{N\hbar\omega_0} = 3\left(\frac{1}{r^2} + r^2\right) - \frac{\gamma}{r^3} \tag{3.48}$$

with $r = d/a_0$, $a_0 = \sqrt{\hbar/M\omega_0}$, and the dimensionless interaction strength

$$\gamma = |g|\frac{4N}{\hbar\omega_0\sqrt{8\pi^3}a_0^3}\,. \tag{3.49}$$

Now, depending on the value of γ the function $v(r)$ may exhibit a local minimum at $r > 0$ separated from the global minimum at $r \to 0$ by a barrier (for $\gamma < \gamma_{\rm c} = 1.07$) or no minimum at all (for $\gamma > \gamma_{\rm c}$) [cf. Fig. 3.9]. In the latter case, the energy functional can only be minimized for $r \to 0$ and the condensate collapses by evaporating atoms, a complicated process which has been recently analyzed experimentally [64]. Of course, for $r \to 0$ the mean field approach breaks down and a true many-body description is required.

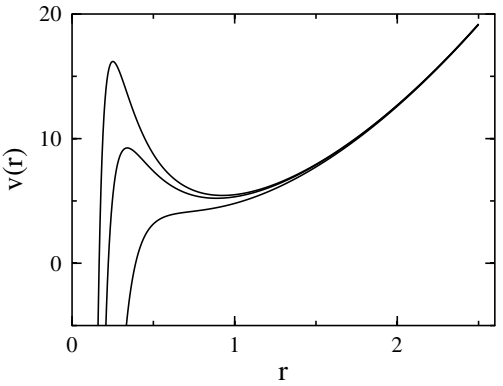

Fig. 3.9. Effective potential $v(r)$ of a condensate with attractive interaction described by the Gaussian trial wave function (3.47) for various values of the parameter γ [see (3.49)]: $\gamma = 0.5, 0.67, 1.2$ (top to bottom).

In the former situation, the condensate is trapped in a metastable well. When the number of bosons N is slightly below $N_{\rm cr}$ (γ slightly below $\gamma_{\rm c}$), the energy barrier will be so low that macroscopic quantum tunneling may occur towards a collapsing state. By taking into account the kinetic energy of the cloud due to zero-point fluctuations around the bottom of the trapping potential (breathing modes), the Euclidian action functional for the partition function is obtained as

$$S_{\rm E}[r]/\hbar = \frac{N}{4}\int d\sigma \left[3\dot{r}(\sigma)^2 + v[r(\sigma)] - v(r_{\rm min})\right] \tag{3.50}$$

with $r_{\rm min}$ the value of r at the bottom of the metastable well $v(r)$. The tunneling rate is then determined by the bounce $r_{\rm B}$ following the formula (3.20). Near the critical point the difference $v(r_{\rm B}) - v(r_{\rm min})$ can be expanded in a harmonic+cubic potential so that the explicit result (3.8) applies. This way, one obtains

$$S_{\rm B}/\hbar = \frac{2}{15}N\sqrt{6v''(r_{\rm min})}(r_{\rm min} - r_0)^2 \tag{3.51}$$

with r_0 the exit point $v(r_{\rm min}) = v(r_0)$, which can be cast into the transparent form

$$S_{\rm B}/\hbar \approx 4.58N\left(1 - \frac{N}{N_{\rm cr}}\right)^{5/4} . \tag{3.52}$$

Eventually, together with the prefactor the tunneling rate is given as

$$\Gamma = 11.8\omega_0\sqrt{N}\left(1 - \frac{N}{N_{\rm cr}}\right)^{7/8} {\rm e}^{-S_{\rm B}/\hbar} \tag{3.53}$$

which vanishes for $N \to N_{\rm cr}$ as expected. For instance, for typical experimental values and $(1 - N/N_{\rm c}) = 5 \times 10^{-3}$, the rate is $\Gamma \approx 1.9/{\rm s}$. We mention

that near the critical point two- and three-body collisions may also play a decisive role and compete with macroscopic quantum tunneling. For further discussions on that point and also on the time evolution of the condensate during the collapse we refer to [71, 72, 73, 74, 75, 76].

3.2 Tunnel Splittings in Bistable Potentials

A bistable potential with a sufficiently high barrier separating two classical ground states has a characteristic energy spectrum, which consists for energies below the barrier of a sequence of doublets. The energy gap of two levels in each doublet is much smaller than the gap between subsequent doublets. In a rough approximation the ground state doublet can be seen as the symmetric and antisymmetric superposition of the harmonic ground states localized in the individual wells, where their overlap in the barrier region determines the splitting between their energies [77]. The splitting is thus a consequence of the quantum coherence between the two stable wells, but is nevertheless usually called tunnel splitting.

This simple model is realized in a variety of systems in physics and chemistry, see e.g. [11]. In fact, the first example was given by Hund already in 1927 [78] to explain spectroscopic data for NH_3. Here, we present a powerful semiclassical technique to extract tunnel splittings in bi- and multistable systems, pioneered in quantum field theory [4, 79] and later on worked out for non-dissipative [80] and dissipative systems [81, 82, 11]. A very recent realization has been achieved by properly tailoring laser beams to form bistable optical potentials, in which the coherent dynamics could be analysed in detail [83].

In the limit of very low temperatures an extended bistable potential can be reduced to a two level system (TLS) with tunnel coupling determined from this semiclassical approach. The thermodynamics and real-time dynamics of the TLS interacting with a heat bath environment, called spin-boson model, has been studied in the last two decades with tremendous efforts, for reviews see [84, 11, 85], and still attracts a substantial amount of research. This is due to the fact that the spin-boson model together with its generalizations to multisite geometry describes a variety of physical systems comprising e.g. quantum Brownian motion, Kondo physics, Luttinger liquids, electron transfer, and decoherence of quantum bits [11, 39]. Despite its simplicity the associated phenomenology is extremely rich, showing different sorts of quantum phase transitions.

In the sequel we describe a path integral technique to extract tunnel splittings in these systems. This method is closely related to the bounce technique introduced in Sect. 3.1.2 the main difference being that here we have to deal with quantum coherence in contrast to tunneling into a continuum. As a consequence, instanton orbits connect alternately one minimum with the other one

and a sum must be performed over all arrangements of instanton chains. The formulation has been extended to the dissipative case as shown in Sect. 5.6.1.

3.2.1 Instanton Technique

In the sequel we consider a symmetric bistable potential $V(q)$ with minima at $q = \pm a$ and a barrier located at $q = 0$ as depicted in Fig. 3.10. Our goal is to calculate the diagonal element

$$\rho_\beta(a, a) = \langle a| \exp(-\beta \hat{H})|a\rangle \tag{3.54}$$

of the unnormalized statistical operator introduced in Sect. 2.4 in the limit of very low temperatures. For this purpose we evaluate the path integral expression (2.41) by means of semiclassical techniques. Accordingly, we start with an analysis of the minimal action paths in the interval $[-\hbar\beta/2, \hbar\beta/2]$ and proceed with the treatment of the fluctuations around them.

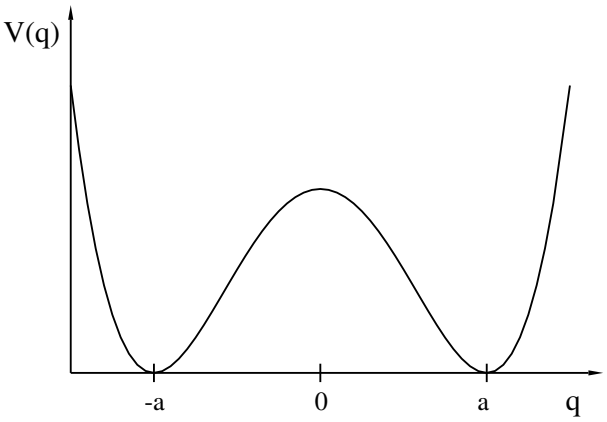

Fig. 3.10. Bistable potential with minima at $q = \pm a$ and a barrier at $q = 0$.

The Euclidian equation of motion following from $\delta S_{\rm E}[q] = 0$ reads

$$M\ddot{q}(\sigma) - V'(q) = 0 \ , \tag{3.55}$$

which for the matrix element in question is supplemented by the boundary conditions $q(\mp\hbar\beta/2) = a$. Obviously, there is one trivial solution $q_a(\sigma) = a$ with the action $S_{\rm E}[q_a] = 0$. In addition, there is a class of dynamical orbits that consists of paths, called instantons, connecting in the inverted potential $-V(q)$ the two maxima at $q = \pm a$. Since $\hbar\beta \to \infty$, the instantons creep most of the time close to these maxima and run through the well at $q = 0$ within a much shorter period of time of the order of $1/\omega_0$, where $\omega_0 = \sqrt{V''(a)/M}$. Hence, strings of instanton-antiinstanton pairs are also proper minimal action

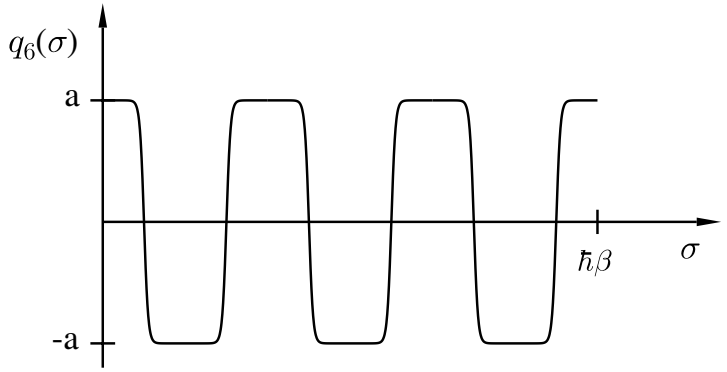

Fig. 3.11. Multi-instanton orbit $q_n(\sigma)$ consisting of $n = 6$ individual instantons connecting the minima $\pm a$ of a bistable potential for $\hbar\beta \to \infty$.

paths obeying the boundary conditions [see Fig. 3.11]. Let us denote such a path by

$$q_{n;\sigma_1,\ldots,\sigma_n}(\sigma)\,, \tag{3.56}$$

where n is the number of traversals and $\sigma_1, \ldots, \sigma_n$ are the consecutive positions of the centers of the individual instantons/antiinstantons with the constraint $-\hbar\beta/2 < \sigma_1 < \cdots < \sigma_n < \hbar\beta/2$. Due to the boundary conditions for paths contributing to $\rho_\beta(a, a)$ the number n must be even. Moreover, we put $q_{n=0} \equiv q_a$.

The crucial assumption is now that the individual instantons in such a string are widely separated meaning that the distances between their centers by far exceed their width of order $1/\omega_0$. This situation resembles that of a dilute gas of independent particles and was thus coined DIGA (Dilute Instanton Gas Approximation) [4]. The validity of the DIGA will be discussed below.

Given the minimal action of an individual instanton $S_\mathrm{I} = S_\mathrm{E}[q_{1;\sigma_1}]$, the action of an n-instanton path is now simply

$$S_\mathrm{E}[q_{n;\sigma_1,\ldots,\sigma_n}(\sigma)] = nS_\mathrm{I}\,. \tag{3.57}$$

We continue by expanding the full action around each minimal action path

$$q(\sigma) = q_{n;\sigma_1,\ldots,\sigma_n}(\sigma) + y(\sigma) \quad , \quad y(-\hbar\beta/2) = y(\hbar\beta/2) = 0\,, \tag{3.58}$$

such that $S_\mathrm{E}[q] \approx nS_\mathrm{I} + \delta_n^2 S_\mathrm{E}[y]$ with the fluctuating part specified in (3.18). The latter one contains the second order variational operator (3.19) which is determined by

$$V_n[y] = \frac{1}{2}V''[q_{n;\sigma_1,\ldots,\sigma_n}]\,y^2\,. \tag{3.59}$$

The corresponding fluctuation path integrals

$$G_n\left(0,\frac{\hbar\beta}{2};0,-\frac{\hbar\beta}{2}\right)= \int\mathcal{D}[y]\exp\left[-\frac{1}{\hbar}\int\limits_{-\frac{\hbar\beta}{2}}^{\frac{\hbar\beta}{2}}\mathrm{d}\sigma\left(\frac{M\dot{y}(\sigma)^2}{2}+V_n[y]\right)\right] \quad (3.60)$$

are thus imaginary time propagators of a particle moving in a harmonic potential with time dependent curvature. Outside the instanton centers the curvature is constant and equal to ω_0, the curvature of the harmonic oscillators at the well bottoms of the bistable potential.

However, we have to be a bit careful in treating the G_n. So far we have not fixed the centers of the instantons and, in fact, in the limit $\omega_0\hbar\beta \gg 1$ the total action is independent of their exact locations inside the interval $[-\hbar\beta/2, \hbar\beta/2]$. This reflects again the time translation symmetry of the action that we have already discussed for the bounce orbit. To deal with this exact invariance, we follow a similar procedure: Select a representative out of the class of equivalent n-instanton paths and sum over the full set by integrating in a time-ordered manner over the locations of the centers. Most conveniently, for the representative one chooses the $\sigma_i, i = 1,\ldots,n$ to lie equidistantly with distances $\hbar\beta/2n$, which are large due to the DIGA. Now, in the G_n for each instanton there must be one direction in function space, i.e. one eigenfunction of the second order variational operator, which generates fluctuations of the instanton centers and has therefore a vanishing eigenvalue. The contributions of these fluctuation modes must be omitted since they are accounted for by the center integrations. In other words, the G_n must be calculated for the representative instanton paths with fixed centers. We denote these restricted path integrals by $\acute{G}_n$.

The element of the density matrix now takes the following form

$$\rho_\beta(a,a)\approx\sum_{n\geq 0,\text{even}}\mathrm{e}^{-nS_\mathrm{I}/\hbar} \times\int\limits_{-\frac{\hbar\beta}{2}}^{\frac{\hbar\beta}{2}}\mathrm{d}\sigma_1\int\limits_{-\frac{\hbar\beta}{2}}^{\sigma_1}\mathrm{d}\sigma_2\cdots\int\limits_{-\frac{\hbar\beta}{2}}^{\sigma_{n-1}}\mathrm{d}\sigma_n\;\acute{G}_n\left(0,\frac{\hbar\beta}{2};0,-\frac{\hbar\beta}{2}\right), \quad (3.61)$$

where only paths with an even number of instantons contributes due to the boundary condition. The $n = 0$ term is just the contribution of the trivial path.

Starting with a single instanton one recalls that $V_1[y]$ reduces to a simple harmonic oscillator potential outside the narrow region of width $1/\omega_0$ around the instanton center. It is thus reasonable to introduce the ratio

$$\tilde{\Delta}=\frac{\acute{G}_1(0,\hbar\beta/2;0,-\hbar\beta/2)}{G_0(0,\hbar\beta/2;-\hbar\beta/2,0)} \quad (3.62)$$

where

$$G_0(0,\hbar\beta/2;-\hbar\beta/2,0)=\sqrt{\frac{M\omega_0}{2\pi\hbar\sinh(\omega_0\hbar\beta)}}\approx\sqrt{\frac{M\omega_0}{\pi\hbar}}\;\mathrm{e}^{-\omega_0\hbar\beta/2} \tag{3.63}$$

is the harmonic propagator in the well. Since $\omega_0\hbar\beta\gg 1$ one shows that $\tilde{\Delta}$ is independent of temperature so that

$$\acute{G}_1(0,\hbar\beta/2;0,-\hbar\beta/2)\approx\tilde{\Delta}\,\sqrt{\frac{M\omega_0}{\pi\hbar}}\;\mathrm{e}^{-\omega_0\hbar\beta/2}\,. \tag{3.64}$$

For multi-instantons basically the same line of reasoning applies due to the DIGA assumption. Cutting the multi-instanton path far away from the instanton centers in segments containing just a single instanton, one finds

$$\acute{G}_n(0,\hbar\beta/2;0,-\hbar\beta/2)\approx\tilde{\Delta}^n\,\sqrt{\frac{M\omega_0}{\pi\hbar}}\;\mathrm{e}^{-\omega_0\hbar\beta/2}\,. \tag{3.65}$$

To obtain this result also the group property (2.19) for the harmonic propagator was used since in each of the segments $-\hbar\beta/2<s_1<s_2<\cdots<s_{n-1}<\hbar\beta/2$ one may put

$$\acute{G}_1(y_l,s_l;y_{l-1},s_{l-1})\approx\tilde{\Delta}\;G_0(y_l,s_l;y_{l-1},s_{l-1})\,. \tag{3.66}$$

The integrals in (3.61) can now explicitly be performed and one arrives at

$$\begin{aligned}\rho_\beta(a,a)&\approx\sqrt{\frac{M\omega_0}{\pi\hbar}}\;\mathrm{e}^{-\omega_0\hbar\beta/2}\sum_{n\geq 0,\mathrm{even}}\frac{1}{n!}\left(\frac{\Delta\hbar\beta}{2}\right)^n\\&=\sqrt{\frac{M\omega_0}{\pi\hbar}}\;\mathrm{e}^{-\omega_0\hbar\beta/2}\cosh(\Delta\hbar\beta/2)\,.\end{aligned} \tag{3.67}$$

Here, we introduced

$$\Delta=2\tilde{\Delta}\;\mathrm{e}^{-S_\mathrm{I}/\hbar}\,, \tag{3.68}$$

which is the frequency corresponding to the energy gap between the lowest lying energies E_1 and E_0 with eigenstates ϕ_1 and ϕ_0. Namely, according to (2.43) at very low temperatures $\omega_0\hbar\beta\to\infty$ the unnormalized statistical operator can be written in form of a spectral decomposition as

$$\rho_\beta(a,a)\approx\frac{1}{2}\sqrt{\frac{M\omega_0}{\pi\hbar}}\;\mathrm{e}^{-\beta(\hbar\omega_0/2-\hbar\Delta/2)}+\frac{1}{2}\sqrt{\frac{M\omega_0}{\pi\hbar}}\;\mathrm{e}^{-\beta(\hbar\omega_0/2+\hbar\Delta/2)}\,. \tag{3.69}$$

Hence, $E_1-E_0=\hbar\Delta$ and $\phi_1(a)^2=\phi_0(a)^2=\sqrt{M\omega_0/4\pi\hbar}$. What remains to do is first to derive an explicit expression for the single instanton ratio $\tilde{\Delta}$ and second to prove the consistency of the DIGA.

In principle, the calculation of $\tilde{\Delta}$ follows the strategy discussed above around (3.20). The integration over the zero mode amplitude y_0 must be

omitted in $\acute{G}_1$ and is carried out according to $\mathrm{d}y_0 = g_0 \mathrm{d}\sigma_1$. The factor g_0 is obtained by exploiting that according to (3.55) $\dot{q}_{1;\sigma_1}$ must be proportional to the zero-mode eigenfunction φ_0. The calculation yields

$$g_0 = \sqrt{\frac{MS_\mathrm{I}}{2\pi\hbar}}\,. \tag{3.70}$$

Note, that in contrast to the bounce orbit the instanton has no turning point so that the zero mode is indeed associated with the lowest eigenvalue of the second order variational operator and no imaginary contribution appears. Then, following again [4] in calculating functional determinants with one direction in function space omitted, one gets

$$\tilde{\Delta} = 2A\sqrt{\frac{M\omega_0^3 a^2}{\pi\hbar}}\,, \tag{3.71}$$

where A is a constant depending on the specific form of the bistable potential and extracted from the asymptotic form of the instanton.

The second point can be discussed by analyzing the sum in (3.67). Its main contributions come from terms where $n \approx \Delta\hbar\beta/2$ so that the density of instantons $n/\hbar\beta \approx \Delta/2$ is exponentially small in accordance with the DIGA. The two underlying ingredients of the DIGA can thus be summarized as (i) the potential barrier separating the two wells by far exceeds $\hbar\omega_0$ and (ii) the temperature is sufficiently low $\omega_0\hbar\beta \gg 1$.

We close this discussion of the instanton technique by presenting some explicit results for a quartic potential

$$V(q) = \frac{M\omega_0^2}{8a}\left(q^2 - a^2\right)^2\,, \tag{3.72}$$

which can be approximated around the well bottoms located at $q = \pm a$ by $V_\pm(q) = (M\omega_0^2/2)(q \pm a)^2$ and around the barrier top located at $q = 0$ by $V_0(q) = (M\omega_0^2 a^2/8) - (M\omega_0^2/4)q^2$. The constant A in (3.71) is gained from the asymptotic behavior of the instanton orbit, which reads

$$q_{1;\sigma_1}(\sigma) = a\,\tanh[\omega_0(\sigma - \sigma_1)/2)\,. \tag{3.73}$$

Hence, for $\omega_0|\sigma| \to \infty$ one has $q_{1,\sigma_1} \to \pm a\,(1 - 2\exp(-\omega_0|\sigma - \sigma_1|)$ so that $A = 2$. The corresponding minimal action reads

$$S_\mathrm{I} = \frac{2}{3}M\omega_0^2 a^2 \tag{3.74}$$

and the tunnel splitting is

$$\Delta = 8\omega_0 \sqrt{\frac{2V_\mathrm{b}}{\pi\hbar\omega_0}}\, \mathrm{e}^{-\frac{16}{3}\frac{V_\mathrm{b}}{\hbar\omega_0}} \tag{3.75}$$

with the barrier height $V_\mathrm{b} = M\omega_0^2 a^2/8$.

We mention that the above semiclassical approach allows to extract exponentially small energy gaps, i.e. gaps which cannot be obtained in any order of perturbation theory in $\hbar$. An extension has been given in [13] to calculate splittings also for higher lying doublets.

3.2.2 SQUIDs

A superconducting ring interrupted by one or more Josephson junctions (JJ) is called a Superconducting Quantum Interference Device (SQUID), see Fig. 3.12. There is a whole variety of SQUID devices, the best known are the rf SQUID and the dc SQUID [7]. The former one contains just a single JJ so that the superconducting loop acts as a shortcut and the voltage drop across the JJ must be read out by a radio frequency (rf) biased tank circuit. The latter one consists of two JJs and effectively represents a JJ with a Josephson coupling tunable by an external magnetic flux threading the loop. Presently, SQUIDS are used as elements for the implementation of superconducting quantum bits [39].

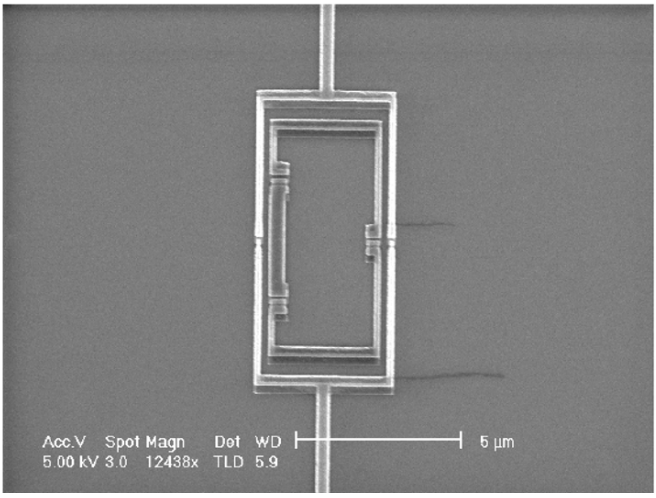

Fig. 3.12. Electron micrograph of a dc-SQUID ring with two JJs (outer ring) surrounding a SQUID ring containing three JJs (inner, darker ring). The outer SQUID is connected with two leads (top and bottom) carrying a bias current and the total circuit is threaded by a magnetic flux. The white bar at the bottom represents a length scale of 5µm. Courtesy of A. Lupascu, ENS Paris.

For the rf SQUID the phase difference δ across the JJ is related to the total magnetic flux Φ through the loop via

$$\delta = -2\pi \left(\frac{\Phi}{\phi_0} - n \right) \ , \ n \text{ integer} \tag{3.76}$$

with the reduced flux quantum ϕ_0 (3.25). The total flux consists of the self-induced flux LI (self-inductance L) and an external flux Φ_x according to $\Phi = \Phi_\mathrm{x} + LI$. Due to the above relation the relevant degree of freedom is now Φ so that the total Hamilton operator of the device including charging energy reads

$$\hat{H} = \frac{\hat{Q}^2}{2C_\mathrm{J}} - E_\mathrm{J} \cos\left(2\pi \frac{\hat{\Phi}}{\phi_0} \right) + \frac{(\hat{\Phi} - \Phi_\mathrm{x})^2}{2L} \tag{3.77}$$

with the charge operator $\hat{Q}$ conjugate to $\hat{\Phi}$. For a large self-inductance $\beta_L = E_\mathrm{J}/(\phi_0^2/4\pi^2 L) \gg 1$ and an external flux Φ_x close to $\phi_0/2$, the potential terms form a double-well with a barrier located near $\Phi = \phi_0/2$ so that with $q = 2\pi\Phi/\phi_0$ one has

$$U(q) = \frac{\phi_0^2}{4\pi^2 l} \left[\beta_L - \frac{\beta_L - 1}{2}(q-\pi)^2 + \frac{\beta_L}{24}(q-\pi)^4 \right] , \tag{3.78}$$

where the barrier height is

$$V_\mathrm{b} = \frac{\phi_0^2}{4\pi^2 L} \frac{3}{2} \frac{(\beta_L - 1)^2}{\beta_L} . \tag{3.79}$$

At sufficiently low temperatures only the lowest lying energy doublet is relevant and has an energy splitting given by (3.75).

Macroscopic quantum phenomena have been observed in rf SQUIDS already in the mid 1980s such as macroscopic quantum tunneling, resonant tunneling, and level quantization [30, 36, 86, 87, 88]. While the level splitting near a degeneracy point has been seen only recently [89, 90] based on a slightly different set-up, quantum coherent oscillations of a superposition of the two lowest lying eigenstates have not been observed yet. This is presumably due to the fact that a large value of β_L is associated with large loops making the system very sensitive to external electromagnetic noise. To overcome this obstacle smaller loops containing three junctions have been successfully manipulated to show e.g. Rabi oscillations [49]. In [91] the changeover from thermal activation to macroscopic quantum tunneling has been observed similar to what has been seen in single JJ circuits, which was theoretically discussed already in the 1980s [92].

The dc SQUID set-up has two JJs in a ring, see Fig. 3.12. The total Hamiltonian is the sum of the Hamiltonians of the individual JJs with phases δ_1 and δ_2, respectively, and the additional constraint $\delta_1 + \delta_2 = -2\pi(\Phi/\phi_0 - n)$. It is thus convenient to switch to the combinations $\delta_\pm = \delta_1 \pm \delta_2$ of phases so that for a low self-inductance loop δ_+ is fixed by the external magnetic flux

$\Phi_\mathrm{x}/\phi_0 = \delta_+$. Then, by using the properties of trigonometric functions one obtains

$$\hat{H} = \frac{\hat{p}^2}{2M} - E_\mathrm{J}(\Phi_\mathrm{x})\cos(\hat{\delta}_-/2) - I_\mathrm{b}\hat{\delta}_- \,, \tag{3.80}$$

where $\hat{p}$ is the conjugate to $\hat{\delta}_-$, I_b is an applied bias current, and

$$E_\mathrm{J}(\Phi_\mathrm{x}) = 2E_\mathrm{J}(0)\cos\left(\frac{\pi\Phi_\mathrm{x}}{\phi_0}\right) \tag{3.81}$$

is the effective Josephson energy. In other words, a low self-inductance dc SQUID is equivalent to a JJ with a tunable critical current. This allows for a much better external control so that dc SQUIDS have been implemented in a variety of circuits, e.g. as measurement devices or artificial atoms [24, 49].

3.3 Tunneling in Higher-dimensional Systems

In the previous Sections we have considered tunneling of a one-dimensional degree of freedom. In principle, an extension of the semiclassical approaches to higher dimensional systems should be possible, practically, however, it is often prohibitive. In general, two types of systems must be distinguished, namely, separable and non-separable ones. For the former one the total Hamiltonian can be cast, possibly after a proper coordinate transformation, into a sum of individual Hamiltonians so that the high-dimensional tunneling problem effectively reduces to independent one-dimensional processes. The challenging situation is the latter one, when such a reduction is not possible.

In the sequel, we first consider a metastable barrier degree of freedom coupled to a large number of harmonic degrees of freedom mimicking a complex environment. Since a collection of harmonic oscillators is always separable, for such a system explicit results for the tunneling rate can be obtained. This is not the case for higher-dimensional anharmonic degrees of freedom, where tunneling may be affected by chaotic phase space structures.

3.3.1 Multi-dimensional Quantum TST

A metastable degree of freedom coupled to N harmonic oscillators is described by

$$H = \frac{p^2}{2M} + V(q, \boldsymbol{x}) + \sum_{j=1}^{N} \frac{p_j^2}{2M_j} \,, \tag{3.82}$$

where

$$V(q, \boldsymbol{x}) = V_0(q) + \frac{1}{2}\sum_{j=1}^{N} M_j\omega_j^2 \left(x_j - \frac{c_j}{M_j\omega_j^2}q\right)^2 \tag{3.83}$$

is an $N+1$-dimensional manifold consisting of the metastable barrier potential $V_0(q)$ and the set of transverse harmonic degrees of freedom. Intuitively, it is clear that the tunneling process is now described in a multi-dimensional landscape with a metastable barrier potential that is deformed due to the presence of the harmonic modes. The idea is to transform to a new curvilinear coordinate system [93, 1, 94]

$$\{q, \boldsymbol{x}\} \longrightarrow \boldsymbol{y} = \{y_0, y_1, \ldots, y_N\} \tag{3.84}$$

with a generalized coordinate y_0 along which the escape happens to occur, the so-called reaction coordinate, and orthogonal degrees of freedom $\{y_j\}_{j\geq 1}$. Along the reaction coordinate tunneling takes place as described above in Sect. 3.1.1 with the crucial difference that the total energy is distributed between the reaction coordinate and the transverse oscillators.

To avoid a cumbersome matching of WKB-wave functions in this high-dimensional space, an explicit expression for the microcanonical rate in (3.1) is required. It is obtained from a formally exact expression for the thermal rate constant derived in [95, 96] and also discussed below in Sect. 6.4.1, namely,

$$\Gamma = \mathrm{Re}\left\{\langle \hat{F}\hat{P}\rangle_\beta\right\} . \tag{3.85}$$

Here the average is taken with respect to the thermal equilibrium $\langle\cdot\rangle_\beta = \mathrm{Tr}\{\exp(-\beta\hat{H})\cdot\}/Z$. Further, $\hat{F}$ is the *flux through dividing surface* operator for the metastable system

$$\hat{F} = \frac{1}{2M}\left[\delta(\hat{y} - y_\mathrm{b})\hat{p}_y + \hat{p}_y\delta(\hat{y} - y_\mathrm{b})\right] \tag{3.86}$$

with the location y_b of the dividing surface being a N-dimensional surface separating the well from the continuum. The projection operator

$$\hat{P} = \lim_{t\to\infty} \mathrm{e}^{\mathrm{i}\hat{H}t/\hbar}\,\theta(\hat{p}_y)\,\mathrm{e}^{-\mathrm{i}\hat{H}t/\hbar} \tag{3.87}$$

projects onto outgoing states in the far future.

By choosing the dividing surface at that point $y_\mathrm{b} = y_0^\ddagger$ where for maximal $V(q, \boldsymbol{x})$ it crosses the reaction coordinate perpendicularly, one puts in the semiclassical limit

$$\hat{F}\hat{P} \longrightarrow \delta(y_0 - y_0^\ddagger)\,\frac{\hat{p}_0}{M}\,\theta(\hat{p}_0) \tag{3.88}$$

with the momentum $\hat{p}_0$ conjugate to y_0. The underlying approximation here is that any recrossing of the dividing surface is neglected once it has been passed. In this sense, (3.88) generalizes the classical result (3.13) to a multi-dimensional quantum transition state theory (MQTST) [1, 97, 98]. One now shows that the thermal rate follows from (3.1) with the Boltzmann distribution $P(E) = \exp(-\beta E)$ (energy measured from the well bottom) and the multi-dimensional escape probability $\mathcal{T}(E) = 2\pi\hbar\rho(E)\Gamma(E)$ given by

$$\mathcal{T}(E) = \lim_{\epsilon\to 0} \mathrm{Im}\left\{ \int_0^\infty \mathrm{d}\sigma \mathrm{e}^{\sigma(E+\mathrm{i}\epsilon)/\hbar} \int \mathrm{d}\boldsymbol{y}\delta(y_0 - y_0^\ddagger) \left|\dot{y}_0^\ddagger\right| \langle \boldsymbol{y}|\mathrm{e}^{-\hat{H}\sigma/\hbar}|\boldsymbol{y}\rangle \right\}. \tag{3.89}$$

In the next step the thermal propagator is approximated by its semiclassical approximation (2.44) and Gutzwiller's periodic orbit theory is applied [93, 99], which yields

$$\mathcal{T}(E) = \sum_{n=1}^{\infty} (-1)^{n-1} \mathrm{e}^{-n2W(E)/\hbar} \prod_{j=1}^{N} \frac{1}{2\sinh[n\tilde{\sigma}(E)\mu_j(E)/2]}\,. \tag{3.90}$$

This results has some similarities to the trace formula (2.38), but is an expression in imaginary time though. The sum collects all multiples of the periodic orbit running with total energy E in the time interval $\tilde{\sigma}(E)$ through the inverted barrier landscape with short action

$$2W(E) = \int_0^{\tilde{\sigma}(E)} \mathrm{d}\sigma \left[M\dot{q}^2(\sigma) + \sum_{j=1}^{N} m_j \dot{x}_j^2(\sigma) \right]. \tag{3.91}$$

The product in (3.90) originates from Gaussian fluctuations perpendicular to the reaction coordinate with the $\{\mu_j\}_{j\geq 1}$ being the dynamical stability frequencies. It turns out that the periodic orbit is indeed unstable in one direction in functions space, but stable in the orthogonal ones. By expanding the sinh-functions, the above expression can be cast into the more appealing form [see also (2.14)] [97]

$$\mathcal{T}(E) = \sum_{n_1,\ldots,n_N=0}^{\infty} \frac{1}{1+\exp[2W(E_{\mathrm{esc}})/\hbar]}\,, \tag{3.92}$$

where we introduced the energy stored in the escape coordinate

$$E_{\mathrm{esc}} = E - \sum_{j=1}^{N} (n_j + 1/2)\hbar\mu_j(E)\,. \tag{3.93}$$

Note that the escape probability at energy E includes a sum over all orthogonal states in the barrier region. Its value may thus exceed 1, in contrast to the uniform transmission probability (2.14), which has a similar form. Now, using this result for $\mathcal{T}(E)$, the thermal rate can be evaluated according to (3.1). In performing the integral one has to distinguish between three regions: (i) the high temperature domain above a crossover temperature $T_{0,\mathrm{R}}$, (ii) the low temperature domain $T < T_{0,\mathrm{R}}$, and (iii) the crossover layer around $T_{0,\mathrm{R}}$.

Due to the harmonic reservoir the actual crossover temperature deviates from the bare one (3.14) and is given by

$$T_{0,\mathrm{R}} = \frac{\hbar\omega_{\mathrm{R}}}{2\pi k_{\mathrm{B}}} \tag{3.94}$$

with the effective barrier frequency determined as the largest positive root of

$$\omega_{\mathrm{R}}^2 + \omega_{\mathrm{R}}\hat{\gamma}(\omega_{\mathrm{R}}) = \omega_{\mathrm{b}}^2 \,. \tag{3.95}$$

We will see in Chap. 5 that the function

$$\hat{\gamma}(z) = \frac{1}{M}\sum_{j=1}^{N} \frac{c_j^2}{M_j\omega_j^2}\frac{z}{\omega_j^2 + z^2} \tag{3.96}$$

coincides in the limit $N \to \infty$ with the Laplace transform of the classical damping kernel.

For high temperatures $T > T_{0,\mathrm{R}}$ we obtain

$$\Gamma = \frac{\omega_{\mathrm{R}}}{2\pi}\frac{\omega_0}{\omega_{\mathrm{b}}}\prod_{j=1}^{\infty}\frac{\nu_j^2 + \omega_0^2 + \nu_j\hat{\gamma}(\nu_n)}{\nu_j^2 - \omega_{\mathrm{b}}^2 + \nu_j\hat{\gamma}(\nu_n)}\,\mathrm{e}^{-\beta V_{\mathrm{b}}} \,. \tag{3.97}$$

This expression is the multi-dimensional generalization of (3.12) to which it reduces for vanishing system-reservoir coupling. The product contains the Matsubara frequencies $\nu_j = 2\pi j/\hbar\beta$ and thus accounts for quantum fluctuations above the crossover.

Below the crossover $T < T_{0,\mathrm{R}}$ one derives the multi-dimensional generalization of the expression (3.10)

$$\Gamma = \frac{1}{Z}\frac{1}{\sqrt{2\pi\hbar|\tau'(E_\beta)|}}\prod_{j=1}^{\infty}\frac{1}{2\sinh[n\hbar\beta\mu_j(E)/2]}\,\mathrm{e}^{-2W(E_\beta)-\beta E_\beta} \tag{3.98}$$

with E_β that total energy for which the period of the periodic orbit equals $\hbar\beta$. The crossover region gives rise to a more involved expression which matches onto the respective formulae specified above. Since in the true dissipative limit all these results coincide with the ImF findings we refer the reader to Chap. 5 for further details.

The above analysis reveals, how transparent expressions for the tunneling rate can be obtained also for multi-dimensional systems by invoking semiclassical periodic orbit theory. This problem was tractable since with the exception of the one-dimensional metastable coordinate, all residual degrees of freedom were harmonic.

3.3.2 Tunneling in Presence of Chaos

When even for a lower dimensional system all degrees of freedom are anharmonic and not separable, the tunneling problem gains new aspects which are related to irregular classical dynamics. In general, there are two types of situations, one in which the classical phase space is basically completely chaotic and another one, where it is mixed consisting of islands supporting regular motion separated by chaotic layers. The first case leads to tunneling between chaotic states, the second one to what is called *dynamical tunneling* or *chaos assisted tunneling* between regular tori.

Tunneling in Chaotic Potentials

The fundamental problem in describing tunneling between chaotic states is that up to now, there is no semiclassical theory for individual chaotic eigenstates. Thus, studies have focused on spectral properties of those systems in terms of periodic orbits based on e.g. Gutzwiller's trace formula (2.38) [100].

As we have seen above an archetypical system to probe tunneling spectra is a symmetric double well potential. However, a standard periodic orbit calculation based exclusively on *real* orbits leads to a set of doubly degenerate levels $E_{\mathrm{sc},n}$ approximating the mean levels. The degeneracy arises since each periodic orbit in one well has a symmetric partner in the other one. The conclusion is that the simple periodic orbit theory fails to predict tunnel splittings. It is thus suggestive to modify this approach to include complex trajectories [101, 102, 103, 104]. As demonstrated in Sect. 3.2, for regular classical motion in one-dimensional bistable systems energy splittings can be calculated based on purely imaginary time instantons. For chaotic maps complex periodic orbits were used to calculate band gaps [105]. In the sequel, we report on an extension of Gutzwiller's trace formula which has been studied in [106, 107, 108].

For this purpose, one considers the splitting-weighted density of states

$$f(E) = \sum_n \Delta E_n \, \delta(E - E_n) \tag{3.99}$$

with splitting ΔE_n of the nth-energy level. Due to the symmetry assumed here, the eigenstates have either even or odd parity so that $f(E) \approx N_+(E) - N_-(E)$, where $N_\pm(E)$ denote the number of states up to energy E. This approximation is valid on scales which are sufficiently larger than the energy splittings. Then, by exploiting that $N_\pm(E)$ are related to the imaginary parts of the symmetry-projected Greens functions [102] [see also (2.36)], one finds that only complex periodic orbits are contained in $N_+ - N_-$. Eventually, upon inserting these findings into Gutzwiller's trace formula (2.38) one arrives at the semiclassical expression

$$f(E) \approx \frac{2}{\pi} \mathrm{Im} \sum_\gamma \beta_\gamma \frac{\mathrm{e}^{\mathrm{i}S_\gamma/\hbar}}{\sqrt{-\det(\mathsf{M}_\gamma - 1)}} \,. \tag{3.100}$$

Here, S_γ and M_γ are the complex action and the corresponding stability matrix, respectively. β_γ is a dimensionless factor taking into account a possibly anomalous reflection coefficient; for most orbits it is $\beta_\gamma = 1$ though.

By way of example, we analyze a symmetric two-dimensional barrier potential of the form

$$V(x, y) = (x^2 - 1)^4 + x^2 y^2 \,, \tag{3.101}$$

in which the classical dynamics is restricted to the well regions for $E < 1$ and basically chaotic for $E > E_\mathrm{c} = 0.236$ [106]. Tunneling is dominated

by a particular set of complex orbits that are confined to the x-axis. The two-dimensional structure of the barrier potential comes into play when calculating the monodromy matrix by embedding them in the other dimension. Accordingly, the simplest complex orbit starts on the x-axis with imaginary momentum and evolves in imaginary time to the symmetry related point on the other side. The corresponding action of this orbit is $S = \mathrm{i}K$ with real $K > 0$. By carefully calculating the corresponding monodromy matrix W one finds

$$f_0(E) = \frac{1}{\pi} \frac{\mathrm{e}^{-K/\hbar}}{\sqrt{-\det(\mathsf{W} - \mathsf{1})}} \,. \tag{3.102}$$

This function describes the average behavior of the tunnel splittings for all energies, i.e. also in the mixed case $E < E_c$. The basic condition is that tunneling is determined by isolated instanton-like orbits.

Upon closer inspection it turns out that there is an oscillatory structure in the splittings not captured by f_0. One thus extends the above analysis to attach to the tunneling orbit real periodic orbits in the wells on either side of the barrier (also with $y = 0$). While one restricts the sum over orbits to those tunneling only once, all multiples of oscillations are taken into account for the

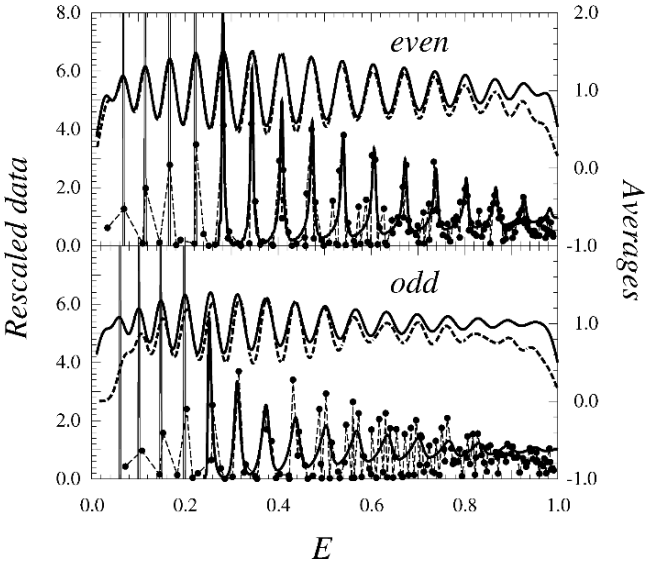

Fig. 3.13. Energy splittings in the potential (3.101) for eigenstates with even (top) and odd (bottom) parity and with the mean $f_0(E)$ scaled out. The dots are the quantum data with dashed lines connecting them. The lower solid curve is $1 + f_{\mathrm{osc}}(E)/f_0(E)$. The upper dashed and solid curves are the corresponding results averaged with a Gaussian with variance 0.15; their scale should be read from the right axis. Reprinted with permission from [106]; ©(1996) by the American Physical Society.

real orbits in the wells. The action of a primitive real orbit is denoted by S_0 so that an orbit with r repetitions gains the action $S = rS_0 + \mathrm{i}K$. The monodromy matrix [cf. (2.30)] follows as $\mathsf{M}_r = \mathsf{W}\mathsf{M}_0^r$ and the total contributions of these orbits give

$$f_{\mathrm{osc}}(E) = \frac{2}{\pi} \sum_{r=1}^{\infty} \frac{\mathrm{e}^{\mathrm{i}(rS_0 - K)/\hbar}}{\sqrt{-\det(\mathsf{W}\mathsf{M}_0^r - 1)}} \,. \tag{3.103}$$

Hence, this expression is similar to that derived in (2.37), where the smooth classical background is given by the Thomas-Fermi density of states. Although in the above problem use was made of the symmetry of the barrier potential, the formulae (3.99) and (3.103) provide a first semiclassical approach to extract information about the relation between tunneling and classical irregular motion.

Dynamical and Chaos Assisted Tunneling

The notion of *dynamical tunneling* was first introduced to describe tunneling between two disjunct regions in phase space separated not by an energy barrier but by the system's dynamics [109, 110]. Typical examples include two-dimensional bound potentials. Later on it was discovered that the same process should occur in driven one-dimensional systems [111, 112, 113], which may exhibit also chaotic domains in phase space. Roughly speaking the situation is then this: Classically, two symmetry related islands with regular motion are separated by a chaotic layer; quantum mechanically the two regular domains can communicate with each other via tunneling through a chaotic sea, thus leading in the energy spectrum to doublets with characteristic tunnel splittings. Accordingly, coherent quantum tunneling as known from a simple double well potential was predicted [113]. Recent experiments with Bose-Einstein condensates in driven optical lattices verified these theories [114].

The presence of chaos can also substantially enhance the tunneling rate between regular islands [115]. Namely, it turns out that the tunneling rate of a wave packet initially localized on one regular island is determined not by the wave packet's overlap with the other island, but by its overlap with the chaotic sea [116]. By increasing the level of chaos in this layer, one finds a strong increase of the splittings, a fact that led to the notion of *chaos assisted tunneling* [117, 118, 119, 120]. It was suggested that the enhancement of the tunneling is actually a resonance phenomenon due to the occurrence of avoided crossings of the tunneling doublet's eigenenergies with the eigenenergy of a state residing on the chaotic phase space layer. This interpretation led to a description in terms of a three-level model (in contrast to standard dynamical tunneling which may be described within a two-level picture) in accordance with the fact that the splittings are rapidly fluctuating quantities with respect to parameters such as e.g. energy and $\hbar$ [117].

Semiclassical approaches for tunneling matrix elements have been put forward for special systems. For instance, for the case of an annular billiard it

was shown [120, 116] by a semiclassical treatment that the distribution of tunneling rates has a power law decay in contrast to the exponential behavior derived in the Sect. 3.3.2. Experimentally, chaos assisted tunneling has been observed first in microwave billiards [121, 122], after it has been studied theoretically. Recently cold atoms in amplitude-modulated optical lattices [123] allowed for a direct observation of this phenomenon.

For both types of phase space tunneling, dynamical and chaos assisted, general semiclassical descriptions are still under development. In contrast to the case of a fully irregular phase space, where the trace formula provides a powerful tool for asymptotic treatments, much less is known about the quantization of mixed systems in terms of classical orbits. The quest for such theories is highly desirable since these systems comprise the majority of dynamical systems found in nature.

References

1. W.H. Miller. *J. Chem. Phys.*, 62:1899, 1975.
2. P. Hänggi, P. Talkner, and M. Borkovec. *Rev. Mod. Phys.*, 62:251, 1990.
3. A.O. Caldeira and A.J. Leggett. *Phys. Rev. Lett.*, 46:211, 1981.
4. S. Coleman. In A. Zichichi, editor, *The Whys of Subnuclear Physics*, Plenum, 1979.
5. G. Gamow. *Z. Phys.*, 51:204, 1928.
6. R.W. Gurney and E.U. Condon. *Nature*, 122:439, 1928.
7. A. Barone and G. Paternó. *Physics and Applications of the Josephson Effect*. Wiley, 1982.
8. K. Likharev. *Dynamics of Josephson Junctions and Circuits*. Gordon and Breach, 1991.
9. A. Schmid. *Ann. Phys. (NY)*, 170:333, 1986.
10. A.O. Caldeira and A.J. Leggett. *Ann. Phys. (USA)*, 149:374, 1983.
11. U. Weiss. *Quantum Dissipative Systems*. World Scientific, 1999.
12. I.K. Affleck. *Phys. Rev. Lett.*, 46:388, 1981.
13. U. Weiss and W. Haeffner. *Phys. Rev. D*, 27:2916, 1983.
14. R. P. Feynman. *Statistical Mechanics*. Benjamin, 1972.
15. H. Kleinert. *Path Integrals in Quantum Mechanics, Statistics, Polymer Physics, and Financial Markets*. World Scientific, 2002.
16. J.S. Langer. *Ann. Phys. (NY)*, 41:108, 1967.
17. W. Miller. *J. Chem. Phys.*, 62:1899, 1975.
18. M. Stone. *Phys. Lett.*, 67B:186, 1977.
19. C.G. Callan and S. Coleman. *Phys. Rev. D*, 16:1762, 1977.
20. P. Reimann, M. Grifoni, and P. Hänggi. *Phys. Rev. Lett.*, 79:10, 1997.
21. M.H. Devoret, D. Esteve, C. Urbina, J. Martinis, A. Cleland, and J. Clarke. In Yu. Kagan and A.J. Leggett, editors, *Quantum Tunneling in Solids*. Elsevier, 1992.
22. D.V. Averin, B. Ruggiero, and P. Silvestrini (eds.). *Macroscopic Quantum Coherence and Quantum Computing*. Kluwer Academic, Plenum, 2001.
23. B. Ruggiero and P. Silvestrini (eds.). *International Workshop on Superconducting Nano-electronic Devices*. Kluwer Academics, Plenum, 2002.

24. D. Vion, A. Aassime, A. Cottet, P. Joyez, H. Pothier, C. Urbina, D. Esteve, and M.H. Devoret. *Science*, 296:886, 2002.
25. J.M. Martinis, S. Nam, J. Aumentado, and C. Urbina. *Phys. Rev. Lett.*, 89:117901, 2002.
26. J.P. Pekola. *Phys. Rev. Lett.*, 93:206601, 2004.
27. J.P. Pekola, T.E. Nieminen, M. Meschke, J.M. Kivioja, A.O. Niskanen, and J.J. Vartiainen *Phys. Rev. Lett.*, 95:197004, 2005.
28. W. den Boer and R. de Bruyn Ouboter. *Physica B*, 98:85, 1980.
29. R.J. Prance, A.P. Long, T.D. Clark, A. Widom, J.E. Mutton, J. Sacco, M.W. Potts, G. Megaloudis, and F. Goodall. *Nature*, 289:543, 1981.
30. R.F. Voss and R.A. Webb. *Phys. Rev. Lett.*, 47:265, 1981.
31. L.D. Jackel, J.P. Gordon, E.L. Hu, R.E. Howard, L.A. Fetter, D.M. Tennant, R.W. Epworth, and J. Kurkijarvi. *Phys. Rev. Lett.*, 47:697, 1981.
32. M.H. Devoret, J.M. Martinis, D. Esteve, and J. Clarke. *Phys. Rev. Lett.*, 53:1260, 1984.
33. M.H. Devoret, J.M. Martinis, and J. Clarke. *Phys. Rev. Lett.*, 55:1908, 1985.
34. J.M. Martinis, M.H. Devoret, and J. Clarke. *Phys. Rev. Lett.*, 55:1543, 1985.
35. M.H. Devoret, D. Esteve, J.M. Martinis, A. Cleland, and J. Clarke. *Phys. Rev. B*, 36:58, 1987.
36. J.M. Martinis, M.H. Devoret, and J. Clarke. *Phys. Rev. B*, 35:4682, 1987.
37. A. Cleland, J.M. Martinis, and J. Clarke. *Phys. Rev. B*, 37:1624, 1988.
38. M.A. Nielsen and I.L. Chuang. *Quantum Computation and Quantum Information*. Cambridge University Press, 2000.
39. Y. Makhlin, G. Schön, and A. Shnirman. *Rev. Mod. Phys.*, 73:357, 2001.
40. A. Cottet *et al. Physica C*, 367:197, 2002.
41. G. Ithier, E. Collin, P. Joyez, D. Vion, D. Esteve, J. Ankerhold, and H. Grabert. *Phys. Rev. Lett.*, 94:057004, 2005.
42. A. Cottet. *Implementation of a quantum bit in a superconducting circuit*. Thesis, available at www-drecam.cea.fr/drecam/spec/Pres/Quantro, 2002.
43. J. Ankerhold and H. Grabert. *Phys. Rev. Lett.*, 91:016803, 2003.
44. L.D. Landau. *Phys. Z. Sowjetunion*, 2:46, 1932.
45. C. Zener. *Proc. R. Soc. London A*, 137:696, 1932.
46. J.R. Friedman and D.V. Averin. *Phys. Rev. Lett.*, 88:050403, 2002.
47. G. Ithier, E. Collin, P.J. Meeson, D. Vion, D. Esteve, F. Chiarello, A. Shnirman, Yu. Makhlin, J. Schriefl, and G. Schön. *Phys. Rev. B*, 72:134519, 2005.
48. M. Duckheim and J. Ankerhold. *Phys. Rev. B*, 71:134501, 2005.
49. I. Chiorescu, Y. Nakamura, C.J.P. Harmans, and J.E. Mooij. *Science*, 299:1869, 2003.
50. O. Mandel, M. Greiner, A. Widera, T. Rom, T.W. Häntsch, and I. Bloch. *Phys. Rev. Lett.*, 91:010407, 2003.
51. S.N. Bose. *Z. Phys.*, 26:178, 1924.
52. A. Einstein. *Sitzber. Kgl. Preuss. Akad. Wiss.*, page 261, 1924.
53. A. Einstein. *Sitzber. Kgl. Preuss. Akad. Wiss.*, page 3, 1925.
54. M.H. Anderson, J.R. Ensher, M.R. Matthews, C.E. Wieland, and E.A. Cornell. *Science*, 269:198, 1995.
55. K.B. Davis, M.-O. Mewes, M.R. Andrews, N.J. van Druten, D.S. Durfee, D.M. Kurn, and W. Ketterle. *Phys. Rev. Lett.*, 75:3969, 1995.
56. F. Dalfovo, S. Giorgini, L.P. Pitaevskii, and S. Stringari. *Rev. Mod. Phys.*, 71:463, 1999.

57. A.J. Leggett. *Rev. Mod. Phys.*, 73:307, 2001.
58. C.C. Bradley, C.A. Sackett, J.J. Hulet, and R.G. Hulet. *Phys. Rev. Lett.*, 75:1687, 1995.
59. C.C. Bradley, C.A. Sackett, and R.G. Hulet. *Phys. Rev. Lett.*, 78:985, 1997.
60. C.A. Sackett, C.C. Bradley, M. Welling, and R.G. Hulet. *Appl. Phys. B*, 65:433, 1997.
61. C.A. Sackett, J.M. Gerton, M. Welling, and R.G. Hulet. *Phys. Rev. Lett.*, 82:876, 1999.
62. J.M. Gerton, D. Strekalov, I. Prodan, and R.G. Hulet. *Nature*, 408:692, 2000.
63. J.L. Roberts, N.R. Claussen, S.L. Cornish, E.A. Donley, E.A. Cornell, and C.E. Wieman. *Phys. Rev. Lett.*, 86:4211, 2001.
64. E.A. Donley, N.R. Claussen, S.L. Cornish ans J.L. Roberts, E.A. Cornell, and C.E. Wieman. *Nature*, 412:295, 2001.
65. Yu. Kagan, G. Shlyapnikov, and J. Walraven. *Phys. Rev. Lett.*, 76:2670, 1996.
66. E. Shuryak. *Phys. Rev. A*, 54:3151, 1996.
67. H.T.C. Stoof. *J. Stat. Phys.*, 87:1353, 1997.
68. M. Ueda and A.J. Leggett. *Phys. Rev. Lett.*, 80:1576, 1997.
69. M. Ueda and A.J. Leggett. *Phys. Rev. Lett.*, 81:1343, 1998.
70. X.-B-Wang, L. Chang, and B.-L. Gu. *Phys. Rev. Lett.*, 81:1342, 1998.
71. Yu. Kagan, E.L. Surkov, and G. Shlyapnikov. *Phys. Rev. Lett.*, 79:2604, 1997.
72. Yu. Kagan, A.E. Muryshev, and G. Shlyapnikov. *Phys. Rev. Lett.*, 81:933, 1998.
73. C.A. Sackett, H.T.C. Stoof, and R.G. Hulet. *Phys. Rev. Lett.*, 80:2031, 1998.
74. H. Saito and M. Ueda. *Phys. Rev. Lett.*, 86:1406, 2001.
75. R.A. Duine and H.T.C. Stoof. *Phys. Rev. Lett.*, 86:2204, 2001.
76. W. Bao, D. Jaksch, and P.A. Markowich. *cond-mat/0307344*, 2003.
77. L.D. Landau and E. Lifshitz. *Quantum Mechanics*. Pergamon, 1976.
78. F. Hund. *Z. Phys.*, 43:803, 1927.
79. J. Zinn-Justin. *Nucl. Phys. B*, 218:333, 1983.
80. B. Felsager. *Geometry, Particles, and Fields*. Odense University Press, 1981.
81. H. Grabert and U. Weiss. *Phys. Rev. Lett.*, 54:1605, 1985.
82. U. Weiss, H. Grabert, P. Hänggi, and P. Riseborough. *Phys. Rev. B*, 35:9535, 1987.
83. D.L. Haycock, P.M. Alsing, I.H. Deutsch, J. Grondalski, and P.S. Jessen. *Phys. Rev. Lett.*, 85:3365, 2000.
84. A.J. Leggett, S. Chakravarty, A.T. Dorsey, M.P.A. Fisher, A. Garg, and W. Zwerger. *Rev. Mod. Phys.*, 59:1, 1987.
85. M. Grifoni and P. Hänggi. *Phys. Rep.*, 304:229, 1998.
86. J. Clarke, N. Cleland, M.H. Devoret, D. Esteve, and J.M. Martinis. *Science*, 239:992, 1988.
87. R. Rouse, S. Han, and J.E. Lukens. *Phys. Rev. Lett.*, 75:1614, 1995.
88. P. Silvestrini, V.G. Palmieri, B. Ruggiero, and M. Russo. *Phys. Rev. Lett.*, 79:3046, 1997.
89. J.R. Friedmann, V. Patel, W. Chen, S.K. Tolpygo, and J.E. Lukens. *Nature*, 406:43, 2000.
90. C.H. van der Waal, A.C.J. ter Haar, F.K. Wilhelm, R.N. Schouten, J.P.M. Harmans, T.P. Orlando, S. Lloyd, and J.E. Mooij. *Science*, 290:773, 2000.
91. V. Corato, S. Rombetto, P. Silvestrini, C. Granata, R. Russo, and B. Ruggiero. *Supercond. Sci. Technol.*, 17:385, 2004.

92. H. Grabert. In *SQUID'85 - Superconducting Quantum Interference Devices and their Applications*. Walter de Gruyter, 1985.
93. M.C. Gutzwiller. *J. Math. Phys.*, 12:343, 1971.
94. M.C. Gutzwiller. *Physica D*, 5:183, 1982.
95. F.J. Mc Lafferty and P. Pechukas. *Chem. Phys. Lett.*, 27:511, 1974.
96. W.H. Miller. *Adv. Chem. Phys.*, XXV:69, 1974.
97. P. Hänggi and W. Hontscha. *J. Chem. Phys.*, 88:4094, 1988.
98. P. Hänggi and W. Hontscha. *Ber. Bunsenges. Phys. Chem.*, 95:379, 1991.
99. M.C. Gutzwiller. *Chaos in Classical and Quantum Mechanics*. Springer, 1990.
100. P. Cvitanović, I. Percival, and A. Wirzba (eds.). *Chaos*, 2, 1992.
101. W.H. Miller. *J. Phys. Chem.*, 83:960, 1979.
102. J.M. Robbins. *Phys. Rev. A*, 40:2128, 1989.
103. J.M. Robbins, S.C. Creagh, and R.G. Littlejohn. *Phys. Rev. A*, 41:6052, 1990.
104. A. Shudo and K.S. Ikeda. *Phys. Rev. Lett.*, 74:682, 1995.
105. P. Lebœuf and A. Mochet. *Phys. Rev. Lett.*, 73:1360, 1994.
106. S.C. Creagh and N.D. Whelan. *Phys. Rev. Lett.*, 77:4975, 1996.
107. S.C. Creagh and N.D. Whelan. *Phys. Rev. Lett.*, 84:4084, 2000.
108. S.C. Creagh and N.D. Whelan. *Ann. Phys. (NY)*, 272:196, 1999.
109. M.J. Davis and E.J. Heller. *J. Chem. Phys.*, 75:246, 1981.
110. S. Tomsovic. *Physica Scripta T*, 90:162, 2001.
111. F. Haake, M. Kus, and R. Scharf. *Z. Phys. B*, 65:381, 1987.
112. B.C. Sanders and G.J. Milburn. *Z. Phys. B*, 77:497, 1989.
113. S. Dyrting, G.J. Milburn, and C.A. Holmes. *Phys. Rev. E*, 48:969, 1993.
114. W.K. Hensinger, H. Häffner, A. Browaeys, N.R. Heckenberg, K. Helmerson, C. McKenzie, G.J. Milburn, W.D. Phillips, S.L. Rolston, H. Rubinsztein-Dunlop, and B. Upcroft. *Nature*, 412:52, 2001.
115. W.A. Lin and L.E. Ballantine. *Phys. Rev. Lett.*, 65:2927, 1990.
116. S.D. Frischat and E. Doron. *Phys. Rev. E*, 57:1421, 1997.
117. O. Bohigas, S. Tomsovic, and D. Ullmo. *Phys. Rep.*, 223:43, 1993.
118. R. Utermann, T. Dittrich, and P. Hänggi. *Phys. Rev. E*, 49:273, 1994.
119. S. Tomsovic and D. Ullmo. *Phys. Rev. E*, 50:145, 1994.
120. E. Doron and S.D. Frischat. *Phys. Rev. Lett.*, 75:3661, 1995.
121. C. Dembowski et al. *Phys. Rev. Lett.*, 84:867, 2000.
122. T. Neicu, K. Schaadt, and A. Kudrolli. *Phys. Rev. E*, 63:026206, 2001.
123. D.A. Steck, H.O. Windell, and M.G. Raizen. *Scince*, 293:274, 2001.

4

Wave-packet Tunneling in Real-time

A dynamical perspective of tunneling is obtained in the time domain. In particular, the time evolution of individual wave packets reveals details of the tunneling process that cannot be gained from energy dependent transmission probabilities alone. Moreover, in situations where barrier penetration is driven by external time dependent forces a description in energy space must fail. The practical reason for applying external driving is the ability to control the time evolution of quantum systems, a field which has seen an enormous amount of research in the last decade [1, 2, 3, 4, 5]. The advent of new laser technologies including optical traps and tailored laser pulses as short as a few femtoseconds and the manipulation of solid state based artificial atoms and molecules on the nanoscale via microwaves have led to the expectation that we have reached a new level of exploring quantum mechanical systems.

In this context the crucial question arises to what extent semiclassical techniques are able to capture tunneling events in the time domain. While within an exact description in terms of the Schrödinger equation a switching from the energy to the time domain does not cause, at least for low-dimensional systems, conceptual difficulties, this is not true for semiclassical approaches [6]. The general reason for that will be discussed at the beginning of this Chapter. The main focus then lies on the analysis of the evolution of pure systems and thus the investigation of wave packet tunneling in real-time. The generalization to density matrices will be the subject of Chap. 7.

While the methods to describe tunneling in the energy domain are well established, see Chap. 3, approaches for time dependent systems are currently still under development. In the sequel we discuss some approaches in more detail. All of them are based on the Hermann-Kluk propagator introduced in Sect. 2.2.

Joachim Ankerhold: *Quantum Tunneling in Complex Systems*
STMP **224**, 61–92 (2007)
DOI 10.1007/3-540-68076-4_4

4.1 Tunneling with Real Classical Trajectories?

Despite the success of semiclassical time-dependent methods in a variety of systems, they encounter fundamental difficulties in describing one of the most striking quantum phenomena, namely, tunneling through potential barriers [7]. The problem was attacked systematically in the 1990s [8, 9, 10, 11, 12], however, corresponding results on the one hand failed for the regime of "deep" tunneling and on the other hand were extremely sensitive to wave packet parameters [7, 12] from which physical observables are supposed to be independent. Common to these treatments is their exclusive use of real-valued trajectories, i.e. orbits running over the barrier, confirming the naive expectation that any simple description of tunneling is hampered by the fact that classical trajectories with energies smaller than the barrier height are reflected completely [13].

Let us take a somewhat closer look upon the problem we encounter here. By way of example imagine a symmetric scattering potential vanishing asymptotically, e.g. an Eckart barrier [14] (cf. Fig. 2.1)

$$V_{\mathrm{Eck}}(q) = \frac{V_0}{\cosh^2(q/l)}\,. \tag{4.1}$$

This barrier potential will be studied in detail below; for the present discussion, the only relevant point is that the underlying scenario is a generic scattering process with asymptotic free states and that the barrier is parabolic around its top. Now, a wave packet $\psi(q_{\mathrm{i}}, 0)$ localized to the far left ($q_{\mathrm{i}} < 0$) is propagated towards the barrier according to

$$\psi(q_{\mathrm{f}}, t) = \int \mathrm{d}q_{\mathrm{i}}\; G_{\mathrm{scl,IVR}}(q_{\mathrm{f}}, t;, q_{\mathrm{i}}, 0)\, \psi(q_{\mathrm{i}}, 0)\,, \tag{4.2}$$

where $G_{\mathrm{scl,IVR}}$ denotes a semiclassical propagator in the initial value representation, e.g. the Hermann-Kluk (HK) propagator (2.27). We are interested in that portion of the packet that after time t arrives on the far right ($q_{\mathrm{f}} = q_{\mathrm{i}} > 0$). All real orbits connecting the two asymptotic regions have $E > V_0$, run over the barrier, and for fixed end-points spend most of their time in the range around $q = 0$ when t becomes large. The marginal stability of trajectories in the parabolic range of the potential around its top causes the semiclassical propagator [cf. (2.25)] to die out exponentially $\propto \exp(-\omega_{\mathrm{b}} t/2)$ (barrier frequency ω_{b}) in contrast to the exact dynamics [6, 13].

To discuss semiclassical tunneling in real-time, a relevant observable, which displays typical quantum mechanical features like interferences, is the time dependent auto correlation function of two Gaussian wave packets, namely,

$$c_{\mathrm{fi}}(t) = \langle \psi_{\mathrm{f}}(0) | \psi_{\mathrm{i}}(t) \rangle = \int\int \mathrm{d}q_{\mathrm{f}} q_{\mathrm{i}}\; \Psi_{\mathrm{f}}^*(q_{\mathrm{f}})\, G_{\mathrm{scl,IVR}}(q_{\mathrm{f}}, t; q_{\mathrm{i}}, 0)\, \Psi_{\mathrm{i}}(q_{\mathrm{i}})\,. \tag{4.3}$$

Here, the initial wave packet is centered around q_{i} and the final one around q_{f}. From this real-time quantity various observables can be derived as e.g.

transmission probabilities, return probabilities etc. One advantage of using $c_{\rm fi}(t)$ is that by inserting the expression (2.27) for $G_{\rm HK}$ into (4.3), the integration over the end-points $q_{\rm i}$, $q_{\rm f}$ can be done analytically and one is left with one phase space integration only (see e.g. see [15]). By way of example, we anticipate here results for the correlation function in the Eckart barrier potential depicted below in Fig. 4.3a. According to the above reasoning, the ordinary HK dynamics dies out *exponentially* on an intermediate time scale in contrast to the exact quantum mechanical behavior. For $\omega_{\rm b}t \to \infty$ the density in phase space of real classical paths connecting the asymptotic regions of the scattering barrier tends to zero. In other words, these paths do not allow to explore regions in phase space which due to energy fluctuations according to the uncertainty relation $\Delta p \Delta q \geq \hbar$ can be visited quantum mechanically. The consequence is that the standard semiclassical HK propagator captures tunneling only in parabolic potentials, but fails for anharmonic ones for longer times when low energy, deep tunneling processes become relevant.

A procedure to effectively account for deep tunneling has been outlined in the previous Chapter based on imaginary time orbits. In fact, it is well-known that complex trajectories do account for tunneling in the energy domain when one exploits the correspondence between real-time propagator and energy dependent Greens function (2.33) [16]. Namely, tunneling at fixed energy can be obtained by performing the time integration in a complex plane meaning that one considers outside the barrier trajectories in real-time and switches to imaginary time trajectories, i.e. paths with imaginary momentum, in the barrier range. However, this type of time contour integration can only be performed by formally using an analytic continuation of the VVG propagator [see (2.23)], since an explicit expression for a semiclassical real-time propagator *including* tunneling is not known. The latter one is clearly required to learn about dynamical properties, particularly in systems with explicitly time dependent Hamiltonians.

In general, there have been two strategies to extend the Hermann Kluk formulation for semiclassical real-time tunneling: One searches for an effective HK propagator still based on one phase space integration but with a modified action contribution, the other one includes a larger number of phase-space integrations when propagating. However, nothing is for free. While the former approaches miss, despite their success, still the mathematical rigor, the latter ones become numerically so expensive that they are practically restricted to low-dimensional undriven systems. In the sequel, the progress that has been achieved in recent years will be addressed in more detail by discussing one formulation in either of the two directions. The first starts from the naive expectation that similar to minimal action paths for fixed energy, but in complex time, there may also exist "tunneling paths" for fixed real time, but with complex energy. Unfortunately, this is not the case [6]. Going back to the real-time path integral (2.17) the conclusion is that there are no minimal action paths even in complex configuration space and tunneling must be ascribed to large fluctuations. The consequences of this finding leads to the construction

of an effective HK propagator that captures deep tunneling and also applies to driven systems, still with one phase space integration only [6, 17, 18]. The second approach determines the correction operator that appears when the standard HK expression is inserted into the time-dependent Schrödinger equation [6]. With this operator at hand one derives an exact asymptotic series with the first term being the standard HK propagator [19, 20, 21]. On the one hand this shows that the HK expression is not just an intelligent guess, but can be put onto a firm mathematical basis [22], and on the other hand it allows for a systematic improvement by systematically extending the number of phase space integrations.

4.2 Semiclassics in Complex Phase Space

Complex trajectories have been used in semiclassical approaches in a variety of scenarios [23, 24, 25, 26, 27], see also Sect. 3.3.2, and particularly for tunneling problems through one-dimensional energy barriers within the HK formulation [7]. It has been conjectured [12] that real-time orbits with complex initial conditions may account for deep tunneling, which was then shown not to be the case [6].

4.2.1 Complex Orbits and the "Tunneling Path"

To explore to what extent also deep tunneling can be incorporated into the HK propagator we turn back to the exact path integral representation (2.17) and restrict ourselves to the case of a particle of mass M in a general one-dimensional barrier potential $V(q)$. The barrier top is located at $q = 0$ with $V(0) = V_0$. According to the previous Section real time orbits cannot capture the long time behavior, where deep tunneling sets in. Classical orbits with $E < V_0$ incident from the far left (right) reach the left (right) flank of the barrier at turning points (TPs) $-q_0$ (q_0). The long time properties of the path integral (2.17) are therefore governed by the dynamics in the "forbidden" range between the TPs. Semiclassically, for $E < V_0$ no *real* stationary phase point to (2.17) obeying the proper boundary conditions exists in function space. In this situation one invokes an analytic continuation, meaning here to extend classical mechanics to the complex coordinate plane. This program has been carried out in [6] for general scattering potentials. In the sequel we review the main results. The formulation is then applicable to all *incoherent* tunneling processes. Further extensions to describe also coherent tunneling, e.g. in a double well potential, may be developed along the lines described below in Sect. 7.3.

Before we focus on specific forms of barrier potentials, we consider some general aspects of the classical dynamics in the complex plane. Newton's equation of motion, $M\ddot{q} + V'(q) = 0$, where $\dot{q} = \mathrm{d}q/\mathrm{d}t$ and $V' = \mathrm{d}V/\mathrm{d}q$, translates for complex $q = x + \mathrm{i}y$ into

$$M\ddot{x} + \frac{\partial r}{\partial x} = 0 \ , \quad M\ddot{y} + \frac{\partial j}{\partial x} = 0. \tag{4.4}$$

Here, we have written $V(q) = r(x, y) + \mathrm{i}j(x, y)$ and further exploited that for analytic functions $V(q)$ Cauchy's relations, i.e.,

$$\begin{aligned} \frac{\partial r(x,y)}{\partial x} &= \frac{\partial j(x,y)}{\partial y}, \\ \frac{\partial r(x,y)}{\partial y} &= -\frac{\partial j(x,y)}{\partial x} \end{aligned} \tag{4.5}$$

apply. From (4.4) one simply finds that the total energy $E = \epsilon_{\mathrm{re}} + \mathrm{i}\epsilon_{\mathrm{im}}$ and its real and imaginary parts

$$\begin{aligned} \epsilon_{\mathrm{re}} &= \frac{M(\dot{x}^2 - \dot{y}^2)}{2} + r(x, y), \\ \epsilon_{\mathrm{im}} &= M\dot{x}\dot{y} + j(x, y) \, , \end{aligned} \tag{4.6}$$

respectively, are constants of motion. With these preliminaries at hand we study the semiclassical complex plane dynamics for two specific barrier potentials, namely, reactive scattering and a metastable well.

4.2.2 Semiclassical Orbits for Reactive Scattering

We examine a generic scattering potential $V(q)$ with the following properties: It is a smooth and analytic function of q, symmetric around $q = 0$, with a barrier of height $V(0) = V_0$, and can be approximated around its top by an inverted harmonic oscillator. For large $|q|$ it falls off as

$$V(q) \to V_0/[q/l]^{2k}, \tag{4.7}$$

with $k \geq 2$ integer, and a characteristic barrier length scale l. Typical examples include algebraic potentials of the form

$$V_k(q) = \frac{V_0}{[1 + (q/l)^2]^k} \, , \tag{4.8}$$

the Eckart barrier (4.1), well-known as a simple model for biochemical reactions, and the Gaussian barrier

$$V(q) = V_0 \exp(-q^2/l^2) \tag{4.9}$$

used in a variety of context, e.g. recently in tunneling of Bose-Einstein condensates through optical mirrors [28].

Since we are mainly interested in deep tunneling, i.e. in the low energy behavior, we restrict ourselves to trajectories the TPs of which lie in the asymptotic region of the potential. Hence, we consider paths starting from

large $q_\mathrm{i} = x_\mathrm{i} < 0$ along the real axis with complex momentum $p_\mathrm{i} \equiv \dot{q}_\mathrm{i} = \dot{x}_\mathrm{i} + \mathrm{i}\dot{y}_\mathrm{i}$. Further, it is convenient to write $V(q) = r(q) + \mathrm{i}j(q)$ as specified in (4.7) in polar coordinates

$$r(R,\phi) = V_0 \frac{\cos(2k\phi)}{(R/l)^{2k}},$$
$$j(R,\phi) = -V_0 \frac{\sin(2k\phi)}{(R/l)^{2k}}. \tag{4.10}$$

Accordingly, trajectories in the complex configuration space are represented as $q(t) = R(t)\mathrm{e}^{\mathrm{i}\phi(t)}$. By solving the respective equations of motion one can basically distinguish three kinds of orbits, see Fig. 4.1. Since the barrier vanishes asymptotically, the classical motion for large distances from the top tends to be a free motion for all of them. As a consequence, for large R orbits run close to straight lines with constant $\phi(q_\mathrm{i}, p_\mathrm{i}) = \phi_\infty$ depending merely on the initial phase space variables.

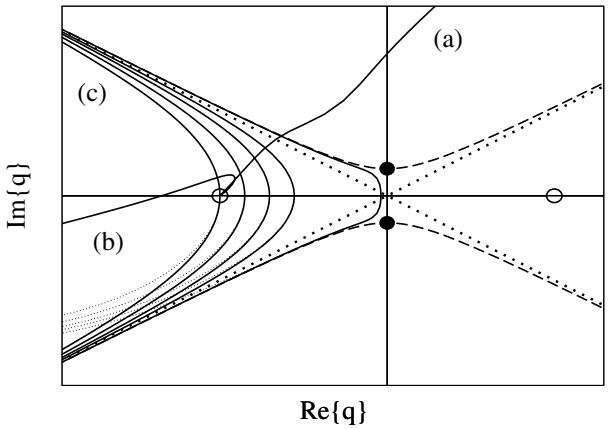

Fig. 4.1. Orbits in the complex plane for $V_2(q)/V_0 = 1/(1+q^2)^2$ [class (a) and (b): solid; class (c) for various x_i: solid for $\epsilon_\mathrm{re} = 0$, dotted (thin) for $\epsilon_\mathrm{re} \neq 0$]. Burning lines are shown for $V_2(q)$ (dashed) and its asymptote $1/q^4$ (dotted, thick); open dots are TPs of the classical motion, solid dots indicate the intersections of the burning lines with the dividing surface.

First, let us have a closer look to class (a) as it is the only one where orbits cross the line $x = 0$ ($\phi = \pi/2$) to reach the other side of the barrier (dividing surface). The imaginary part $j(R,\phi)$ of the potential vanishes along $\phi = \pi/2$ so that due to energy conservation $\epsilon_\mathrm{im} = M(\dot{x}\dot{y})(\phi = \pi/2) = M\dot{x}_\mathrm{i}\dot{y}_\mathrm{i} > 0$ [cf. (4.6)]. It follows that starting on the left side ($q < 0$) a successful crossing of the dividing surface at $q = 0$ must happen with positive real momentum $\dot{x}(\pi/2) > 0$ and thus positive imaginary momentum $\dot{y}(\pi/2) > 0$. For the energy required to reach the dividing surface one derives $|\epsilon_\mathrm{im}| > r(x_\mathrm{i}, 0) =$

$V(x_\mathrm{i})$. Starting, however, from the imaginary axis with $\dot{x} > 0$ and $\dot{y} > 0$, i.e. in the direction of decreasing $|V(q)|$, always generates an orbit reaching the asymptotic right side of the barrier far from the real axis ($\phi > 0$). Therefore class (a) orbits are not capable to provide a connection between the asymptotic segments along the positive and negative real axis. Opposite to the naive expectation a simple "tunneling path" running through the barrier range via a tour through the complex plane does not exist.

This finding is in sharp contrast to tunneling for fixed energy. There, as mentioned above, the energy dependent Greens function $G(q_\mathrm{f}, q_\mathrm{i}, E)$ exhibits stationary phase points in imaginary time corresponding to classical paths running with energy E in the inverted potential through the barrier range from $-q_0$ to q_0. Here, for real-time tunneling a stationary phase under-barrier-path to the quantum propagator $G(q_\mathrm{f}, t;, q_\mathrm{i}, 0)$ even with complex energy *cannot* be found.

For our analysis the consequences are two-fold: on the one hand complex trajectories in class (a) do not play any role for a semiclassical approximation to $G(q_\mathrm{f}, t; q_\mathrm{i}, 0)$ and on the other hand in the low energy sector, dominated by tunneling, the path integral in (2.17) is completely governed by fluctuations. To find its dominant contributions thus means to detect the dominant fluctuations as points in function space which lie close to orbits with $\delta S[q] = 0$ and also obey the proper boundary conditions.

Hence we turn to the remaining two classes of orbits. The second class (b) contains paths with small but non-vanishing energies $0 < |\epsilon_\mathrm{im}| < r(x_\mathrm{i}, 0)$. Since they may exhibit TPs in the complex plane and always live on the same side of the barrier, they do not provide a connection either.

In class (c) trajectories have small real total energy $E = \epsilon_\mathrm{re}$ and consequently start with purely imaginary momenta $\dot{x}_\mathrm{i} = 0$, cf. (4.6). These orbits display crucial features as we will explain in the following. For that purpose we first focus on the limit $\epsilon_\mathrm{re} = 0$ and follow paths with $x_\mathrm{i} < 0, \dot{y}_\mathrm{i} > 0$. Writing asymptotically $q(t) = R(t)\mathrm{e}^{\mathrm{i}\phi}$, one obtains

$$\phi_\infty(x_\mathrm{i}, \dot{y}_\mathrm{i}) \equiv \phi_\mathrm{c}^- = \pi - \frac{\pi}{2(k+1)}\,. \tag{4.11}$$

Accordingly, after a transient period of time *all* those orbits run along the *same* line in the complex plane independent of their starting points x_i. Due to symmetry mirror images of this line exist for corresponding orbits along $-\phi_\mathrm{c}^-$ and $\pi \pm \phi_\mathrm{c}^-$, respectively. Since trajectories merging along these lines carry the same energy, they are also focused in phase space and thus define caustics (burning lines).

Typically, a caustic is associated with unstable orbits and large fluctuations connecting them which renders a simple Gaussian semiclassics insufficient [29]. To verify this scenario here, we consider small deviations $\delta q = \delta x + \mathrm{i}\delta y$ around a certain orbit $\bar{q}(x_\mathrm{i}; t)$ with initial point x_i and $E = 0$. By linearizing the equations of motion (4.4) one gains

$$\begin{pmatrix} \delta\ddot{x} \\ \delta\ddot{y} \end{pmatrix} = \hat{K} \begin{pmatrix} \delta x \\ \delta y \end{pmatrix} , \tag{4.12}$$

where $\hat{K}$ evaluated along $\bar{q}(x_\mathrm{i};t)$ is a matrix containing the stability information. Along the line $\phi = \phi_\mathrm{c}^-$ it takes the form

$$\hat{K} = \left(\begin{array}{cc} -\frac{\partial^2 r}{\partial x \partial x} & -\frac{\partial^2 r}{\partial y \partial x} \\ -\frac{\partial^2 j}{\partial x \partial x} & -\frac{\partial^2 j}{\partial y \partial x} \end{array} \right) \Bigg|_{\phi=\phi_\mathrm{c}^-} = \begin{pmatrix} -\bar{r}_{xx} & 0 \\ 0 & -\bar{r}_{xx} \end{pmatrix} \tag{4.13}$$

with diagonal elements $-\bar{r}_{xx} > 0$ so that all trajectories merging along the burning lines are unstable. As a consequence small deviations in phase space can lead from an orbit $\bar{q}(x_\mathrm{i};t)$ to another one $\bar{q}(x_\mathrm{i}';t)$ and even allow for a turn from positive to negative momentum to run along the $\bar{q}(x_\mathrm{i}';t)$-orbit back towards x_i' on the real axis. As asymptotically paths creep along ϕ_c^-, those jumps from very small positive to negative momenta require only tiny fluctuations. The "reflected" orbit crosses the real axis at x_i' and approaches the complementary burning line $-\phi_\mathrm{c}^-$ in the lower half-plane. There, a similar kind of deviation drives it to still another $\bar{q}(x_\mathrm{i}'';t)$ to reach again ϕ_c^- and so forth and back. By subsequently running through these cycles between the caustics at $\pm\phi_\mathrm{c}^-$ a net-motion into the direction of the barrier top may be generated. On the right side of the barrier ($x_\mathrm{i} > 0$) the same kind of scenario exists and at the top $x = 0$ the burning lines intersect (depending in detail on $V(q)$ within $|q/l| < 1$, see Fig 4.1.) so that small deviations in the vicinity of the bottleneck $x = 0$ may lead from the set of left-barrier cycles to that of right-barrier cycles and vice versa. This allows for a motion starting in $x_\mathrm{i} < 0$ to eventually reach the range on the opposite side of the barrier. So far the above discussion is restricted to class (c)-orbits with $\epsilon_\mathrm{re} = 0$. For finite but small ϵ_re the orbits do not merge asymptotically along a single line, cf. Fig. 4.1, but still approach each other closely in the barrier region and are then unstable so that they may be connected by small fluctuations, too.

The conclusion is that the incoming and outgoing real axis segments of a scattering path with TPs at q_0 and $-q_0$ and energy $E = V(q_0)$, respectively, are linked by a sequence of real-time complex plane orbits with the same energy $E(q_0) = \epsilon_\mathrm{re}$ that are tied together by small fluctuations near caustic lines. Since this under-barrier-motion is not a purely stationary one obeying (4.4), but rather can be seen as nearly stationary as it follows classical orbits most of the time, it describes quasi-stationary fluctuations (QSF). The QSF allow to move from $q_\mathrm{i} < 0$ through the barrier range towards $q_\mathrm{f} > 0$ and this way dominate in absence of true stationary points, $\delta S[q] = 0$ with $q(0) = q_\mathrm{i}, q(t) = q_\mathrm{f}$, the path integration in $G(q_\mathrm{f}, t; q_\mathrm{i}, 0)$ between the TPs. In the sequel we will refer to these dominant fluctuations also as *fluctuation paths*.

4.2.3 Complex Orbits for Metastable Potentials

While for scattering barriers QSF on both sides of the barrier show the same features, the situation is different for quasi-bound states tunneling through a

barrier into a continuum. As an example we discuss here a metastable potential of the form

$$V(q) = \frac{M\omega_0^2}{2} q^2 \left[1 - \frac{q}{l}\right], \tag{4.14}$$

where the well is located at $q = 0$, the barrier at $q_\mathrm{b} = 2l/3$, and the barrier height is $V_\mathrm{b} = V(q_\mathrm{b}) = 2M\omega_0^2 l^2/27$. The exit point of the potential, i.e. its zero on the continuum side of the barrier, is given by $q = l$.

We are interested in the escape from the well through the barrier and thus proceed in searching for QSF as orbits with small $E = \epsilon_\mathrm{re}$ starting near $q = 0$ along the real axis with purely imaginary momentum. Based on the equations of motion (4.4) and energy conservation (4.6) the following scenario for the relevant classical mechanics is gained (see Fig. 4.2). For each fixed energy $0 \leq E \leq V_\mathrm{b}$ there is a starting point x_i^0 with $E = V(x_\mathrm{i}^0)$ being the TP of a real periodic orbit in the well (i.e. oscillating along the real axis). For $x_\mathrm{i} > x_\mathrm{i}^0$ and same energy E this real periodic orbit is "unfolded" to a loop in the complex plane; particularly for $E = 0$ one has $x_\mathrm{i}^0 = 0$. A certain set of periodic orbits can thus be characterized by its energy $E = V(x_\mathrm{i}^0)$ with $0 \leq x_\mathrm{i}^0 \leq q_\mathrm{b}$ where the various paths within this set differ only by their individual starting points $x_\mathrm{i} > x_\mathrm{i}^0$ with $0 \leq x_\mathrm{i} \leq l$. All paths in such a set not only share the same energy but also have the same period and action for one round trip.

In the barrier range $0 \leq x_\mathrm{i} \leq l$ orbits lie arbitrarily close to each other. Along the real axis we then find for the elements of the stability matrix $\hat{K}$ that non-diagonal elements $j_{xx}(x_\mathrm{i})$ vanish, while the diagonal elements read $r_{xx}(x_\mathrm{i}) = M\omega_0^2(1 - 3x_\mathrm{i}/l)$. Hence, in the well for $x_\mathrm{i} < l/3$ one recovers the elliptic stability of a harmonic oscillator ($r_{xx} > 0$), while for $x_\mathrm{i} > l/3$ all orbits

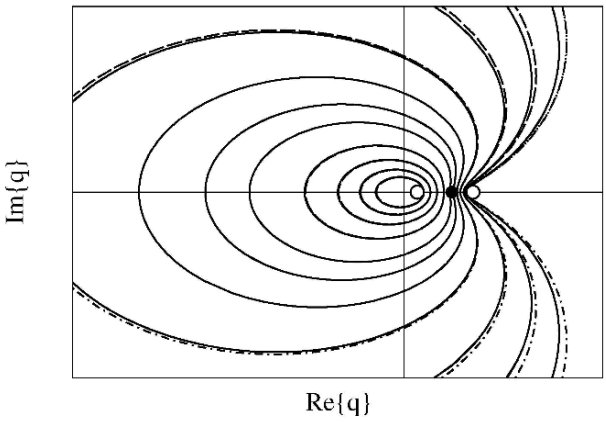

Fig. 4.2. Quasi stationary orbits in the complex plane for the cubic potential (4.14) and various x_i and $\dot{y}_\mathrm{i} > 0$, $\dot{y}_\mathrm{i} < 0$. Zero energy (solid) and finite, but small energy (dotted-dashed) orbits are shown. Open circles denote the entrance and exit points, respectively, and the filled circle indicates the location of the barrier top.

become unstable. This way, each time a loop crosses the real axis in the barrier range at a certain x_i small fluctuations may drive it to another one with a different x_i' within the same set of paths. Such "phase fluctuations" generate effectively a spiraling motion towards the exit point q_c where orbits accumulate. The continuum along the real axis to the right of q_c is again reached by small fluctuations. It is this spiraling quasi-stationary motion around the well that defines the QSF.

While for scattering potentials under-barrier reflection paths are tied together by fluctuations, here, tunneling results from fluctuations between under-barrier periodic orbits. In both cases barrier penetration cannot be described by a single tunneling path, but only by a sort of "diffusion" on certain sets of classical complex plane orbits. Since this under-barrier dynamics follows most of the time Newton's equation of motion it dominates the path integral of the propagator in the semiclassical limit and allows to explicitly calculate its corresponding action. For other barrier potentials the QSF show qualitatively features either from one or even both of the archetypical situations discussed here, namely, tunneling into asymptotically free and out of quasi bound states, respectively.

4.2.4 Extension of the Hermann Kluk Propagator

Based on the above analysis we are now in a position to include also deep tunneling in the HK propagator scheme. Before we do so, one comment is in order: The ordinary HK propagator has not been directly derived from the exact path integral expression (2.17) as a leading term of a consistent $\hbar$ expansion. Nevertheless it has been proven in numerous applications that for practical purposes the HK approach is extremely powerful and very convenient to be implemented into numerical algorithms. Accordingly, we do not derive in a strict mathematical sense an extended HK formalism, but rather follow a semiclassical guideline by incorporating contributions of the QSF into the HK phase-space integrand as additional action and phase factors.

Since the ordinary HK propagator captures tunneling for parabolic barriers, we start by formally splitting the propagator in total phase space as

$$G_\mathrm{HK}(q_\mathrm{f}, t; q_\mathrm{i}, 0) = G_>(q_\mathrm{f}, t; q_\mathrm{i}, 0) + G_<(q_\mathrm{f}, t; q_\mathrm{i}, 0). \tag{4.15}$$

Here, $G_>$ and $G_<$ comprise integrations over phase-space volumes $E \geq V_0$ and $E < V_0 - \delta_\mathrm{pb}$, respectively, with δ_pb defining the lower bound in energy where a parabolic approximation around the barrier top is valid. $G_>$ is taken to coincide with the ordinary G_HK as specified in (2.27), thus describing the time evolution up to moderate times. The part $G_<(t)$ gives the long time behavior and is the crucial extension we are looking for. In order to construct the latter, one first observes that for $E < V_0$ the ordinary semiclassical propagation, (2.27), works outside the barrier range. The missing link are the QSF discussed in Sect. 4.2.3. To determine their contribution explicitly, it is more instructive

to consider a specific example, generalizations are then straightforward. For that purpose we stick to the scattering situation of Sect. 4.2.2.

The action contributions for motions from q_i to the left TP $-q_0$ and from the right TP q_0 to q_f are simply evaluated. The same is true for the Gaussian fluctuations around these segments. The contribution of the QSF is composed of simple cycles, each of them connecting a real axis point x_i with another one $x_\mathrm{i}' > x_\mathrm{i}$ by an orbit running from x_i along $\bar{q}(x_\mathrm{i}, t)$ towards a caustic line and then backwards along $\bar{q}(x_\mathrm{i}', t)$ to x_i' (see Fig. 4.1). The action of a simple cycle in the time interval δt then reads

$$S(x_\mathrm{i}', x_\mathrm{i}, \delta t) = \int\limits_{\bar{q}(x_\mathrm{i})} \mathrm{d}qp(q) - \int\limits_{\bar{q}(x_\mathrm{i}')} \mathrm{d}qp(q) + \delta F - E\delta t\,. \tag{4.16}$$

The first two parts are just the short actions along the contours of $\bar{q}(x_\mathrm{i})$ and $\bar{q}(x_\mathrm{i}')$, respectively, and the portion δF takes into account the phase-space jump along the caustic line. The short actions are evaluated by closing the integration contour with a segment of the real axis connecting x_i with x_i'. Since all singularities of the potential lie beyond the caustic and orbits creep with almost vanishing momentum along the caustic, we find

$$\int\limits_{\bar{q}(x_\mathrm{i})} \mathrm{d}qp(q) - \int\limits_{\bar{q}(x_\mathrm{i}')} \mathrm{d}qp(q) = \int_{x_\mathrm{i}}^{x_\mathrm{i}'} \mathrm{d}qp(q) \equiv W(x_\mathrm{i}', x_\mathrm{i}). \tag{4.17}$$

Apparently, the short action $W(x_\mathrm{i}', x_\mathrm{i})$ is imaginary. For the jump contribution we write $\delta F = \Delta p\, \Delta q$. The momentum jump is estimated from typical momentum fluctuations on the barrier length scale l, i.e. $\Delta p = \hbar/l$, while the position space jump is asymptotically much smaller $\Delta q \ll l$ (in fact, e.g. for an Eckart barrier it is exponentially small). Hence, $\delta F/\hbar \ll 1$ so that (4.16) provides up to negligible corrections $S(x_\mathrm{i}', x_\mathrm{i}, \delta t) \approx W(x_\mathrm{i}', x_\mathrm{i}) - E\delta t$. The sum of cycles linking $-q_0$ with q_0 immediately follows and we obtain

$$S(q_0, -q_0, \Delta t) \approx \mathrm{i}|W(q_0, -q_0)| - E\Delta t\,, \tag{4.18}$$

where Δt is the time spent between the TPs. This way, the QSF effectively provide an imaginary part to the real-time action which coincides with the Euclidian instanton action from $-q_0$ to q_0 in the inverted potential.

Apart from the action of the QSF there is also a pure phase factor which must be taken into account. This is due to the fact that the segments of the real time motion outside the barrier have to match at the TPs onto the QSF under the barrier. At the TPs small fluctuations drive the motion into/out of the complex plane starting/arriving with purely imaginary momenta. The corresponding rotation in phase space $\Delta p \to \mathrm{i}\Delta p$ leads to a phase factor $\mathrm{e}^{\mathrm{i}\pi/2}$ at each TP. Thus, we recover the connection rules (2.9) known from the ordinary WKB approximation. Moreover, it turns out that these phase factors also ensure the continuity of the monodromy matrix (2.29).

In principle, we could now combine the respective contributions outside and under the barrier to arrive at an integrand for the phase space integration in the low energy sector. However, so far the "tunneling time" Δt is not yet determined. In fact, as discussed above, there is no unique Δt as the QSF do not correspond to a ballistic classical motion, but rather contain "diffusive" segments along the caustics. The notion of a definite tunneling time is thus obsolete and we could only attempt to estimate the most likely time for the QSF to run through the barrier. According to the semiclassical limit, however, we proceed by assuming that the time spent outside the barrier is much larger than the time spent under the barrier. In other words, we assume that the semiclassical tunneling process occurs instantaneously on the time scale on which the outside barrier motion takes place. We mention in passing that empirically one finds that in the exact wave packet dynamics a transmitted portion of the wave packet can be observed immediately after the tail of the packet has entered the barrier range.

Eventually, on this coarse grained time scale we arrive for the low energy part of the propagator and for q_i and q_f on opposite sides of the barrier at

$$G_<^{\mathrm{HK}}(q_\mathrm{f},t;q_\mathrm{i},0) = \int\limits_{E<V_0-\delta_{\mathrm{pb}}} \frac{\mathrm{d}p'\mathrm{d}q'}{2\pi\hbar}\; g_\gamma(q_t',p_t',q_\mathrm{f})\, R_<(p',q',t)\, T(q',p') \times \mathrm{e}^{\frac{\mathrm{i}}{\hbar}S_<(p',q',t)}\, g_\gamma^*(q',p',q_\mathrm{i})\,. \tag{4.19}$$

Above, an orbit runs in time t from $\{p',q'\}$ along the real axis to its TP $\{0,-q_0(q',p')\}$, jumps to $\{0,q_0(q',p')\}$ to finally reach $\{p(t),q(t)\}$. This classical real axis motion leads to a fluctuation prefactor

$$R_<(p',q',t) = \det\left[\frac{1}{2}\,\mathrm{e}^{\mathrm{i}\pi}\left(\mathrm{m}_{11}+\mathrm{m}_{22}-\mathrm{i}\gamma\mathrm{m}_{21}-\frac{1}{\mathrm{i}\gamma}\mathrm{m}_{12}\right)\right]^{1/2} \tag{4.20}$$

with the monodromy matrix elements m_{ij} [see (2.30)] and action $S_<(p',q',t)$. The position space jump costs the action contribution of the QSF,

$$T(q,p) = \mathrm{e}^{-\frac{1}{\hbar}|W[-q_0(q,p),q_0(q,p)]|}\,, \tag{4.21}$$

and $G_<$ results from phase space averaging. In (4.19) the phase factor $\mathrm{e}^{\mathrm{i}\pi}$ has been incorporated into $R_<$ ensuring its continuity when jumping from $-q_0$ to q_0. Importantly, $G_<$ follows *not* just from switching in the integrand of the ordinary HK propagator (2.17) to imaginary times in regions where $E<V(q)$.

The semiclassical dynamics based on the extended HK propagator $G_<+G_>$ turns out to be in excellent agreement with exact results for end points $q_\mathrm{i}, q_\mathrm{f}$ which are sufficiently away from the barrier range. Its only drawback is the changeover from short and moderate times, where $G_>$ dominates, to large times, where $G_<$ prevails. Namely, for energies approaching the transition layer $(V_0-\hbar\omega_\mathrm{b}, V_0)$ around the barrier top from below, the exponential factor $T(q,p)$ in $G_<$ does not give the correct semiclassical transmission amplitude since it neglects multiple traversals of the barrier range by the QSF.

Practically, one can partially compensate for this deficiency by adjusting the parameter $\delta_{\rm pb}$ properly, but this *ad hoc* method is, of course, not very satisfying. Matching procedures are common to semiclassical approximations and the usual way to circumvent them is to resort to uniform approximations. Uniform transmission probabilities have been derived by carefully analyzing analytic properties of the action [30] as seen in (2.14). Here, we summarize these results by following an intuitive argument based on the complex mechanics. From (4.21) the transition probability in lowest order reads $p_0 = |T|^2$. The process where QSF traverse the barrier range once, but then *return* to the left side of the barrier, occurs with a probability $p_2 = |T|^4$ and effectively reduces the total transmission probability. Hence, an odd number $2k+1, k = 1, 2, 3, \ldots$ of traversals through the barrier range (coming from the left) gives a contribution $|T|^{2k+2}$ and enhances the transmission probability, while an even number $2k, k = 1, 2, 3, \ldots$ of traversals leads to $|T|^{2k+2}$ and diminishes the transmission probability. After summing up both contributions, one obtains the known result $p_{\rm tot} = |T_{{\rm uni},<}(q,p)|^2$ with the absolute transmission amplitude [cf. (2.14)]

$$T_{{\rm uni},<}(q,p) = \frac{T(q,p)}{\sqrt{1+T(q,p)^2}}\,. \tag{4.22}$$

This expression is valid from low energies up to energies close to the transition layer. In the layer it reduces up to negligible corrections to the absolute of the transmission amplitude through a parabolic barrier

$$T_{\rm pb}(q,p) = \frac{1}{\sqrt{1+\exp\{2\pi[V_0 - E(q,p)]/\hbar\omega_{\rm b}\}}}\,. \tag{4.23}$$

However, tunneling through the parabolic range is already accounted for in the ordinary HK ($G_>$) by summing exclusively over orbits with $E > V_0$. When we define

$$\alpha = \frac{|T_{{\rm uni},<} - T_{\rm pb}|}{T_{{\rm uni},<}}\,, \tag{4.24}$$

we find for all trajectories with $V_0 - \hbar\omega_{\rm b} < E < V_0$ that $\alpha \ll 1$, while outside the layer $\alpha > 1$. To exclude orbits in the layer from the phase-space integration in $G_<$ one may use an appropriate function $f(\alpha)$ with $f(\alpha \ll 1) \to 0$ and $f(\alpha > 1) \to 1$. We found the simplest choice to be $f(\alpha) = \theta(\alpha - \delta')$ with $\theta(\cdot)$ the step function and δ' a parameter the precise value of which does not sensitively affect the dynamics as long as $0 < \delta' \ll 1$. This way, we obtain

$$T_{\rm uni}(q,p) = \begin{cases} T_{{\rm uni},<}(q,p)\;\theta(\alpha-\delta') & \text{for } E(q,p) < V_0 \text{ with } \delta' \ll 1 \\ 1 & \text{for } E(q,p) \geq V_0 \end{cases}\,. \tag{4.25}$$

The uniform extended HK propagator then reads

$$\begin{aligned} G_{\rm uni,eHK}(q_{\rm f},t;q_{\rm i},0) = \int \frac{{\rm d}p'{\rm d}q'}{2\pi\hbar}\; & g_\gamma(q_t',p_t',q_{\rm f})\,R_<(p',q',t)\,T_{\rm uni}(q',p') \\ & \times\, {\rm e}^{\frac{\rm i}{\hbar}S_<(p',q',t)}\,g_\gamma^*(q',p',q_{\rm i})\,. \end{aligned} \tag{4.26}$$

For a purely parabolic barrier $T_{\rm uni} = 1$ ensures that $G_{\rm uni,eHK}$ coincides with the ordinary HK. For anharmonic barrier potentials the ordinary HK is recovered for all energies down to $E = V_0$ describing also tunneling through the vicinity of the top, while for low energy orbits $T_{\rm uni} \to T$ and $G_<$ (4.19) is regained. The above expression (4.26) allows to describe incoherent tunneling dynamics in terms of classical real time motion. We will illustrate its power in the next Sect. 4.2.5 by applying it to various barrier penetration processes. In particular, it gives astonishingly accurate results even for externally driven systems where so far no other semiclassical approach was available.

For end points on the same side of the barrier the propagator for reflection is needed. To gain its semiclassical expression one exploits quantum mechanical current conservation: $T_{\rm uni}(q,p)^2 + R_{\rm uni}(q,p)^2 = 1$ where $R_{\rm uni}(q,p)$ is the absolute of the reflection amplitude. Hence, we have

$$R_{\rm uni}(q,p) = \sqrt{1 - T_{\rm uni}(q,p)}\,. \tag{4.27}$$

The semiclassical HK propagator for reflection follows from (4.26) by replacing $T_{\rm uni}$ with $R_{\rm uni}(q,p)$. Of course, the expression (4.26) also applies to asymmetric scattering situations where $|q_0^{\rm left}(q,p)| \neq q_0^{\rm right}(q,p)$ and other barrier potentials. The only restriction is that the quantum mechanical barrier penetration has to be an incoherent process.

4.2.5 Driven Tunneling for Reactive Scattering

The Eckart barrier already specified in (4.1) has been of wide use as a simple model for bimolecular reaction dynamics, e.g. for the H+H_2 exchange reaction. It further serves as a nontrivial test case for the accuracy of semiclassical approximations since the stationary Schrödinger equation can be solved analytically. Asymptotically $V_{\rm Eck}(q)$ drops faster than any power of q so that one has $\phi_{\rm c}^- \to 0$ and burning lines stretch parallel to the real axis. In the sequel, we assume an initial wave packet $\psi_{\rm i}(0)$ located to the far left that runs towards the barrier with a mean kinetic energy $p_{\rm i}^2/2M \ll V_0$. This ensures that the main portion of the packet experiences deep tunneling, while the above-barrier part–though always present in the high energy tail of the packet's energy distribution–is much smaller. The final wave packet $\psi_{\rm f}$ sits to the far right and has the same width as $\psi_{\rm i}(0)$.

Let us first consider the static situation. The standard semiclassical result for the correlation function (4.3) has been discussed already in Sect. 4.1). As expected (see Fig. 4.3a) the ordinary HK dynamics dies out exponentially on an intermediate time scale. In contrast the extended HK time evolution keeps close to the exact dynamics also for very large times when the low energy components of the wave packet dominate. By using $G_{\rm uni,eHK}$ a matching procedure between short/moderate and long time propagation according to (4.19) is avoided. It has been shown that a very sensitive observable for the accuracy of a real-time treatment is the transmission probability $P(E)$ calculated by numerically Fourier transforming $c_{\rm fi}(t)$. The ordinary HK approach

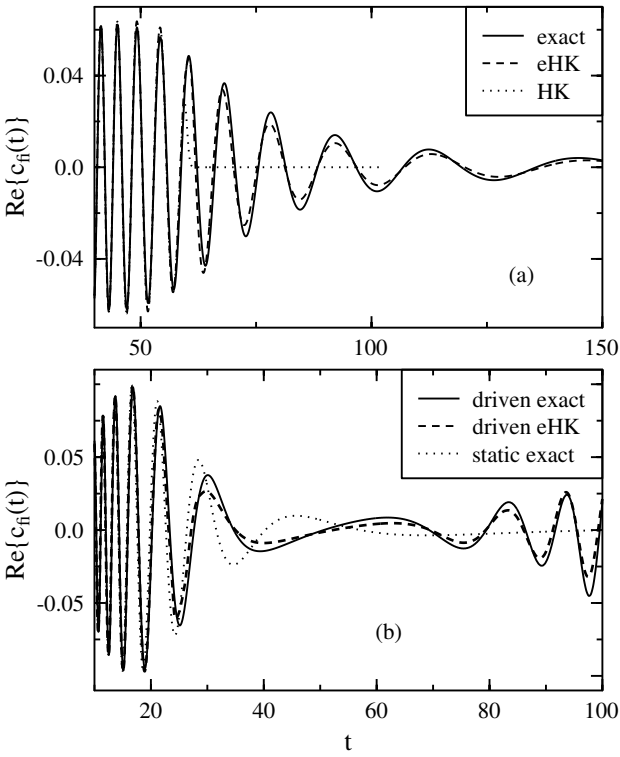

Fig. 4.3. Real part of the correlation function $c_{\rm fi}$ vs. time for scattering in a static (a) and driven (b) Eckart barrier (4.1). Parameters are $\gamma l^2 = 6$, $V_0/(p_{\rm i}^2/2M) = 8$, and (a) $q_{\rm i}/l = -q_{\rm f}/l = 40$, (b) $q_{\rm i}/l = -q_{\rm f}/l = 15$ with $q_{\rm i}A/V_0 = -0.75$, $\Omega/\sqrt{V_0/2Ml^2} = 0.02$.

gives satisfactory results only for energies sufficiently close to the barrier top. Its fundamental deficiency, however, is that its $P(E)$ strongly depends on $q_{\rm i}, q_{\rm f}$ such that with increasing end-points the semiclassical transmission probability tends towards the classical result. Here, we get accurate data also for very low energies (Fig. 4.4) apart from small oscillations typical for real-time calculations [9]. In the moderate energy range $E/V_0 > 0.5$ the real-time $P(E)$ even improves the uniform WKB result. Further, it saturates for end-points $q_{\rm i}, q_{\rm f}$ sufficiently away from the barrier range.

The performance of the $G_{\rm uni,eHK}$ is very promising. The typical number of trajectories for the set of parameters is $1 \cdot 10^5$. In order to speed up the convergence process a tuned equidistant integration grid can be used which for one-dimensional systems is superior to a Monte Carlo procedure. Newton's equation of motion and the phase space integration are efficiently evaluated with the Verlet-Algorithm and an symplectic integrator of 6th order [31], respectively. In contrast to previous approaches [32] convergence of $G_{\rm uni,eHK}$ is achieved for roughly the same number of trajectories as for the

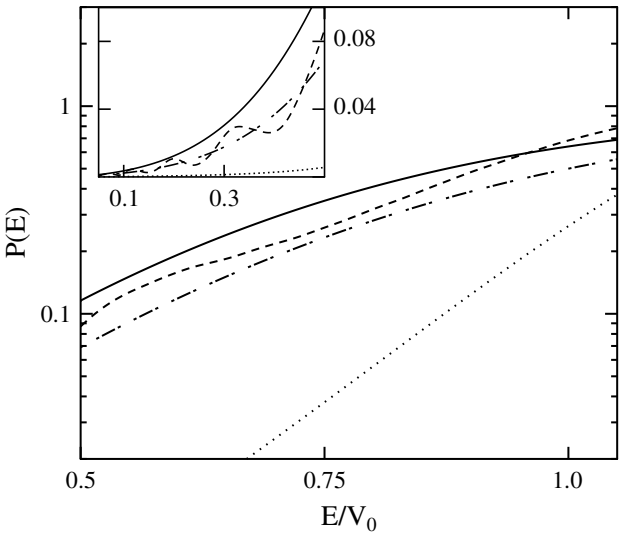

Fig. 4.4. Transmission probability vs. E/V_0 for an Eckart barrier. Exact (solid), conventional HK (dotted), eHK (dashed), and uniform WKB (dotted-dashed) results are shown.

one-dimensional $G_{\rm HK}$ in non-tunneling situations so that also an extension to two or three dimensional barriers systems seems feasible. The main obstacle then will be the proliferation of orbits at the left TP. However, since the transmission amplitude depends very sensitively on the length of the under-barrier paths, we expect only a sufficiently small subset of orbits to be actually relevant in the phase-space integration.

A dynamical semiclassical approach is clearly required for Hamilton operators that are explicitly time dependent. It is worthwhile to note that e.g. for periodic driving the naive procedure to switch under the barrier from real to imaginary times leads to unrealistic transmission probabilities due to an exponentially increasing driving force. As an example, we turn to an Eckart barrier driven by a periodic signal

$$V(q) = V_{\rm Eck}(q) + qA\sin(\Omega t) \tag{4.28}$$

and focus on the range of non-resonant driving and weak to moderate driving amplitudes. In this case already the exact numerics is non-trivial since it is the long time tunneling behavior which is most sensitively affected by the driving and leads to a strong spreading of the wave packet. Further, absorption and emission of field quanta *under* the barrier are excluded from the $G_{\rm uni,eHK}$ scheme according to the time coarse graining on which it is based. Typical results for the correlation function $c_{\rm fi}(t)$ are shown in Fig. 4.3b. Compared to the static case one sees phase shifted oscillations and a revival type of phenomenon. Semiclassically, both effects originate from an intimate

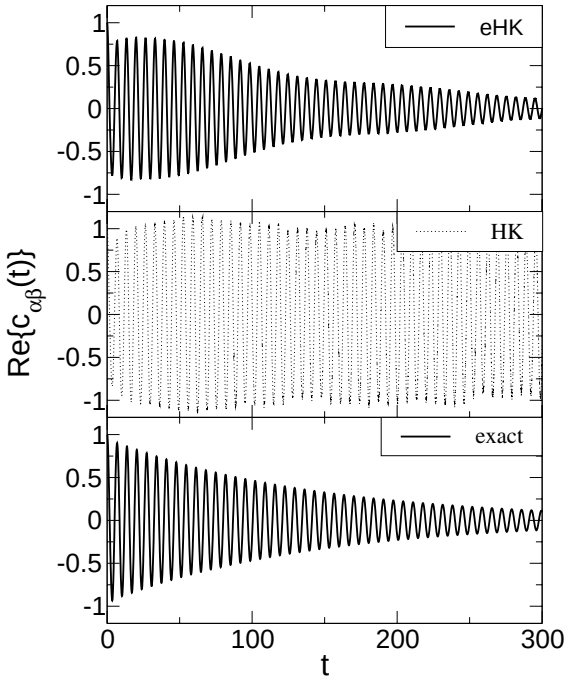

Fig. 4.5. Real part of the correlation c_{fi} vs. time for the static metastable well (4.14). Results for eHK (top), HK (middle), and exact (bottom) dynamics are shown. Parameters are $V_{\mathrm{b}}/\hbar\omega_0 = 0.93$, and $q_{\mathrm{i}}/l = q_{\mathrm{f}}/l = 0$.

interference of (fast) above-barrier-paths ($E > V_0$), which cross the barrier and are then back-scattered, and (slow) driven tunneling orbits ($E < V_0$). Even in this time-dependent case the accuracy of the eHK in amplitude as well as in phase is remarkable.

4.2.6 Resonant Decay out of Metastable Wells

Tunneling out of a metastable well through a high barrier into a continuum can be found in many areas of physics and chemistry. One of the most prominent examples is the decay of the zero voltage state of a current biased Josephson junction as described in Sect. 3.1.3. In particular, microwave driven junctions have recently gained much interest as solid-state based devices to realize and control quantum bits in the context of quantum computing [33]. There, decoherence and dephasing play a crucial role and it is thus desirable to have a semiclassical real-time approach at hand which may also allow to take into account environmental degrees of freedom.

To be specific, we consider the quadratic+cubic potential in (4.14). The escape dynamics from this well can simply be understood in terms of quasi-stationary energy levels $E_n = \epsilon_n - \mathrm{i}\hbar\Gamma_n/2$ with a well energy ladder $\epsilon_0 <$

$\epsilon_1 < \ldots$ and decay rates $\Gamma_0 \ll \Gamma_1 \ll \ldots$. Preparing the system initially in a normalized linear combination of well states $\psi(q,0)$, the dynamical quantity of interest is the survival probability in the well

$$P_0(t) = |c_{\rm fi}(t)|^2 = |\langle\psi(q,t)|\psi(q,0)\rangle|^2. \tag{4.29}$$

For very long times this probability is expected to decay mono-exponentially as the decay is then dominated by tunneling from the ground state, i.e. $P_0(t) \rightarrow {\rm e}^{-\Gamma_0 t}$. WKB results for tunneling rates have been obtained in Sect. 3.1.1, in particular, the tunneling rate for the ground state is specified in (3.8).

Now, let us first study a potential with $V_{\rm b}/\hbar\omega_0 = 0.93$ corresponding to only one quasi-eigenstate in the well. While for the ordinary HK all orbits with $E < V_{\rm b}$ remain trapped in the well and no decay is seen for longer times (Fig. 4.5), the eHK describes the quantum escape quite well. Only for small times where the eHK basically coincides with the ordinary HK there is a slight unphysical increase of the oscillation amplitudes which in case of the eHK lives on a short transient period of time while in case of the HK it drives the amplitudes even beyond ± 1. This effect is well-known and reflects the violation of the norm conservation in the HK approach. The performance of the eHK becomes even more pronounced when comparing escape rates (Fig. 4.6): The exact and eHK rate differ by $\approx 5\%$, while the ordinary WKB result (3.8) completely fails in this low barrier regime. For higher barriers the accuracy of the WKB rate improves, of course, the dynamics of $P_0(t)$, however, can only be captured by the eHK scheme.

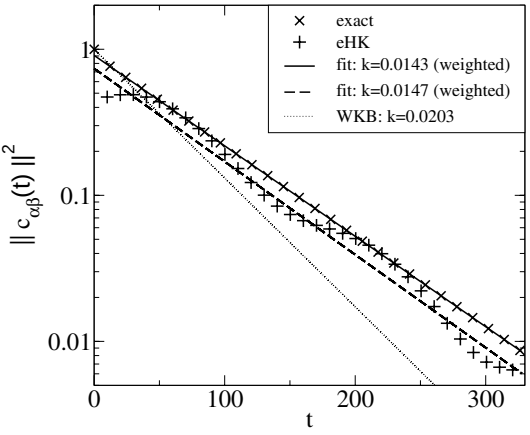

Fig. 4.6. Real part of $c_{\rm fi}$ vs. time for the static metastable well (4.14). Results for the eHK, the HK, and the exact dynamics are shown. Parameters are $V_{\rm b}/\hbar\omega_0 = 0.93$, and $q_{\rm i}/l = q_{\rm f}/l = 0$. Solid and dashed lines are fits to extract decay rates $k = \Gamma_0/\omega_0$; the dotted line depicts the WKB result.

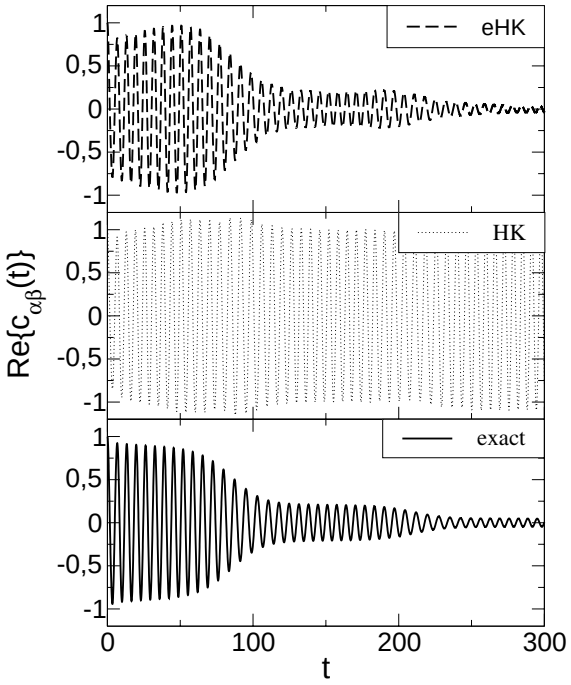

Fig. 4.7. Real part of c_{fi} vs. time for a driven metastable well with weaker driving. Results for eHK (top), HK (middle), and exact (bottom) dynamics are shown. The external driving is characterized by $\Omega/\omega_0 = 0.05$ and $Al = 0.4V_{\mathrm{b}}$. Other parameters are as in Fig. 4.5.

Is it possible to describe also driven decay within the eHK? To study this question we consider again a periodic driving force of the from $qA\sin(\Omega t)$ and start with a well supporting in the static case only one well state. The driving amplitude is adjusted in such a way that the well state lies either slightly below (Fig. 4.7) or slightly above (Fig. 4.8) the barrier top when the barrier reaches its minimal height. With $\Omega = 0.05$ the driving frequency is far below any resonance frequency. Apparently, the HK again fails, even in the case of the larger amplitude when escape is essentially governed by above-barrier paths, while the eHK follows closely the exact dynamics for many periods of the driving force.

More ambitious is the case of resonant driving (photon assisted tunneling) which is the most difficult process to describe within a semiclassical formalism. Although the driving amplitude is taken to be very small compared to the barrier height, a driving frequency in resonance with the spacing of a pair of quasi-energy levels in the well leads to strongly enhanced tunneling from excited well states. Here, parameters are chosen such that the well supports two states with $\Delta\omega_{10} = (\epsilon_1 - \epsilon_0)/\hbar$. Indeed, the influence of the external

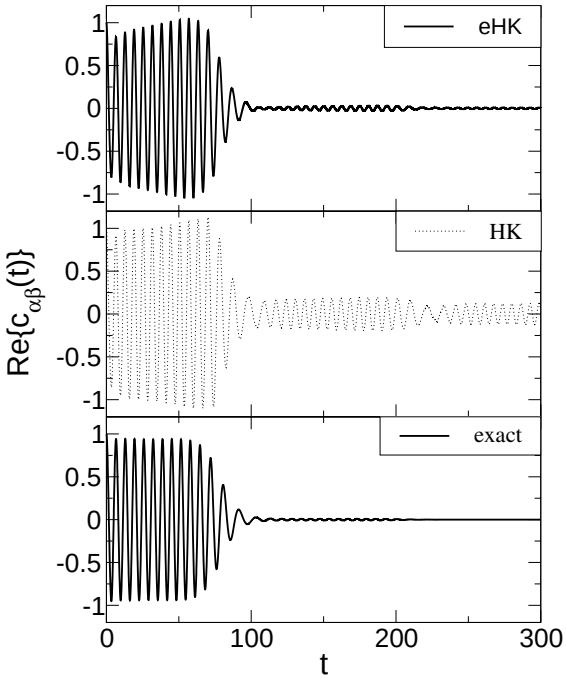

Fig. 4.8. Real part of c_{fi} vs. time for a driven metastable well with stronger driving. Results for eHK (top), HK (middle), and exact (bottom) dynamics are shown. Parameters are $\Omega/\omega_0 = 0.05$, $Al = 1.0V_{\mathrm{b}}$. Other parameters are as in Fig. 4.5.

driving remains very small away from the resonance and a decay is basically absent for this set of parameters and ranges of time.

This changes abruptly in the vicinity of the resonance. Typical results are shown in Fig. 4.9 where a clear decay due to tunneling from the excited state is observable. The difference between the exact and the semiclassical resonance frequency is about 5% and the eHK shows a fine agreement with the exact dynamics that is completely absent in the HK propagation. For longer times an increase of the amplitudes in the eHK data can be seen which again can be traced back to a break-down of the norm conservation and becomes a severe problem in the very long time domain. Moreover, in all these cases we found that the eHK exhibits much better convergence properties than the usual HK. The transmission/reflection factor acts like a filter and damps out the impact of chaotic trajectories and corresponding diverging prefactors which are a serious problem of the ordinary HK.

4.2.7 Tunneling Ionization in Laser Fields

Ionization in strong laser fields takes place in two channels. Either the bound electron absorbs photons from the external field (photoionization) or it may

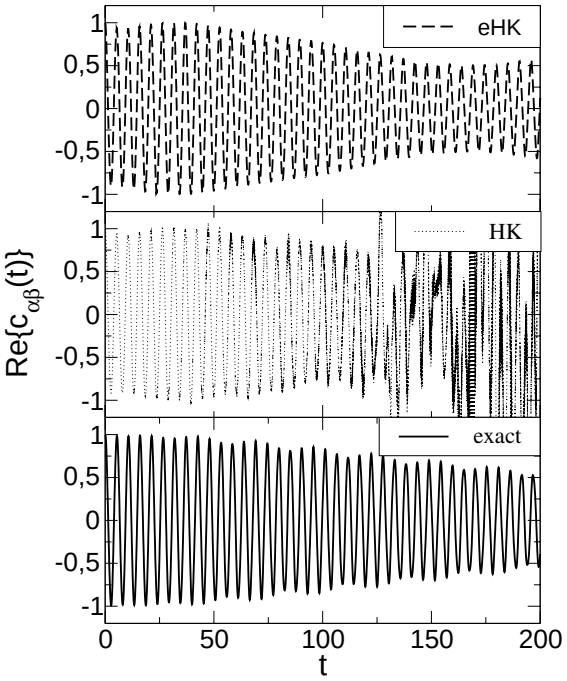

Fig. 4.9. Real part of $c_{\rm fi}$ vs. time for the driven metastable well for resonant driving. Results for eHK (top), HK (middle), and exact (bottom) dynamics are shown. Parameters are $V_{\rm b}/\hbar\omega_0 = 2$, $q_{\rm i}/l = q_{\rm f}/l = 0$, and $Al = 0.04V_{\rm b}$. Frequencies are $\Omega/\omega_0 = 2.135$ (exact resonance) and $\Omega/\omega_0 = 2.335$ (semiclassical resonance).

tunnel through the Coulomb potential tilted by the field (tunnel ionization) [34]. The parameter which controls the two ranges is the so-called Keldysh parameter [35]

$$\gamma_K = \sqrt{\frac{I_{\rm P}}{2U_{\rm P}}} = \sqrt{2I_{\rm P}}\frac{\omega_{\rm ex}}{A}\,, \tag{4.30}$$

where $I_{\rm P}$ is the ionization potential and $U_{\rm P} = A^2/(4\omega_{\rm ex}^2)$ the mean kinetic energy that a free electron gains in a laser field of amplitude A and frequency $\omega_{\rm ex}$. For $\gamma_{\rm K} \gg 1$ multi-photonionization prevails and may lead e.g. to Above Threshold Ionization (ATI). In the opposite range $\gamma_K < 1$ the electron may tunnel through the tilted Coulomb-barrier. Subsequently, it is accelerated in the electromagnetic field, returns in the next cycle of the field, which tilts the Coulomb potential to the other direction, back to the atom, where it may recombine and emit photons. Typically, this phenomenon is described in a three step process, where the first and third step are quantum mechanical events, while the intermediate one is assumed to be classical [36, 37, 38]. Eventually, this may generate higher harmonics [39, 40]. The extended HK formalism provides a possible basis to describe the whole process within one consistent

approach and may thus also be able to capture interferences between the emitted and back-scattered electronic wave packet.

In a first step towards this goal we report on some results for a driven Morse oscillator [18]

$$V_{\mathrm{Morse}} = V_0 \left(1 - \mathrm{e}^{-q/l}\right)^2 , \tag{4.31}$$

common in molecular physics. By applying an external field of the form

$$V_{\mathrm{ex}}(q,t) = q\,A\,\sin^2(\omega_{\mathrm{ex}} t)\,\Theta(n2\pi/\omega_{\mathrm{ex}} - t) \tag{4.32}$$

and choosing $n = 1$, we aim to simulate two laser pulses acting on the potential ($\Theta(\cdot)$ is the unit step function). The $\sin^2$ term ensures, that the deviation of the original shape of the potential is only in one direction. This allows us to study only the incoherent tunneling process. As the observable of interest we study the ionisation probability

$$P_{\mathrm{Ion}}(t) = 1 - \sum_n |\langle\phi_n|\psi(t)\rangle|^2 = 1 - \sum_n P_n(t)\,, \tag{4.33}$$

where P_n is the probability of being in the nth eigenstate $\langle\phi_n|$. For the potential parameters we have $V_0/(\hbar\omega_0) = 1.58$ for the depth of the well and $l/\sqrt{\hbar/(M\omega_0)} = 1.78$ for its width. Further, the external field has amplitude $\sqrt{\hbar/(M\omega_0)}A/V_0 = -0.146$ and frequency $\omega_{\mathrm{ex}}/\omega_0 = 0.0785$. This corresponds to a Keldysh parameter $\gamma_{\mathrm{K}} \approx 0.16$ ensuring a typical situation for ionization via tunneling [35]. Fig. 4.10 shows the time dependent probability of being in the ground and first excited state, respectively. One first observes that the eHK result follows the exact one quite accurately. However, for short times both HK based results overestimate the exact calculation. This effect is due to the violation of the norm conservation of the HK mechanism. While the eHK procedure recovers from this violation up to a certain extent, the result of the conventional HK formalism does not, leading to a probability amplitude for the ground state much larger than one. Calculating the ionization probability after the two external pulses, i.e. $n = 1$ in (4.32), using (4.33) gives $\approx 60\%$ for the exact result, $\approx 53\%$ for the result obtained with the eHK formalism, and a negative ionization probability $\approx -8\%$ predicted by the original HK formalism. Assuming that the ground state probability obtained by the eHK formalism is overestimated in the same way as the one obtained by the conventional HK result, leads to a naive correction to $P_0(t)$ simply by subtraction. Therefore one may correct the eHK result to $P_{\mathrm{Ion}}(t) \approx 61\%$, which is in very good agreement with the exact result.

4.3 Systematic Expansion of the HK Propagator

As already mentioned in Sect. 2.2, the HK propagator was originally not derived as a *systematic* stationary phase solution to the exact expression [41,

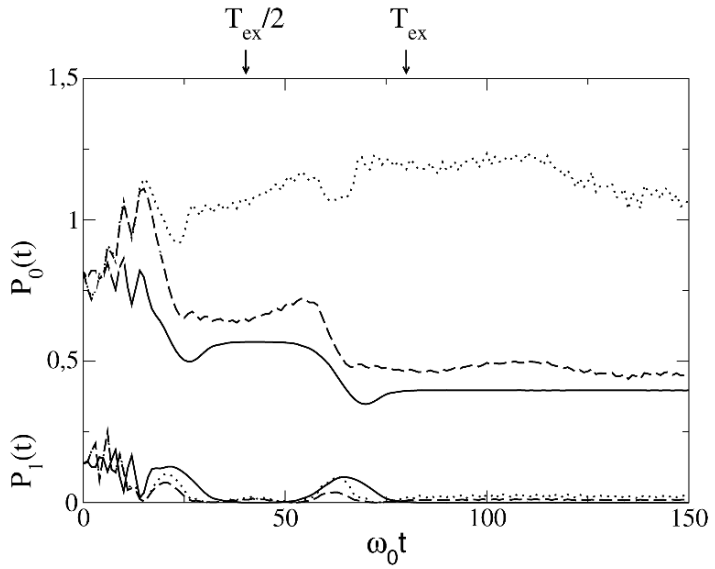

Fig. 4.10. Survival probability for ground (P_0) and first excited state (P_1) of a Morse potential driven by an external sinusodial field (4.32). Exact (solid), eHK (long-dashed), and HK (dotted) results are shown. For comparison the light grey line depicts results calculated with the conventional HK, but with renormalized wave packets at each time step. $T_{\rm ex}$ denotes the period of the external driving.

42, 43]. In contrast to the Van Vleck propagator, which due to its derivation as an asymptotic expansion to the exact path integral representation of the time evolution operator can be systematically improved, at least in principle, the semiclassical IVR was *constructed* to agree with the Van Vleck propagator in the sense of a stationary phase approximation but is useful only, if its phase space integration is evaluated numerically exactly. Thus, one computes the quantity of interest, using the IVR, but there is no real control as to the accuracy of the resulting approximation. Studies in this direction and also attempts to develop a firm basis of the HK propagator have been performed though, see e.g. [44, 45, 46, 47, 48, 49, 50, 51, 52, 53, 54]. Only very recently has this seed led to a consistent mathematical foundation [6, 22, 55].

The HK propagator has to fulfill the Schrödinger equation up to a correction which must be in some sense small. Based on this observation a deeper analysis leads to an exact representation of the quantum propagator in terms of an asymptotic IVR series with the HK propagator being the leading order contribution [19, 20, 22, 55]. Hence, a systematic improvement of the HK expression is available, which in particular allows to capture deep tunneling by higher order phase space integrations [21, 56].

4.3.1 Correction Operator

The exact quantum mechanical propagator $\hat{G} = \mathrm{e}^{-\mathrm{i}\hat{H}t/\hbar}$ obeys

$$\mathrm{i}\hbar\frac{\mathrm{d}}{\mathrm{d}t}\hat{G} = \hat{H}\hat{G}\,. \tag{4.34}$$

Now, upon inserting the expression (2.27) for the semiclassical IVR propagator $\hat{G}_{\mathrm{HK}}$ into this equation, one finds that it obeys

$$\mathrm{i}\hbar\frac{\mathrm{d}}{\mathrm{d}t}\hat{G}_{\mathrm{HK}} = \hat{H}\hat{G}_{\mathrm{HK}} + \hat{C}(t)\,, \tag{4.35}$$

where the correction operator $\hat{C}(t)$ is found to be

$$\hat{C}(t) = \int_{-\infty}^{\infty}\frac{\mathrm{d}p\mathrm{d}q}{2\pi\hbar}\left(\frac{\hbar^2\gamma^2}{2}[\hat{q}-q(t)]^2 - \frac{\hbar^2}{2}\gamma + \mathrm{i}\hbar\frac{\frac{\mathrm{d}R(p,q,t)}{\mathrm{d}t}}{R(p,q,t)} + V[q(t)] - V(\hat{q})\right.$$
$$\left. + V'[q(t)][\hat{q}-q(t)]\right) R(p,q,t)\,\mathrm{e}^{iS(p,q,t)/\hbar}|g_\gamma(p,q,t)><g_\gamma(p,q,0)| \tag{4.36}$$

and the prime denotes differentiation with respect to the argument.

It is straightforward to derive an explicit expression for the correction operator at time $t = 0$. Using Hamilton's equations of motion and (2.29) we have

$$\dot{R}(p,q,t) = \frac{1}{4R(p,q,t)}\left(-\frac{\partial V'[q(t)]}{\partial p} + \frac{\partial p(t)}{\partial q} - \mathrm{i}\hbar\gamma\frac{\partial p(t)}{\partial p} + \frac{1}{\mathrm{i}\hbar\gamma}\frac{\partial V'[q(t)]}{\partial q}\right). \tag{4.37}$$

Therefore, at time $t = 0$,

$$\dot{R}(p,q,0) = -\frac{\mathrm{i}\hbar\gamma}{4}\left(1 + \frac{V''(q)}{\hbar^2\gamma^2}\right). \tag{4.38}$$

This means that at the initial time the correction operator $\hat{C}(0)$ is Hermitian and depends only on the coordinate operator. Defining the average

$$< f(q) > \equiv \sqrt{\frac{\gamma}{\pi}}\int_{-\infty}^{\infty}\mathrm{d}q\;\mathrm{e}^{-\gamma(\hat{q}-q)^2}f(q) \tag{4.39}$$

and integrating by parts the terms with V' and V'', one readily finds that at $t = 0$

$$\hat{C}(0) = < \frac{3}{2}V(q) - \gamma V(q)(\hat{q}-q)^2 > -V(\hat{q})\,. \tag{4.40}$$

Hence, as to be expected, for a harmonic potential the correction operator vanishes.

4.3.2 Asymptotic Series

After having derived an explicit expression for the correction operator, one can view (4.35) as an inhomogeneous differential equation for $\hat{G}_{\mathrm{HK}}(t)$ supplemented with the boundary condition $\hat{G}_{\mathrm{HK}}(0) = \hat{I}$. Then, according to (4.34) the exact propagator is the solution of its homogeneous part so that the formally exact solution to (4.35) is given by

$$\hat{G}_{\mathrm{HK}}(t) = \hat{G}(t) - \frac{\mathrm{i}}{\hbar} \int_0^t \mathrm{d}s \; \hat{G}(t-s)\, \hat{C}(s)\,. \tag{4.41}$$

This can be written in form of a recursive equation for the exact propagator similar to a Born or Dyson series

$$\hat{G}(t) = \hat{G}_{\mathrm{HK}}(t) + \frac{\mathrm{i}}{\hbar} \int_0^t \mathrm{d}s \; \hat{G}(t-s)\, \hat{C}(s)\,. \tag{4.42}$$

By using $\hat{G}_{\mathrm{HK}}(t)$ as the 0th order term one may now represent the exact propagator as a series in which the nth element is of order $\hat{C}(t)^n$, i.e.,

$$\hat{G}(t) = \sum_{n=0}^{\infty} \hat{G}_n(t) \tag{4.43}$$

with $\hat{G}_0(t) = \hat{G}_{\mathrm{HK}}(t)$ and the recursion relation

$$\hat{G}_{n+1}(t) = \frac{\mathrm{i}}{\hbar} \int_0^t \mathrm{d}s \; \hat{G}_n(t-s)\, \hat{C}(s)\,. \tag{4.44}$$

Provided that the above series converges, it allows to actually compute the propagator, where a semiclassical IVR approximation beyond the HK expression is obtained when only a finite number terms is taken into account.

As an example, one considers [19] increasing orders of time dependent autocorrelation functions of a Gaussian wave packet $|\psi\rangle$, see (4.3),

$$c_k(t) = \sum_{n=0}^{k} \langle \psi | G_n(t) | \psi \rangle\,. \tag{4.45}$$

Already the second order approximation almost coincides with the exact quantum mechanical result. It turns out that the convergence towards the latter one is non-monotone and strongly depends on the time domain. For instance, the first order approximation c_1 gives for longer times a result much worse than c_0. This deterioration is cured by the next order term c_2. However, going to even longer times also this approximant fails and even higher order terms are required. While numerically the above integrals are very effectively evaluated by means of Monte Carlo techniques, in the long time range the increasing number of phase space integrations [$2(n+1)$ integrations in order c_n]

is plagued by another problem: The sign problem which is due to the oscillatory integrands and can be traced back to quantum mechanical interferences. Hence, practically depending on the problem in question the systematically improved semiclassics becomes no longer feasible though. The same is true for higher dimensional systems, where the number of phase space integrations increases with the dimension d as $2d(n+1)$. For instance, while for $d=1$ the c_2 requires to perform 6 integration, for $d=3$ already the c_1 needs 12. In addition, the calculation of the determinant in the prefactor of the HK propagator becomes increasingly expensive and turns out to be a crucial bottleneck. We will address this issue briefly in the next Sect. 4.3.3. On the other hand, one has to recall that also an exact solution of the time dependent Schrödinger equation becomes increasingly demanding for very long times and/or in higher dimensions.

4.3.3 Deep Tunneling with Real-valued Trajectories

To demonstrate the ability of the approach outlined in the previous Section to deal with deep tunneling, penetration through an Eckart barrier has been studied in [21]. According to the series (4.43) there is no longer one real-valued trajectory, but rather a total path connecting a fixed point on the left with another one on the right side of the barrier is composed of segments with discontinuous jumps in phase space between end- and starting points of adjacent segments. It turns out that compared to the exact data very accurate results for transmission probabilities and real-time correlation functions are already obtained for $n=2$ [(4.43)], see Fig. 4.11. In particular, note the convergence to the numerically exact values in the low energy regime, where deep tunneling prevails. We remark that in this study a prefactor-free semiclassical initial value representation was used. Accordingly, the action factor needs to be modified in order to obey Heisenberg's equation of motion. Even though the corresponding propagator is slightly less accurate than the HK representation, its advantage is a substantial speed-up of the numerics, especially, for the higher order corrections. Namely, the computational bottleneck of the HK-scheme is the calculation of the prefactor, which as a determinant requires to perform $\propto N^3$ numerical operations for an $N \times N$-matrix. Hence, since in order n one has $2(n+1)$ phase space integrations, the number of operations grows like $8(n+1)^3$ that have to be performed at each time step and for each trajectory. Together with the above mentioned sign problem which requires an increasing number of orbits with growing n, the HK scheme soon becomes numerically no longer tractable. A prefactor-free formulation has the merit of being much more efficient and thus allows to over-compensate its slightly smaller accuracy.

Based on a variational method, tunneling splittings in a double well potential have been obtained in [56] from a semiclassical time evolution of wave packets in the short time domain. Again the number of iterations in (4.44) to reach sufficiently accurate data is small ($n=3$). Further, the time interval

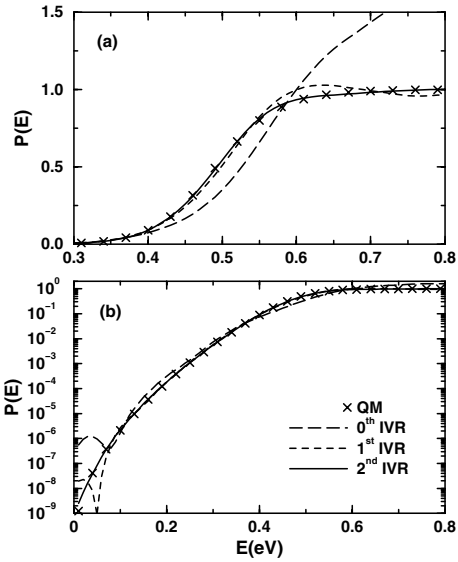

Fig. 4.11. Energy dependent transmission probability for a symmetric Eckart barrier potential. Panel (a) depicts results on a linear scale, panel (b) on a logarithmic scale for various orders of iteration of the IVR series. Courtesy of E. Pollak, Weizmann Institute of Science.

over which the semiclassical dynamics has to be determined is short, i.e. much shorter than the Fourier time $2\pi\hbar/\Delta E$ for a tunnel splitting ΔE.

From a conceptual point of view, the interesting aspect here is that semiclassical dynamics is known to work quite well precisely for shorter times as we have discussed above. Of course, in order to retrieve information about tunneling in this time domain, necessitates an extremely accurate calculation of details of the dynamics. This idea has also been exploited in an alternative semiclassical real-time approach to be addressed in the following Sect. 4.4.

4.4 Alternative Approaches

One of the first attempts to attack the real-time tunneling problem beyond the standard HK propagator has been developed in [32] on the basis of a splitting of that propagator. The underlying idea is to combine segments of real-valued classical trajectories such that the end-point of the first and the initial point of the next one do not coincide in phase space so that a larger area in phase space can be explored. Namely, due to the half-group property of the quantum operator (2.19), the splitting into n segments accounts for n additional intermediate integrations. In principle, for $n \to \infty$ this leads to the exact path integral representation (2.17). However, when only a finite number

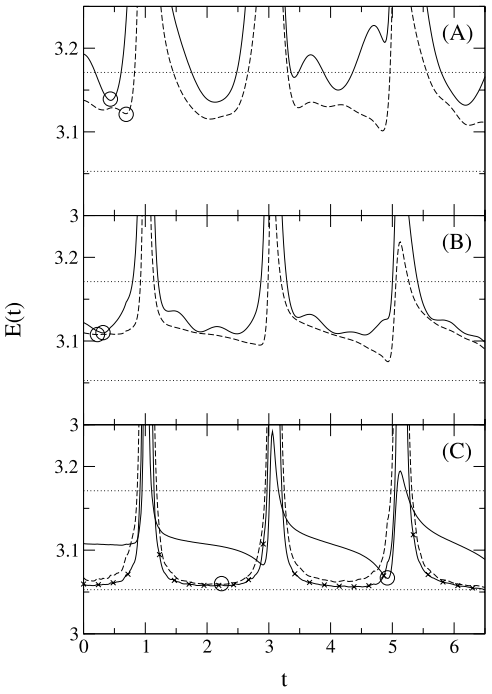

Fig. 4.12. The iterative variational method for computing the ground state tunneling energy in a quartic double well potential. Panel (A) shows the zero-th and first iteration. The small circles denote the respective time dependent minima ($t_1 = 0.435$ for the zero-th order functional and $t_2 = 0.69$ for the first iterated functional). Panel (B) depicts the same for the next two iterations ($t_3 = 0.315$, $t_4 = 0.225$) and panel (C) shows the final two iterations ($t_5 = 4.92$, $t_6 = 2.235$). The horizontal dotted lines denote the ground and first excited state eigenvalues as determined by an exact diagonalization. The line with crosses in (C) depicts the energy after the sixth iteration. Courtesy of E. Pollak, Weizmann Institute of Science.

of splittings is considered and for each time segment the exact quantum propagator is approximated by the HK propagator, one may expect an improved semiclassical approximation.

By way of example, let us consider the case $n = 1$. Then, one has

$$G_{\mathrm{HK}}(q_{\mathrm{f}}, t; q_{\mathrm{i}}, 0) = \int \mathrm{d}\, x G_{\mathrm{HK}}(q_{\mathrm{f}}, t; x, t/2)\, G_{\mathrm{HK}}(x, t/2; q_{\mathrm{i}}, 0)\,, \tag{4.46}$$

which upon inserting the expression for the HK propagator (2.27) and performing the x integrations leads to

$$G_{\mathrm{HK}}(q_{\mathrm{f}},t;q_{\mathrm{i}},0) = \int \frac{\mathrm{d}p\mathrm{d}q}{2\pi\hbar} \int \frac{\mathrm{d}p'\mathrm{d}q'}{2\pi\hbar}\, g_\gamma[p'(t/2),q'(t/2);q_{\mathrm{f}}]\, R\left(p',q',\frac{t}{2}\right) \mathrm{e}^{\mathrm{i}S(p',q',\frac{t}{2})/\hbar} \times \langle g'_\gamma | g_\gamma(t/2)\rangle\, R\left(p,q,\frac{t}{2}\right) \mathrm{e}^{\mathrm{i}S(p,q,\frac{t}{2})/\hbar}\, g_\gamma(p,q;q_{\mathrm{i}})\,. \tag{4.47}$$

Here, the expressions in (2.28) and (2.29) for the Gaussian wave packets and the prefactors have been used. Further, the intermediate x-integration gives rise to the overlap of the two Gaussians

$$\langle g'_\gamma | g_\gamma(t/2)\rangle = \exp\left\{ -\frac{\gamma}{4}[q'-q(t/2)]^2 + \frac{\mathrm{i}}{2\hbar}[q'-q(t/2)][p'+p(t/2)] - \frac{1}{4\gamma\hbar^2}[p'-p(t/2)]^2 \right\}. \tag{4.48}$$

Note that the expression for the HK propagator is regained when the additional integral in (4.46) is performed in stationary phase. The crucial point is that this is not done here, in order to obtain a more accurate semiclassical approximation. In the light of our discussion in Sect. 4.1, any additional splitting allows for a spawning of classical orbits in the barrier range to cover a larger domain in phase space.

This concept has been shown to substantially improve the performance of the HK in case of tunneling through an Eckart barrier [32]. The number of additional splittings did not exceed three, but could reach the accuracy of the uniform WKB result from moderate energies to energies around the barrier top. The only bottleneck of the approach is again the increasing number of phase space integrations in time and in higher dimensions. In fact, the numerical effort did not allow to treat driven systems explicitly, when the method was introduced. One may assume that this may change with a still ongoing increase in computer power.

Another approach has been laid out on the basic insight that according to the spectral representation (2.32) of the quantum propagator, in principle, information about the tunneling process is already contained in the short time domain. The only problem is that the corresponding exponentially small contributions are hidden behind a dominating background. Hence, to avoid a semiclassical time evolution for longer times, one needs a very sensitive method to retrieve the "needles in a haystack" by accumulating enough information in the short time range. Such a method is provided by a high resolution spectral analysis based on the filter diagonalization method (FDM) [57, 58, 59, 60, 61]. For a time signal originating from a quantum mechanical time evolution, e.g. an auto-correlation function (4.3), it is suggestive to assume a form

$$C(t) = \sum_l b_l \mathrm{e}^{-iE_l t/\hbar}\,. \tag{4.49}$$

The goal is then to determine the amplitudes b_l and energies E_l by fitting $C(t)$ to the semiclassical data. This type of problem is known as a harmonic inversion problem and an efficient way to solve it is given by the FDM. Very successful applications of this procedure comprise the extraction of eigenenergies [62] and periodic orbit quantization [63, 64].

However, by considering a tunneling situation just a single correlation function for shorter times is not sufficient to extract tunneling amplitudes – the information content is too small. Thus, one takes into account a whole family of correlation functions [65]

$$C_{\mu\nu}(t) = \langle\psi_\mu|\exp(-\mathrm{i}Ht/\hbar)|\psi_\nu\rangle \quad , \quad \mu,\nu = 1,2,\ldots,K\,, \tag{4.50}$$

where the $\{\psi_\mu\}$ are Gaussian wave packets that for $K \to \infty$ define a complete basis set. In this limit, the calculation of the set of correlation functions is identical to an exact diagonalization of the propagator. The idea is now, to use only a certain subset of states such that the FDM delivers tunneling amplitudes being independent of time in the short time range after some transient time scale. The harmonic inversion problem then reads

$$C_{\mu\nu}(t) = \sum_l b_{\mu l}\, b_{\nu l}\, \mathrm{e}^{-\mathrm{i}E_l t/\hbar}\,. \tag{4.51}$$

This program has been successfully applied to determine tunnel splittings in a one-dimensional double well potential, where $K = 7$. Even a two-dimensional problem could been attacked again with a still feasible number of states $K = 7$. For explicit time dependent problems (external driving) this methodology has not been applied so far.

References

1. S. Mukamel. *Principles of Nonlinear Spectoscropy.* Oxford University Press, 1995.
2. M. Grifoni and P. Hänggi. *Phys. Rep.*, 304:229, 1998.
3. D. Tannor. *Introduction to Quantum Mechanics, A Time Dependent Perspective.* University Science Books, 2003.
4. P.W. Brumer and M. Shapiro. *Principles of the Quantum Control of Molecular Processes.* Wiley-VCH, 2003.
5. V.M. Akulin. *Coherent Dynamics of Complex Quantum Systems.* Theoretical and Mathematical Physics.
6. J. Ankerhold, M. Saltzer, and E. Pollak. *J. Chem. Phys.*, 116:5925, 2002.
7. K.G. Kay. *J. Chem. Phys.*, 107:2313, 1997.
8. B.W. Spath and W.H. Miller. *J. Chem. Phys.*
9. S. Garashchuk and D. Tannor. *Chem. Phys. Lett.*, 262:477, 1996.
10. S. Keshavamurthy and W.H. Miller. *Chem. Phys. Lett.*, 218:189, 1994.
11. X. Sun, H. Wang, and W.H. Miller. *J. Chem. Phys.*, 109:4190, 1998.
12. F. Grossmann and E.J. Heller. *Chem. Phys. Lett.*, 241:45, 1995.

13. N.T. Maitra and E.J. Heller. *Phys. Rev. Lett.*, 78:3035, 1997.
14. C. Eckart. *Phys. Rev.*, 35:1303, 1930.
15. D. Tannor and S. Garashchuk. *Annu. Rev. Phys. Chem.*, 51:553, 2000.
16. W.H. Miller. *J. Phys. Chem.*, 83:960, 1979.
17. M. Saltzer and J. Ankerhold. *Phys. Rev. A*, 68:042108, 2003.
18. M. Saltzer and J. Ankerhold. In *Recent Research in Quantum Theory*. Nova Publishers, 2004.
19. S. Zhang and E. Pollak. *Phys. Rev. Lett.*, 91:190201, 2003.
20. S. Zhang and E. Pollak. *J. Chem. Phys.*, 119:11058, 2003.
21. S. Zhang and E. Pollak. *Phys. Rev. Lett.*, 93:140401, 2004.
22. K.G. Kay. *Chem. Phys.*, 322:3, 2006.
23. M. Wilkinson and J.H. Hannay. *Physica D*, 27:201, 1987.
24. J.M. Robbins. *Phys. Rev. A*, 40:2128, 1989.
25. J.M. Robbins, S.C. Creagh, and R.G. Littlejohn. *Phys. Rev. A*, 41:6052, 1990.
26. P. Lebœuf and A. Mochet. *Phys. Rev. Lett.*, 73:1360, 1994.
27. A. Shudo and K.S. Ikeda. *Phys. Rev. Lett.*, 74:682, 1995.
28. L. Salasnich, A. Parola, and L. Reatto. *Phys. Rev. A*, 64:023601, 2001.
29. L.S. Schulman. *Techniques and Applications of Path Integrals*. Wiley, 1981.
30. D.M. Brink and U. Smilansky. *Nuc. Phys. A*, 405:301, 1983.
31. H. Yoshida. *Phys. Lett. A*, 150:1, 1990.
32. F. Grossmann. *Phys. Rev. Lett.*, 85:903, 2000.
33. J.M. Martinis, S. Nam, J. Aumentado, and C. Urbina. *Phys. Rev. Lett.*, 89:117901, 2002.
34. E. Mevel, P. Breger, R. Trainham, G. Petite, P. Agostini, A. Migus, J.-P. Chambaret, and A. Antonetti. *Phys. Rev. Lett.*, 70:406, 1993.
35. L.V. Keldysh. *Sov. Phys. JETP*, 20:1307, 1965.
36. P.B. Corkum. *Phys. Rev. Lett.*, 71:1994, 1993.
37. M. Lewenstein, Ph. Balcou, M.Yu. Ivanov, A. L'Huillier, and P.B. Corkum. *Phys. Rev. A*, 49:2117, 1994.
38. M.Y. Kuchiev and V.N. Ostrovsky. *Phys. Rev. A*, 60:3111, 1999.
39. A. L'Huillier et al. *Phys. Rev. A*, 46:2778, 1992.
40. M. Protopapas, C. Keitel, and P.L. Knight. *Rep. Prog. Phys.*, 60:389, 1997.
41. M.F. Herman and E. Kluk. *Chem. Phys.*, 91:27, 1984.
42. E. Kluk, M.F. Herman, and H.L. Davis. *J. Chem. Phys.*, 84:326, 1995.
43. M.F. Herman. *J. Chem. Phys.*, 85:2969, 1996.
44. K.G. Kay. *J. Chem. Phys.*, 100:4377, 1994.
45. M.F. Herman. *Annu. Rev. Phys. Chem.*, 45:83, 1994.
46. W.H. Miller. *Adv. Chem. Phys.*, 101:853, 1997.
47. W.H. Miller. *Faraday Discuss.*, 110:1, 1998.
48. F. Grossmann and A.L. Xavier. *Phys. Lett. A*, 243:243, 1998.
49. W.H. Miller. *Mol. Phys.*, 100:397, 2002.
50. T. Yamamoto and W.H. Miller. *J. Chem. Phys.*, 118:2135, 2003.
51. B. Hu, Q. Jie, B. Li, and S. Wang. *Phys. Rev. A*, 63:044102, 2001.
52. M. Baranger, M.A.M. de Aguiar, F. Keck, H.J. Korsch, and B. Schellhaaß. *Phys. Rev. A*, 35:9493, 2002.
53. M. Baranger, M.A.M. de Aguiar, and H.J. Korsch. *J. Phys. A*, 36:9795, 2003.
54. S. Yoshida, F. Grossmann, E. Person, and J. Burgdörfer. *Phys. Rev. A*, 69:043410, 2004.
55. E. Pollak and J. Shao. *J. Phys. Chem. A*, 107:7112, 2003.

56. M. Saltzer and E. Pollak. *J. Chem. Theory Comput.*, 1:439, 2005.
57. S.K. Gray. *J. Chem. Phys.*, 96:6543, 1996.
58. M.R. Wall and D. Neuhauser. *J. Chem. Phys.*, 102:8011, 1995.
59. V.A. Mandelshtam and H.S. Taylor. *J. Chem. Phys.*, 106:5085, 1997.
60. V.A. Mandelshtam and H.S. Taylor. *Phys. Rev. Lett.*, 78:3274, 1997.
61. V.A. Mandelshtam and H.S. Taylor. *J. Chem. Phys.*, 107:6756, 1997.
62. F. Grossmann, V.A. Mandelshtam, H.S. Taylor, and J.S. Briggs. *Chem. Phys. Lett.*, 279:355, 1997.
63. J. Main, V.A. Mandelshtam, and H.S. Taylor. *Phys. Rev. Lett.*, 78:4351, 1997.
64. J. Main, V.A. Mandelshtam, and H.S. Taylor. *Phys. Rev. Lett.*, 79:825, 1997.
65. V.A. Mandelshtam and M. Ovchinikov. *J. Chem. Phys.*, 108:9206, 1998.

5

Tunneling in Open Systems: Thermodynamical Approaches

A complete description of tunneling processes in real systems has to take into account the presence of environmental degrees of freedom. In fact, this has led at the beginning of the 1980s to fundamental questions such as [1]: To what extent is quantum coherence observable on a macroscopic level? Is quantum mechanics valid to describe, at least in principle, macroscopic objects? How does a complex surrounding destroy quantum non-locality and the superpositions of eigenstates? Since quantum tunneling is one of the most striking consequences of quantum mechanics, the study of those questions in the context of barrier penetration in complex systems has triggered a substantial amount of research on tunneling of macroscopic variables – to be more precise, of collective degrees of freedom consisting of a macroscopically large number of individual degrees of freedom [2, 3, 4, 5, 6, 7]. Particular emphasis has been put on superconducting mesoscopic systems, as e.g. Josephson junctions and liquid Helium, and on the role of dissipation due to their contact with the macroscopic world [8, 9]. For a detailed discussion of the experimental results we refer to [10, 11]. In parallel to these efforts the theoretical foundations for the description of quantum dissipative systems in general [12, 13, 14] and for decay processes in particular have been developed [14, 15].

The foundations for a classical rate theory were laid in 1940 with a seminal work by Kramers [29]. He derived a rate expression in presence of a heat bath within a dynamical description based on a Fokker-Planck equation. This work has further been extended in the 1980s and since then has grown into a broad field along the borderline between statistical and chemical physics [14, 15]. We will give a brief survey of the main results in the next Sect. 5.1.

Quantum mechanically the situation is much more complicated. First, a simple modification of the Schrödinger equation to include dissipation [16, 17] does not work since it leads to contradictions with fundamental laws as e.g. the uncertainty relation [18]. Indeed, dissipation cannot be understood as an intrinsic process, but rather as the consequence of reducing our interest to a small subsystem embedded into a much larger surrounding. Thus, one starts from a Hamiltonian of the whole compound comprising system, interaction,

Joachim Ankerhold: *Quantum Tunneling in Complex Systems*
STMP **224**, 93–130 (2007)
DOI 10.1007/3-540-68076-4_5

and bath and eliminates the latter degrees of freedom. Second, quantum mechanical non-locality renders any Markovian (time-local) approximation for the reduced dynamics to break down at sufficiently low temperatures meaning that a "simple" equation of motion for the reduced density matrix does in general not exist [14], a subject that will be discussed in more detail in Chap. 6.

A breakthrough was achieved by Caldeira and Leggett who exploited path integral techniques to adapt a thermodynamical approach pioneered by Langer to calculate the tunneling rate in presence of a dissipative environment [19, 20, 21]. In Sect. 3.1.2 we already discussed this method, known as ImF approach, for non-dissipative systems and showed that in this limit it is indeed completely equivalent to the WKB approximation. As also mentioned, the real power of the formulation lies in the fact that the path integrals allow for a straightforward generalization to dissipative systems. The corresponding rate expressions derived over the whole temperature range [22, 23, 24, 25, 26] have been tested with remarkable accuracy against experimental data [10] so that transparency and elegance of the approach have turned it into *the* standard tool for quantum rate calculations at least in physics and in fields as diverse as cosmology, condensed matter, and nuclear physics. A more detailed discussion will be presented in the main body of this Chapter.

However, the ImF method has one drawback, namely, it has not been rigorously derived from first principles for dissipative systems in the domain of finite temperatures. And it is well known that it certainly fails for certain ranges in parameters space, e.g. in the weak damping regime, where classically the escape process is limited by energy diffusion. Further, as a thermodynamical approach it does not allow to describe tunneling processes driven by external time dependent sources. Hence, a description based on a real-time evolution of the reduced density matrix is strongly desired. Foundations for such an approach will be presented in Chaps. 6 and 7.

5.1 Classical Kramers' Rate Theory: A Brief Survey

The dynamics of a classical particle of mass M moving in a metastable well $V(q)$ and subject to thermal noise follows from

$$M\ddot{q} + M\gamma\dot{q} + V'(q) = \xi(t)\,. \tag{5.1}$$

Here, the stochastic force with zero mean $\langle\xi(t)\rangle = 0$ is related to the damping constant γ via the dissipation fluctuation theorem

$$\langle\xi(t)\xi(t')\rangle = 2M\gamma k_{\rm B}T\,\delta(t-t')\,. \tag{5.2}$$

Further, the barrier top is located at $q = q_{\rm b}$ and to the right of a well region around $q = 0$ with $V(0) = 0$ so that $V_{\rm b} = V(q_{\rm b})$ is the barrier height. Equivalently, the above dynamics is described by the Fokker-Planck equation (FPE) [27]

$$\dot{P}(p,q,t) = \left\{ \frac{p}{M}\partial_q - \partial_p \left[V'(q) + \gamma p\right] + M\gamma k_{\mathrm{B}} T \partial_p^2 \right\} P(p,q,t)\,. \tag{5.3}$$

The basic assumption in Kramers' theory [15, 29] is a time scale separation between relaxation in the well and escape over the barrier. It turns out that this imposes

$$V_{\mathrm{b}} \gg k_{\mathrm{B}} T \tag{5.4}$$

meaning that the thermal activation driven by the noise is a rare event. In fact, the time scale separation is a prerequisite for a sensible definition of a rate constant. The strategy to calculate it is then this: (i) Look for a stationary solution of the above FPE corresponding to a stationary flux across the barrier when initially a local thermal equilibrium is restricted to the well region, (ii) calculate the stationary flux J_{st} and the population in the well N_{well}, and (iii) determine the escape rate from the *flux over population*

$$\Gamma = \frac{J_{\mathrm{st}}}{N_{\mathrm{well}}}\,. \tag{5.5}$$

The crucial point is thus the calculation of the stationary flux solution P_{flux}. Of course, the above FPE has always one trivial stationary solution, namely, the thermal equilibrium related to a vanishing flux

$$P_\beta(p,q) = \frac{1}{Z}\, \mathrm{e}^{-\beta p^2/2M - \beta V(q)}\,, \tag{5.6}$$

with a constant Z that must be chosen properly since this distribution is not normalizable in the usual sense. However, there is another stationary solution P_{flux} which obeys the boundary conditions

$$P_{\mathrm{flux}}(p,q) \to 0 \quad \text{for} \quad q \gg q_{\mathrm{b}} \quad \text{and} \quad P_{\mathrm{flux}}(p,q) \to P_\beta(p,q) \quad \text{for} \quad q \ll q_{\mathrm{b}} \tag{5.7}$$

and describes a nonequilibrium situation. For sufficiently strong damping, the deviation of P_{flux} from the thermal equilibrium is restricted to a small range around the barrier top, where the barrier potential can be approximated by an inverted harmonic oscillator potential. Hence, one writes

$$P_{\mathrm{flux}}(p,q) = P_\beta(p,q)\; g_{\mathrm{fl,cl}}(p,q)\,, \tag{5.8}$$

where $g_{\mathrm{fl,cl}}$ captures the nonequilibrium features and drops from 1 to 0 within the vicinity of q_{b}. Accordingly, the above FPE turns into an equation for $g_{\mathrm{fl,cl}}(p,q)$, which becomes an ordinary differential equation, if one introduces the combination

$$u = q - q_{\mathrm{b}} - a_{\mathrm{cl}}\, p \quad \text{with} \quad a_{\mathrm{cl}} = \frac{\lambda_+}{M\omega_{\mathrm{b}}^2}\,. \tag{5.9}$$

Here $\omega_{\mathrm{b}}^2 = |V''(q_{\mathrm{b}})/M|$ and

$$\lambda_\pm = -\frac{\gamma}{2} \pm \sqrt{\omega_{\mathrm{b}}^2 + \frac{\gamma^2}{4}} \tag{5.10}$$

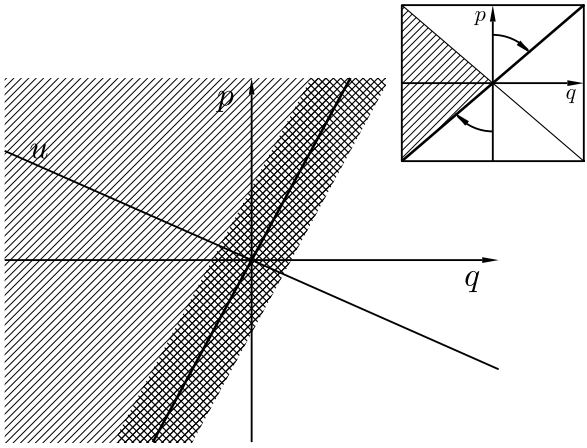

Fig. 5.1. Phase-space structure of the nonequilibrium flux distribution (5.8) with (5.11) around a barrier top located at $q = q_\mathrm{b}$ and for finite friction. A well is located to the left and sufficiently away from the barrier top. In the simple shaded area the distribution coincides with the thermal equilibrium and the double shaded domain shows the layer, where this equilibrium tends to a vanishing distribution to the right of the barrier. The relevant coordinate u (5.9) is shown as a thin straight line, while the thick line refers to $u = 0$, where $g_{\mathrm{fl,cl}} = 1/2$. The inset displays the situation for vanishing friction: a thermal distribution initially localized to the left of $q = q_\mathrm{b}$ will for long times only survive in the shaded area, where $E < V_\mathrm{b}$. Orbits with $E > V_\mathrm{b}$ will asymptotically evolve along the unstable direction (thick line) so that the domains $E > V_\mathrm{b}$ are completely depleted.

denote the characteristic roots for the dynamics in an inverted harmonic potential. This new coordinate u has an interesting physical meaning: In phase-space and for zero friction two branches of the separatrix deviding regions with $E < V_\mathrm{b}$ from those with $E > V_\mathrm{b}$ cross at q_b. Hence, at q_b one finds two stable directions along $v = q - q_\mathrm{b} + p/M\omega_\mathrm{b} = 0$ (corresponding to λ_-) and two unstable ones along $u = q - q_\mathrm{b} - p/M\omega_\mathrm{b} = 0$ (corresponding to λ_+). From the latter ones only that with $p > 0$ is associated with a successful escape event. Now, suppose that initially a thermal equilibrium to the left of the line $q = q_\mathrm{b}$ is prepared. For vanishing friction, in the far future all states in the domain $E > V_\mathrm{b}$ of phase space will then evolve along the unstable v-direction (see Fig. 5.1, inset) and the domains $E > V_\mathrm{b}$ will be depleted completely. In case of non-zero friction the slopes of the stable and unstable branches must change to account for the energy loss when passing the barrier top [28]. Additional noise (due to re-scattering back into the well) maintains the thermal equilibrium in a much broader region and restricts the domain of depletion to a boundary layer near the barrier top as depicted in Fig. 5.1. The coordinate u measures the distance from this boundary layer.

Within the new coordinate system the flux solution is easily found to read [15]

$$g_{\mathrm{fl,cl}}(p,q) = \frac{1}{\sqrt{\pi}} \int_{\xi(p,q)}^{\infty} \mathrm{d}x\, \mathrm{e}^{-x^2} \tag{5.11}$$

with

$$\xi(p,q) = \sqrt{\frac{M\beta\omega_\mathrm{b}^2}{2\gamma\lambda_+}} \left[\omega_\mathrm{b}(q-q_\mathrm{b}) - \frac{p}{M}\frac{\lambda_+}{\omega_\mathrm{b}}\right] . \tag{5.12}$$

This function is constant outside the boundary layer around $\xi(p,q) = 0$ and approaches 0 for $q - q_\mathrm{b} \gg \lambda_+ p/(M\omega_\mathrm{b}^2)$ and 1 for $q - q_\mathrm{b} \ll \lambda_+ p/(M\omega_\mathrm{b}^2)$, see also Fig. 5.1. The stationary flux now follows with (5.8) from

$$J_\mathrm{st} = \frac{1}{M} \int_{-\infty}^{\infty} \mathrm{d}p\, \frac{p}{M}\, P_\mathrm{flux}(p, q_\mathrm{b}) \tag{5.13}$$

and the well population is given by

$$N_\mathrm{well} = \int_\mathrm{well} \mathrm{d}q\mathrm{d}p\, P_\beta(p,q)\,, \tag{5.14}$$

with the integral restricted to the well region where the barrier potential can be approximated by a harmonic oscillator with frequency $\omega_0^2 = V''(0)/M$. Eventually, the rate expression is gained according to (5.5) as

$$\Gamma = \frac{\omega_0}{2\pi}\frac{\lambda_+}{\omega_\mathrm{b}}\, \mathrm{e}^{-\beta V_\mathrm{b}} . \tag{5.15}$$

This result differs from the simple transition state theory formula (3.13) by the additional factor λ_+/ω_b which for finite friction is always smaller than 1 and captures re-crossing processes after a particle has been kicked over the barrier. As long as this effect associated with a flux back towards the well is sufficiently strong, the nonequilibrium state is indeed restricted in position space around the barrier top. This leads to a condition for the validity of the above flux solution from the requirement that $g_\mathrm{flux,cl}$ must approach 1 within a range in position space where the harmonic approximation is still valid, i.e. on a length scale much smaller than q_b. While this condition is always fulfilled for stronger friction, it defines a lower bound on friction in the underdamped case, namely,

$$\frac{\gamma}{\omega_\mathrm{b}} > \frac{1}{\beta W(V_\mathrm{b})}\,, \tag{5.16}$$

where $W(E) = \oint p\mathrm{d}q$ is the action for one round trip in the well. For instance, in case of a harmonic+cubic potential one has $W(V_\mathrm{b}) = 36V_\mathrm{b}/(5\omega_\mathrm{b})$. When this condition is violated, the nonequilibrium state covers the entire well region in position space and the diffusion process across the barrier is not limited by friction in position space, but by energy diffusion [15, 29]. Kramers' found a solution also in this domain by transforming the FPE from (p,q) to (E,ϕ)

space, where E denotes the energy, an almost conserved quantity for weak friction, and $\phi = \omega(E)t$ the phase along an oscillating orbit in the well, a fast moving variable compared to E. The phase can thus be eliminated adiabatically and one arrives at an effective FPE in energy space. Then, the same line of reasoning as above applies, now, however, in energy space meaning that $g_{\mathrm{flux,cl}}(E)$ approaches 1 for energies slightly below $E = V_b$. As a result one finds

$$\Gamma = \frac{\omega_0}{2\pi} \frac{\gamma W(V_\mathrm{b})}{k_\mathrm{B} T} \, \mathrm{e}^{-\beta V_\mathrm{b}} \, . \tag{5.17}$$

The rate expression (5.15) yields a decreasing rate for large friction $\gamma/\omega_\mathrm{b} \gg 1$ according to $\Gamma \propto 1/\gamma$, while the above result provides a vanishing rate for small friction $\gamma/\omega_\mathrm{b} \ll 1$ according to $\Gamma \propto \gamma$. Hence, for intermediate values of γ there is a turnover between these two regimes, which necessitates a more involved description. The underlying idea is to analyze the well dynamics along the unstable coordinate introduced above. This way, one obtains a framework which provides a common description for all friction strengths [30, 31] with the rate being of the form $\Gamma = (\omega_0/2\pi)\kappa \exp(-\beta V_\mathrm{b})$, where the transmission coefficient reads

$$\kappa = \frac{\lambda_+}{\omega_\mathrm{b}} \exp\left\{ \frac{1}{\pi} \int_{-\infty}^{\infty} \frac{\mathrm{d}x}{1+x^2} \ln\{1 - \exp[-\delta(1+x^2)/4]\} \right\} . \tag{5.18}$$

Here, $\delta = \beta \Delta E$ is the dimensionless energy loss of the unstable normal mode during one round trip in the well. For $\delta \ll 1$ one regains (5.17), while for $\delta \gg 1$ the result (5.15) is recovered.

So far our discussion has focused on memory-less friction, but it has been shown that these findings can also be generalized to friction with finite memory time [32, 33]. Essentially, this amounts to the fact to substitute in the rate expressions specified above the friction constant γ by $\hat{\gamma}(\omega)$, where $\hat{\gamma}(\omega)$ is the Laplace transform of the time dependent damping kernel $\gamma(t)$ [see (5.23)]. Accordingly, the characteristic frequency λ_+ is given by the so-called Grote-Hynes frequency already introduced in (3.95).

5.2 ImF for Open Systems

The general concept of the *Imaginary part of the Free energy method* (ImF-method) has already been discussed in Sect. 3.1.2 for the case of vanishing friction, where it is equivalent to the WKB approximation. The advantage of the underlying path integral formulation is that it allows to include additional degrees of freedom to introduce dissipation. According to the introductary discussion, the goal is to calculate a reduced partition function, where the bath degrees of freedom are traced out and where the dominant contributions are provided by minimal action paths.

5.2.1 System+Reservoir Model

The standard model to describe dissipation is based on a separation of the total system under investigation in a small relevant part, the actual system we are interested in, and in a much larger part containing macroscopically many degrees of freedom [14]. This latter part constitutes a heat bath in thermal equilibrium specified by a temperature T. Hence, one writes for the total Hamiltonian

$$H = H_{\mathrm{S}} + H_{\mathrm{B}} + H_{\mathrm{I}}\,, \tag{5.19}$$

where H_{S} denotes the system part, H_{B} the heat bath part, and H_{I} the coupling between them. Note that the underlying idea of this separation is that dissipation is not something intrinsic, but something that is born out of our ignorance to focus on a small subsystem only. In this way, we observe energy transfer from the system to the outside world, i.e. relaxation, while in the total system energy is of course conserved. The simplest assumption one can make about the nature of the heat bath is that it obeys Gaussian statistics. In fact, due to the large number of degrees of freedom the *central limit theorem* guarantees this to be true for most types of environments and even for those, which are explicitly non-Gaussian, the Gaussian part is always prevailing. As a consequence, the heat bath can be modeled by a large collection of independent harmonic oscillators bilinearly coupled to the system, i.e.,

$$H_{\mathrm{B}} + H_{\mathrm{I}} = \sum_{i=1}^{N} \left[\frac{p_i^2}{2M_i} + \frac{M_i\omega_i^2}{2} \left(x_i - \frac{c_i}{M_i\omega_i^2} q \right)^2 \right] \tag{5.20}$$

with q being the system degree of freedom interacting with the surrounding. The coupling term contains the so-called counter term which removes the non-dynamical influence of the heat bath and corresponding instabilities in the system's dynamics. An other way to rationalize it, is to require that on average the system Hamiltonian is supposed to be identical with H_{S} meaning that

$$H_{\mathrm{S}} = \langle H \rangle_{\mathrm{B}} = -\frac{1}{\beta} \ln \mathrm{Tr}_{\mathrm{B}} \left\{ \mathrm{e}^{-\beta H} \right\}\,, \tag{5.21}$$

where the trace is performed over the bath degrees of freedom only.

In the sequel let us consider a Hamiltonian of the standard form

$$H_{\mathrm{S}} = \frac{p^2}{2M} + V(q)\,. \tag{5.22}$$

Classically, dissipation and noise in these systems has been studied already since the late 1950s [34, 35] and was shown to reproduce a generalized Langevin equation [14, 36] in the system's subspace: One solves the equations of motion for the bath oscillators and inserts these solutions into the system equation, which leads in a first step to

$$M\ddot{q} + M \int_0^\infty \gamma(t-s)\dot{q}(s) + V'(q) = \xi(t)\,. \tag{5.23}$$

Here, the friction kernel is defined as

$$\gamma(t) = \sum_{i=1}^{N} \frac{c_i^2}{M M_i \omega_i^2} \cos(\omega t) \tag{5.24}$$

and the stochastic force by

$$\xi(t) = -\sum_{i=1}^{N} c_i \left\{ \left[x_i(0) - \frac{c_i}{M_i \omega_i^2} q(0) \right] \cos(\omega_i t) + \frac{\dot{x}_i(0)}{\omega_i} \sin(\omega_i t) \right\} . \tag{5.25}$$

When averaging over the bath degrees of freedom according to the distribution $\exp[-\beta(H_\mathrm{B} + H_\mathrm{I})]$, the stochastic force obeys $\langle \xi(t) \rangle_\beta = 0$ and is related to the friction kernel via the dissipation fluctuation theorem $\langle \xi(t)\xi(s) \rangle = 2Mk_\mathrm{B}T\gamma(t-s)$.

In a second step one performs the limit $N \to \infty$ with a quasi-continuum of bath frequencies so that Poincare's recurrence time tends to infinity. Accordingly, one introduces a bath spectral density

$$I(\omega) = \frac{\pi}{2} \sum_{i=1}^{N} \frac{c_i^2}{M_i \omega_i} \delta(\omega - \omega_i) \tag{5.26}$$

so that the kernel takes the form

$$\gamma(t) = \frac{2}{M} \int_0^\infty \frac{\mathrm{d}\omega}{\pi} \frac{I(\omega)}{\omega} \cos(\omega t) . \tag{5.27}$$

The impact of the heat bath onto the system's dynamics is thus completely defined by temperature T and spectral density $I(\omega)$. The latter one can either be calculated numerically e.g. by means of molecular dynamics simulations or extracted experimentally by exploiting the fluctuation dissipation theorem and measuring the force-force correlation function of the bath.

Based on the Hamiltonian (5.19) the total system can now be quantized. As we have already mentioned above, this is most conveniently done in the path integral formulation, an approach pioneered by Caldeira and Leggett [20] and with numerous extensions since then [14, 37].

5.2.2 Partition Function for Quantum Dissipative Systems

Within the path integral representation (2.42) of the partition function we have for the model described in the previous Sect. 5.2.1

$$Z = \oint \mathcal{D}[q] \oint \mathcal{D}[\boldsymbol{x}] \, \mathrm{e}^{-[\bar{S}_\mathrm{S}[q] + (\bar{S}_\mathrm{B} + \bar{S}_\mathrm{I})[q, \boldsymbol{x}]]/\hbar} , \tag{5.28}$$

where $\bar{S}_\mu$, μ =S, I, B denote the Euclidian actions according to the three parts of the Hamiltonian (5.19) and $\boldsymbol{x}$ is the collection of oscillator degrees of

freedom in the environment. The Gaussian integrals over these latter paths can be done exactly which generates the effective action

$$\bar{S}_{\rm eff}[q] = \int_0^{\hbar\beta} {\rm d}\tau \left[\frac{M}{2}\dot{q}^2 + V(q)\right] + \frac{1}{2}\int_0^{\hbar\beta} {\rm d}\tau \int_0^{\hbar\beta} {\rm d}\sigma k(\tau-\sigma)\, q(\tau)q(\sigma) \quad (5.29)$$

with the kernel

$$k(\tau) = \frac{M}{\hbar\beta}\sum_{n=-\infty}^{\infty} |\nu_n|\hat{\gamma}(|\nu_n|)\, {\rm e}^{{\rm i}\nu_n\tau}\,, \quad (5.30)$$

which contains the Matsubara frequencies $\nu_n = 2\pi n/\hbar\beta$ and the Laplace transform $\hat{\gamma}$ of the classical damping (5.27). This last part in (5.29) due to the bath is also called influence functional. Thus, the quantum dissipative system is determined by the same information about the bath as the classical one, namely, temperature and spectral density. The above kernel describes a self-interaction of the system, which is non-local in (Euclidian) time and has the property

$$\int_0^{\hbar\beta} {\rm d}\tau\, k(\tau) = 0\,. \quad (5.31)$$

To be specific, in the sequel we consider an archetypical barrier potential $V(q)$ of the form (3.7) with a well located at $q = 0$ and a barrier at $q = q_{\rm b}$. In the spirit of a semiclassical evaluation of the partition function sketched for the undamped case in Sect. 3.1.2, the dominant contributions are provided by the minimal action paths and fluctuations in their vicinity. We recall the conditions for the validity of this approximation: $V_{\rm b} \gg k_{\rm B}T, \hbar\omega_0$, where $V_{\rm b}$ is the barrier height and ω_0 describes the frequency for small oscillations around the well bottom. For the minimal action paths one finds from $\delta S_{\rm eff}[q] = 0$ that

$$M\ddot{q}(\tau) - V'(q) - \int_0^{\hbar\beta} {\rm d}\sigma\, k(\tau-\sigma)\, q(\sigma) = 0 \quad (5.32)$$

and one seeks for periodic solutions with $q(0) = q(\hbar\beta)$ and $\dot{q}(0) = \dot{q}(\hbar\beta)$. In absence of dissipation these correspond to real time orbits in the inverted potential $-V(q)$, while for the dissipative case this analogy is only true qualitatively due to the periodicity of $k(\tau)$ with period $\hbar\beta$. The most convenient way to solve (5.32) is to switch to the Fourier representation

$$q(\tau) = \frac{1}{\hbar\beta}\sum_{n=-\infty}^{\infty} q_n {\rm e}^{{\rm i}\nu_n\tau}\,, \quad (5.33)$$

which leads to

$$(M\nu_n^2 + |\nu_n|\hat{\gamma}(|\nu_n|) + M\omega_0^2)q_n - \frac{3M\omega_0^2}{2q_0}\sum_{m=-\infty}^{\infty} q_m\, q_{m-n} = 0\,. \quad (5.34)$$

The full effective action is then expanded around the minimal action paths $\{q_{\rm min}^{(\alpha)}(\tau)\}_\alpha$, where in Gaussian approximation only the second order term is

taken into account, see (3.18). This fluctuation contribution is determined by the corresponding second order variational operator which reads in generalization of (3.19)

$$L_\alpha[y] = \left(-M\frac{\mathrm{d}^2}{\mathrm{d}\tau^2} + \left.\frac{\mathrm{d}^2 V(q)}{\mathrm{d}q^2}\right|_{q=q_{\min}^{(\alpha)}(\tau)} \right) y(\tau) + \int_0^{\hbar\beta} \mathrm{d}\sigma\, k(\tau-\sigma) y(\sigma)\,. \quad (5.35)$$

5.2.3 From Thermal Activation to Quantum Tunneling

For sufficiently short time intervals $\hbar\beta$, i.e. for sufficiently high temperatures, the minimal action paths coincide with the trivial paths residing at the well bottom and at the barrier top, respectively. The corresponding actions read $S[q(\tau)=0]=0$ and $S[q(\tau)=q_\mathrm{b}]=V_\mathrm{b}$. A periodic path around $q(\tau)=0$ may be written as $x(\tau)=\sum_n X_n \exp(\mathrm{i}\nu_n\tau)$ so that one has for the full action up to second order

$$S[x] = \frac{M\hbar\beta}{2} \sum_{n=-\infty}^{\infty} \Lambda_n^0\, X_n X_{-n} \quad (5.36)$$

with the eigenvalues

$$\Lambda_n^0 = \nu_n^2 + \omega_0^2 + |\nu_n|\hat{\gamma}(|\nu_n|) \quad (5.37)$$

of the second order variational operator (5.35). Likewise, for paths around $q(\tau)=q_\mathrm{b}$ one writes $y(\tau)=q_\mathrm{b}+\sum_n Y_n \exp(\mathrm{i}\nu_n\tau)$ which gives for the full action

$$S[y] = \hbar\beta V_\mathrm{b} + \frac{M\hbar\beta}{2} \sum_{n=-\infty}^{\infty} \Lambda_n^\mathrm{b}\, Y_n Y_{-n} \quad (5.38)$$

with

$$\Lambda_n^b = \nu_n^2 - \omega_\mathrm{b}^2 + |\nu_n|\hat{\gamma}(|\nu_n|)\,. \quad (5.39)$$

Here we used that $V''(q_\mathrm{b}) = -M\omega_\mathrm{b}^2$. As we already know from the undamped case in Sect. 3.1.2, there is one negative eigenvalue $\Lambda_0^\mathrm{b} = -\omega_\mathrm{b}^2$ which reflects the fact that the barrier top is a marginal point. As described there, the integral over the corresponding unstable fluctuation mode is performed by analytic continuation giving rise to an imaginary part to the partition function $Z = Z_0 + \mathrm{i}|Z_\mathrm{b}|$, where Z_0 is the well contribution and $\mathrm{i}|Z_\mathrm{b}|$ the barrier part. Accordingly, one has $F = (-1/\beta)\ln(Z_0+\mathrm{i}|Z_\mathrm{b}|) \approx (-1/\beta)\ln(Z_0) - (\mathrm{i}/\beta)|Z_\mathrm{b}|/Z_0$. Eventually, based on the relation (3.17) for temperatures above the crossover temperature and in generalization of the result (3.12), we find [38, 39, 40, 41, 42]

$$\Gamma = \frac{\omega_0}{2\pi}\frac{\omega_\mathrm{R}}{\omega_\mathrm{b}}\, f_\mathrm{q}\, \mathrm{e}^{-\beta V_b}\,, \quad (5.40)$$

where ω_R is the Grote-Hynes frequency specified in (3.95) and f_q collects the contributions of the stable fluctuation modes

$$f_\mathrm{q} = \prod_{n=1}^{\infty} \frac{\Lambda_n^0}{\Lambda_n^\mathrm{b}} = \prod_{n=1}^{\infty} \frac{\nu_n^2 + \omega_0^2 + \nu_n\hat{\gamma}(\nu_n)}{\nu_n^2 - \omega_\mathrm{b}^2 + \nu_n\hat{\gamma}(\nu_n)}\,. \quad (5.41)$$

This result coincides with the one derived within a multi-dimensional formulation in Sect. 3.3.1, which also proves that the ImF relations (3.17) apply to the damped case. The crossover temperature $T_{0,\mathrm{R}}$ defined in (3.94) follows here as the temperature, where the second least eigenvalues $\Lambda_1^{\mathrm{b}} = \Lambda_{-1}^{\mathrm{b}}$ vanish. Then, fluctuations in the corresponding direction in function space can no longer be treated in Gaussian approximation, but rather higher order terms must be taken into account. We will continue this discussion below and first analyse the impact of the quantum prefactor f_{q} in more detail (cf. Fig. 5.2 and also Fig. 5.3).

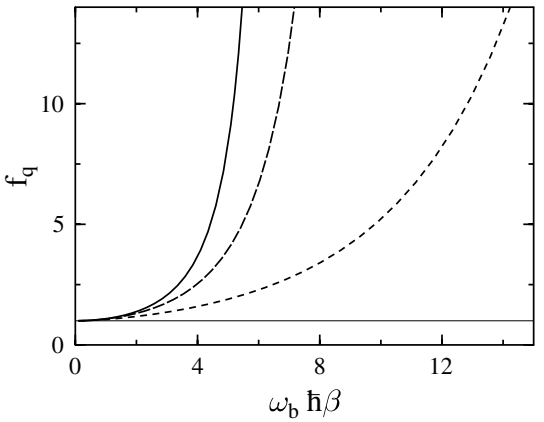

Fig. 5.2. Prefactor f_{q} (5.41) of the decay rate for $T > T_{0,\mathrm{R}}$ collecting the contributions from quantum fluctuations. Shown are data for a metastable potential with $\omega_{\mathrm{b}} = \omega_0$ and various damping strengths $\gamma/\omega_0 = 0.1$ (solid), 1 (long-dashed), and 5 (short-dashed). The thin horizontal line depicts the classical result $f_{\mathrm{q}} = 1$.

For higher temperatures, where $\omega_0\hbar\beta \ll 1$ one has in leading order

$$f_{\mathrm{q}} \approx \exp\left[\frac{\hbar^2\beta^2}{24}(\omega_0^2 + \omega_{\mathrm{b}}^2)\right] \tag{5.42}$$

with corrections of order $(\omega_0\hbar\beta)^4$ independent of the dissipation mechanism. Further, for ohmic friction with $\hat{\gamma}(z) = \gamma$ the explicit expression reads [26]

$$f_{\mathrm{q}} = \frac{\Gamma(1 - \lambda_{\mathrm{b}}^+/\nu_1)\Gamma(1 - \lambda_{\mathrm{b}}^-/\nu_1)}{\Gamma(1 - \lambda_0^+/\nu_1)\Gamma(1 - \lambda_0^-/\nu_1)}\,, \tag{5.43}$$

where $\Gamma(\cdot)$ denotes the Gamma-function and

$$\lambda_{\mathrm{b}}^{\pm} = -\frac{\gamma}{2} \pm \sqrt{\omega_{\mathrm{b}}^2 + \frac{\gamma^2}{4}} \quad , \quad \lambda_0^{\pm} = -\frac{\gamma}{2} \pm \sqrt{\frac{\gamma^2}{4} - \omega_0^2}\,. \tag{5.44}$$

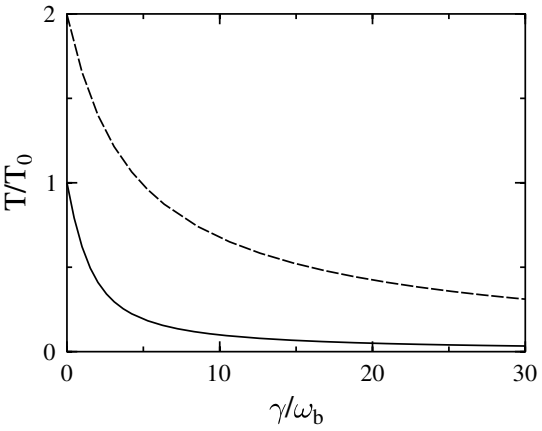

Fig. 5.3. Crossover temperature $T_{0,\mathrm{R}}$ (3.95), solid, and critical temperature T_c (6.72), dashed, for a barrier potential with frequency ω_b and ohmic friction of strength γ in units of the crossover temperature T_0 (3.14) for vanishing dissipation.

In case of very strong friction $\gamma \gg \omega_0, \omega_\mathrm{b}$ this expression simplifies to

$$f_\mathrm{q} = \exp\left\{\frac{T_{0,\mathrm{R}}}{T}\left[1+\frac{\omega_0^2}{\omega_\mathrm{b}^2}\right]\left[\Psi\left(1+\frac{\gamma^2}{\omega_\mathrm{b}^2}\frac{T_{0,\mathrm{R}}}{T}\right)-\Psi(1)\right]\right\} \tag{5.45}$$

with the digamma function $\Psi(x)$. For strong ohmic friction the crossover temperature is obtained as [see (3.95)] $T_{0,\mathrm{R}} \approx (\hbar/2\pi k_\mathrm{B})\omega_\mathrm{b}^2/\gamma$ so that $(\gamma^2/\omega_\mathrm{b}^2)T_{0,\mathrm{R}}/T = \hbar\beta\gamma/2\pi$. Then, we can look either for the high temperature limit ($\hbar\beta\gamma \ll 1$), which corresponds to the classical Smoluchowski limit, or to the range where $\hbar\beta\gamma \gg 1$, recently coined the quantum Smoluchowski range and discussed in more detail in Sect. 6.5. In the first case, (5.45) reduces to (5.42), while in the latter case one obtains

$$f_\mathrm{q} = \exp\left[\beta(M\Lambda/2)(\omega_0^2+\omega_\mathrm{b}^2)\right] \tag{5.46}$$

with the quantum Smoluchowski coefficient $\Lambda = (\hbar/\pi\gamma M)\ln(\hbar\beta\gamma/2\pi)$. This result is remarkable since it shows that even far above the crossover temperature the rate can be enhanced quite substantially, e.g. for $T = 4T_{0,\mathrm{R}}$ and $\omega_0 = \omega_\mathrm{b}$, one has $f_\mathrm{q} \approx \gamma/2\omega_\mathrm{b}$.

Let us now turn to the question about the approach of the crossover temperature [23, 24, 25, 26]. As pointed out above, when lowering the temperature from above the two eigenvalues $\Lambda_{\pm 1}^\mathrm{b}$ tend to zero and higher order terms in the expansion of the full action around the minimal action path $q(\tau) = q_\mathrm{b}$ are relevant. The actual calculation shows that this eventually leads in (5.41) to the replacement of $1/\Lambda_1^\mathrm{b}$ by

$$\frac{1}{\lambda_1^\mathrm{b}} = \frac{iM\beta}{2\pi}\int_{-\infty}^{\infty}\mathrm{d}Y_1\int_{-\infty}^{\infty}\mathrm{d}Y_{-1}\mathrm{e}^{-s_1^\mathrm{b}(Y_{-1},Y_1)/\hbar}\,. \tag{5.47}$$

The action contribution from the marginal modes is

$$s_1^{\mathrm{b}}(Y_{-1}, Y_1) = M\hbar\beta \left(\Lambda_1^{\mathrm{b}} Y_1 Y_{-1} + B\, Y_1^2 Y_{-1}^2\right) \tag{5.48}$$

with the constant B depending on the anharmonicities of the barrier potential. This action has an interesting physical meaning, which reveals the change of stability that happens to occur in the region around $T_{0,\mathrm{R}}$. Namely, upon introducing polar coordinates $Y_{\pm 1} = \rho \exp(\pm \mathrm{i}\phi)$ the action s_1^{b} depends on the amplitude ρ only and, when sweeping through the crossover, changes its topology: while for $T > T_{0,\mathrm{R}}$ the fluctuation potential $s_1^{\mathrm{b}}(\rho)$ exhibits only one minimum, it develops a bistable form for $T < T_{0,\mathrm{R}}$; at the crossover $T = T_{0,\mathrm{R}}$ the quadratic term vanishes and the potential becomes very flat around its minimum. This behavior reminds on properties known from the Landau theory of second order phase transitions, where ρ plays the role of an order parameter. Note though that this is a purely formal analogy, which was first suggested in [24, 25] and later analysed in detail in [43, 44, 45]. The described behavior of s_1^{b} displays the appearance of new minimal action paths below the crossover, the bounce paths. In the direction of the $Y_{\pm 1}$ modes these latter paths are stable for $T < T_{0,\mathrm{R}}$, while the trivial path $q(\tau) = q_b$ which is stable for $T > T_{0,\mathrm{R}}$ becomes unstable also in the Y_1, Y_{-1}-directions in function space. We recall that both types of paths are always unstable with respect to one direction in function space orthogonal to the Y_1, Y_{-1} modes. Physically, this changeover marks the setting in of deep quantum tunneling. In the crossover region the rate obeys an interesting scaling behavior of the form $y/y_0 = F(x/x_0)$, where $F(z) = \mathrm{erfc}(z)\, \exp(z^2)$ is a universal function independent of the form of the barrier potential and the dissipative mechanism and $y = \Gamma \exp(\beta V_{\mathrm{b}})$, $x = T - T_{0,\mathrm{R}}$, and with a temperature scale x_0 and a frequency scale y_0 (see [26]).

5.2.4 The Regime of Very Low Temperatures

For temperatures sufficiently below the crossover Gaussian approximations around each of the separated minima of s_1^b dominate against the contribution of the local maximum. Hence, one arrives at the situation where the bounce paths provide the leading contributions to the imaginary part of the partition function. These latter paths cover the entire barrier range so that for their explicit form one has to rely on numerical solutions of (5.33). As discussed in detail in Sect. 3.1.2, the bounce comes with one negative eigenvalue and one zero mode for the operator (5.35). The former one is treated according to Langer's analytic continuation, the latter one, which reflects time translation invariance, must be taken into account exactly. This is done by integrating the phase of the bounce over the time interval $\hbar\beta$ providing just a prefactor since the full action is independent of the phase. Accordingly, one arrives for the rate at the formal expression (3.20), where the determinants included in the prefactor must be calculated numerically as well.

Some analytical results are available at temperatures around $T = 0$, for ohmic friction, and a harmonic+cubic potential (3.7) with barrier height V_b. For the bounce action one finds for weak damping and small temperatures [26]

$$S_\mathrm{B} = \frac{36}{5}\frac{V_\mathrm{b}}{\omega_0}\left[1 + \frac{45\zeta(3)}{2\pi^3}\frac{\gamma}{\omega_0} - \frac{5}{2\pi}\left(\frac{\nu_1}{\omega_0}\right)^2 - \frac{\pi}{12}\frac{\gamma}{\omega_0}\left(\frac{\nu_1}{\omega_0}\right)^4\right] \tag{5.49}$$

with $\zeta(3) = 1.202\ldots$ being a Riemann number. Here, corrections are of order $(\gamma/\omega_0)^2, (\gamma/\omega_0)\nu_1^6/\omega_0^6$. In the opposite limit of strong friction the result reads [25, 26]

$$S_\mathrm{B} = 3\pi\frac{\gamma}{\omega_0}\frac{V_\mathrm{b}}{\omega_0}\left[1 - \frac{4\pi}{3}\left(\frac{\gamma}{\omega_0^2\hbar\beta}\right)^2\right] \tag{5.50}$$

with corrections of order ω_0/γ. For the prefactor of the quantum rate appearing in the form $\Gamma = \Omega_\mathrm{q}\exp(-S_\mathrm{B}/\hbar)$ the calculation at zero temperature yields for weak friction

$$\Omega_\mathrm{q} = 6\omega_0\sqrt{\frac{6V_\mathrm{b}}{\pi\hbar\omega_0}}\left(1 + c\frac{\gamma}{2\omega_0}\right) \tag{5.51}$$

with a constant $c \approx 2.8$ [25, 46]. In the opposite limit of strong friction one has in leading order [26]

$$\Omega_\mathrm{q} = 8\omega_0\sqrt{\frac{6V_\mathrm{b}}{\hbar\omega_0}}\left(\frac{\gamma}{2\omega_0}\right)^{7/2}. \tag{5.52}$$

Hence, due to the dynamics of the bounce orbit, friction now appears not only in the prefactor, but also in the action. The rate becomes thus very sensitive to the strength of dissipation (cf. Fig. 5.4) with the overall tendency that increasing friction suppresses the tunneling.

The enhancement of quantum tunneling by finite temperature fluctuations is according to the above results of the form $\Gamma(T) = \Gamma(T=0)\exp(A_2\,T^2)$. The quadratic temperature dependence originates from low frequency fluctuation modes in the bath and is specific for an ohmic environment [47]. More generally, it has been shown that for spectral densities of the form $I(\omega) \propto \omega^s$ the temperature enhancement is given by $\exp(A_s\,T^{s+1})$ [14].

5.2.5 Validity of the ImF Approach

According to Sect. 3.1.2, for vanishing friction the ImF approach can for all temperatures directly be derived from a WKB type of calculation and tends for very high temperatures towards the classical TST expression (3.13). The only requirement here are sufficiently high barriers $V_b \gg \hbar\omega_0, k_\mathrm{B}T$ to justify the semiclassical approximation and the corresponding rates must be understood in the sense of a quantum transition state theory.

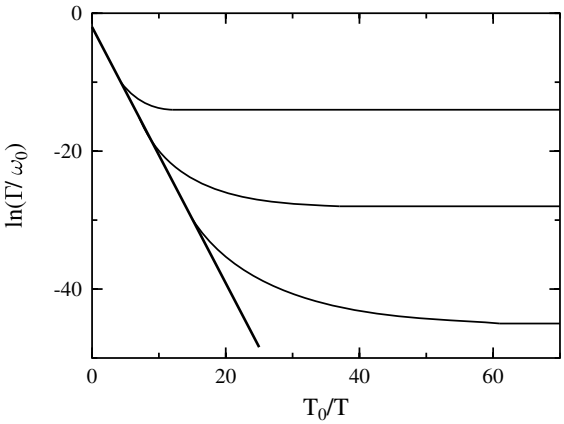

Fig. 5.4. Decay rate vs. inverse temperature for a cubic potential (3.7) and various ohmic friction strengths $\gamma/\omega_0 = 0$ (top), 1 (middle), 2 (bottom). Barrier height is $V_\mathrm{b}/\hbar\omega_0 = 5$ and the thick straight line depicts the classical result.

In the dissipative case one knows that for high temperatures the ImF rate reproduces (5.40) with $f_q = 1$, which is the Kramers rate in the spatial diffusion limit, i.e. for sufficiently strong friction. This indicates that there must be an additional condition on friction for the applicability of the method. In fact, as a thermodynamical approach the ImF technique assumes that locally thermal equilibrium is maintained inside the well region. For temperatures above the crossover this means that friction must be strong enough to restrict the nonequilibrium state to the vicinity of the barrier top. On the other hand, for very low temperatures only the ground state of the quasi-stationary energy states in the well is basically populated so that deviations from thermal equilibrium are absent. Hence, the range of validity of the ImF method with respect to friction grows towards lower temperatures to apply for sufficiently low temperatures for basically all damping strengths [15]. Explicit conditions, however, can only be obtained within a real-time formulation addressed in Chap. 6.

5.3 Decay of the Zero Voltage State in Josephson Junctions

The Josephson junction has been introduced in Sect. 3.1.3 as a mesoscopic device to experimentally study the tunneling out of a metastable well. While a qualitative understanding of the experimental data is provided by the rate theory for vanishing friction, a quantitative comparison necessitates the inclusion of dissipation [10, 26]. At temperatures above the crossover temperature friction appears in the prefactor of the rate only [cf. (5.40)], while at very low

temperatures the bounce action depends very strongly on the damping mechanism due to the fact that the bounce is a dynamical orbit [cf. (5.49), (5.50)]. For the analysis of the experimental data and the verification of theoretical predictions, it is convenient to work with the escape temperature $T_{\rm esc}$, see (3.36). Then, one has in the classical regime [48]

$$T_{\rm esc} = \frac{T}{1 - p_{\rm cl}}\,, \tag{5.53}$$

where $p_{\rm cl} = \ln(\omega_{\rm R}/\omega_0)/(\beta V_{\rm b})$ with the plasma frequency ω_0 specified in (3.32). In the moderate friction range, where most experiments are performed, $p_{\rm cl}$ is much smaller than 1. At very low temperatures, the escape temperature saturates to reach at $T = 0$ for weaker friction [see (5.49)]

$$T_{\rm esc} = \frac{\hbar\omega_0}{7.2 k_{\rm B}} \frac{1}{(1 + 0.87/Q)(1 - p_{\rm q})} \tag{5.54}$$

with $p_{\rm q} = \ln(2\pi\Omega_{\rm q}/\omega_0)/[(7.2V_{\rm b}/\hbar\omega_0)(1+0.87/Q)]$, where Q denotes the quality factor of the junction $Q = \omega_0/\gamma$. The quantum correction $p_{\rm q}$ is large enough to contribute substantially. Experimental data have been shown to be in remarkable agreement with these predictions of the ImF theory [10, 48]. In particular, the crossover from thermal activation to quantum tunneling has been observed (see Fig. 5.5) and quantitatively followed the theoretical predictions. At very low temperatures the strong suppression of the tunneling rate with increasing friction, i.e. with a decreasing Q-factor, has been verified. The

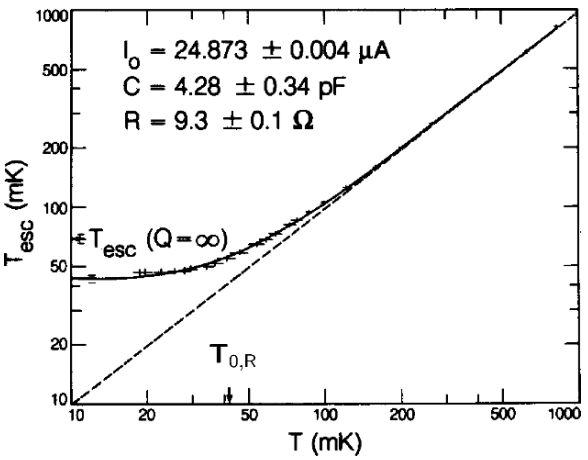

Fig. 5.5. Escape temperature (3.36) vs. temperature for a shunted JJ with $Q = 1.8$. The solid curve depicts the full theoretical and the dashed line the classical prediction. The crossover temperature and the predicted $Q = \infty$ (no dissipation) escape temperature are indicated (arrows). Courtesy of the Quantronics Group (SPEC), CEA Saclay.

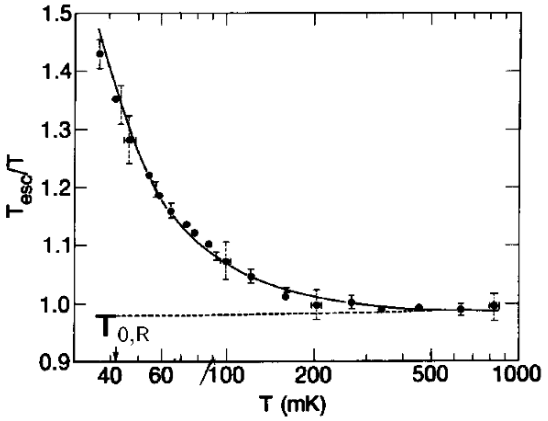

Fig. 5.6. Rate enhancement $T_{\rm esc}/T$ (solid) above the classical value (dashed) for temperatures above the crossover temperature $T_{0,\rm R}$ (cf. Fig. 5.2). Parameters are the same as in Fig. 5.5. Courtesy of the Quantronics Group (SPEC), CEA Saclay.

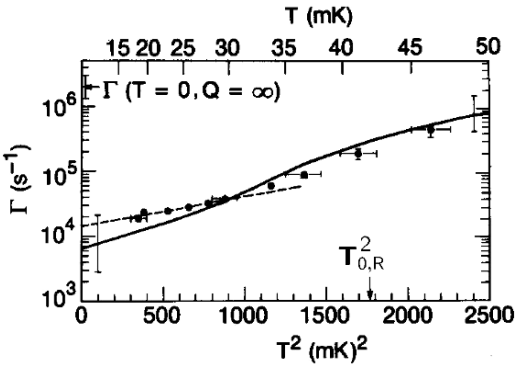

Fig. 5.7. Escape rate as a function of the square of the temperature. Theory (solid line) predicts a T^2 dependence in the low temperature regime. Parameters are the same as in Fig. 5.5. Courtesy of the Quantronics Group (SPEC), CEA Saclay.

same is true for the influence of quantum fluctuations above the crossover. Deviations of $T_{\rm esc}/T$ from unity clearly reveal the role of the enhancement factor $f_{\rm q}$ (5.41) and are in good agreement with the theoretical expressions (see Fig. 5.6). As mentioned in the previous Section, a striking prediction of the theory is a rate enhancement $\Gamma(T)/\Gamma(T=0) \propto T^2$ due to low frequency environmental modes. This has been tested as well (see Fig. 5.7) and gives direct information about the nature of the electrical environment since this quadratic dependence is a characteristic signature of an ohmic bath. For spectral densities of the form $I(\omega) \propto \omega^{\alpha-1}$ one expects an enhancement according to $\Gamma(T)/\Gamma(T=0) \propto T^{\alpha}$ [14].

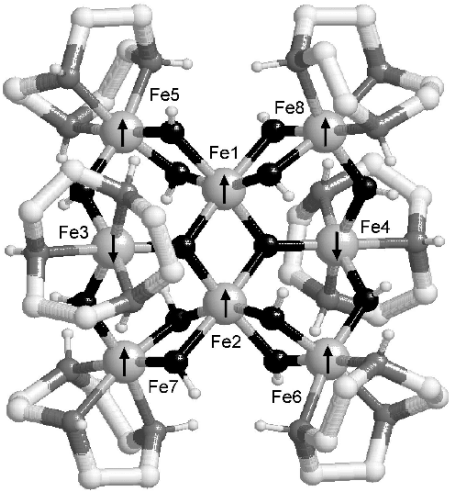

Fig. 5.8. Schematic view of the magnetic core of a Fe_8 cluster. The oxygen atoms are black, the nitrogen atoms are gray, and carbon atoms are white. The arrows represent the spin structure of the ground state $S = 10$ as experimentally determined through polarized neutron diffraction experiments [61]. Courtesy of W. Wernsdorfer, University Grenoble.

5.4 Tunneling of Magnetization

In crystals of Mn_{12} and Fe_8 clusters interatomic correlations lead to an alignment of the atomic spins such that effectively each cluster constitutes a nanomagnet with net spin $S = 10$ and longitudinal and transverse anisotropy [49]. While early research has focused on these types of molecular structures, meanwhile a variety of other materials has been shown to reveal a similar type of behavior. Comprehensive reviews are given in [49, 50]. Due to the anisotropy the spin states along the easy axis (say, the z-axis) are not eigenstates, but rather may tunnel. In contrast to tunneling of a continuous coordinate, here, the tunneling process occurs between discrete spin states. When an external magnetic field is applied along the easy axis the relative position of these states can be tuned and resonant tunneling may appear. The presence of environmental degrees of freedom such as phonons, nuclear spins, and dipolar fields, introduce dissipation in the process of spin tunneling [51, 52, 53]. In fact, not only thermally activated escape and quantum tunneling between ground states have been observed [54, 55, 56, 57], but also phonon assisted tunneling [58, 59, 60], termed thermally activated tunneling (TAT).

The simplest model describing the spin system of Fe_8 molecular clusters has the Hamiltonian

$$H = -DS_z^2 + E(S_x^2 - S_y^2) - g\mu_{\rm B}\boldsymbol{S}\boldsymbol{H}\,, \tag{5.55}$$

where S_x, S_y, S_z are the three components of the spin, $D > 0$ and $E > 0$ are anisotropy constants, and the last term describes the coupling to an external field with Bohr magneton μ_B and gyromagnetic moment $g > 0$. Note that here and in the following $\hbar$ has been absorbed in the coefficients such that the spin operators are dimensionless and S_z has eigenstates $S_z|S, M\rangle = M|S, M\rangle$ with eigenvalues M, $-10 \leq M \leq 10$. Since $D \gg E$, for vanishing external field $\boldsymbol{H} = 0$ the energy levels are approximately given by $E_M = -DM^2$ so that there is an energy barrier between the two ground states $M = \pm 10$ (see Fig. 5.9). Experimentally, this barrier was determined to be about 70 K for Mn_{12} and 25 K for Fe_8 [62, 63]. The anisotropy in the transverse directions induces tunneling between these levels, which without an external field is, at least for transitions between lower lying states, extremely small though. When an external field $-H_z$ along the easy axis is applied, energy levels with $M < 0$ increase, while those with $M > 0$ decrease. Hence, for fields for which $E_M + g\mu_B M H_z = E_{M'} + g\mu_B M' H_z$ resonant tunneling occurs. When the field is applied along the x-axis, tunneling can also be enhanced and even Landau-Zener transitions can be induced [64, 65].

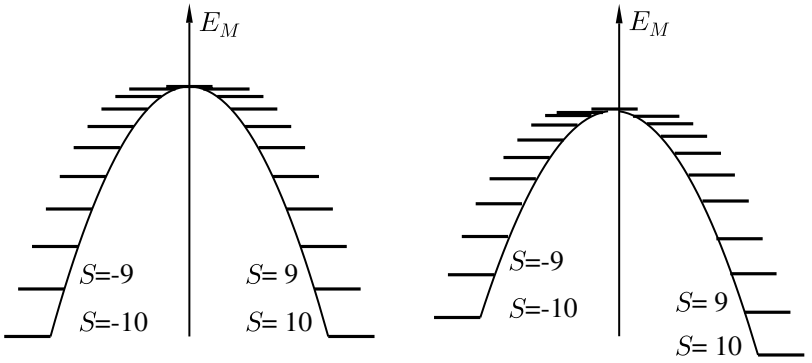

Fig. 5.9. Energy levels of a nanomagnet with $S = 10$ unbiased (left) and biased by an external magnetic field (right). See text for details.

Theories to calculate tunneling rates for these systems have exploited the ImF method as well, where $1/S$ serves as the semiclassical expansion parameter [66, 67]. The first step is to write a path integral expression for the partition function. This is conveniently done in a coherent spin basis [68]

$$|\boldsymbol{n}\rangle = \mathrm{e}^{\mathrm{i}\theta(\boldsymbol{n}\times\boldsymbol{n}_0)\boldsymbol{S}}\,|S, S\rangle \tag{5.56}$$

with $\boldsymbol{n} = (\cos(\phi)\sin(\theta), \sin(\phi)\sin(\theta), \cos(\theta))$ and $\boldsymbol{n}_0 = (0, 0, \cos(\theta))$. In order to calculate tunneling rates one considers transition matrix elements $R = \langle \boldsymbol{n}_1| \exp(-TH)|\boldsymbol{n}_2\rangle$ for very large T. Here, $\boldsymbol{n}_1 = \boldsymbol{n_2}$ is the metastable direction in case of tunneling out of a metastable state, while $\boldsymbol{n}_1$ and $\boldsymbol{n_2}$ denote

energetically degenerate ground states in case of macroscopic quantum coherence. Since for large T one has $R \to \exp(-E_0 T)$, where due to the instability the ground state energy E_0 carries a small imaginary part, the rate follows according to ImF theory as $\Gamma = (-2/T)\mathrm{Im}\{\ln(R)\}$. The spin-coherent-state path integral representation of the matrix element R is then given by [68]

$$R = N \int \mathcal{D}\boldsymbol{n}\ \mathrm{e}^{-S_\mathrm{E}[\boldsymbol{n}]/\hbar} \tag{5.57}$$

with a normalization N and the Euclidian action

$$S_\mathrm{E}[\boldsymbol{n}] = \int_{-T/2}^{T/2} \mathrm{d}\tau \left[-\mathrm{i}\hbar S \cos(\theta)\dot{\phi} + E(\theta,\phi) \right] , \tag{5.58}$$

where $E(\theta,\phi) = \langle \boldsymbol{n}|H|\boldsymbol{n}\rangle$. All paths run from $\boldsymbol{n}(-T/2) = \boldsymbol{n}_1$ to $\boldsymbol{n}(T/2) = \boldsymbol{n}_2$. The first term in (5.58) is the so-called Wess-Zumino term and a result of the topology of the Bloch sphere on which the spin coherent states live. Now, in the second step the minimal action paths need to be determined, which in turn causes a problem. Namely, the two equations of motion for the minimal action paths $\bar{\theta}(\tau)$ and $\bar{\phi}(\tau)$ are only first order in time due to the fact that the above action does not contain a kinetic energy contribution. Since one has four boundary conditions to obey, the problem is overdetermined and a solution does in general not exist. This problem can be resolved by adding a regularization term $\eta S [\dot{\theta}^2 + \sin^2(\theta)\dot{\phi}^2]$ to the integrand (5.58) with the prescription to take the limit $\eta \to 0$ at the very end [69]. As a consequence, the classical paths develop a boundary layer at $\tau = \pm T$ with width of order η, where they jump from the original boundary values to new ones $\boldsymbol{n}_1', \boldsymbol{n}_2'$. One can then work with the original equations of motion supplemented with these new boundary conditions outside the boundary layer. Eventually, the tunneling rate takes the usual form

$$\Gamma = A\ \mathrm{e}^{-S_\mathrm{ma}/\hbar} \tag{5.59}$$

with the minimal action S_ma and the fluctuation prefactor A.

To be specific, we consider a model Hamiltonian similar to (5.55), namely, $H = -DS_z^2 + ES_y^2 + \gamma S_z H_z$ [67] . In the coherent spin state representation one has up to a constant

$$E(\theta,\phi) = \left[D + E\sin^2(\phi) \right] \sin^2(\theta) + \gamma S H_z \cos(\theta) . \tag{5.60}$$

In the limit of small $\epsilon = 1 - H_z/H_\mathrm{c}$ with $H_\mathrm{c} = 2D/(S\gamma)$ this reduces for small θ up to a constant to

$$E(\theta,\phi) \approx D\epsilon\theta^2 + E\theta^2\sin^2(\phi) - \frac{D}{4}\theta^4 , \tag{5.61}$$

thus describing a metastable well. The corresponding minimal action paths read $\bar{\theta}(\tau) = 2\sqrt{\epsilon}/\sinh(\omega\tau)$ and $\bar{\phi}(\tau) = -\mathrm{i}\sqrt{D\epsilon/E}\tanh(\omega\tau) + n\pi$, where $\omega = (2/\hbar S)\sqrt{DE\epsilon}$ and $n = 0$ or $n = 1$. Hence, the minimal action is gained as

$$S_{\rm ma} = \sqrt{\frac{64D}{9E}}\,\epsilon^{3/2}\hbar S\,, \tag{5.62}$$

while the fluctuation prefactor is obtained as $A = 2\omega\sqrt{12S_{\rm ma}/2\pi}$.

Another example is a Hamiltonian of the form $H = -DS_z^2 - \gamma H_x S_x + \gamma^2 H_x^2 S^2/4D$ (see [67] for details), which describes an isolated Mn_{12} cluster in a transverse magnetic field and neglecting the fourth order anisotropy. Then, one has

$$E(\theta,\phi) = D[\sin(\theta) - \sin(\theta_0)] + 2D\sin(\theta_0)\sin(\theta)[1-\cos(\phi)] \tag{5.63}$$

with $\sin(\theta_0) = H_x\gamma S/2D$. In this case one has two degenerate ground states at angles $\theta = \theta_0, \phi = 0$ and $\theta = \pi - \theta_0, \phi = 0$, respectively, connected by macroscopic spin coherence. The calculation gives for the tunnel splitting

$$\Delta = \frac{8D}{\sqrt{\pi\hbar^2 S}}\frac{\cos^{5/2}(\theta_0)}{\sin(\theta_0)}\left[\frac{1-\cos(\theta_0)}{1+\cos(\theta_0)}\right]^{\cos(\theta_0)/2} {\rm e}^{-S_{\rm ma}/\hbar} \tag{5.64}$$

with

$$S_{\rm ma} = 2S\hbar\left\{-\cos(\theta_0) + \frac{1}{2}\ln\left[\frac{1+\cos(\theta_0)}{1-\cos(\theta_0)}\right]\right\}. \tag{5.65}$$

In the limit of $H \to 2D/\gamma S$, i.e. $\theta_0 \to \pi/2$, one regains the known result for the tunnel splitting of the ground state doublet in a double well potential (3.75).

The type of calculation sketched above, allows also to include dissipative effects, which turned out to be crucial for understanding the experimental data [51, 52, 53]. Experiments [54, 57] revealed that the relaxation of an initially prepared magnetization displays a clear signature for the crossover from thermal activation to temperature independent quantum tunneling. Figure 5.10 displays a nice example for Fe_8 clusters, where for lower temperatures the relaxation rate becomes temperature independent compared to the classical regime of thermal activation. However, not only the expected relatively sharp crossover between these two regime has been seen, but also a rather smooth one, which has been interpreted as TAT [58, 59, 60], see Fig. 5.11 for results on Mn_{12} nanomagnets. Apparently, at temperatures far below the energy barrier (below 2K), the location of the peaks corresponding to resonant tunneling move gradually to higher external fields with descreasing temperature and saturate only in the low temperature regime (below 1K). In this intermediate temperature range not only resonant tunneling transitions occur, but also phonon induced transitions to nearest and next nearest energy levels from which tunneling is greatly enhanced, which leads also to a specific broadening of the resonances. This phenomenon has been described in terms of master equations with a Caldeira-Leggett type of phonon bath [70, 71].

The nanomagnets discussed above have all an even net spin. One may wonder whether there is a deeper reason for this and indeed that is the case.

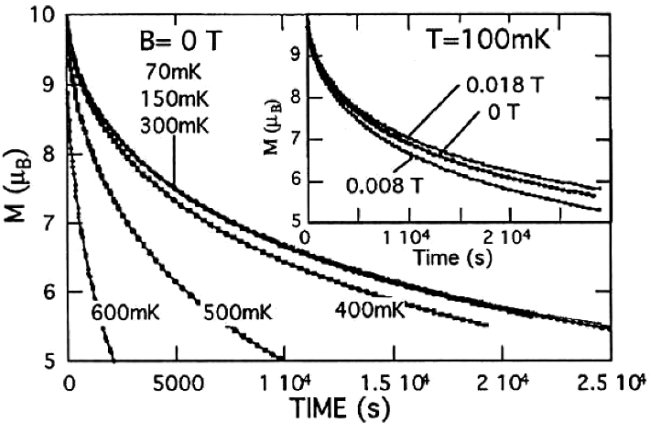

Fig. 5.10. Relaxation of the magnetization in Fe_8 clusters measured at $B = 0$T after first saturating in a field of 3.5 T. For $T < 4$mK curves superimpose showing that the relaxation is independent of temperature T. Inset shows subtle field dependence near resonance. Reprinted with permission from [58]; ©(1997) by the American Physical Society.

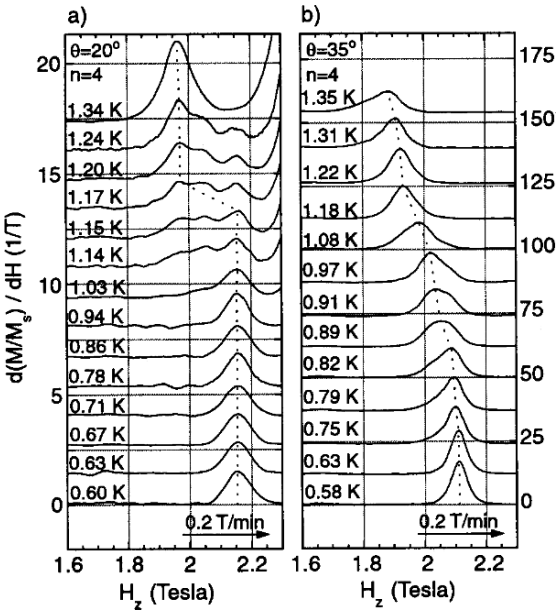

Fig. 5.11. Field derivative of normalized magnetization vs H_z at different temperatures for Mn_{12} clusters and for two orientations of the applied field and magnetic easy axis: (a) $\theta = 20°$, showing an abrupt crossover, and (b) $\theta = 35°$, showing a smooth crossover to quantum tunneling. The curves are offset for clarity. The dashed lines mark the position of the maximum dM/dH. Note that the data on graphs (a) and (b) are plotted on different scales. Reprinted with permission from [59]; ©(2000) by the American Physical Society.

Namely, it has been shown theoetically within semiclassical type of arguments that due to the topological Wess-Zumino term quantum tunneling is completely suppressed for half integer spin systems according to a destructive interference of tunneling paths on the Bloch sphere [72, 73]. This result can also be seen as a direct consequence of the so-called Kramers' theorem [74].

5.5 MQT in Presence of Non-Gaussian Noise

So far we have assumed that the environmental fluctuations obey Gaussian statistics. However, this is sometimes only a very good approximation to reality. An important example for this situation is the current noise produced when charges flow through a mesoscopic conductor. The granularity of the charges generates in the simplest case shot noise, already discussed by Schottky in 1918 [75]. Within the last decade, electrical noise has moved into the focus of research activities on electronic transport in nanostructures [76], since it provides information on microscopic mechanisms of the transport not available from the voltage dependence of the average current. Presently, attention has turned from the noise auto-correlation function (shot noise) to higher order cumulants of the current fluctuations characterizing non-Gaussian statistics [77, 78].

While theoretical attempts to predict these cumulants for a variety of devices are quite numerous [78], experimental observation is hard because of small signals, large bandwidth detection, and strict filtering demands. As a pioneering result the third moment of current noise produced in a tunnel junction has been extracted in [79] by analog amplifiers and filtering techniques and later on also in [80]. Since then strong efforts have been made towards on-chip detection schemes, first because they are faster and second because they give access to finite frequency noise properties. Lately, in [81, 82] the full distribution of charges flowing through a quantum dot has been detected in the low frequency regime. The goal now is to push devices forward into higher frequency ranges (GHz), where quantum effects, electron-electron interactions, and plasmon dynamics are relevant. In this context several new proposals for experimental set-ups have been put forward, some of which are based on Josephson junctions (JJ) as noise detectors [83, 84, 85, 86]. In the sequel we analyse how to exploit the exponential sensitivity of the tunneling rate on noise to extract information about the current statistics [87].

In experimental set-ups to measure higher order cumulants, heating (due to residual thermal noise and the Gaussian portion of the electrical noise) is one of the major experimental obstacles [88, 86]. Thus, many experiments have primarily attempted to establish just the unspecified non-Gaussian nature of the noise or to measure the third cumulant (skewness). The latter one is particularly accessible since it can be discriminated from purely Gaussian noise due to its asymmetry, e.g. when inverting the current through the conductor. This is in contrast to the fourth order cumulant (sharpness), which

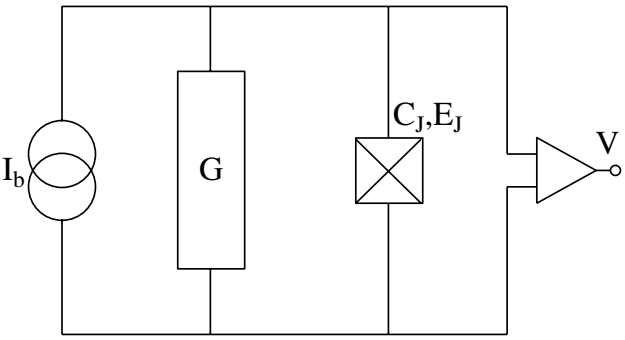

Fig. 5.12. Electrical circuit containing a mesoscopic conductor G in parallel to a JJ with capacitance $C_{\rm J}$ and coupling energy $E_{\rm J}$ biased by an external current $I_{\rm b}$. The switching out of the zero voltage state of the JJ by MQT is detected as a voltage pulse V.

on the one hand due to heating effects may be completely hidden behind the second and the third one, but on the other hand is required to gain an essentially complete characterization of the distribution of current fluctuations. In the set-up we consider in the sequel, see Fig. 5.12, a nanoscale conductor is placed in parallel to a current biased JJ in the zero voltage state, so that no heating occurs prior to the decay of this state by MQT (Macroscopic Quantum Tunneling). However, the MQT rate is modified in a specific way by the even higher order cumulants characterizing the non-Gaussian current fluctuations of the conductor.

The complete statistics of current noise generated by a mesoscopic conductor can be gained from the generating functional

$$G[\phi] = \mathrm{e}^{-S_{\rm G}[\phi]} = \left\langle \mathcal{T} \exp\left[\frac{\mathrm{i}}{e}\int_{\mathcal{C}} dt I(t)\phi(t)\right]\right\rangle , \tag{5.66}$$

where $I(t)$ is the current operator and $\mathcal{T}$ the time ordering operator along the Kadanoff-Baym contour $\mathcal{C}$. Time correlation functions of arbitrary order of the current are determined from functional derivatives of $G[\phi]$, in particular, the average current

$$C_1(t) = \langle I(t)\rangle = \mathrm{i}e\ \partial S_{\rm G}[\phi]/\partial\phi(t)|_{\phi=0} \tag{5.67}$$

and the current auto-correlation function

$$C_2(t,t') = \langle I(t)\, I(t')\rangle = e^2\ \partial^2 S_{\rm G}[\phi]/\partial\phi(t)\partial\phi(t')\big|_{\phi=0} . \tag{5.68}$$

Higher order functional derivatives give the cumulants related to non-Gaussian current fluctuations

$$C_n(t_1,\ldots,t_n) = -(-\mathrm{i}e)^n\ \partial^n S_{\rm G}[\phi]/\partial\phi(t_1)\cdots\partial\phi(t_n)|_{\phi=0} . \tag{5.69}$$

We remark that the functional $S_{\rm G}[\phi]$ carries the full frequency dependence of all current cumulants and not just their time averaged zero frequency values usually studied in the field of full counting statistics [77].

To see the relation with the Gaussian heat baths discussed previously, let us consider an Ohmic resistor of resistance R in thermal equilibrium at inverse temperature β. Then, the functional $S_{\rm G}[\phi] \equiv S_R[\phi]$ takes the well-known form

$$S_{\rm R}[\phi] = \frac{1}{2}\frac{h}{e^2 R}\int_{\mathcal{C}} {\rm d}t \int_{\mathcal{C}} {\rm d}t'\, \alpha(t-t')\ \phi(t)\,\phi(t')\,, \tag{5.70}$$

where

$$\alpha(t) = \frac{\pi}{2\,(\hbar\beta)^2\,\sinh^2(\pi t/\hbar\beta)}\,. \tag{5.71}$$

The quadratic action $S_{\rm R}$ turns out to be identical to the influence functional in (5.29), which adds to the bare action of the system to give the effective action. Hence, the functional $S_{\rm G}$ generalizes the concept of an influence functional to non-Gaussian environments. For instance, for a tunnel junction with many transmission channels, where each channel has a small transmission coefficient T_i leading to the dimensionless conductance $g_{\rm T} = h/(4\pi\, e^2 R_{\rm T}) = \pi \sum_i T_i$, with $R_{\rm T}$ being the tunneling resistance, one has [89]

$$S_{\rm T}[\phi] = -4 g_{\rm T} \int_{\mathcal{C}} {\rm d}t \int_{\mathcal{C}} {\rm d}t'\, \alpha(t-t') \sin^2\left[\frac{\phi(t)-\phi(t')}{2}\right]. \tag{5.72}$$

Here, the periodicity in ϕ reflects the discreteness of the transferred charges associated with non-Gaussian current fluctuations.

The MQT rate Γ can now be calculated in the standard way from the ImF method with the effective action $S_{\rm eff}[\theta] = S_{\rm JJ}[\theta] + S_{\rm G}[\theta/2]$. Here

$$S_{\rm JJ}[\theta] = \frac{1}{\hbar}\int_0^{\hbar\beta} {\rm d}\tau \left[\frac{1}{2}\phi_0^2 C_{\rm J}\dot{\theta}(\tau)^2 + U(\theta)\right] \tag{5.73}$$

is the action of the bare JJ and $S_{\rm G}$ is the generating functional of current fluctuations of the conductor introduced above. In (5.73) $\phi_0 = \hbar/2e$ denotes the reduced flux quantum, $C_{\rm J}$ is the capacitance of the JJ, and the tilted washboard potential is $U(\theta) = -E_{\rm J}[\cos(\theta) - s\,\theta]$, where $E_{\rm J}$ is the Josephson energy and $s = I_{\rm b}/I_{\rm c}$. The factor of 2 in the argument of $S_{\rm G}$ arises from the fact that the voltage across the conductor equals the voltage $V_{\rm J} = (\hbar/e)(\dot{\theta}/2)$ across the JJ.

In the MQT regime, where the contribution of the bounce paths dominate, the partition function can now be calculated for arbitrary coupling between detector and conductor based on a numerical scheme sketched above around (5.34) and further elaborated in [26]. For this purpose, one approximates a well-barrier segment of $U(\theta)$ around a well minimum $\theta_{\rm m}$ by a harmonic+cubic potential, $V(\delta\theta) = (M\Omega^2/2)\,\delta\theta^2(1 - \delta\theta/\delta\theta_0)$ with $\delta\theta = \theta - \theta_{\rm m}$ and $\Omega = \Omega(s)$ the frequency for small oscillations around the well bottom (plasma

frequency). Analytical progress is made when the noise generating element has a dimensionless conductance $g_\mathrm{T} \ll E_\mathrm{J}/\hbar\Omega$ so that the influence of the noise on the MQT rate can be calculated by expanding about the unperturbed bounce at vanishing temperature

$$\theta_B(\tau) = \frac{\delta\theta_0}{\cosh^2(\Omega\tau/2)}\,. \tag{5.74}$$

This gives the approximate tunneling rate

$$\Gamma = \Gamma_0\, \mathrm{e}^{-S_\mathrm{G}[\theta_\mathrm{B}/2]}\,, \tag{5.75}$$

where Γ_0 is the tunneling rate in absence of the environment [see (3.8)]. The correction $S_\mathrm{G}[\theta_\mathrm{B}/2]$ is usually dominated by the second cumulant C_2 and the fourth cumulant C_4. Note that this approximation still contains the full dynamics of detector and noise source since any approximation relying on a time scale separation, as e.g. the adiabatic limit considered in [90], is usually not applicable.

Now, in case of a tunnel junction as noise element one finds for $S_\mathrm{G}[\theta_\mathrm{B}/2] \equiv S_\mathrm{T}[\theta_\mathrm{B}/2]$ from (5.71) and (5.72)

$$S_\mathrm{T}[\theta_\mathrm{B}/2] = \frac{g_\mathrm{T}}{4\pi}\int_0^\infty \mathrm{d}\omega\,\omega\,|\tilde{\rho}(\omega)|^2 \tag{5.76}$$

with

$$\tilde{\rho}(\omega) = \int_{-\infty}^{\infty}\mathrm{d}\tau\,\mathrm{e}^{\mathrm{i}\theta_\mathrm{B}(\tau)/2}\,\mathrm{e}^{\mathrm{i}\omega\tau}\,.$$

We note in passing that a finite capacitance C_T of the tunnel junction can easily be taken into account by replacing C_J by $C = C_\mathrm{J} + C_\mathrm{T}$. By expanding the first exponential and performing the Fourier transform for each power of $\theta_\mathrm{B}(\tau)$ separately, the relevant part $\rho(\omega) = \tilde{\rho}(\omega) - 2\pi\delta(\omega)$ reads

$$\rho(\omega) = \frac{\pi}{4}\frac{\omega}{\sinh(\pi\omega/\Omega)}\sum_{k=1}^{\infty}\frac{(2\mathrm{i}\delta\theta_0)^k}{k!\,(2k-1)!}\prod_{l=1}^{k-1}\left(\frac{\omega^2}{\Omega^2}+l^2\right). \tag{5.77}$$

This way, the result (5.76) can be cast into

$$S_\mathrm{T}[\theta_\mathrm{B}/2] = \frac{g_\mathrm{T}}{4\pi^3}\sum_{k,k'=1}^{\infty} I_{k,k'}\,\delta\theta_0^{k+k'} \tag{5.78}$$

with the coefficients

$$I_{k,k'} = \frac{(-1)^{(3k+k')/2}\,2^{k+k'}}{k!k'!(2k-1)!(2k'-1)!}\,A_{kk'}\,. \tag{5.79}$$

Here,

$$A_{kk'} = \int_0^\infty dy \frac{y^3 \mathrm{e}^y}{(\mathrm{e}^y - 1)^2} \left[\prod_{l=1}^{k-1} \left(\frac{y^2}{4\pi^2} + l^2\right)\right] \left[\prod_{l=1}^{k'-1} \left(\frac{y^2}{4\pi^2} + l^2\right)\right] \tag{5.80}$$

with $A_{kk'} = A_{k'k}$ so that $I_{k,k'} \neq 0$ only for $k + k'$ even. This means that all odd cumulants of the fluctuating current vanish according to a vanishing net current $\langle I(t)\rangle = 0$ through the conductor. Specifically, one finds

$$\begin{aligned} A_{11} &= 6\zeta(3) \\ A_{22} &= 6\zeta(3) + \frac{5!\,\zeta(5)}{2\pi^2} + \frac{7!\,\zeta(7)}{16\pi^4} \\ A_{31} &= 24\zeta(3) + 5\frac{5!\,\zeta(5)}{4\pi^2} + \frac{7!\,\zeta(7)}{16\pi^4}\,. \end{aligned} \tag{5.81}$$

The terms in the sum (5.78) related to a contribution of order $\delta\theta_0^{k+k'}$ determine the impact of the $(k + k')$th-moment of the current fluctuations of the tunnel junction onto the MQT process. Since in (5.77) the term of order $\delta\theta_0^k$ contains contributions centered around $\omega \approx 0, \Omega \ldots, k\Omega$, the influence of the $(k + k')$th-moment results from mode mixing between fluctuations with frequencies $l\,\Omega$ and $l'\,\Omega$ where $l \leq k, l' \leq k'$.

In lowest order, $k + k' = 2$, one gains from (5.78) the Gaussian noise contribution providing a correction to the bare MQT rate [cf. (5.49)]

$$\Gamma_{\mathrm{T}}^{(2)} = \Gamma_0 \exp\left[-\frac{6\zeta(3)\,g_{\mathrm{T}}}{\pi^3}\,\delta\theta_0(s)^2\right]. \tag{5.82}$$

At order $\delta\theta_0^4$ the sum (5.78) gives three contributions, namely, $k = 1, k' = 3$ and $k = 3$, $k' = 1$ with $A_{13} = A_{31}$ as well as $k = 2, k' = 2$ with A_{22}. This leads to

$$\Gamma_{\mathrm{T}}^{(4)} = \Gamma_{\mathrm{T}}^{(2)} \exp\left[\frac{4\,g_{\mathrm{T}}}{\pi^3}\,(2A_{31} - A_{22})\,\delta\theta_0(s)^4\right] \tag{5.83}$$

so that the fourth order cumulant of the current noise contains both, fluctuations that suppress tunneling (related to A_{22}) and fluctuations that increase MQT (related to A_{31}). Since $2A_{31} - A_{22} > 0$, the total impact of the fourth moment leads to an *enhancement* of the MQT rate.

For the on-chip detection circuit proposed here, the impact of the fourth order cumulant needs to be clearly distinguishable from effects of purely Gaussian noise. This is provided by considering the function

$$B(x) = -\ln[\Gamma(x)/\Gamma_0(x)] \tag{5.84}$$

with the variable $x = (1 - s^2)/s^2$. It allows to discriminate between weak Gaussian and non-Gaussian noise due to a qualitatively different scaling behavior: as Fig. 5.13 illustrates, at low temperatures purely Gaussian noise results essentially in a straight line for $B(x)$, while non-Gaussian noise displays a nonlinear behavior. Even more pronounced are the differences in the

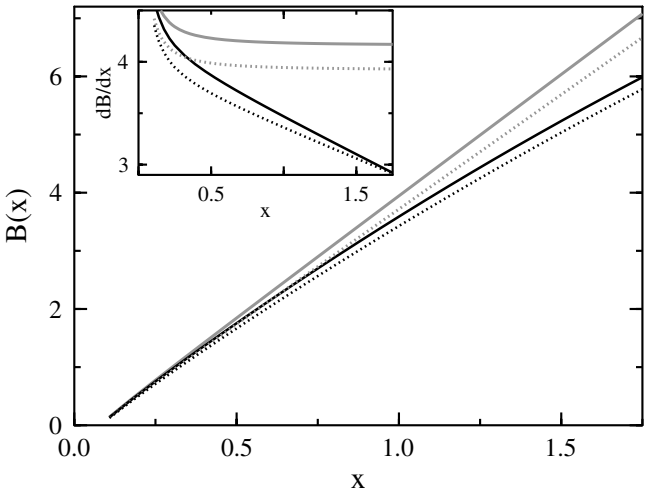

Fig. 5.13. $B(x) = -\ln[\Gamma(x)/\Gamma_0(x)]$ vs. $x = (1-s^2)/s^2$ (dimensionless bias current s) for a tunnel junction (black) and an ohmic resistor (grey) with identical second cumulant. Solid lines display the situation in absence, dashed lines in presence of additional Gaussian noise in the wiring with $R/R_{\rm T} = 0.05$. The inset displays the corresponding slopes $dB(x)/dx$. Parameters are $\sqrt{E_{\rm J}/E_{\rm C}} = 10, g_{\rm T} = 2$, $\Omega(s = 0)$=100 GHz.

slopes $\mathrm{d}B(x)/\mathrm{d}x$, which saturate in the former case away from the domain of small x-values, but strongly decrease with increasing x in the latter one. Hence, determining from $B(x)$ the derivatives $\mathrm{d}B(x)/\mathrm{d}x$ gives direct access to the impact of higher than second order cumulants in the noise fluctuations of the conductor. This scaling property is rather robust, since it holds for any sort of Gaussian/non-Gaussian noise. In particular, additional Gaussian noise present in the wiring and comprised in an additional resistor with resistance $R \ll R_{\rm T}$ [cf. Eq. (5.70)] merely shifts $\mathrm{d}B(x)/\mathrm{d}x$ and thus does not spoil the scaling behavior originating from C_4 (see Fig. 5.13). Further, by fitting $\mathrm{d}B(x)/\mathrm{d}x$ with (5.82), the coefficient $2A_{31} - A_{22}$ related to C_4 in (5.83) can be extracted.

5.6 Dissipative Tunneling in Bistable Potentials

The calculation of tunnel splittings in bistable systems is based on the instanton approach presented for the non-dissipative case in Sect. 3.2. In case of interaction with a thermal environment the situation becomes much more complex, because the system, initially confined in one the wells, may not only coherently oscillate between the minima (quantum coherence), but also irreversibly decay towards equilibrium (incoherent decay). In the sequel we

first collect some main theoretical results and then turn to a specific system, namely, rotational tunneling in molecular complexes.

5.6.1 Instantons and Dissipation

To be specific, let us consider a double well potential of the form shown in Fig. 3.10 with potential minima located at $\pm a$ separated by a barrier of height V_b and with a frequency ω_0 around the well bottoms. We also allow for a small aysmmetry $\hbar\epsilon = V(-a) - V(a)$ between the well minima. Then, the parameters which govern the different dynamical situations are the non-dissipative tunnel splitting Δ, the typical frequency for the separation of adjacent energy doublets ω_0 with $\omega_0 \gg \Delta$, temperature $k_\mathrm{B}T$, and dimensionless friction strength $\alpha = M\gamma a^2/(2\pi\hbar)$ [γ is the friction strength appearing in the classical Langevin equation, see (5.1)]. In principle, also the nature of the spectral bath density matters but for the moment we assume an ohmic bath with a very large cut-off. Coherent tunneling then only exists in the parameter range (see Fig. 5.14)

$$\alpha < \frac{1}{2} \quad , \quad \frac{k_\mathrm{B}T}{\hbar\Delta} \ll \frac{1}{\alpha} \quad , \quad \epsilon < \Delta \,. \tag{5.85}$$

Apart from this domain, the situation is a follows. For $V_\mathrm{b} \gg k_\mathrm{B}T \gg \hbar\omega_0$ quantum effects are weak and the relaxation from one well to the other occurs dominantly by incoherent thermal activation, at somewhat lower temperatures influenced by quantum fluctuations. Accordingly, the results derived from the ImF theory above the crossover apply so that one finds for the difference $P(t)$ between populations in left and right well

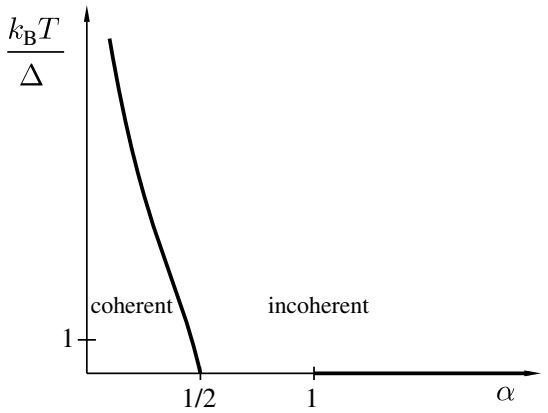

Fig. 5.14. Sketch of the phase diagram for a symmetric bistable potential. Shown are the regions of coherent dynamics (tunneling oscillations) and of incoherent decay. The thick solid line for $T = 0$ and $\alpha \geq 1$ indicates the domain of completely frozen dynamics (localization).

$$P(t) = P_\infty + (1 - P_\infty)\,\mathrm{e}^{-\Gamma t}\,, \tag{5.86}$$

where $P_\infty = \tanh(\hbar\beta\epsilon)/2$ is the thermal value of $P(t)$ and $\Gamma = \Gamma_+ + \Gamma_-$ is the total rate as a sum of forward Γ_+ and backward rate Γ_-. The latter ones are related by detailed balance via $\Gamma_- = \Gamma_+ \exp(-\hbar\beta\epsilon)$, so that it suffices to gain one of these rates from the ImF calculation. Note that the partition function must be calculated here in a subspace of the total Hilbert space only, because otherwise an imaginary part would not appear due to the stability of the system.

For temperatures $V_\mathrm{b} \gg \hbar\omega_0 \gtrsim k_\mathrm{B}T \gg \hbar\Delta$ and apart from the range of very small values of α [cf. 5.85)], incoherent tunneling dominates the relaxation and the ImF approach adapted to the bistable situation can be applied as well. It turns out that a treatment based on single instanton paths leads to infrared divergencies in case of ohmic friction. These divergencies cancel when one considers pairs of instantons and anti-instantons, so-called extended bounces, which then leads to an approximate scheme generalizing the dilute instanton gas approximation to the dilute bounce gas approximation (DBGA). Namely, the intra-bounce interactions introduced by dissipation are much stronger than those between different bounces. The dilute gas of instantons thus becomes a dilute gas of bounces or equivalently, the gas of charged particles turns into a gas of strongly bound dipoles. The full action is invariant against translations of the center of mass of an extended bounce and the corresponding zero mode is treated as described above. The relative separation of the instanton–anti-instanton pair is related to an unstable fluctuation mode, the breathing mode, which gives rise to the imaginary part of the partition function. Eventually, the forward rate is obtained as

$$\Gamma_+ = \frac{\Delta_*^2}{4}\,\frac{1}{\omega_0}\left(\frac{2\pi}{\omega_0\hbar\beta}\right)^{2\alpha-1} \mathrm{e}^{\hbar\beta\epsilon/2}\,\frac{|\Gamma(\alpha + \mathrm{i}\hbar\beta\epsilon/(2\pi))|^2}{\Gamma(2\alpha)}\,, \tag{5.87}$$

where the contribution with a dressed tunnel splitting Δ_* reads

$$\frac{\Delta_*^2}{4} = \frac{1}{2\pi\hbar}\left(\prod_{n=0}^{\infty} \Lambda_n^{(0)} \Big/ \prod_{n=2}^{\infty} \Lambda_n^{(\mathrm{B})}\right)^{1/2} \sqrt{\rho}\;\mathrm{e}^{-S_\mathrm{B}/\hbar}\,. \tag{5.88}$$

In this expression S_B is the action of the bounce without the interaction between instanton and anti-instanton and without a contribution due to the asymmetry given by $\hbar\epsilon\tau_1$ with τ_1 being the length of the extended bounce. Further, $\Lambda_n^{(0)}$ are the eigenvalues of the second order variational operator in the well, while $\Lambda_n^{(\mathrm{B})}$ are those around the bounce, and

$$\rho = \int_{-\hbar\beta/2}^{\hbar\beta/2} \mathrm{d}\tau \left[\frac{\partial q_\mathrm{B}(\tau,\tau_s)}{\partial\tau}\right]^2 \times \int_{-\hbar\beta/2}^{\hbar\beta/2} \mathrm{d}\tau \left[\frac{\partial q_\mathrm{B}(\tau,\tau_s)}{\partial\tau_s}\right]^2 \tag{5.89}$$

with the bounce orbit $q_\mathrm{B}(\tau,\tau_s)$ of length $\tau_s = (\hbar\beta/\pi)\mathrm{arccot}[\hbar\beta\epsilon/(2\pi\alpha)]$. The result (5.87) indicates that the tunneling process is dominated by the contribution of a single bounce, i.e. two traversals of the barrier range. The dilute bounce gas approximation is valid as long as $\tau_s\Gamma_+ \ll 1$ meaning that

$\tau_s \ll 1/\Delta_*^2$, which is valid for $\epsilon = 0$ down to $T \to 0$ if $\alpha > 1$; for finite ϵ the range of validity down to $T = 0$ is even broader. Specifically, one finds from (5.87) at $T = 0$ and for $\epsilon > 0$ [i.e. $V(-a) > V(a)$] that

$$\Gamma_+ = \frac{\Delta^2}{2\omega_0} \frac{\pi}{\Gamma(2\alpha)} \left(\frac{\epsilon}{\omega_0}\right)^{2\alpha-1} , \tag{5.90}$$

while for $\epsilon < 0$ the forward rate vanishes, $\Gamma_+ = 0$. At zero temperature and for $\epsilon = 0$ even a phase transition occurs at $\alpha = 1$ such that for larger friction the incoherent tunneling dynamics is completely frozen, i.e. $\Gamma_+ = \Gamma_- = 0$, and the initially prepared wave packet remains trapped (localization), see Fig. 5.14.

At temperatures $V_\mathrm{b} \gg \hbar\omega_0 \gg k_\mathrm{B}T, \hbar\Delta, \hbar\epsilon$ the continuous bistable potential can be truncated to its lowest lying doublet, thus leading to a spin boson (SB) description [14]. The two level system is parametrized by the asymmetry ϵ and the dressed tunnel coupling Δ_* so that its Hamiltonian reads $H_\mathrm{TLS} = -(\hbar\Delta_*/2)\sigma_x + (\hbar\epsilon/2)\sigma_z$ with the Pauli-matrices σ_x, σ_z. The SB model is an archetypical model on its own with various realizations in physics. The literature about its thermodynamic and real-time properties is huge and we refer to [14] for more details since its study is not directly related to semiclassical approximations for tunneling processes. Basically, the tunneling in the coherent domain (5.85) occurs via damped oscillations and the explicit calculation gives for $\epsilon = 0$

$$P(t) = \frac{\cos(\Omega t - \phi)}{\cos(\phi)} \, \mathrm{e}^{-\Gamma t} \tag{5.91}$$

with $\tan(\phi) = \Gamma/\Omega$. The tunnel frequency is obtained as

$$\Omega = \Delta_\mathrm{eff} \left\{1 + 2\alpha \left[\mathrm{Re}\{\psi(\mathrm{i}\hbar\beta\Delta_\mathrm{eff}/2\pi) - \ln(\hbar\beta\Delta_\mathrm{eff}/2\pi)\right]\right\} \tag{5.92}$$

and the relaxation rate is given by

$$\Gamma = \frac{\pi\alpha}{2} \Delta_\mathrm{eff} \coth(\hbar\beta\Delta_\mathrm{eff}/2) \, . \tag{5.93}$$

Here, it has been convenient to introduce an effective tunnel splitting

$$\Delta_\mathrm{eff} = [\Gamma(1-2\alpha)\cos(\pi\alpha)]^{1/2/(1-\alpha)} \left(\frac{\Delta_*}{\omega_0}\right)^{\alpha/(1-\alpha)} \Delta_* \, , \tag{5.94}$$

which is apparently the actual frequency scale for oscillations between the two states. The result for finite ϵ has also been gained, although by extending the scheme of the dilute bounce gas approximation [for the spin boson system the DBGA has been coined non-interacting blip approximation (NIBA)]. Namely, for a biased system ($\epsilon \neq 0$) the NIBA predicts a wrong asymptotic population difference P_∞ due to the fact that inter-blip correlations are neglected. For the explicit treatment beyond NIBA we refer to [14]. In case of vanishing friction

the known coherent oscillations are regained from the expression (5.90) with a frequency calculated in Sect. 3.2.

The dynamics in dissipative bistable systems has seen an intensive amount of work in the past, cf. [14]. Here, we address some recent developments and discuss an explicit example in the next Section. One has appeared in the context of quantum information processing based on superconducting circuits. There, two-level systems or qubits are implemented at low temperatures in SQUID devices so that only the ground state doublet of the SQUID potential for the magnetic flux matters [91] (see Sect. 3.2.2). Noise processes induce dephasing and, to a weaker extent, also relaxation in these systems causing e.g. Rabi-oscillations to decay on time scales of a few hundred nanoseconds. A detailed understanding of this decay is necessary to develop efficient schemes to fight against noise sources. Another field of application is related to the relaxation dynamics in molecular nanomagnets described in the previous Sect. 5.4. As seen there, noise from residual degrees of freedom gives rise to a complex tunneling dynamics of the collective spin which includes photon assisted tunneling. Accordingly, the two level description must be extended to include higher lying doublets [92].

5.6.2 Rotational Tunneling in Metal Hydride Complexes

Rotational tunneling has been found in a variety of compounds, where small molecular groups are attached to larger structures [93]. Since tunneling frequencies depend very sensitively on the shape of the rotational barrier, spectroscopy provides insight in the energy landscape of complex molecules.

As a particular example, we discuss here diatomic hydrogen molecules in form of H_2 or D_2 that can bind to transition metal complexes to built strongly bound dihydrides [94], for recent reviews see [95, 96]. In these compounds the individual hydrogen atoms are not fixed in space, but can exchange their positions while keeping the distances between each other and between the metal complex constant. Accordingly, their mutual exchange can be seen as a hindered 180° rotation around the axis intersecting the metal–dihydrogen angle [97]. The rotational barrier originates primarily from the chemical structure of the binding to the metal and in some cases also from crystal effects of neighboring molecules.

The simplest model to describe this situation is that of a one-dimensional rigid rotator with angular position ϕ as the only degree of freedom. The corresponding Hamilton operator reads

$$H_{\rm rot} = -\frac{\hbar^2}{2Mr^2}\frac{{\rm d}^2}{{\rm d}\phi^2} - V_0\,[1-\cos(2\phi)]\;, \tag{5.95}$$

where $2V_0$ is the height of the rotational barrier. Due to symmetry the spatial eigenfunctions of this Hamiltonian decompose into classes with even and odd parity, respectively, and tunnel splittings occur between adjacent states with

opposite symmetry (doublets). These wave functions are connected to spin states in such a way that the total wave functions are either antisymmetric (in the fermionic case H_2) or symmetric (in the bosonic case D_2). Accordingly, a spin tunnel Hamiltonian can be defined that describes the splitting within each doublet which in turn, via the corresponding tunnel frequency, is directly visible in measured spectra [98]. These frequencies vary from 10^{12} Hz for dihydrogen in gas phase, where fast coherent oscillations have been detected by incoherent neutron scattering (INS), to a few Hz in the liquid phase, where NMR spectroscopy has been applied (see e.g. [99]). In particular, NMR techniques have been used to study solid state structures with di-deuterons as metal ligands [96, 98].

In addition to coherent processes the interaction with residual vibronic degrees of freedom leads to incoherent transitions (thermal activation), particularly, at sufficiently high temperatures. Usually, several pairs of eigenstates are thermally populated so that the effective frequency of coherent oscillations and the effective incoherent rate result, in a rough estimate, from a thermal average over the individual tunnel frequencies and incoherent transition rates, respectively. Experimentally, the spin-system in thermal equilibrium is prepared via a $\pi/2$-pulse and the corresponding relaxation of the nonequilibrium state is observed [95, 98]. To theoretically describe this process in different temperature domains requires a density matrix approach, where here a weak coupling Born-Markov type of master equation applies. Typical spectral data are depicted in Fig. 5.15. While for temperatures above 20 K a broad central line indicates purely incoherent decay, at lower temperatures the width of the central line increases and additional satellites appear at frequencies of about ± 60 kHz. It turns out that these data can be understood by assuming a superposition of coherent and incoherent transitions. The strong temperature dependence of the latter ones is clearly seen in the Arrhenius plot, see Fig. 5.16, where in contrast the tunneling frequency is basically constant. Note that the incoherent rate exhibits a bi-exponential behavior, which cannot be reproduced in a one-dimensional tunneling model [Bell model, which is based on a WKB-type evaluation of (3.1)], but necessitates the treatment of at least a two-dimensional process. Anyway, the changeover from purely incoherent to a mixed incoherent/coherent and eventually a prevailing coherent tunneling process is clearly seen and illustrates the theoretical findings discussed in the previous Section.

5.7 Centroid Theory

The idea of the *centroid theory* is to calculate the quantum rate from a thermodynamic distribution that can be seen as the quantum analog to the classical Boltzmann distribution $\exp[-\beta V(q)]$ [100, 101]. Accordingly, one introduces the center of mass of a minimal action path $q(\tau)$ of the Euclidian path integral of the partition function Z, the so-called centroid, as

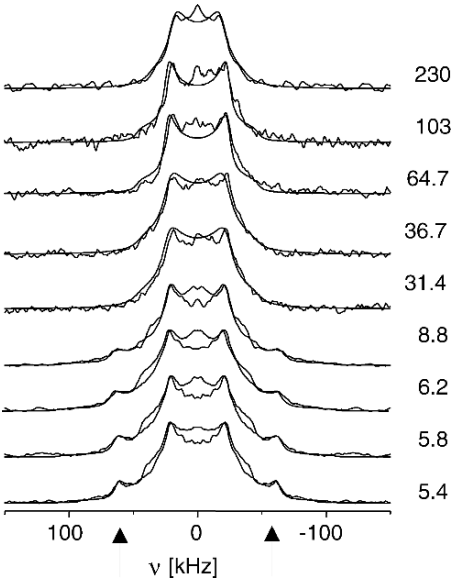

Fig. 5.15. Experimental and simulated (smooth curves) ^{2}H NMR spectra of a Ru-D_2 complex, measured in the temperature range from 5.4. to 230 K. At temperatures below 8.8 K a splitting in the line shape is clearly visible (arrows). This splitting can be explained by a coherent tunneling of the deuterons in the Ru–D_2 sample. For the details of the simulations see [98]. Courtesy of G. Buntkowsky, University of Jena.

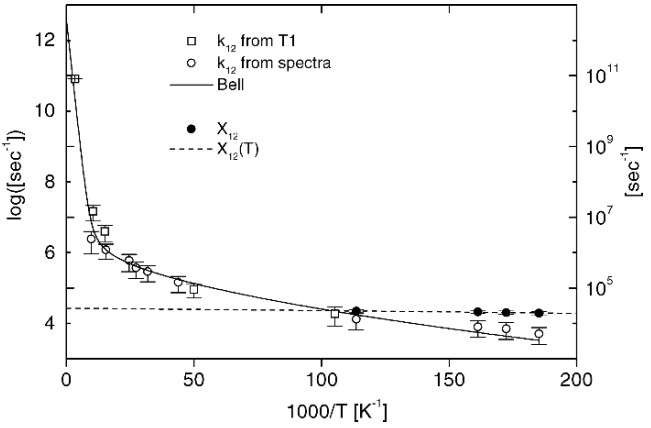

Fig. 5.16. Arrhenius plot of the temperature dependence of the coherent (X_{12}, black dots, right scale) and incoherent (k_{12}, open squares and dots, left scale) exchange rates extracted from Fig. 5.15. The solid line is the result of a fit of the temperature dependence of the incoherent rates using a modified tunnel model (see [98] for details). The dashed line is a simple linear fit to the coherent tunnel frequencies. Courtesy of G. Buntkowsky, University of Jena.

$$q_0 = \frac{1}{\hbar\beta}\int_0^{\hbar\beta} \mathrm{d}\tau\, q(\tau)\,. \tag{5.96}$$

The probability distribution or centroid density with q_0 constrained to some particular position R is then

$$\begin{aligned}\rho(R) &= \frac{1}{Z}\mathrm{Tr}\left\{\delta(q_0 - R)\mathrm{e}^{-\beta H}\right\} \\ &= \frac{1}{Z}\oint \mathcal{D}[q]\ \delta(q_0 - R)\mathrm{e}^{-S_E[q]/\hbar}\end{aligned} \tag{5.97}$$

with $Z = \int \mathrm{d}\, R\rho(R)$. Indeed, for all temperatures above the crossover temperature, where $q(\tau)$ collapses to either $q(\tau) = 0$, the constant path at the well bottom, or $q(\tau) = q_b$, the constant path at the barrier top, for the latter one we have $\rho(q_b) \propto \exp(-\beta V_b)$. Below the crossover the bounce paths dominate over the constant barrier path. Thus, fixing the center of mass of the bounce is equivalent as to fixing its phase. In the spirit of our discussion in Sect. 3.1.2 this means that one picks a certain representative out of the set of equivalent bounces, the action of which then, as we have seen, provides the exponential contribution to the tunneling rate. In this sense the centroid theory is completely equivalent to the ImF approach [102, 103] and provides a powerful tool to numerically evaluate, e.g. by means of equilibrium Monte Carlo techniques, the partition function and the corresponding rate.

However, there are differences. Namely, from the formally exact expression for the rate (3.85) one derives that the rate can be cast into the form

$$\mathit{\Gamma} = \frac{1}{Z}\int \mathrm{d}R\ \rho(R)\,\nu(R) = \rho(q^*)\,\bar{v} \tag{5.98}$$

where q^* denotes the transition point, in the simplest case $q^* = q_\mathrm{b}$, and $\nu(R)$ collects the real-time contributions. Further, one defines the average (dynamical factor)

$$\bar{v} = \int \mathrm{d}R\ \nu(R)\,[\rho(R)/\rho(q^*)] \tag{5.99}$$

so that the thermodynamic part is factorized from the dynamical part [104, 105, 106, 107, 108]. The former one is, as we have seen, responsible for the exponential in the rate and can be calculated also numerically. There, the location of q^* may even serve as a variational parameter to find the state where $\rho(R)$ is the smallest, i.e. the bottleneck of the transition. The more complicated task though is the dynamical factor $\bar{v}$. In general, an exact evaluation requires a full real-time evolution of the problem even for long times which is out of reach for complex systems. In this situation various approximations have been invoked comprising analytical results for the parabolic barrier or semiclassical approximations [104, 105].

Without going into further details, we note that the advantage of the centroid method is that it allows for efficient numerical simulations of the

decay since one needs to create only configuration near the transition point q^*. On the other hand, one still relies on the factorization (5.98) with certain assumptions about the dynamical factor. These are based on the observation that in many cases the dynamical factor $\nu(R)$ is sharply peaked around $R = q^*$, where $\rho(R)$ is minimal. However, cases have been analysed [109] where this is not true so that this empirical finding cannot be turned into a rigorous statement.

References

1. A.J. Leggett. *Prog. Theor. Phys. (Suppl.)*, 69:80, 1980.
2. W. den Boer and R. de Bruyn Ouboter. *Physica B*, 98:85, 1980.
3. R.J. Prance, A.P. Long, T.D. Clark, A. Widom, J.E. Mutton, J. Sacco, M.W. Potts, G. Megaloudis, and F. Goodall. *Nature*, 289:543, 1981.
4. R.F. Voss and R.A. Webb. *Phys. Rev. Lett.*, 47:265, 1981.
5. L.D. Jackel, J.P. Gordon, E.L. Hu, R.E. Howard, L.A. Fetter, D.M. Tennant, R.W. Epworth, and J. Kurkijarvi. *Phys. Rev. Lett.*, 47:697, 1981.
6. M.H. Devoret, J.M. Martinis, and J. Clarke. *Phys. Rev. Lett.*, 55:1908, 1985.
7. J.M. Martinis, M.H. Devoret, and J. Clarke. *Phys. Rev. Lett.*, 55:1543, 1985.
8. S. Washburn, R.A. Webb, R.F. Voss, and S.M. Faris. *Phys. Rev. Lett.*, 54:2712, 1985.
9. D.B. Schwartz, B. Sen, C.N. Archie, and J.E. Lukens. *Phys. Rev. Lett.*, 55:1547, 1985.
10. M.H. Devoret, D. Esteve, C. Urbina, J. Martinis, A. Cleland, and J. Clarke. In Yu. Kagan and A.J. Leggett, editors, *Quantum Tunneling in Solids*. Elsevier, 1992.
11. S. Tagaki. *Macroscopic Quantum Tunneling*. Cambridge, 2002.
12. H. Grabert, P. Schramm, and G.-L. Ingold. *Phys. Rep.*, 168:115, 1988.
13. A.0. Caldeira and A.J. Leggett. *Physica A*, 121:587, 1983.
14. U. Weiss. *Quantum Dissipative Systems*. World Scientific, 1999.
15. P. Hänggi, P. Talkner, and M. Borkovec. *Rev. Mod. Phys.*, 62:251, 1990.
16. M.D. Kostin. *J. Chem. Phys.*, 57:3589, 1972.
17. H. Dekker. *Phys. Rev. A*, 16:2116, 1977.
18. W.H. Louisell. *Quantum Statistical Properties of Radiation*. Wiley, 1973.
19. A.O. Caldeira and A.J. Leggett. *Phys. Rev. Lett.*, 46:211, 1981.
20. A.O. Caldeira and A.J. Leggett. *Ann. Phys. (USA)*, 149:374, 1983.
21. A.O. Caldeira and A.J. Leggett. *Ann. Phys. (USA)*, 153:445(E), 1984.
22. H. Grabert, U. Weiss, and P. Hänggi. *Phys. Rev. Lett.*, 52:2193, 1984.
23. H. Grabert and U. Weiss. *Phys. Rev. Lett.*, 53:1787, 1984.
24. A.I. Larkin and Yu.N. Ovchinnikov. *Sov. Phys.-JETP*, 37:382, 1983.
25. A.I. Larkin and Yu.N. Ovchinnikov. *Sov. Phys.-JETP*, 59:420, 1984.
26. H. Grabert, P. Olschowski, and U. Weiss. *Phys. Rev. B*, 36:1931, 1987.
27. H. Risken. *The Fokker Planck Equation*. Springer, 1984.
28. D.J. Tannor and D. Kohen. *J. Chem. Phys.*, 100:4932, 1994.
29. H.A. Kramers. *Physica*, 7:284, 1940.
30. H. Grabert. *Phys. Rev. Lett.*, 61:1683, 1988.
31. E. Pollak, H. Grabert, and P. Hänggi. *J. Chem. Phys.*, 91:4073, 1989.

32. R.F. Grote and J.T. Hynes. *J. Chem. Phys.*, 73:2715, 1980.
33. P. Hänggi and F. Mojtabai. *Phys. Rev. A*, 26:1168, 1982.
34. V.B. Magalinskiĭ. *Sov. Phys. JETP*, 9:1381, 1959.
35. P. Ullersma. *Physica*, 32:27,56,74,90, 1966.
36. R. Zwanzig. *J. Stat. Phys.*, 9:215, 1973.
37. H.P. Breuer and F. Petruccione. *The Theory of Open Quantum Systems*. Oxford University Press, 2002.
38. P.G. Wolynes. *Phys. Rev. Lett.*, 47:968, 1981.
39. V.I. Melnikov and S.V. Meshkov. *JETP Letters*, 38:130, 1983.
40. P. Hänggi, H. Grabert, G.L. Ingold, and U. Weiss. *Phys. Rev. Lett.*, 55:761, 1985.
41. E. Pollak. *Phys. Rev. A*, 33:4244, 1986.
42. E. Pollak. *Chem. Phys. Lett.*, 177:178, 1986.
43. E. Chudnovsky. *Phys. Rev. A*, 46:8011, 1992.
44. E.M. Chudnovsky and D.A. Garanin. *Phys. Rev. Lett.*, 79:4469, 1997.
45. S.P. Kou, J.Q. Liang, and F.C. Pu. *J. Phys.: Condensed Matter*, 13:2627, 2001.
46. E. Freidkin, P.S. Riseborough, and P. Hänggi. *Phys. Rev. A*, 32:237, 1986.
47. J.M. Martinis and H. Grabert. *Phys. Rev. B*, 38:2371, 1988.
48. J.M. Martinis, M.H. Devoret, and J. Clarke. *Phys. Rev. B*, 35:4682, 1987.
49. L. Gunther and B. Barbara, editors. *Quantum Tunneling of Magnetization – QTM94*. Kluwer, 1995.
50. E. Chudnovsky and J. Tejada. *Macroscopic Quantum Tunneling of the Magnetic Moment*. Cambridge, 2005.
51. A. Garg. *Phys. Rev. Lett.*, 70:1541, 1993.
52. N.V. Prokof'ev and P.C.E. Stamp. *J. Phys.: Condens. Matter*, 5:L663, 1993.
53. A. Garg. *J. Appl. Phys.*, 76:6168, 1994.
54. J.R. Friedman, M. Sarachik, J. Tejada, and R. Ziolo. *Phys. Rev. Lett.*, 76:3830, 1996.
55. J.M. Hernandez, X.X. Zhang, F. Louis, J. Bartolome, J. Tejada, and R. Ziolo. *Europhys. Lett.*, 35:301, 1996.
56. J.M. Hernandez, X.X. Zhang, F. Louis, J. Tejada, J.R. Friedmann, M.P. Sarachik, and R. Ziolo. *Phys. Rev. B*, 55:5858, 1996.
57. L. Thomas, F. Lionti, R. Ballou, D. Gatteschi, R. Sessoli, and B. Barbara. *Nature*, 383:145, 1996.
58. C. Sangregorio, T. Ohm, C. Paulsen, R. Sessoli, and D. Gatteschi. *Phys. Rev. Lett.*, 78:4645, 1997.
59. L. Bokacheva, A.D. Kent, and M.A. Walters. *Phys. Rev. Lett.*, 85:4803, 2000.
60. I. Chiorescu, R. Giraud, A.G.M. Jansen, A. Caneschi, and B. Barbara. *Phys. Rev. Lett.*, 85:4807, 2000.
61. W. Wernsdorfer. *Adv. Chem. Phys.*, 118:99, 2001.
62. R. Sessoli, D. Gatteschi, A. Caneschi, and M.A. Novak. *Nature*, 365:141, 1993.
63. A.-L-Barra, P. Debrunner, D. Gateschi, C.E. Schulz, and R. Sessoli. *Europhys. Lett.*, 35:133, 1996.
64. W. Wernsdorfer and R. Sessoli. *Science*, 284:133, 1999.
65. W. Wernsdorfer, R. Sessoli, A. Caneschi, D. Gatteschi, and A. Cornia. *Europhys. Lett.*, 50:552, 2000.
66. E.M. Chudnovsky and L. Gunther. *Phys. Rev. Lett.*, 60:661, 1988.
67. A. Garg and G.-H. Kim. *Phys. Rev. B*, 45:12921, 1991.
68. E. Fradkin. *Field Theories of Condensed Matter Systems*. Addison-Wesley, 1991.

69. J.R. Klauder. *Phys. Rev. D*, 19:2349, 1979.
70. D.A. Garanin and E.M. Chudnovsky. *Phys. Rev. B*, 56:11102, 1997.
71. M.N. Leuenberger and D. Loss. *Phys. Rev. B*, 61:1286, 2000.
72. D. Loss, D.P. DiVincenzo, and G. Grinstein. *Phys. Rev. Lett.*, 69:3232, 1992.
73. J. van Delft and C.L. Henle. *Phys. Rev. Lett.*, 69:3236, 1992.
74. L.D. Landau and E. Lifshitz. *Quantum Mechanics*. Pergamon, 1976.
75. W. Schottky. *Ann. Phys. (Leipzig)*, 57:541, 1918.
76. Y.M. Blanter and M. Büttiker. *Phys. Rep.*, 336:1, 2000.
77. L.S. Levitov, H.B. Lee, and G.B. Lesovik. *J. Math. Phys.*, 37:4845, 1996.
78. Y.V. Nazarov, editor. *Quantum Noise in Mesoscopic Physics*, NATO Science Series in Mathematics, Physics and Chemistry, Kluwer, 2003.
79. B. Reulet, J. Senzier, and D.E. Prober. *Phys. Rev. Lett.*, 91:196601, 2003.
80. Yu. Bomze *et al. Phys. Rev. Lett*, 95:176601, 2005.
81. T. Fujisawa, T. Hayashi, Y. Hirayama, H.D. Cheong, and Y.H. Jeong. *Appl. Phys. Lett.*, 84:2343, 2004.
82. S. Gustavsson, R. Leturcq, B. Simovič, R. Schleser, T. Ihn, P. Studerus, K. Ensslin, D.C. Driscoll, and A.C. Gossard. *Phys. Rev. Lett.*, 96:076605, 2006.
83. J. Tobiska and Y.V. Nazarov. *Phys. Rev. Lett.*, 93:106801, 2004.
84. R.K. Lindell, J. Delahaye, M.A. Sillanpää, T.T. Heikkilä, E.B. Sonin, and P.J. Hakonen. *Phys. Rev. Lett.*, 93:197002, 2004.
85. T.T. Heikkila, P. Virtanen, G. Johansson, and F.K. Wilhelm. *Phys. Rev. Lett.*, 93:247005, 2004.
86. J.P. Pekola *et al. Phys. Rev. Lett.*, 95:197004, 2005.
87. J. Ankerhold and H. Grabert. *Phys. Rev. Lett.*, 95:186601, 2005.
88. B. Reulet. *cond-mat/0502077*, 2005.
89. G. Schön and A.D. Zaikin. *Phys. Rep.*, 198:237, 1990.
90. J.P. Pekola. *Phys. Rev. Lett.*, 93:206601, 2004.
91. I. Chiorescu, Y. Nakamura, C.J.P. Harmans, and J.E. Mooij. *Science*, 299:1869, 2003.
92. M. Thorwart, M. Grifoni, and P. Hänggi. *Phys. Rev. Lett.*, 85:860, 2000.
93. T. Miyazaki (Ed.). *Atom Tunneling Phenomena in Physics, Chemistry and Biology*. Springer, 2006.
94. G.J. Kubas, R.R. Ryan, B.I. Swanson, P.J. Vergamini, and H.J. Wassermann. *J. Am. Chem. Soc.*, 116:451, 1984.
95. G. Buntkowsky and H.H. Limbach. *J. Low. Temp. Phys.*, in press, 2006.
96. G. Buntkowsky and H.H. Limbach. In H.H. Limbach, editor, *Handbook on Hydrogen Transfer*. Wiley-VCH, 2006.
97. H.H. Limbach, G. Scherer, and M. Maurer. *Angew. Chem.*, 104:1414, 1992.
98. F. Wehrmann, T.P. Fong, R.H. Morris, H.H. Limbach, and G. Buntkowsky. *Phys. Chem. Chem. Phys.*, 1:4033, 1999.
99. H.H. Limbach, S. Ulrich, S. Gründemann, G. Buntkowsky, S. Sabo-Etienne, B. Chaudret, G.J. Kubas, and J. Eckert. *J. Am. Chem. Soc.*, 120:7929, 1998.
100. M.J. Gillan. *Phys. Rev. Lett.*, 58:563, 1987.
101. M.J. Gillan. *J. Phys. C*, 20:3621, 1987.
102. J. Cao and G.A. Voth. *J. Chem. Phys.*, 105:6856, 1996.
103. S. Jang and G.A. Voth. *J. Chem. Phys.*, 112:8747, 2000.
104. G.A. Voth, D. Chandler, and W.H. Miller. *J. Chem. Phys.*, 91:7749, 1989.
105. G.A. Voth, D. Chandler, and W.H. Miller. *J. Phys. Chem.*, 93:7009, 1989.
106. G.A. Voth. *Chem. Phys. Lett.*, 170:289, 1990.
107. G.A. Voth. *J. Phys. Chem.*, 97:8365, 1993.
108. G.A. Voth. *Adv. Chem. Phys.*, 93:135, 1996.
109. R. Egger and C.H. Mak. *J. Chem. Phys.*, 99:2541, 1993.

6

Tunneling in Open Systems: Dynamics

The dynamics of quantum dissipative systems displays a fascinating variety of phenomena approaching for deep temperatures and weak friction the pure quantum mechanical domain and for high temperatures the realm of classical physics. Accordingly, a theoretical description has been a formidable task. In the 1960s the real-time dynamics of open quantum systems has been treated for the case of weak system-bath interaction, which allows for a perturbative treatment in terms of Born-Markov approximations [1, 2]. This way, various types of master equations have been derived and quite successfully applied to a number of fields as e.g. nuclear magnetic resonance [3, 4], quantum optics [5] and, most recently, quantum information processing [6]. Based on the work by Feynman and Vernon [7], in the 1980s the path integral formulation was shown to allow for an exact elimination of the bath degrees of freedom, thus leading to a formally exact expression for the reduced density matrix [8, 9, 10], the quantum version of the classical phase-space distribution. For a review of the recent progress in the description of the real-time dynamics of open quantum systems we refer to [11].

Unfortunately, in general "simple" equations of motion for the reduced dynamics do not exist due to long-time retardations in the influence functional at lower temperatures [10, 12, 13, 14]. Techniques for an explicit numerical evaluation have been developed by means of e.g. quantum Monte Carlo methods, but for long times and very low temperatures such simulations are basically prohibitive. In this situation semiclassical approaches offer promising tools to attack the problem. For processes including quantum tunneling a bunch of complications arises though: (i) quantum mechanical non-locality renders the notion of a transition point in position space meaningless [52]; (ii) a semiclassical approximation to the path integral of the reduced density matrix cannot follow the prescriptions specified in Chap. 2 since the fluctuation prefactor cannot be calculated according to the Gelfand-Yaglom formula [15] due to time irreversibility; (iii) according to Chap. 4 the inclusion of deep tunneling into a semiclassical approximation of the real-time propagators is rather

Joachim Ankerhold: *Quantum Tunneling in Complex Systems*
STMP **224**, 131–170 (2007)
DOI 10.1007/3-540-68076-4_6

non-trivial and cannot be done on the level of the standard van Vleck-Gutzwiller or Hermann-Kluk approximations.

Progress can be achieved in two directions. First, one may look for a generalization of the classical Kramers' theory to the quantum regime and focus on a moderate temperature range, where quantum fluctuations become relevant, but where the nonequilibrium state is still sufficiently localized around the barrier top. This theory will be discussed in the first part of this Section. Second, one may look for a regime, where friction is so strong that the system's dynamics follows closely a classical one. For sufficiently high temperatures one then approaches the classical overdamped regime, called Smoluchowski limit. Interestingly though, it turns out that the same also applies for substantially lower temperatures, where the non-dissipative system would be completely governed by quantum mechanics. In this regime quantum fluctuations generated by the strong interaction with the surrounding appear as corrections so that a type of semiclassical approximation is again feasible. Due to the large friction, the dynamics in the position degree of freedom is decelerated so strongly that on the time scale of its relaxation, the time evolution is effectively Markovian, thus allowing for an effective equation of motion. Within this framework quantum rate calculations resemble classical rate calculations, while the explicit rate expressions show a sensitive dependence on quantum fluctuations. We will present this *Quantum Smoluchowski Theory* in the second part of the Chapter.

6.1 Real-time Dynamics of Quantum Dissipative Systems

We consider a dissipative system as described in Sect. 5.2.1 with a system+bath Hamiltonian of the form (5.19) and an environment consisting of a large collection of harmonic oscillators. Since our focus lies on the dynamics of a small relevant subsystem, we are only interested in the quantum dynamics of the reduced system, i.e.,

$$\rho(t) = \mathrm{Tr_B}\left\{\exp(-\mathrm{i}Ht/\hbar)\; W(0)\; \exp(\mathrm{i}Ht/\hbar)\right\}\,, \tag{6.1}$$

where $W(0)$ describes the initial state of the total compound. In the ordinary Feynman-Vernon theory [7, 16] this state is assumed to be a factorizing state, $W(0) = \rho_{\mathrm{S}}(0)\,\exp(-\beta H_{\mathrm{B}})/Z_{\mathrm{B}}$ (Z_{B} is the bath partition function), so that each one, system and equilibrated bath, lives in splendid isolation at $t = 0$. While this assumption may be justified in the weak damping/high temperature limit, it certainly fails for moderate to strong friction and/or lower temperatures. It can be shown explicitly that in the classical limit even the Langevin equation is not regained, but differs by initial boundary terms that may persist up to long times [17]. A more realistic description thus starts with a correlated initial state [9] of the form

$$W(0) = \sum_j O_j \exp(-\beta H) O_j'/Z \tag{6.2}$$

with preparation operators O_j and O'_j acting onto the system degree of freedom only and the total partition function Z. For transparency, in the sequel we assume these operators to be diagonal in position (for generalizations see [9]) so that the initial density for an one-dimensional system reads in position representation

$$\rho(q_\mathrm{i}, q'_\mathrm{i}, t=0) = \rho_\beta(q_\mathrm{i}, q'_\mathrm{i})\, \lambda(q_\mathrm{i}, q'_\mathrm{i}) \tag{6.3}$$

with the reduced thermal equilibrium density matrix

$$\rho_\beta(q, q') = \mathrm{Tr}_\mathrm{B} \langle q| \exp(-\beta H) |q'\rangle \tag{6.4}$$

and the coordinate representation of the preparation operators

$$\lambda(q, q') = \sum_j \langle q|O_j|q\rangle \langle q'|O'_j|q'\rangle \,. \tag{6.5}$$

For a specific initial state, one does not need to know the specific form of these operators (which may be very complicated), but rather chooses the preparation function properly.

The reduced quantum dynamics (6.1) starting with an initial state (6.3) is now obtained within the position representation by employing the path integral formalism. Since the bath contains harmonic degrees of freedom only, it can be integrated out exactly, as shown for the imaginary time path integral in Sect. 5.2.2, and one arrives at

$$\rho(q_\mathrm{f}, q'_\mathrm{f}, t) = \int \mathrm{d}q_\mathrm{i} \mathrm{d}q'_\mathrm{i}\; \tilde{J}(q_\mathrm{f}, q'_\mathrm{f}, t, q_\mathrm{i}, q'_\mathrm{i})\, \lambda(q_\mathrm{i}, q'_\mathrm{i}) \,, \tag{6.6}$$

where the propagating function $\tilde{J}(\cdot)$ is a threefold path integral – two in real time, one in imaginary time – over the system degree of freedom only

$$\tilde{J}(q_\mathrm{f}, q'_\mathrm{f}, t, q_\mathrm{i}, q'_\mathrm{i}) = \frac{1}{Z} \int \mathcal{D}[q]\mathcal{D}[q']\mathcal{D}[\bar{q}]\; \mathrm{e}^{\mathrm{i}\Sigma[q,q',\bar{q}]/\hbar} \tag{6.7}$$

with $Z = \mathrm{Tr}\{\exp(-\beta H)\}/Z_\mathrm{B}$. The two real time paths $q(s)$ and $q'(s)$ connect in time t the initial points q_i and q'_i with fixed end points q_f and q'_f, while the imaginary time path $\bar{q}(\sigma)$ runs from q_i to q'_i in the interval $\hbar\beta$, see Fig. 6.1. The contribution of each path is weighted with an effective action $\Sigma[q, q', \bar{q}] = S_\mathrm{S}[q] - S_\mathrm{S}[q'] + \mathrm{i}\bar{S}[\bar{q}] + \mathrm{i}\phi[q, q,', \bar{q}]$ which consists of the actions of the bare system in real and imaginary time, respectively, and an additional interaction contribution (influence functional) non-local in time. The latter one can be written as

$$\phi[\tilde{q}] = \int \mathrm{d}z \int_{z>z'} \mathrm{d}z'\; \tilde{q}(z)\, K(z-z')\, \tilde{q}(z') + \frac{\mathrm{i}}{2}\mu \int \mathrm{d}z \tilde{q}(z)^2 \tag{6.8}$$

where the ordered time integration is understood along the contour: $z = s$ from $t \to 0$, $z = -\mathrm{i}\tau$ from $0 \to \hbar\beta$, $z = -\mathrm{i}\hbar\beta + s$ from $0 \to t$ with

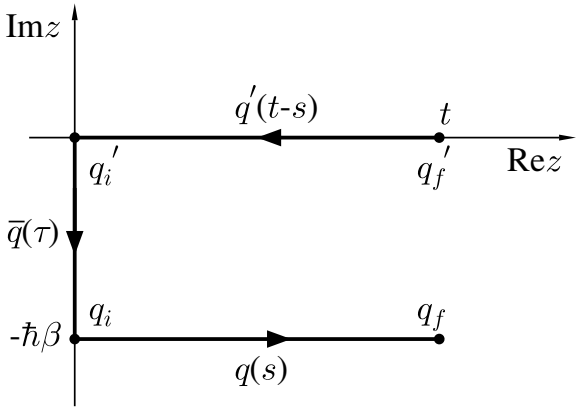

Fig. 6.1. Real and imaginary time paths in the complex time plane $z = s - i\tau$ contributing to the propagating functional; see text for details.

$$\tilde{q}(z) = \begin{cases} q'(s) & \text{for } z = s & 0 \le s \le t \\ \bar{q}(\tau) & \text{for } z = -\mathrm{i}\tau & 0 \le \tau \le \hbar\beta \\ q(s) & \text{for } z = -\mathrm{i}\hbar\beta + s & 0 \le s \le t \end{cases} . \tag{6.9}$$

The effective impact of the bath is completely controlled by the damping kernel

$$K(z) = \int_0^\infty \frac{\mathrm{d}\omega}{\pi}\, I(\omega)\, \frac{\cosh[\omega(\hbar\beta - \mathrm{i}z)]}{\sinh(\omega\hbar\beta/2)} , \tag{6.10}$$

where $I(\omega)$ denotes the spectral density (5.26) of the environment. As expected $\hbar K(z)$ coincides with the autocorrelation function of the bath force $\sum_i c_i x_i$ acting on the system. In particular, for real times the kernel $K(s) = K'(s) + \mathrm{i}K''(s)$ is related to the macroscopic damping kernel entering the classical generalized Langevin equation (5.24) via $K''(s) = (M/2)d\gamma(s)/ds$ and $K'(s) \to M\gamma(s)/\hbar\beta$ in the classical limit (M is the mass of the Brownian particle). The term with $\mu = \lim_{\hbar\beta\to 0} \hbar\beta K(0)$ in (6.8) cancels a time-local contribution from the first integral so that the environment affects the system only dynamically.

In the classical limit $\hbar\beta \to 0$ the imaginary time paths $\bar{q}(\tau)$ reduce to constants and one derives from the expression (6.6) the generalized Langevin equation (5.23) [10, 18].

6.2 Quantum Kramers Theory

With a non-perturbative formalism for the time evolution of the reduced density matrix at hand, one can now develop the generalization of Kramers' theory to the quantum domain. In the sequel, we consider the region of high to intermediate temperatures, where local harmonic approximations for the

barrier potential around the well region and the barrier top are still sufficient but quantum effects become important [19, 20].

6.2.1 Reduced Dynamics at a Parabolic Barrier

In the spirit of Kramers' theory in Sect. 5.1, the local dynamics around the barrier of a metastable potential is assumed to determine the stationary non-equilibrium flux state also for somewhat lower temperatures. This assumption will be confirmed self-consistently by deriving precise conditions for such a local treatment. Hence, we consider here an inverted harmonic potential $V(q) = -(M\omega_b^2/2)q^2$, for which the path integrals involved in the propagating function can be solved exactly [9]. The explicit calculation is performed in [19] and the result takes the form

$$\rho(x_\mathrm{f}, r_\mathrm{f}, t) = \int \mathrm{d}x_\mathrm{i}\, \mathrm{d}r_\mathrm{i}\; \tilde{J}(x_\mathrm{f}, r_\mathrm{f}, t, x_\mathrm{i}, r_\mathrm{i})\, \lambda(x_\mathrm{i}, r_\mathrm{i})\,, \tag{6.11}$$

where we have introduced sum and difference coordinates

$$x = q - q', \qquad r = (q + q')/2 \tag{6.12}$$

for q_f, q'_f and q_i, q'_i, respectively. For the propagating function one obtains

$$\begin{aligned}\tilde{J}(x_\mathrm{f}, r_\mathrm{f}, t, x_\mathrm{i}, r_\mathrm{i}) = \frac{1}{Z}\,\frac{1}{4\pi|A(t)|}\,\frac{1}{\sqrt{\omega_0^2\hbar\beta|\Lambda|}}\sqrt{\frac{M}{2\pi\hbar^2\beta}}\,\left(\prod_{n=1}^{\infty}\nu_n^2\,u_n\right)\\ \times\exp\left[\frac{\mathrm{i}}{\hbar}\Sigma_\beta(x_\mathrm{i}, r_\mathrm{i}) + \frac{\mathrm{i}}{\hbar}\Sigma_t(x_\mathrm{f}, r_\mathrm{f}, t, x_\mathrm{i}, r_\mathrm{i})\right]\,.\end{aligned} \tag{6.13}$$

Here,

$$\Sigma_\beta(x, r) = \mathrm{i}\frac{M}{2\Lambda_\mathrm{b}}r^2 + \mathrm{i}\frac{M\Omega_\mathrm{b}}{2}\,x^2 \tag{6.14}$$

is the minimal imaginary-time action of a damped inverted harmonic oscillator, where

$$\Lambda_\mathrm{b} = \frac{1}{\hbar\beta}\sum_{n=-\infty}^{\infty} u_n \tag{6.15}$$

and

$$\Omega_\mathrm{b} = \frac{1}{\hbar\beta}\sum_{n=-\infty}^{\infty}\left(|\nu_n|\hat{\gamma}(|\nu_n|) - \omega_\mathrm{b}^2\right)u_n. \tag{6.16}$$

Furthermore, $\nu_n = 2\pi n/(\hbar\beta)$ are Matsubara frequencies and

$$u_n = \left(\nu_n^2 + |\nu_n|\hat{\gamma}(|\nu_n|) - \omega_b^2\right)^{-1} \tag{6.17}$$

with $\hat{\gamma}(z)$ being the Laplace transform of the macroscopic damping kernel $\gamma(t)$. We note that for a harmonic oscillator the functions Λ_b and Ω_b correspond to the variance of the position and of the momentum, respectively

[9]. However, for a barrier there is no obvious physical meaning since e.g. for high temperatures one has $\Lambda_\mathrm{b} < 0$. When the temperature is lowered, $|\Lambda_\mathrm{b}|$ becomes smaller and vanishes for the first time at a critical temperature T_c [19]. As seen from (6.13) and (6.14), this leads to a divergence of the propagating function. Similar as for the Gaussian semiclassics of the non-dissipative statistical operator [cf. the discussion below (2.44)], the harmonic approximation is thus limited to temperatures above the critical temperature T_c, which in turn defines a lower bound in temperature for a quantum Kramers theory. This point will be further discussed in Sect. 6.3.

Apart from the pre-exponential factor the time dependence of the propagating function is contained in the second part of the exponent of (6.13). It reads explicitly [19]

$$\begin{aligned}
&\Sigma_t(x_\mathrm{f}, r_\mathrm{f}, t, x_\mathrm{i}, r_\mathrm{i}) = \\
&\quad x_\mathrm{f} r_\mathrm{f} M \frac{\dot{A}(t)}{A(t)} + x_\mathrm{i} r_\mathrm{f} \frac{\hbar}{2A(t)} - r_\mathrm{i} x_\mathrm{i} \frac{MS(t)}{2\Lambda_\mathrm{b} A(t)} + r_\mathrm{i} x_\mathrm{f} \frac{M^2}{\hbar} \left(\frac{\dot{S}(t)}{\Lambda_\mathrm{b}} - \frac{S(t)}{\Lambda_\mathrm{b}} \frac{\dot{A}(t)}{A(t)} \right) \\
&\quad + \frac{\mathrm{i}}{2} x_\mathrm{i}^2 M \left[-\Omega_\mathrm{b} + \frac{\hbar^2 \Lambda_\mathrm{b}}{4M^2 A(t)^2} \left(1 - \frac{M^2 S(t)^2}{\hbar^2 \Lambda_\mathrm{b}^2} \right) \right] \\
&\quad - \mathrm{i} x_\mathrm{i} x_\mathrm{f} \frac{\hbar \Lambda_\mathrm{b}}{2A(t)^2} \left[\dot{A}(t) \left(\frac{M^2 S(t)^2}{\hbar^2 \Lambda_\mathrm{b}^2} - 1 \right) - A(t) \frac{S(t) \dot{S}(t) M^2}{\Lambda_\mathrm{b}^2 \hbar^2} \right] \\
&\quad + \frac{\mathrm{i}}{2} x_\mathrm{f}^2 M \left[\Omega_\mathrm{b} + \Lambda_\mathrm{b} \frac{\dot{A}(t)^2}{A(t)^2} - \frac{M^2}{\hbar^2 \Lambda_\mathrm{b}} \left(\dot{S}(t) - \frac{\dot{A}(t)}{A(t)} S(t) \right)^2 \right] . \qquad (6.18)
\end{aligned}$$

The dynamics at a parabolic barrier is essentially determined by the functions $A(t)$ and $S(t)$, which are given by the Laplace transforms of [9]

$$\hat{A}(z) = -\frac{\hbar}{2M} \left(z^2 + z\hat{\gamma}(z) - \omega_\mathrm{b}^2 \right)^{-1} \qquad (6.19)$$

and

$$\hat{S}(z) = \frac{2}{\hbar\beta} \sum_{n=-\infty}^{\infty} \frac{z}{z^2 - \nu_n^2} \left(\hat{A}(z) - \hat{A}(|\nu_n|) \right) . \qquad (6.20)$$

Within the harmonic approximation the above formulas (6.11)–(6.20) determine the time evolution of the density matrix near the top of a potential barrier starting from an initial state with a deviation from thermal equilibrium described by the preparation function $\lambda(x_\mathrm{i}, r_\mathrm{i})$. Here, this state is taken as the thermal equilibrium state restricted to the well region $q < 0$ [19], i.e.,

$$\lambda(x_\mathrm{i}, r_\mathrm{i}) = \Theta(-r_\mathrm{i}) \qquad (6.21)$$

so that according to (6.11) the dynamics is given by

$$\rho(x_\mathrm{f}, r_\mathrm{f}, t) = \int \mathrm{d}x_\mathrm{i}\, \mathrm{d}r_\mathrm{i}\, \tilde{J}(x_\mathrm{f}, r_\mathrm{f}, t, x_\mathrm{i}, r_\mathrm{i})\, \Theta(-r_\mathrm{i}) . \qquad (6.22)$$

Since the exponents (6.14) and (6.18) in the propagating function are bilinear functions of the coordinates, the integrals in (6.22) are Gaussian and can be evaluated exactly. After determining the extremum of the exponent in the propagating function (6.22) with respect to x_i and r_i, one first evaluates the x_i–integral. Then, after simple manipulations of the remaining r_i–integral, the time dependent density matrix may be written in the form [20]

$$\rho(x_\mathrm{f}, r_\mathrm{f}, t) = \rho_\beta(x_\mathrm{f}, r_\mathrm{f})\, g(x_\mathrm{f}, r_\mathrm{f}, t). \tag{6.23}$$

Here,

$$\rho_\beta(x, r) = \frac{1}{Z} \frac{1}{\sqrt{\omega_\mathrm{b}^2 \hbar\beta |\Lambda_\mathrm{b}|}} \sqrt{\frac{M}{2\pi\hbar^2\beta}} \left(\prod_{n=1}^{\infty} \nu_n^2\, u_n \right) \exp\left(\frac{\mathrm{i}}{\hbar} \Sigma_\beta(x, r) \right) \tag{6.24}$$

is the equilibrium density matrix for an inverted harmonic oscillator and

$$\begin{aligned} g(x, r, t) &= \frac{1}{\sqrt{\pi}} \int_{-\infty}^{u(x,r,t)} \mathrm{d}z\, \mathrm{e}^{-z^2} \\ &= \frac{1}{2} \mathrm{erfc}\left[-u(x, r, t) \right] \end{aligned} \tag{6.25}$$

is a form factor describing deviations from equilibrium with

$$u(x, r, t) = \sqrt{\frac{M}{2\hbar|\Lambda_\mathrm{b}|}} \left(1 - \frac{\hbar^2 \Lambda_\mathrm{b}^2}{M^2 S(t)^2} \right)^{-1/2} \left(-r + \mathrm{i}|\Lambda_\mathrm{b}| \frac{\dot{S}(t)}{S(t)}\, x \right). \tag{6.26}$$

One comment is in order here: One observes that the reduced dynamics factorizes in a thermodynamic part and a dynamical part, where, as we know from the classical limit, the latter one reduces to unity away from the barrier top towards the well region so that the former one yields the exponential in the rate expression. Accordingly, the above result is already of the form that Kramers exploited in the classical domain for the stationary flux state (5.8). Indeed, for sufficiently long times the above expression becomes time independent as well.

To see this in detail, we investigate the dynamics of the density matrix (6.23) starting at $t = 0$ [20]. Note that the time dependence of the form factor (6.23) is completely determined by the function $S(t)$. Firstly, let us consider small times $\omega_\mathrm{b} t \ll 1$. There, one has [9]

$$S(t) = \frac{\hbar\Lambda_\mathrm{b}}{M} - \frac{\hbar\Omega_\mathrm{b}}{2M} t^2 + \mathcal{O}(t^4)\,, \tag{6.27}$$

which leads to

$$1 - \frac{\hbar^2 \Lambda_\mathrm{b}^2}{M^2 S(t)^2} = \frac{\Omega_\mathrm{b}}{|\Lambda_\mathrm{b}|} t^2 + \mathcal{O}(t^3)\,. \tag{6.28}$$

Then, the function $u(x, r, t)$, which gives the upper bound of integration in (6.25), reads

$$u(x,r,t) = -r\sqrt{\frac{M}{2\hbar\Omega_\mathrm{b}}}\,\frac{1}{t} + \mathrm{i}x\sqrt{\frac{M\Omega_\mathrm{b}}{2\hbar}} + \mathcal{O}(t)\,. \tag{6.29}$$

Hence, using the asymptotic formula

$$\int_z^\infty \mathrm{d}x\ \mathrm{e}^{-x^2} \simeq \frac{1}{2z}\mathrm{e}^{-z^2} \quad \text{for } \mathrm{Re}\{z\} \to \infty\,, \tag{6.30}$$

where Re denotes the real part, the leading order expression for the form factor (6.25) in the limit $\omega_\mathrm{b} t \ll 1$ is found to read for finite r

$$g(x,r,t) = \Theta(-r) + \sqrt{\frac{\hbar\Omega_\mathrm{b}}{2M\pi}}\,\frac{t}{r}\exp\left(-\frac{Mr^2}{2\hbar\Omega_\mathrm{b}t^2} + \mathrm{i}\frac{Mxr}{\hbar t} + \frac{M\Omega_\mathrm{b}}{2\hbar}x^2\right)\,, \tag{6.31}$$

while for $r = 0$

$$g(x,0,t) = \frac{1}{2} + \frac{1}{\sqrt{\pi}}\int_0^{\mathrm{i}x\sqrt{M\Omega_\mathrm{b}/2\hbar}} \mathrm{d}z\,\mathrm{e}^{-z^2} + \mathcal{O}(t)\,. \tag{6.32}$$

Clearly, for $t \to 0+$ and $r \neq 0$ the form factor reduces to the Θ function contained in the initial preparation (6.21) as expected. On the other hand, at $r = 0$ the $t \to 0+$ limit differs from the $t \to 0-$ limit by an imaginary part due to the discontinuity of the Θ function. Defining the width $\Delta(t)$ in position space of the nonequilibrium state (6.23) as that value of $|q|$, $q < 0$ where $u(0,q,t) = 1$, one gets

$$\Delta(t) = \sqrt{\frac{2\hbar|\Lambda_b|}{M}}\,\left(1 - \frac{\hbar^2\Lambda_\mathrm{b}^2}{M^2S(t)^2}\right)^{1/2}\,. \tag{6.33}$$

This reduces to $\Delta(t) = \sqrt{2\hbar\Omega_\mathrm{b}/M}t$ for small times in accordance with (6.31).

For large times, i.e. times larger than $1/\omega_\mathrm{R}$, the functions $A(t)$ and $S(t)$ are obtained in leading order as

$$A(t) = -\frac{\hbar}{2M}\,\frac{1}{2\omega_\mathrm{R} + \hat{\gamma}(\omega_\mathrm{R}) + \omega_\mathrm{R}\hat{\gamma}'(\omega_\mathrm{R})}\,\mathrm{e}^{\omega_\mathrm{R}t} \tag{6.34}$$

and

$$S(t) = -\frac{\hbar}{2M}\,\cot(\frac{\omega_\mathrm{R}\hbar\beta}{2})\,\frac{1}{2\omega_\mathrm{R} + \hat{\gamma}(\omega_\mathrm{R}) + \omega_\mathrm{R}\hat{\gamma}'(\omega_\mathrm{R})}\,\mathrm{e}^{\omega_\mathrm{R}t}\,. \tag{6.35}$$

Here, $\hat{\gamma}'(z)$ denotes the derivative of $\hat{\gamma}(z)$, and ω_R is the Grote-Hynes frequency (3.95). Equations (6.34) and (6.35) describe the unbounded motion at the parabolic barrier with corrections that are exponentially decaying in time (see [19, 20] for details). Consequently, the function $u(x,r,t)$ in (6.26) approaches a stationary value

$$u_\infty(x,r) = \sqrt{\frac{M}{2\hbar|\Lambda_\mathrm{b}|}}\,(-r + \mathrm{i}|\Lambda_\mathrm{b}|\,\omega_\mathrm{R}\,x)\,, \tag{6.36}$$

and the density matrix (6.23) reduces to a stationary nonequilibrium state $\rho_{\rm flux}(x,r) = \rho_\beta(x,r)\, g_{\rm fl}(x,r)$ with

$$g_{\rm fl}(x,r) = \frac{1}{\sqrt{\pi}} \int_{-\infty}^{u_\infty(x,r)} {\rm d}z\, {\rm e}^{-z^2}\,. \tag{6.37}$$

This time independent state describes a constant flux across the potential barrier and generalizes the Kramers flux state (5.8) to the temperature region where quantum effects are important. The width $\Delta(t)$ from (6.33) saturates for large times at the finite value

$$\Delta_\infty = \sqrt{\frac{2\hbar|\Lambda_{\rm b}|}{M}}\,, \tag{6.38}$$

which coincides with the width of the diagonal part of the equilibrium distribution (6.24). The position dependent part of the corresponding function $g_{\rm fl}(0,q)$ is depicted in Fig. 6.2 for various values of temperature.

Range of Validity

Before we proceed, let us discuss the validity of the harmonic approximation in more detail. It turns out that this analysis will impose certain conditions on temperature and on friction.

As addressed above, the temperature dependent function $\Lambda_{\rm b}$ in (6.15) vanishes at a temperature $T_{\rm c}$ leading to a divergence of the harmonic propagating function. While a further analysis will be given below in the Sect. 6.3, here, we conclude that the above flux solution is only valid for temperatures sufficiently above $T_{\rm c}$.

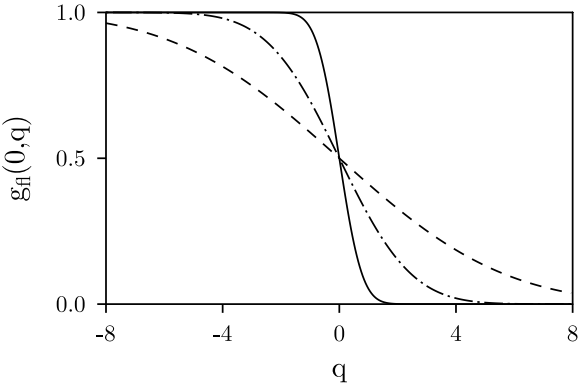

Fig. 6.2. "Form factor" $g_{\rm fl}(x,r)$ of the quantum stationary flux distribution (6.37) describing deviations from thermal equilibrium around the barrier top. Shown is the diagonal part $g_{\rm fl}(0,q)$ for various temperatures $\omega_{\rm b}\hbar\beta$ =0.1 (dashed), 1 (dotted-dashed), and 2 (solid) for ohmic friction with $\gamma/\omega_{\rm b} = 1$.

In the time domain, a lower bound for the existence of the stationary flux solution is derived from $\omega_{\mathrm{R}} t_< \gg 1$. An upper bound follows from the fact that for extremely long times the depletion of states deep inside the potential well leads to a flux decreasing in time. Hence, for very long times anharmonicities of the barrier potential influence the dynamics even for $T > T_{\mathrm{c}}$. For a barrier potential with a quartic term as leading order anharmonicity an upper bound in time where the density matrix (6.23) is valid has been estimated by the condition $\exp(\omega_{\mathrm{R}} t_>) \ll q_a \sqrt{2M\omega_{\mathrm{b}}/\hbar|\Lambda_{\mathrm{b}}|}$ where q_a denotes a typical distance from the barrier top for which the anharmonic part of the potential becomes essential. This intermediate time range $t_< < t < t_>$ defines the so-called plateau region.

Now, within this window the flux state must also match onto the equilibrium state in the well. This means that the solution (6.23) must reduce to the thermal equilibrium state for coordinates q_{f}, q'_{f} on the left side of the barrier at distances small compared with q_a. One obtains the condition [19]

$$|\Lambda| \ll \frac{V_{\mathrm{b}}}{\hbar\omega_{\mathrm{b}}^2}\left(1 - \omega_{\mathrm{R}}^2 \frac{|\Lambda_{\mathrm{b}}|}{\Omega_{\mathrm{b}}}\right), \tag{6.39}$$

where V_{b} is the barrier height with respect to the well bottom. From a physical point of view (6.39) specifies the range in parameter space (temperature, friction strength, barrier height) where the influence of the heat bath on the escape dynamics is strong enough to equilibrate particles on a length scale smaller than the scale where anharmonicities become important. Only then remain nonequilibrium effects localized around the barrier range within the plateau region. In the classical limit where $k_{\mathrm{B}}T \gg \hbar\omega_{\mathrm{b}}$ and for Ohmic damping $\hat{\gamma}(z) = \gamma$ the condition (6.39) reduces to the Kramers condition [see also (5.16)] $k_{\mathrm{B}}T\omega_{\mathrm{b}}/V_{\mathrm{b}} \ll \gamma$. Here, $1 - \omega_{\mathrm{R}}^2 \approx \gamma$ for small damping has been used. When the temperature is lowered, $|\Lambda_{\mathrm{b}}|$ decreases and the range of damping where the stationary solution (6.23) is valid becomes larger. For an extended discussion of this issue we refer to [19].

6.2.2 Phase Space Representation

The comparison between the classical and the quantum results can be revealed even better by transforming the result (6.37) to phase space via a Wigner transformation

$$W_{\mathrm{flux}}(p,q) = \frac{1}{2\pi\hbar}\int \mathrm{d}x\, \rho_{\mathrm{flux}}(x,r)\, \mathrm{e}^{ixp/\hbar}\,. \tag{6.40}$$

Accordingly, the quantum generalization of the classical Kramers distribution (5.8) with (5.10) reads

$$W_{\mathrm{flux}}(p,q) = \frac{1}{Z}\mathrm{e}^{-p^2/2\Omega_{\mathrm{b}} + q^2/2|\Lambda_{\mathrm{b}}|}\,\frac{1}{\sqrt{\pi}}\int\limits_{\xi_{\mathrm{qm}}(p,q)}^{\infty} \mathrm{d}y\, \mathrm{e}^{-y^2} \tag{6.41}$$

with

$$\xi_{\rm qm}(p,q) = \left(\frac{2M^4\omega_{\rm b}^4|\Lambda_{\rm b}|}{\Omega_{\rm b}^2\gamma\lambda_+}\right)^{1/2} \frac{\frac{\Omega_{\rm b}}{M^2\omega_{\rm b}|\Lambda_{\rm b}|}\,q - \frac{\lambda_+}{M\omega_{\rm b}}\,p}{\sqrt{1+(\Omega_{\rm b}-M^2\omega_b^2|\Lambda_{\rm b}|)/(\Omega_{\rm b}\gamma\lambda_+)}} \tag{6.42}$$

and $\omega_{\rm R} \equiv \lambda_+$. For high temperatures one regains with $|\Lambda_{\rm b}| = 1/M\omega_{\rm b}^2\beta$ and $\Omega_{\rm b} = M/\beta$ the classical expression (5.12). The quantum version of the parameter $a_{\rm cl}$ related to the unstable/stable directions in phase space (5.9) is thus given by

$$a_{\rm qm} = a_{\rm cl}\,\frac{M^2\omega_{\rm b}^2|\Lambda_{\rm b}|}{\Omega_{\rm b}}\,. \tag{6.43}$$

Since $|\Lambda_{\rm b}|$ is smaller than its classical value, while $\Omega_{\rm b}$ is larger, one has $a_{\rm qm} \leq a_{\rm cl}$ and the boundary layer near the barrier top (see Fig. 5.1) tends towards the p-axis. As a consequence, the nonequilibrium distribution in q becomes narrower, while that in p broadens, which reflects the fact that quantum mechanically the barrier becomes transparent near the top with a steeper distribution in q accompanied by larger quantum fluctuation in p.

The flux solution (6.41) has also been derived from a quantum Fokker Planck equation [21], where one introduces in the classical FPE (5.3) for a parabolic barrier quantum diffusion by replacing $\gamma M/\beta \to \gamma\Omega_{\rm b}$ and by adding a term $(M\omega_{\rm b}^2|\Lambda_{\rm b}| - \Omega_{\rm b}/M)\partial^2/\partial q\partial p$. We remark that an analysis of the phase space structure of barrier penetration in the non-dissipative case has been given in [22] based on the real-time dynamics of wave packets.

6.2.3 Decay Rate

The solution (6.23) now allows to evaluate the total probability flux $J(t)$ at the barrier top $q = 0$. The expression

$$J(t) = \frac{1}{2M}\langle\hat{p}\delta(\hat{q}) + \delta(\hat{q})\hat{p}\rangle_t\,, \tag{6.44}$$

where the expectation value $\langle\cdot\rangle_t$ is calculated with respect to the time dependent nonequilibrium state, reads in coordinate representation

$$J(t) = \frac{\hbar}{iM}\frac{\partial}{\partial x_{\rm f}}\,\rho(x_{\rm f},0,t)\bigg|_{x_{\rm f}=0}\,. \tag{6.45}$$

Since the essential contribution to the population in the well comes from the region near the well bottom, the normalization constant Z in (6.45) can be approximated by the partition function of a damped harmonic oscillator with frequency ω_0 at the well bottom, i.e.

$$Z = \frac{1}{\omega_0\hbar\beta}\left(\prod_{n=1}^{\infty}\frac{\nu_n^2}{\nu_n^2 + |\nu_n|\hat{\gamma}(|\nu_n|) + \omega_0^2}\right)\mathrm{e}^{\beta V_{\rm b}}\,. \tag{6.46}$$

Note that the potential was set to 0 at the barrier top so that its energy at the well minimum is $-V_\mathrm{b}$. Upon inserting (6.23) for $r_f = 0$ and (6.46) into (6.45) one gains the time dependent flux [20]

$$J(t) = \Gamma\, \eta(t)\,, \tag{6.47}$$

where

$$\Gamma = \lim_{t\to\infty} J(t) = \frac{\omega_0}{2\pi}\frac{\omega_\mathrm{R}}{\omega_\mathrm{b}}\, f_\mathrm{q}\, \mathrm{e}^{-\beta V_\mathrm{b}} \tag{6.48}$$

denotes the decay rate of the metastable system with the quantum mechanical prefactor f_q specified in (5.41) and the Grote-Hynes frequency ω_R given in (3.95). The above rate expression exactly coincides with the one derived in (5.40) within the ImF approach for temperatures above the crossover temperature. The real-time approach thus provides (i) a proof for the validity, at least in the temperature range above T_c, and (ii) precise conditions in parameter space for the applicability of this thermodynamic method.

For the time dependence of the flux we obtain

$$\eta(t) = \frac{\dot{S}(t)}{\omega_\mathrm{R}\, S(t)}\left(1 - \frac{\hbar^2 \Lambda_\mathrm{b}^2}{M^2 S(t)^2}\right)^{-1/2}. \tag{6.49}$$

This way we have found an analytical result for the dynamical behavior of the average flux which is usually studied numerically, see e.g. [23]. For long times $\omega_\mathrm{R} t \gg 1$ the function $\eta(t)$ approaches 1. For short times one derives from (6.27) that

$$\eta(t) = \frac{1}{\omega_\mathrm{R}}\sqrt{\frac{\Omega_\mathrm{b}}{|\Lambda_\mathrm{b}|}} + \mathcal{O}(t^2)\,, \tag{6.50}$$

which gives a finite flux for $t \to 0+$ while, according to the initial preparation (6.21), the limit $t \to 0-$ leads to a vanishing flux [see also (6.31) and (6.32)]. Specifically, for finite damping

$$\eta(0) = \frac{1}{\omega_\mathrm{R}}\sqrt{\frac{\Omega_\mathrm{b}}{|\Lambda_\mathrm{b}|}} \tag{6.51}$$

is always larger than 1. As a consequence, the probability flux for $t \to 0+$ exceeds the rate (6.48). For very high temperatures where $\omega_\mathrm{b}\hbar\beta \ll 1$, (6.51) reduces to $\eta(0) = \omega_\mathrm{b}/\omega_\mathrm{R}$ and the corresponding probability flux $J(0) = \Gamma\omega_\mathrm{b}/\omega_\mathrm{R}$ coincides with the result of the classical transition state theory (3.13)

$$\Gamma_\mathrm{cl,TST} = \frac{\omega_0}{2\pi}\,\mathrm{e}^{-\beta V_\mathrm{b}}\,. \tag{6.52}$$

For lower temperatures $|\Lambda_\mathrm{b}|$ decreases and $\eta(0)$ becomes larger than $1/\omega_\mathrm{R}$ which means that the transition state result $J(0)$ overestimates the true rate Γ even stronger in the quantum domain.

An Example: Drude Damping

To illustrate the above results we now study a Drude model with $\gamma(t) = \gamma\omega_{\rm D}\exp(-\omega_{\rm D}t)$. Clearly, in the limit $\omega_{\rm D} \gg \omega_{\rm b}, \gamma$ the Drude model behaves like an Ohmic model except for very short times of order $1/\omega_{\rm D}$. With the Laplace-transform of $\gamma(t)$, i.e.

$$\hat{\gamma}(z) = \gamma\frac{\omega_{\rm D}}{\omega_{\rm D}+z}\,, \tag{6.53}$$

we get from (6.15) and (6.16)

$$\Lambda_{\rm b} = \frac{1}{\hbar\beta}\sum_{n=-\infty}^{\infty}\frac{1}{\nu_n^2+|\nu_n|(\gamma\omega_{\rm D}/\omega_{\rm D}+|\nu_n|)-\omega_{\rm b}^2} \tag{6.54}$$

and

$$\Omega_{\rm b} = \frac{1}{\hbar\beta}\sum_{n=-\infty}^{\infty}\frac{|\nu_n|(\gamma\omega_{\rm D}/\omega_{\rm D}+|\nu_n|)-\omega_{\rm b}^2}{\nu_n^2+|\nu_n|(\gamma\omega_{\rm D}/\omega_{\rm D}+|\nu_n|)-\omega_0^2}. \tag{6.55}$$

The time dependence of the nonequilibrium state results from the function $S(t)$ in (6.20). Explicitly, one obtains

$$S(t) = \frac{\hbar}{M}\sum_{i=1}^{3}\left[\frac{c_i}{2}\cot\left(\frac{\lambda_i\hbar\beta}{2}\right)\exp(\lambda_i t)\right] - \zeta(t)\,, \tag{6.56}$$

where λ_i, $i = 1, 2, 3$ denote the poles of $\hat{A}(z)$ given by the three solutions of

$$z^3 + \omega_{\rm D}z^2 + z(\gamma\omega_{\rm D} - \omega_{\rm b}^2) - \omega_{\rm D} = 0\,. \tag{6.57}$$

For the coefficients c_i we have

$$c_1 = (\lambda_2^2-\lambda_3^2)/\epsilon \quad , \quad c_2 = (\lambda_3^2-\lambda_1^2)/\epsilon \quad , \quad c_3 = (\lambda_1^2-\lambda_2^2)/\epsilon\,, \tag{6.58}$$

where

$$\epsilon = (\lambda_1-\lambda_2)\lambda_1\lambda_2 + (\lambda_2-\lambda_3)\lambda_2\lambda_3 + (\lambda_3-\lambda_1)\lambda_1\lambda_3\,. \tag{6.59}$$

Further, we have introduced the time dependent function

$$\zeta(t) = \frac{\gamma\omega_{\rm D}^2}{\hbar\beta}\sum_{n=-\infty}^{\infty}\frac{|\nu_n|\,\exp(-|\nu_n|t)}{(\lambda_1^2-\nu_n^2)(\lambda_2^2-\nu_n^2)(\lambda_3^2-\nu_n^2)}\,, \tag{6.60}$$

which can also be written in terms of hypergeometric functions as

$$\zeta(t) = -\frac{1}{\hbar\beta}\sum_{i=1}^{3}\frac{c_i}{\lambda_i}\left[F(1,\frac{\lambda_i}{\nu};1+\frac{\lambda_i}{\nu};{\rm e}^{-\nu t}) - F(1,-\frac{\lambda_i}{\nu};1-\frac{\lambda_i}{\nu};{\rm e}^{-\nu t})\right]. \tag{6.61}$$

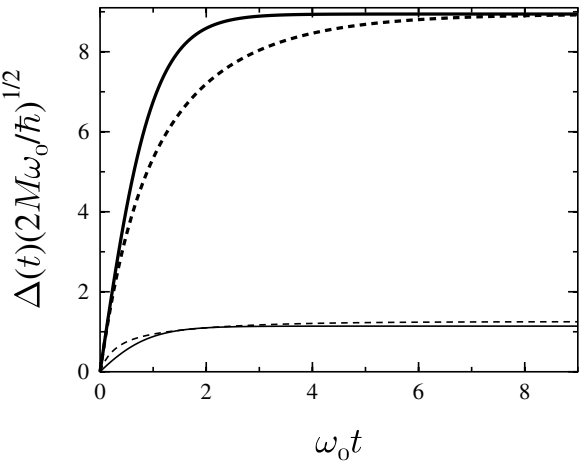

Fig. 6.3. Width $\Delta(t)$ in position space of the nonequilibrium state for $\hbar\beta\omega_0 = 0.05$ (thick lines) and $\hbar\beta\omega_0 = 2.0$ (thin lines) for a Drude damping with $\omega_D/\omega_0 = 100$. Solid lines depict weak friction $\gamma/\omega_0 = 0.1$, dashed lines strong damping $\gamma/\omega_0 = 3$.

With these findings for Λ_b, Ω_b, and $S(t)$, the time evolution of the nonequilibrium state has been evaluated explicitly for a Drude frequency $\omega_D = 100\omega_b$. In Fig. 6.3 the width $\Delta(t)$ of the nonequilibrium state in position space, given in (6.33), is depicted as a function of t for various temperatures. For high temperatures damping effects are relevant for intermediate times only while for lower temperatures they are essential for all times. For short times $\Delta(t)$ grows faster for stronger damping and reaches a larger asymptotic value for long times. This is due to the quantum mechanical effect that stronger damping suppresses the fluctuations of the coordinate and therefore enhances fluctuations of the momentum.

The relaxation of the time dependent flux (6.47) across the potential barrier towards the time independent decay rate (6.48) is determined by the function $\eta(t)$ in (6.49). In Fig. 6.4 the dynamics of $\eta(t)$ is depicted for various temperatures. One sees that in the region of moderate damping the simple TST result $J(0) = \Gamma\eta(0)$ for the rate constant gives a satisfactory estimate of the true rate only for high temperatures. When the temperature is decreased $\eta(0)$ grows and depends strongly on the damping strength. Furthermore, for lower temperatures the average flux across the barrier becomes stationary faster for stronger damping.

6.2.4 Correlation Functions

The propagating function can also be used to determine correlation functions [20], which we will use in Sect. 6.4.1 to illustrate the relation between the above quantum Kramers theory and alternative approaches. Of particular relevance is the right–left spatial correlation function

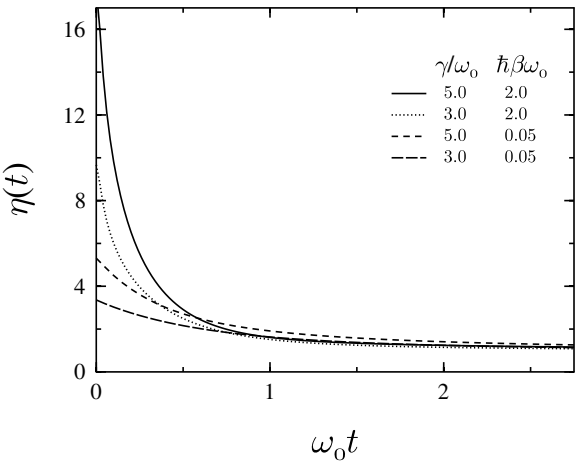

Fig. 6.4. Dynamics of the average flux across a barrier $J(t)$ in units of the stationary decay rate Γ: $\eta(t) = J(t)/\Gamma$ for different temperatures and a Drude model with $\omega_{\rm D}/\omega_0 = 100$ and various damping strengths.

$$C_q(t) = \frac{1}{Z}\mathrm{Tr}\left\{\Theta[q(t)]\Theta[-q]\mathrm{e}^{-\beta H}\right\} = \langle\Theta[q(t)]\,\Theta[-q]\rangle_\beta\,, \tag{6.62}$$

where $\Theta(\cdot)$ denotes the step function being unity on the product side and zero otherwise. Time derivatives of $C_q(t)$ lead to further correlation functions, e.g. the flux-flux correlation.

Now, let us evaluate $C_q(t)$ explicitly. Within the presented real time approach this correlation function may formally be looked upon as the expectation value of $\Theta(q)$ at time t of a system with an initial "density matrix" $\Theta(-q)\rho_\beta$. The corresponding preparation function then takes the form

$$\lambda(x_{\rm i}, r_{\rm i}) = \Theta\left(-r_{\rm i} - x_{\rm i}/2\right)\,. \tag{6.63}$$

This way, using (6.11), the correlation function may be written as

$$\begin{aligned} C_q(t) &= \int \mathrm{d}r_{\rm f}\mathrm{d}x_{\rm i}\mathrm{d}r_{\rm i}\,\Theta(r_{\rm f})\Theta\left(-r_{\rm i} - x_{\rm i}/2\right)\,\tilde{J}(0, r_{\rm f}, t, x_{\rm i}, r_{\rm i}) \\ &= \int \mathrm{d}r_{\rm f}\mathrm{d}x_{\rm i}\mathrm{d}r'_{\rm i}\,\Theta(r_{\rm f})\Theta(-r'_{\rm i})\,\tilde{J}(0, r_{\rm f}, t, x_{\rm i}, r'_{\rm i} - x_{\rm i}/2) \end{aligned} \tag{6.64}$$

with the propagating function $\tilde{J}(x_{\rm f}, r_{\rm f}, t, x_{\rm i}, r_{\rm i})$ given in (6.13). We proceed as before and first evaluate the $x_{\rm i}$ and afterwards the $r'_{\rm i}$ integration. Here, the maximum of the exponent in the propagating function with respect to $x_{\rm i}$ and $r'_{\rm i}$ lies at

$$\begin{aligned} x_{\rm i}^0 &= \mathrm{i}\frac{2M\omega_{\rm b}}{\hbar}A(t)\frac{r_{\rm f}}{\Lambda_{\rm b}} \\ r_{\rm i}'^0 &= \frac{M}{\hbar}[S(t) + \mathrm{i}A(t)]\frac{r_{\rm f}}{\Lambda_{\rm b}}. \end{aligned} \tag{6.65}$$

Introducing shifted coordinates $\hat{x}_\mathrm{i} = x_\mathrm{i} - x_\mathrm{i}^0$ and $\hat{r}'_\mathrm{i} = r'_\mathrm{i} - r'^0_\mathrm{i}$ a straightforward calculation shows that

$$\Sigma_\beta(x_\mathrm{i}, r'_\mathrm{i} - x_\mathrm{i}/2) + \Sigma_t(0, r_\mathrm{f}, t, x_\mathrm{i}, r'_\mathrm{i} - x_\mathrm{i}/2) = \frac{\mathrm{i}M(\hat{r}'_\mathrm{i})^2}{2\Lambda_\mathrm{b}} - \frac{\mathrm{i}M\hat{x}_\mathrm{i}^2}{8\Lambda_\mathrm{b}A(t)^2}\left\{[S(t)+\mathrm{i}A(t)]^2 - \frac{\hbar^2\Lambda_\mathrm{b}^2}{M^2}\right\} - \frac{M\hat{x}_\mathrm{i}\hat{r}'_\mathrm{i}}{2\Lambda_\mathrm{b}A(t)}\left[S(t)+\mathrm{i}A(t)\right]. \quad (6.66)$$

The Gaussian integrals with respect to $\hat{x}_\mathrm{i}$ and $\hat{r}'_\mathrm{i}$ are now readily performed. Eventually, after some further manipulations, we end up with

$$\begin{aligned} C_q(t) &= \frac{1}{Z}\frac{1}{\pi\omega_\mathrm{b}\hbar\beta}\left(\prod_{n=1}^{\infty}\nu_n^2\,u_n\right)\int_0^\infty \mathrm{d}x\exp(x^2)\int_{x/z(t)}^\infty \mathrm{d}y\,\exp(-y^2) \\ &= \frac{1}{Z}\frac{1}{4\pi\omega_\mathrm{b}\hbar\beta}\left(\prod_{n=1}^{\infty}\nu_n^2\,u_n\right)\log\left(\frac{1+z(t)}{1-z(t)}\right), \end{aligned} \quad (6.67)$$

where

$$z(t) = \left\{1 - \frac{\hbar^2\Lambda_\mathrm{b}^2}{M^2[S(t)+iA(t)]^2}\right\}^{1/2}. \quad (6.68)$$

For $t \to 0$ one has from (6.19)

$$A(t) = -\frac{\hbar}{2M}t + O(t^3) \quad (6.69)$$

and $z(t)$ tends to zero so that $C_q(t)$ vanishes for $t \to 0$ as expected. The time derivative of (6.67) yields the flux-position correlation

$$\begin{aligned} C_{fq}(t) &\equiv \dot{C}_q(t) = \langle\hat{F}(t)\Theta(-q)\rangle_\beta \\ &= \frac{1}{Z}\frac{1}{2\pi\omega_\mathrm{b}\hbar\beta}\left(\prod_{n=1}^{\infty}\nu_n^2\,u_n\right)\frac{|\dot{S}(t)| + \mathrm{i}|\dot{A}(t)|}{\left\{[S(t)+\mathrm{i}A(t)]^2 - \hbar^2\Lambda_\mathrm{b}^2/M^2\right\}^{1/2}}, \end{aligned} \quad (6.70)$$

where

$$\hat{F} = \frac{1}{2M}\left[p\delta(q) + \delta(q)p\right] \quad (6.71)$$

is the symmetrized flux operator at $q = 0$. Finally, a second time derivative gives the flux-flux correlation $C_f(t) \equiv \ddot{C}_q(t) = \langle\hat{F}(t)\hat{F}\rangle_\beta$.

6.2.5 Crossover Temperature

The semiclassical approximation presented above breaks down at a critical temperature T_c defined by

$$\Lambda(T_\mathrm{c}) = \frac{1}{\hbar\beta}\sum_{n=-\infty}^{\infty}\frac{1}{\nu_n^2 - \omega_\mathrm{b}^2 + |\nu_n|\hat{\gamma}(|\nu_n|)}\bigg|_{T=T_\mathrm{c}} = 0. \quad (6.72)$$

For the undamped case one has $T_c = \omega_b \hbar/(\pi k_B)$, thus being exactly *twice* the crossover temperature T_0, see (3.14) and Fig. 5.3. For finite friction T_c as well as T_0 are shifted to lower values so that for strong damping T_c follows from the solution of $\omega_b \hbar\beta_c \ln(\omega_b \hbar\beta_c) = \pi\gamma/\omega_b$ and is then substantially higher than $T_{0,R}$. In case of purely ohmic friction, T_c is conveniently obtained from the first zero of

$$\Lambda_b = \frac{1}{M\omega_b^2\beta} + \frac{1}{2\pi(\lambda_+ + \gamma/2)}\left[\Psi\left(1 - \frac{\hbar\beta\lambda_+}{2\pi}\right) - \Psi\left(1 - \frac{\hbar\beta\lambda_-}{2\pi}\right)\right] \quad (6.73)$$

with the digamma function Ψ and the frequencies $\lambda_\pm$ as in (5.10).

Around T_c the reduced density matrix diverges due to a divergent semiclassical expression for the equilibrium density matrix contained in (6.13). Namely, it turns out that at the temperature T_c new minimal action paths in imaginary time appear [24, 25] associated with a change of stability. For instance, while for $T > T_c$ the only path obeying $q(0) = q(\hbar\beta)$ is $q(\tau) = 0$, for $T < T_c$ orbits oscillating for half a period to the left or to the right are possible. This also explains that for zero friction $T_c = 2T_0$, because at T_0 orbits oscillating for a *full* period arise.

A proper description of this bifurcation necessitates the inclusion of anharmonicities in the barrier potential and a semiclassical treatment for the fluctuations which goes beyond the Gaussian approximation [24, 25]. This situation has some similarities with the semiclassical evaluation of the partition function around $T_{0,R}$ [see Sect. 5.2.3], but differs in detail since here not only periodic paths must be taken into account. Accordingly, there is a crucial difference between semiclassical rate theories based onto the full dynamics and those based onto thermodynamics. While both give the same results for $T > T_c$, as we have seen above, and also sufficiently below $T_{0,R}$, as we will see in Sects. 7.3.4 and 7.4.3, it cannot be expected that they lead to identical rate expressions in the intermediate temperature range $T_c > T > T_{0,R}$.

Due to the large excursions of the newly emerging orbits, for temperatures below T_c the parabolic approximation for the reduced dynamics is no longer valid even for coordinates in the close vicinity of the barrier top. The new oscillating minimal action paths then provide the dominant contributions to the semiclassical equilibrium density matrix and describe the on-set of quantum mechanical non-locality related to tunneling [26, 27]. In this situation analytical progress can only be made for vanishing friction as we will discuss in detail in Chap. 7.

6.3 Nuclear Fission

One of the first applications of the quantum theory of tunneling came actually from nuclear physics to understand the emission of α-particles from heavy nuclei [28, 29, 30]. Later it was discovered that two fundamental processes of nuclear matter, namely fission and fusion, can be understood as decay

and formation, respectively, of a many-body system in presence of potential barriers [31]. The first expression for a microcanonical decay rate was provided in 1939 by Bohr and Wheeler [32] in terms of level densities. In fact, it was this dissipation-less expression that motivated Kramers in 1940 [33] to lay the foundations for a dynamical rate theory including friction (see Sect. 5.1). The main difference to the situations we have considered so far is though that here the reaction coordinate describes actually a collective excitation of a strongly interacting many-body system [34]. The problem one encounters when one wants to adopt the methodology of dissipative systems is thus to identify parameters such as mass, friction, and frequencies. In this sense nuclear fission is also a nice example of the broad applicability of the Brownian motion model for metastable decay. Fission and fusion processes have regained new interest recently due to experimental efforts for the production of super-heavy nuclei [35, 36, 37]

Transport Coefficients

A microscopic description of nuclear matter as a many-body system consisting of protons and neutrons is based on a Hamiltonian with two-particle interaction of the form

$$\mathcal{H} = \sum_{ij} T_{ij} a_i^\dagger a_j + \frac{1}{2} \sum_{ijkl} V_{ijkl} a_i^\dagger a_j^\dagger a_l a_k \tag{6.74}$$

with fermionic creation and annihilation operators $a_i^\dagger$ and a_i, respectively, and corresponding matrix elements T_{ij} and V_{ijkl}. This Hamiltonian can be cast into a sum of separable interactions [38]

$$\mathcal{H} = \sum_{ij} H_{ij} a_i^\dagger a_j + \frac{1}{2} \sum_{\mu} k_\mu F_\mu F_\mu \tag{6.75}$$

with $F_\mu = \sum_{ij} F_{\mu;ij} a_i^\dagger a_j$. Several methods have been developed to extract from this microscopic Hamiltonian collective coordinates based on a type of Born-Oppenheimer approximation: The time scale for the dynamics of the nucleons is assumed to be much shorter than this of density variations [39]. Other methods to extract collective coordinates from the strongly correlated many-problem are based on a random phase approximation [40, 41] and the path integral representation [42, 43].

By way of example, let us illustrate how this allows to determine transport coefficients entering Langevin and Fokker-Planck equations [34, 44, 45]. We consider a simplified Hamiltonian with just one interaction term

$$\mathcal{H} = H(Q_0) + \frac{k(Q_0)}{2} F(Q_0) F(Q_0)\,, \tag{6.76}$$

where Q_0 denotes the (unknown) equilibrium value of a collective coordinate $Q(t)$. Within the mean field ansatz

$$Q(t) - Q_0 = k\langle F\rangle_t \tag{6.77}$$

for deviations from Q_0, one arrives at the *renormalized mean field* Hamiltonian

$$\mathcal{H}_{\mathrm{RMF}} = H(Q_0) + (Q - Q_0)F - \frac{1}{2k}(Q - Q_0)^2 \,. \tag{6.78}$$

The last term guarantees that the expectation value of $\mathcal{H}_{\mathrm{RMF}}$ coincides with the total energy of $\mathcal{H}$ in (6.76). Now, one looks at the linear response limit to derive response functions according to

$$\delta\langle F\rangle_t = -\int_{-\infty}^{\infty} \mathrm{d}s\ \chi(t-s)\ [Q(s) - Q_0] \tag{6.79}$$

with

$$\chi(t-s) = \frac{\mathrm{i}}{\hbar}\Theta(t)\,\langle [F(t), F(s)]\rangle_{Q_0} \,. \tag{6.80}$$

This response function, which depends on temperature due to the Q_0 average, can be expressed in terms of one-particle Greens-functions within the so-called *independent particle model*, where one assumes uncorrelated particles and holes. Residual interactions are taken into account by introducing phenomenologically parametrized self-energies. Accordingly, one obtains self-consistently an equation for the frequencies of the collective coordinate Q from $1 + \tilde{\chi}(\omega) = 0$ with $\tilde{\chi}(\omega)$ being the Fourier transform of $\chi(t)$. This local response function of the intrinsic degrees of freedom is related to the response function χ_{coll} of the collective coordinate by

$$\tilde{\chi}_{\mathrm{coll}} = \frac{\tilde{\chi}(\omega)}{1 + k\tilde{\chi}(\omega)} \,. \tag{6.81}$$

Around a certain root ω_0 of $1+\tilde{\chi}(\omega) = 0$, where $\tilde{\chi}$ is calculated microscopically for a specific nuclei, one fits $\tilde{\chi}_{\mathrm{coll}}$ onto the response function of a damped harmonic system

$$\tilde{\chi}_{\mathrm{osc}}(\omega) = \frac{-1}{M\omega^2 + \mathrm{i}\gamma|\omega| + C} \tag{6.82}$$

with effective mass M, friction constant γ, and stiffness C. Note that these coefficients depend on ω_0 and temperature, i.e. $M = M(Q,T), \gamma = \gamma(Q,T), C = C(Q,T)$. The collective coordinate Q is now interpreted as that of a fictitious particle that for a fission process moves in a metastable potential (cf. Fig. 6.5). The dependence of the transport coefficients on temperature and collective coordinate, however, cannot result from the standard Caldeira-Leggett Hamiltonian (5.20), so that application of the latter is always a reduction of the full many-problem and is thus not able to capture specific phenomena of nuclear matter.

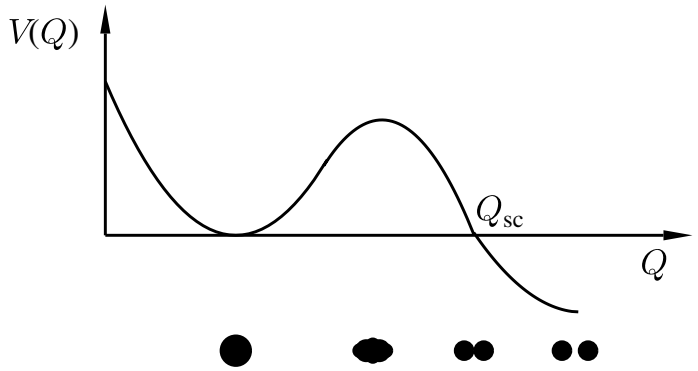

Fig. 6.5. Nuclear fission along a collective coordinate Q as decay from a metastable state. The deformation of the nucleus along the reaction path is sketched below.

Dwell Time and Decay Rates

For the decay process the typical time the system spends in the barrier region is of considerable interest (dwell time). Of course, access to this observable is only provided by a real-time calculation [46] presented in Sects. 6.2.1, 6.2.3. Using the same symbols as introduced there, the dwell time is defined as

$$t_{\rm dw} = \frac{1}{J_{\rm flux}} \int_0^{Q_{\rm sc}} {\rm d}Q \int_{-\infty}^{\infty} {\rm d}P_Q \; P_{\rm flux}(P_Q, Q)\,, \tag{6.83}$$

where the integral gives the fraction of the flux population which is located to the right of the barrier from the barrier top at $Q = 0$ to the scission point $Q_{\rm sc}$ being identical to the exit point of the metastable potential (3.7), see Fig. 6.5. It turns out that the dwell time solely depends on local properties around the barrier top so that the transport coefficients can be put to constants with values determined by those at the saddle. Then, with the results specified in Sects. (6.2.1) and (6.2.3) one obtains for temperatures above $T_{\rm c}$ [21]

$$\mathrm{t}_{\rm dw} = \frac{2\lambda_+}{\omega_{\rm b}^2} \mathcal{R}\left(\sqrt{M\omega_{\rm b}^2 \beta Q_{\rm sc}^2/2}\,/\,\sqrt{-\Lambda_{\rm b}\hbar\omega_{\rm b}^2\beta} \right) \tag{6.84}$$

with the Rosser function $\mathcal{R} = \int_0^x {\rm d}y \exp(y^2) \int_y^\infty {\rm d}z \exp(-z^2)$. The first factor in the argument is the ratio of the energy difference between saddle and scission and temperature, while the second one carries the impact of quantum fluctuations. As depicted in Fig. 6.6 the dwell time is enhanced compared to its classical value for lower temperatures, which can be attributed to the fact that the barrier tends to become transparent and the density of states under the barrier larger.

To complete this discussion, we specify the fission rate for temperatures above the crossover. A convenient way to derive it when starting with the microscopic Hamiltonian (6.76), is the path integral representation of the grand

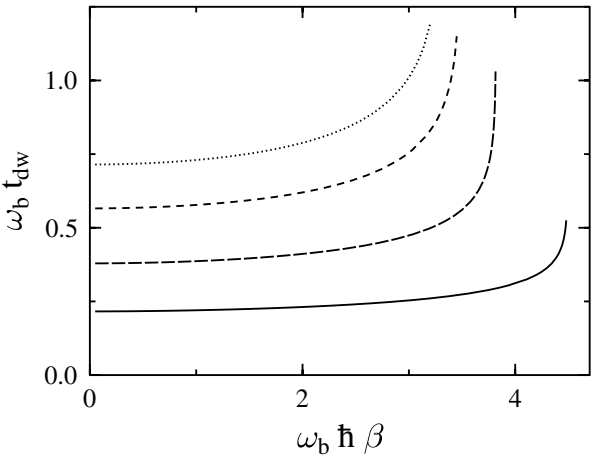

Fig. 6.6. Dwell time (6.84) of a nuclear fission process over a barrier with height $M\omega_b^2\beta Q_{sc}^2/2 = 5$ vs. inverse temperature and for various values of friction: $\gamma/\omega_b = 0.25$ (dotted), 0.5 (short-dashed), 1 (long-dashed), 2 (solid).

canonical partition function [47, 48, 49, 50]. The collective coordinate then appears as a Hubbard Stratonovich field and the rate is gained via the ImF method. Note though that one has to take into account that the transport coefficient are only locally defined and may considerably vary between well and barrier top. This leads to a more involved expression [47, 49, 50] than that specified in (5.40), namely,

$$\Gamma = \frac{\omega_R(\beta)}{2\pi}\sqrt{\frac{C_0(\beta)}{C_b(\beta)}}\, f_{qm}\, e^{-\beta B(\beta)}\,, \tag{6.85}$$

where the indices "b" and "0" refer to the corresponding functions taken at the barrier and the well, respectively. $B(\beta)$ denotes the temperature dependent barrier height and the quantum prefactor reads

$$f_{qm} = \left(\prod_n \frac{\nu_n^2 + \nu_n/\tau_{kin}^b(\beta) + \Omega_b^2(\beta)}{\nu_n^2 + \nu_n/\tau_{kin}^b(\beta) - \omega_b^2(\beta)}\right)\left(\prod_n \frac{\nu_n^2 + \nu_n/\tau_{kin}^0(\beta) + \Omega_0^2(\beta)}{\nu_n^2 + \nu_n/\tau_{kin}^0(\beta) + \omega_0^2(\beta)}\right)^{-1} \tag{6.86}$$

with typical nucleonic frequencies $\Omega_{0,b}$ gained from the nuclear shell model and the momentum relaxation time τ_{kin}^α ($\alpha = b, 0$) related to mass and friction coefficient by $\tau_{kin}^\alpha = (M/\gamma)|_\alpha$. The frequencies of the collective motion are always much smaller than those of the nucleonic one.

6.4 Alternative Dynamical Theories

Dynamical approaches for rate calculations have already been derived in the 1970s and later on extended to dissipative systems. These formulations do not

start from the general expression for the time evolution of the reduced density matrix, but rather from rate expressions derived within scattering theory.

6.4.1 Formally Exact Rate Expressions

A formally exact expression for the decay rate has been derived in [51] and [52], from which we started already in Sect. 3.85 to develop a multi-dimensional transition state theory. For the sake of convenience, let us recall this formula:

$$\Gamma = \frac{1}{Z} \lim_{t\to\infty} \mathrm{ReTr}\left\{\hat{F}\hat{P}(t)\mathrm{e}^{-\beta H}\right\} . \tag{6.87}$$

Here $\hat{F}$ is the flux operator introduced in (6.71), which for a general location q^* of the dividing surface reads

$$\hat{F} = \frac{1}{2M}\left[\delta(q-q^*)p + p\delta(q-q^*)\right] . \tag{6.88}$$

Note that q may be a generalized coordinate corresponding in a multi-dimensional space to the reaction path. The real-time dynamics is contained in the projection operator

$$\hat{P}(t) = \lim_{t\to\infty} \mathrm{e}^{iHt/\hbar}\Theta(p)\mathrm{e}^{-iHt/\hbar} \tag{6.89}$$

projecting in the long time limit only onto outgoing states. In this limit the step function in momentum can also be replaced by $\Theta(q-q^*)$, the step function in position being unity on the product side and 0 otherwise. Note that in case of a metastable potential here and in the sequel the large time limit must be understood in the sense of a plateau time.

From this expression three different forms for the rate constant have been obtained [53] based on the position autocorrelation $C_q(t)$ defined in (6.62). First, one has from (6.87)

$$\Gamma = \lim_{t\to\infty} \frac{\mathrm{d}}{\mathrm{d}t} C_q(t) . \tag{6.90}$$

As seen in Sect. 6.2.4, $C_q(t)$ is related to the position-flux and the flux-flux correlations simply by taking time derivatives: $C_{f,q}(t) = \dot{C}_q(t)$ and $C_f(t) = \ddot{C}_q(t)$, respectively. In these latter expressions it is advantageous to work with the thermal flux operator $\hat{F}_\beta = \exp(-\beta H/2)\hat{F}\exp(\beta H/2)$ so that

$$C_{fq}(t) = \frac{1}{Z}\mathrm{Tr}\left\{\hat{F}_\beta\hat{P}(t)\right\}, \quad C_f(t) = \frac{1}{Z}\mathrm{Tr}\left\{\hat{F}_\beta\hat{F}(t)\right\} . \tag{6.91}$$

This yields a second and a third expression

$$\Gamma = \lim_{t\to\infty} C_{f,q}(t), \quad \Gamma = \int_0^\infty \mathrm{d}t\; C_f(t) . \tag{6.92}$$

Apart from the conceptual point of view, the reason for deriving these alternative formulas is mainly practical so as to minimize the length of the time interval over which a numerical simulation has to be performed or to reduce the dimension of the basis set to represent the operators. For instance, the thermal flux operator is a low rank object (for one-dimensional systems of rank 2) [54], so that the time evolution needed for the rate calculation is restricted to the relatively small basis set of this operator. A very efficient numerical scheme for dissipative rate calculations, known as *Quasi-adiabatic Path Integral* (QUAPI) approach, is based on a path integral representation of the respective correlation functions combined with an exact diagonalization of the free system propagator [55, 56, 57, 58].

According to the discussion in Sect. 3.85, the exact expressions specified above lay also the basis for approximate treatments [59, 60, 61, 62, 63, 64, 65]. One option is, as done there, to approximate the dynamical operator $\hat{P}(t)$ by its form at $t = 0$. To go beyond this type of quantum transition state theory, the real-time propagators contained in $\hat{P}(t)$ can be represented by their semiclassical expressions, most conveniently in Hermann-Kluk form [see (2.27)]. This program has been further elaborated in the works cited above, particularly, by modeling dissipation by explicitly taking into account a moderate number of bath oscillators distributed according to a given spectral density. The fundamental problem is though that the standard types of semiclassical propagation schemes do not include the domain of deep tunneling (see Chap. 4) meaning that these studies are restricted to the range of moderate to high temperatures. For many chemical system, especially in gas phase, this is certainly sufficient; for more details we refer to the original literature.

We conclude this discussion by revealing the relation between the above correlation functions and the dynamical approach based on the reduced density matrix, which we have outlined in Sect. 6.2.4. Interestingly, this also provides a link to a rate expression derived by Yamamoto [66] based on Kubo's linear response theory, i.e.,

$$\Gamma = \lim_{t\to\infty} \frac{1}{\hbar\beta} \int_0^{\hbar\beta} \mathrm{d}\lambda \langle \Theta[-q(-\mathrm{i}\lambda)]\dot{\Theta}[-q(t)]\rangle_\beta \,. \tag{6.93}$$

Namely, the right hand side can be transformed to read

$$\frac{1}{\hbar\beta} \int_0^{\hbar\beta} \mathrm{d}\lambda \langle \Theta[-q(-\mathrm{i}\lambda)]\dot{\Theta}[-q(t)]\rangle_\beta = \frac{\mathrm{i}}{\hbar\beta} \langle [\Theta[-q(t)], \Theta[-q]]\rangle_\beta \,. \tag{6.94}$$

On the other hand, taking into account that $\Theta(q) = 1 - \Theta(-q)$ one has from (6.62)

$$\mathrm{Im}\,\{C_q(t)\} = -\mathrm{Im}\,\{C_{-q}(t)\} = \frac{\mathrm{i}}{2} \langle [\Theta[-q(t)]\,, \Theta[-q]]\rangle_\beta \tag{6.95}$$

so that we get from (6.94)

$$\Gamma = \frac{2}{\hbar\beta} \lim_{t\to\infty} \mathrm{Im}\,\{C_q(t)\} \,. \tag{6.96}$$

The result (6.67) can now be inserted into this rate formula. From (6.34) and (6.35) one obtains for times $\omega_{\rm R} t \gg 1$

$$\mathrm{Im}\left\{\log\left(\frac{1+z(t)}{1-z(t)}\right)\right\} = 2\arctan\left[A(t)/S(t)\right] . \tag{6.97}$$

Thus, we gain from (6.67)

$$\lim_{t\to\infty} \mathrm{Im}\left\{C_q(t)\right\} = \frac{\omega_{\rm R}\hbar\beta}{2\omega_0}\frac{1}{Z}\frac{1}{2\pi\hbar\beta}\left(\prod_{n=1}^{\infty}\nu_n^2\, u_n\right) , \tag{6.98}$$

which combines with (6.96) and the normalization (6.46) to yield the escape rate (6.48).

On the other hand, the time derivative $\dot{C}_q(t)$ given in (6.70) determines the rate according to (6.90). In the long time limit the imaginary part of $\dot{C}_q(t)$ becomes exponentially small and

$$\lim_{t\to\infty} \dot{C}_q(t) = \frac{1}{Z}\frac{1}{2\pi\omega_0\hbar\beta}\left(\prod_{n=1}^{\infty}\nu_n^2\, u_n\right)\omega_{\rm R} \tag{6.99}$$

yields again the rate (6.48).

6.4.2 Phase Space Approach

The Wigner representation of quantum mechanics often reveals interesting aspects of the dynamics due to its close relation to the classical phase-space picture [cf. Sect. 6.2.2)]. Moreover, it gives insight into appropriate semiclassical approximations for the exact rate expression (6.87).

The Wigner representation [67] of an operator is defined as

$$A(p,q) = \frac{1}{2\pi\hbar}\int_{-\infty}^{\infty} \mathrm{d}x\ \mathrm{e}^{ipx/\hbar}\ \langle q - \frac{x}{2}|\hat{A}|q + \frac{x}{2}\rangle\,, \tag{6.100}$$

from which one derives the important property that the Wigner representation of a product of two operators is identical to the product of the individual Wigner respresentations. Accordingly, the quantum rate (6.87) may be cast into the form [68]

$$\Gamma = \frac{2\pi\hbar}{Z}\int \mathrm{d}p\mathrm{d}q\ P(p,q)\, F_\beta(p,q) \tag{6.101}$$

with the Wigner representation $P(p,q)$ and $F_\beta(p,q)$ of the operators $\hat{P}$ and $\hat{F}_\beta$, respectively.

For a one-dimensional barrier system with no dissipation, semiclassical expressions for the Wigner representations of the flux operator have been

found in [68]. For higher temperatures, where a local parabolic approximation applies, one has

$$F_\beta(p,q) = \frac{1}{2\pi\hbar M}\sqrt{\frac{2M\omega_\mathrm{b}}{\pi\hbar\sin(\omega_\mathrm{b}\hbar\beta)}} \times \exp\left[-\frac{M\omega_\mathrm{b}^2 q^2}{\hbar\tan(\omega_\mathrm{b}\hbar\beta/2)} - \frac{p^2\,\tan(\omega_\mathrm{b}\hbar\beta/2)}{M\omega_\mathrm{b}\hbar}\right] \quad (6.102)$$

with the barrier frequency ω_b. This expression also diverges at the critical temperature T_c introduced already in (6.72), where $\omega_\mathrm{b}\hbar\beta_\mathrm{c} = \pi$ which is not surprising since a semiclassical approximation of the thermal flux operator includes the equilibrium density matrix and not the partition function. For temperatures below T_c the corresponding result is rather involved and we refer to the literature for more details [68].

The simplest choice of a semiclassical approximant for the dynamical factor is

$$P(p,q)_\mathrm{sc} = \frac{1}{2\pi\hbar}\Theta\left[p \pm \sqrt{-2MV(q)}\right], \quad (6.103)$$

where the plus [minus] sign is taken for positive [negative] q and the barrier potential $V(q)$ is taken such that $q = 0$ is the location of the barrier with $V(0) = 0$. Apparently, the projector projects onto that range in phase-space, where all trajectories reach in the infinite time limit the product side. Based on an exact evaluation of the flux operator in combination with the above classical approximation for the dynamical projection operator, rate calculations have been successfully performed [69, 70, 71] as long as tunneling is not too strong. In this context we note that the first three time derivatives of an operator in the Wigner representation are identical to the classical ones, so that their short time properties coincide [72, 73].

By replacing the exact Wigner representations in (6.101) by semiclassical ones, semiclassical rate expressions are found. For temperatures above T_c the rate coincides with the result specified in (3.12). For temperatures below T_c, the rate consists of an exponential factor which contains only half of the bounce action corresponding to the action of a closed path that connects its end-points in half a period and not in a full one. The related rate enhancement in $T_\mathrm{c} > T > T_0$ is partially compensated for by the fact that the flux exhibits positive and negative contributions over which one has to sum. In comparison with exact data for e.g. an Eckart barrier potential [74] very good agreement is found above T_c, while deviations grow below; see also Table 7.1 at the end of Sect. 7.4.3. How from this approximation the known tunneling rate with the full bounce action arises for very low temperatures, is not known yet. One problem may be again the semiclassical approximation of the dynamical factor $P(p,q)$, which for lower temperatures must include modifications of the standard semiclassical real-time propagators to capture deep tunneling.

6.5 Quantum Smoluchowski Limit

In Sect. 6.1 it was argued that the reduced quantum dynamics is subject to time retarded self-interactions mediated by the surrounding. A full dynamical rate calculation becomes thus very demanding since the evaluation of the path integrals contained in (6.6) is much more involved than the solution of a time-local equation of motion. As addressed above, progress can be made in the limits of weak and very strong friction. In the former range so-called master equations have been derived. The opposite domain of strong friction, classically known as the Smoluchowski limit [75], has been studied for low temperatures only recently leading to a quantum version of the classical Smoluchowski dynamics [76, 77, 78]. In this Section we will discuss the main results of this analysis and illustrate its applicability as a very elegant tool to gain quantum decay rates for strongly condensed phase systems.

6.5.1 Quantum Smoluchowski Equation

The classical Smoluchowski limit is related to a separation of time scales between fast equilibration of momentum and slow equilibration of position [75]. This way, the Fokker-Planck equation for the phase space distribution (5.3) can be adiabatically reduced to a Smoluchowski equation for the marginal distribution in position space [79]. For quantum dissipative systems the expectation is that friction makes the system to behave more classically so that for strong friction the complicated path integral expression (6.6) simplifies considerably. This is indeed the case as has been shown recently [76].

A typical damping strength in the long time limit is defined as

$$\gamma \equiv \hat{\gamma}(0) = \lim_{\omega \to 0} \frac{I(\omega)}{M\omega}\,, \tag{6.104}$$

where $\hat{\gamma}(\omega)$ is the Laplace transform of the classical damping kernel $\gamma(t)$. For ohmic friction, $I(\omega) = M\tilde{\gamma}\omega$, for instance, one finds $\gamma = \tilde{\gamma}$. The same is true for the more realistic Drude damping $I(\omega) = M\tilde{\gamma}\omega\omega_c^2/(\omega^2 + \omega_c^2)$ with cut-off frequency ω_c. Now, given a typical frequency ω_0 of the bare system (e.g. its ground state frequency) by strong damping we then mean (cf. Fig. 6.7)

$$\frac{\gamma}{\omega_0^2} \gg \frac{\hbar\beta}{2\pi}, \frac{1}{\omega_c}, \frac{1}{\gamma}\,. \tag{6.105}$$

Hence, one extends the time scale separation known from the classical Smoluchowski range to incorporate the time scale for quantum fluctuations $\hbar\beta$.

The idea is now, to evaluate for strong friction $\gamma/\omega_0 \gg 1$ the path integral expression (6.6) on the coarse-grained times scale $t \gg \hbar\beta, 1/\omega_c, 1/\gamma$ and $\tau \gg 1/\omega_c, 1/\gamma$, respectively. The consequences are the following: (i) Non-diagonal elements of the reduced density matrix are strongly suppressed during the time evolution, (ii) the real time part of the kernel $K(s)$ [see (6.10)] becomes local

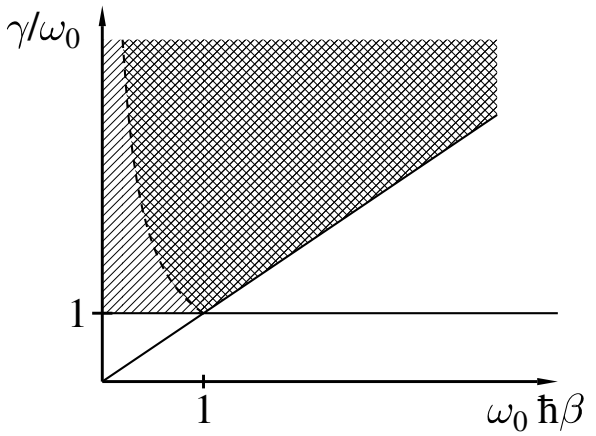

Fig. 6.7. Quantum Smoluchowski range according to (6.105) (shaded). The classical range $\gamma\hbar\beta < 1$ is simple shaded, the quantum range $\gamma\hbar\beta > 1$ double shaded.

on the coarse grained time scale, and (iii) initial correlations described by (6.3) survive for times of order γ/ω_0^2 verifying that factorizing initial states cannot be used. Accordingly, the strong friction limit corresponds to a semiclassical approximation where inverse friction plays the role of the small parameter.

The classical Smoluchowski equation for the marginal distribution $P(q,t)$ reads $\dot{P}(q,t) = (1/\gamma M)\partial_q L_{\rm S} P(q,t)$ with the flux operator

$$L_{\rm S} = V'(q) + k_{\rm B}T\partial_q \,. \tag{6.106}$$

We seek for a generalization of this equation to the quantum regime in a form, where $[1 + \delta h]\, L_{\rm QS}$ replaces $L_{\rm S}$ so as to preserve the structure of a continuity equation and thus probability conservation. In case of a harmonic potential $V(q) = M\omega_0^2 q^2/2$, where the full nonequilibrium dynamics can be solved analytically [9], one finds [76] that

$$L_{\rm QS,harm} = M\omega_0^2 q + M\omega_0^2\langle q^2\rangle\partial_q \,, \tag{6.107}$$

where for strong friction (6.105) the variance reads $\langle q^2\rangle = 1/(M\omega_0^2\beta) + \Lambda$ [77] with

$$\begin{aligned}\Lambda &= \frac{2}{M\beta}\sum_{n=1}^{\infty}\frac{1}{\nu_n^2 + \nu_n\gamma} \\ &= \frac{\hbar}{M\gamma\pi}\left[\Psi\left(\frac{\gamma}{\nu}\right) - C + \frac{\nu}{\gamma}\right]\end{aligned} \tag{6.108}$$

with the Euler constant $C = 0.577\ldots$ and the digamma function Ψ. In the high temperature domain $\gamma\hbar\beta \ll 1$, we have $\Lambda \approx \hbar^2\beta/12M$. The dependence on friction appears for lower temperatures as a genuine quantum effect and in the

quantum Smoluchowski range $\gamma\hbar\beta \gg 1$ one obtains $\Lambda \approx (\hbar/M\gamma\pi)\ln(\gamma\hbar\beta/2\pi)$. Quantum fluctuations in position are thus suppressed by friction, not algebraically though, but much weaker. They also show a nonlinear dependence on $\hbar$ meaning that for $\gamma\hbar\beta \gg 1$ we work in a deep quantum domain even though $\langle q^2\rangle$ is in leading order given by the classical result. The correction function δh carries dynamical corrections which are at most of order $1/\gamma$ or smaller [80].

Equilibrium Distribution

To extend this finding to anharmonic potentials, in a first step, the diagonal part of the equilibrium density matrix $P_\beta(q) = \rho_\beta(q,q)$ is calculated, which in turn determines $L_{\rm QS}$ from the condition of a vanishing flux in thermal equilibrium. In the path integral representation of the position distribution

$$\rho_\beta(q,q) = \frac{1}{Z'}\int \mathcal{D}[q]\, \mathrm{e}^{-\bar{S}_{\rm eff}[q]/\hbar} \tag{6.109}$$

with a proper normalization Z' and the effective Euclidian action specified in (5.29), one sums over all paths with $q(0) = q(\hbar\beta) = q$, where the minimal action paths $\bar{q}$ are determined by (5.32). We now look for a solution of this equation in the limit of very strong friction by Fourier transforming it via (5.33). Since (5.33) periodically continues $\bar{q}(\tau)$ outside $[0,\hbar\beta]$, we have to supplement (5.32) on the right hand side by the boundary term $Mb : \delta(\tau) :$ with the periodically continued δ-function $: \delta(\tau) := (1/\hbar\beta)\sum_n \exp(\mathrm{i}\nu_n\tau)$ and $b = \dot{\bar{q}}(\hbar\beta) - \dot{\bar{q}}(0)$ [9]. Accordingly, we have

$$-\nu_n^2 q_n - \gamma|\nu_n| q_n + v_n/M = b \tag{6.110}$$

with $v_n = \int_0^{\hbar\beta} \mathrm{d}\tau V'[\bar{q}(\tau)]\exp(-\mathrm{i}\nu_n\tau)$. From this expression one observes that for all $n \neq 0$ friction dominates and $q_n, n \neq 0$, are formally of order $1/\gamma$. Hence, the $n = 0$ part provides the leading order contribution $\bar{q}(\tau) \approx q_0/\hbar\beta \approx q$ according to the boundary conditions and (6.110) is solved by $b = (\hbar\beta/M)V'(q)$. In next order, $n \neq 0$, one has

$$q_n = -\frac{b}{\nu_n^2 + \gamma|\nu_n|}\ ,\ n \neq 0\,, \tag{6.111}$$

where we retained the kinetic term to include also the strong friction/high temperature domain ($\gamma\hbar\beta \ll 1$), where ν_n^2 dominates. Note that corrections due to $V[\bar{q}(\tau)] \approx V(q) + V'(q)\delta q$, where δq collects the $n \neq 0$-terms in (5.33), yield negligible contributions as long as $|V''(q)|/M \ll \gamma/\hbar\beta$ for low temperatures and $\hbar^2\beta^2 V''(q)/M \ll 1$ for high temperatures. Both conditions are fulfilled for sufficiently smooth potentials and under the restrictions (6.105). Now, the next order correction to q_0 is obtained from $\bar{q}(0) = q$ as $q_0 = q + bM\Lambda/\hbar$ with Λ in (6.108).

The corresponding minimal action is gained from (5.29) after partial integration as

$$\bar{S}_{\min} = \frac{M}{2} b\, q + \int_0^{\hbar\beta} \mathrm{d}\tau \left[V(\bar{q}) - \frac{\bar{q}}{2} V'(\bar{q}) \right] , \tag{6.112}$$

which yields

$$\bar{S}_{\min}(q) = \hbar\beta V(q) - \frac{\hbar\beta^2 \Lambda}{2} V'(q)^2 . \tag{6.113}$$

This gives the dominant contribution to the path integral (6.106) as $P_\beta(q) \propto \exp[-\bar{S}_{\min}(q)/\hbar]$. In fact, for a harmonic potential, where the exact result is $\bar{S}_{\min} = \hbar q^2/2\langle q^2\rangle$, the expansion of $\langle q^2\rangle$ according to (6.108) reproduces in leading order the above expression.

What remains to do is to evaluate the fluctuation integral. Due to the large friction this can be done by expanding the full action according to $q(\tau) = \bar{q}(\tau) + y(\tau)$, $y(0) = y(\hbar\beta) = 0$, up to second order leading to Gaussian integrals. This way, we write $P_\beta(q) = F(q) \exp[-\bar{S}_{\min}(q)/\hbar]/Z'$ where

$$F(q) = \int \mathcal{D}[y] \exp\left[-\frac{1}{\hbar} \int_0^{\hbar\beta} \mathrm{d}\tau\, y(\tau) L[y] \right] \tag{6.114}$$

with the second order variational operator (5.35). This operator has eigenfunctions $\propto \exp(\mathrm{i}\nu_n\tau)$ so that one works with the Fourier representation (5.33) for the $y(\tau)$ as well. However, also the boundary conditions have to be imposed, which is most conveniently done by introducing $\delta[y(0)] = \delta[(1/\hbar\beta)\sum_n y_n]$ in the path integral and representing the δ function by an integral over an auxiliary variable μ. Thus,

$$F(q) = N \int_{-\infty}^{\infty} \mathrm{d}\mu \prod_{n=-\infty}^{\infty} \int_{-\infty}^{\infty} \mathrm{d}y_n \exp\left[\frac{\mathrm{i}}{\hbar\beta}\, \mu y_n - \frac{M}{\hbar^2\beta}\, \zeta_n\, y_n^2 \right] \tag{6.115}$$

and the eigenvalues read in leading order $\zeta_n = \nu_n^2 + |\nu_n|\gamma + V''(q)/M$. N is a proper normalization to ensure the correct free particle limit. After performing the corresponding integrations we arrive at

$$F(q) = N' \left[1 + \beta\Lambda V''(q)\right]^{-1/2} \prod_{n=1}^{\infty} \frac{\nu_n^2 + \nu_n\gamma}{\nu_n^2 + \nu_n\gamma + V''(q)/M} , \tag{6.116}$$

where N' collects constant factors from the normalization of the path integral. For strong friction the product can be further evaluated by writing $\prod f_n = \exp(\sum \ln f_n)$ and approximating $f_n \approx 1 - [V''(q)/M]/(\nu_n^2 + \nu_n\gamma)$. Hence, up to a constant factor and including at most terms of order Λ one finds $\prod f_n \propto \exp[-\beta V''(q)\Lambda/2] \approx 1 - \beta V''(q)\Lambda/2$. Eventually, the equilibrium probability distribution reads in the strong friction regime

$$P_\beta(q) = \frac{1}{Z} \left[1 - \beta V''(q)\Lambda\right]\ \mathrm{e}^{-\beta V(q) + \beta^2 \Lambda V'(q)^2/2} , \tag{6.117}$$

where we absorbed normalization factors from $F(q)$ in a new normalization Z and expanded the prefactor $(1-\beta V''\,\Lambda/2)(1+\beta V''\,\Lambda)^{-1/2}$ up to first order in Λ. Note that in the first derivation of the equilibrium distribution [76] the product in $F(q)$ has been gained with a wrong factor Λ instead of $\Lambda/2$ so that the contribution from the fluctuations was obtained as $1-(3\Lambda/2)\beta V''$.

The result (6.117) can also be generalized to the nondiagonal elements of the density matrix $\rho_\beta(q,q')$ following the procedure described above. The result is

$$\rho_\beta(\bar{x},\bar{r}) = \frac{1}{Z}\,\left[1-\beta V''(\bar{r})\Lambda\right]\;\mathrm{e}^{-\beta V(\bar{r})-\Omega\,\bar{x}^2/2\hbar^2+\Lambda\beta^2 V'(\bar{r})^2/2}\,, \tag{6.118}$$

where $\bar{r}=(q+q')/2$ and $\bar{x}=q-q'$. The function Ω has been specified for arbitrary friction in (6.16). For strong friction and Drude damping (6.53) with a high frequency cut-off $\omega_\mathrm{c}\gg\gamma$, it can be expressed in terms of Ψ functions as

$$\Omega \approx \frac{M\hbar\gamma}{\pi}\left[\Psi\left(\frac{\omega_\mathrm{c}}{\nu}\right)-\Psi\left(\frac{\gamma}{\nu}+\frac{\gamma^2}{\nu\omega_\mathrm{c}}\right)-\frac{\nu}{2\gamma}+\frac{2\nu}{\omega_\mathrm{c}}\right]. \tag{6.119}$$

In the high temperature range $\gamma\hbar\beta\ll 1$, we regain $\Omega\approx M/\beta$ so that the Wigner transform of (6.118) reduces to the classical phase space distribution, while for lower temperatures $\gamma\hbar\beta\gg 1$ one has $\Omega\approx(M\hbar\gamma/\pi)\ln(\omega_\mathrm{c}/\gamma)$. Since according to (6.108) the position variance shrinks when lowering the temperature, the momentum variance grows with friction to guarantee Heisenberg's uncertainty relation. In particular, for a harmonic potential the above distribution reduces to the known result [81]. Accordingly, as assumed above, off-diagonal elements of the distribution $\rho_\beta(q,q')$ are strongly suppressed with $|\bar{x}|$ being of order $1/\sqrt{\gamma\ln(\omega_\mathrm{c}/\gamma)}$ or smaller. We mention in passing that higher order corrections in Λ are associated with higher than second order derivatives of the potential $V(q)$.

Current Operator and Quantum Smoluchowski Equation

We are now in a position to determine the quantum flux operator L_QS from the condition that $L_\mathrm{QS}P_\beta(q)=0$. The expression (6.117) leads to

$$L_\mathrm{QS} = V'(q) + k_\mathrm{B}T\partial_q\frac{1}{1-\beta\Lambda V''(q)}\,. \tag{6.120}$$

We mention that in the spirit of our small Λ expansion, the diffusion term could also be written as $1/[1-\beta\Lambda V''(q)]\approx 1+\beta\Lambda V''(q)$ as it was done in [76]. Then, however, a vanishing equilibrium current is guaranteed only up to terms of order Λ^2. While this is consistent with the perturbative treatment, in direct numerical integrations it is more convenient to work with the expression (6.120) to avoid any spurious violations of the second law of thermodynamics [82].

Following the lines above, now, a possible dynamical correction δh must be analysed. Since it gives a negligible contribution in case of a harmonic oscillator, we deduce that if this term contributes in order Λ for anharmonic potentials, it must carry higher than second order derivatives of the potential. While in principle we could now proceed to study the reduced dynamics in real time according to Sect. 6.1 for the total distribution $\rho(q_\mathrm{f}, q'_\mathrm{f}, t)$ [83], it is sufficient to concentrate on the relevant diagonal part $P(q_\mathrm{f}, t) = \rho(q_\mathrm{f}, q_\mathrm{f}, t)$ [76]. Hence, the preparation function in (6.6) is taken as $\lambda(q_\mathrm{i}, q'_\mathrm{i}) = \lambda_0(q_\mathrm{i})\delta(q_\mathrm{i} - q'_\mathrm{i})$. In fact, one can show that off-diagonal elements relax to thermal equilibrium with respect to the instantaneous position of the Brownian particle on a time scale of order $1/\gamma$ [84]. For the semiclassical evaluation of the propagating function in (6.6) one thus exploits that difference paths $x(s) = q(s) - q'(s)$ remain small during the dynamics, namely at most of order $(\hbar^2\beta/M\gamma t)^{1/2}$. Further, since we are looking for a time independent correction δh on the coarse grained time scale (6.105), it suffices to work in the range $\hbar\beta, 1/\gamma \ll t \ll \gamma/\omega_0^2$. The explicit evaluation is somewhat tedious, but reveals that δh is at most of order Λ/γ or smaller and can thus safely be disregarded.

Finally, the dynamics of $P(q, t)$ can be cast into an equation of motion, the so-called *Quantum Smoluchowski Equation* (QSE),

$$\frac{\partial P(q,t)}{\partial t} = \frac{1}{\gamma M}\frac{\partial}{\partial q}\left[V'(q) + k_\mathrm{B}T\frac{\partial}{\partial q}D(q)\right] P(q,t)\,. \tag{6.121}$$

Here,

$$D(q) = \frac{1}{1 - \Lambda\beta V''(q)} \tag{6.122}$$

is an effective position dependent diffusion coefficient. We mention that here in contrast to the original derivation [76] no correction to the potential term appears due to (6.117).

The quantum analog to the classical Langevin equation in the strong damping limit can also be gained (in the Ito sense) from (6.121) as

$$M\gamma\dot{q} + V'(q) = \xi(t)\sqrt{D(q)} \tag{6.123}$$

with Gaussian white noise $\langle\xi(t)\rangle = 0, \langle\xi(t)\xi(t')\rangle = 2M\gamma k_\mathrm{B}T\delta(t - t')$. Equations (6.121) and (6.123) describe the reduced dynamics of an overdamped quantum system from high down to very low temperatures and show that the corresponding quantum stochastic process is equivalent to a classical process with multiplicative noise [85, 86].

6.5.2 Quantum Decay Rate for Strong Friction

The QSE can be used to derive escape rates within a dynamical formulation in the range $\gamma\hbar\beta \gg 1$. We remark that the condition for a time scale separation $\hbar\beta \ll \gamma/\omega_0^2$ is only fulfilled above the crossover temperature, which for strong

friction reads $T_{0,\mathrm{R}} \approx (\hbar/2\pi k_\mathrm{B})\omega_0^2/\gamma$. The corresponding rate expression has already been derived within the thermodynamic ImF theory in (5.40) together with the quantum prefactor in (5.46). Here, we regain it in a much simpler way.

The situation we consider is again this: a metastable potential $V(q)$ with a barrier of height $V_\mathrm{b} \gg k_\mathrm{B}T, \hbar\omega_0$ separates a well region (well frequency ω_0) from a continuum. Initially particles stay in local thermal equilibrium inside the well. As time elapses, particles surmount the barrier and for intermediate times (plateau range) their position distribution becomes quasi-stationary $P(q,t) \to P_\mathrm{flux}(q)$ describing a constant flux across the barrier. From the QSE one then has

$$J_\mathrm{st} = -\frac{1}{\gamma M} L_\mathrm{QS} P_\mathrm{flux} \tag{6.124}$$

and the escape rate follows as

$$\Gamma = \frac{J_\mathrm{st}}{Z_\mathrm{well}} \tag{6.125}$$

with the well population Z_well. For strong friction the changeover from quasi-equilibrium in the well around $q = 0$ and nonequilibrium on the other side of the barrier is restricted to the vicinity of the barrier top located at $q_\mathrm{b} = 0$. The stationary distribution takes the known form $P_\mathrm{flux}(q) = P_\beta(q)\, g_\mathrm{fl}(q)$ with a form factor obeying $g_\mathrm{fl}(q) \to 1$ in a close range to the left of q_b and $g_\mathrm{fl}(q) \to 0$ in a close range to the right of q_b. A direct integration of (6.124) yields

$$P_\mathrm{flux}(q) = \frac{M\gamma\beta J_\mathrm{st}}{D(q)}\ \mathrm{e}^{-\beta\psi(q)} \int_q^\infty dy\ \mathrm{e}^{\beta\psi(y)} \tag{6.126}$$

with $\psi(q) = V(q) - \beta\Lambda V'(q)^2/2$. Upon inserting $Z_\mathrm{well} = \int_{-\infty}^{q_\mathrm{b}} dq P_\mathrm{st}(q)$ into (6.125) and by invoking a harmonic approximation around the well minimum and the barrier top, we obtain the rate in the quantum Smoluchowski range

$$\Gamma_\mathrm{QSR} = \frac{\sqrt{V''(0)|V''(q_\mathrm{b})|}}{2\pi M\gamma}\ \mathrm{e}^{-\beta V_b}\ \mathrm{e}^{\beta(\Lambda/2)(V''(0)+|V''(q_\mathrm{b})|)}\,. \tag{6.127}$$

In this expression the second exponential accounts for quantum fluctuations, while the first factors coincide with the overdamped Kramers rate. Note that Λ dependent terms enter exponentially and thus substantially enhance the quantum rate compared to the classical one (see Fig. 6.8). The above result is indeed identical to the one that has been obtained in (5.46) from the ImF theory, however, after evaluating a complicated path integral expression. As shown in Fig. 6.8 the QSE result agrees already for moderate friction well with the full solution (5.40). Remarkably, the rate enhancement is observable already at relatively high temperatures $\omega_0\hbar\beta < 1$ provided damping is sufficiently strong to guarantee $\gamma\hbar\beta \gg 1$.

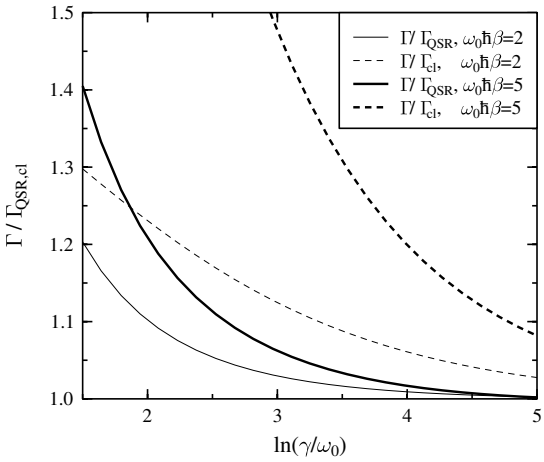

Fig. 6.8. Ratio of the exact rate with the classical (dashed) and the QSE (solid) rate vs. friction for $|V''(q_{\rm b})| = V''(0) = M\omega_0^2$.

6.6 Applications

In the sequel we discuss two applications of the quantum Smoluchowski theory, one is related to the transfer of Cooper pairs through Josephson junctions in low impedance environments, the other one reveals the strong impact of even small quantum fluctuations on mean currents in adiabatically driven ratchet potentials.

6.6.1 Quantum Phase Diffusion in Josephson Junctions

The Josephson junction (JJ) has been introduced in Sect. 3.1.3, to which we refer for further details. Based on the Josephson relation its transport dynamics can be understood as the diffusive motion of a fictitious particle in a tilted washboard potential. The translation rules between the circuit parameters R and C (resistance and capacitance) and mass and friction coefficients of the mechanical analog are

$$M = \left(\frac{\hbar}{2e}\right)^2 C \ , \quad \gamma = \frac{1}{RC} \, . \tag{6.128}$$

In the classical strong friction limit the phase diffusion of the JJ has been analysed by Ivanchenko/Zil'berman [87] and Ambegaokar/Halperin [88]. Here we present the low temperature generalization within the QSE theory [89]. Recently, also noise properties of variances of the current have been studied for this system [90].

We start by translating the constraints for the QSE dynamics to the case of JJs. Here, we also have to take into account that typically the junction

is subject to an external voltage (or a corresponding current). Accordingly, in order for the momentum $M\dot{\phi}$ to relax within the $RC = 1/\gamma$-time to a Boltzmann-like distribution around $\langle\dot{\phi}\rangle$, the external voltage V is restricted by $eV \ll \hbar\gamma$. By combining $\gamma^2/\omega_0^2 \gg 1, \gamma\hbar\beta$, where $\omega_0 = \sqrt{2E_{\rm c}E_{\rm J}}/\hbar$ is the plasma frequency of the unbiased JJ, with this latter condition and expressing them in junction parameters we expect the QSE to capture quantum phase diffusion in JJs, if

$$\frac{E_{\rm c}}{E_{\rm J}2\pi^2\rho^2} \gg 1, \ \frac{\beta E_{\rm c}}{2\pi^2\rho}, \ \frac{V}{RI_{\rm c}} \tag{6.129}$$

with $\rho = R/R_{\rm Q}$ and the resistance quantum $R_{\rm Q} = h/4e^2$. Since typically $\rho \ll 1$ the above condition allows for a broad range of values for $E_{\rm c}/E_{\rm J}$, $\beta E_{\rm J}$, and also large voltages $V/RI_{\rm c}$. Further, the relation also ensures that the actual non-ohmic impedance seen by the junction can effectively be treated as ohmic.

Now, the potential entering the QSE (6.121) reads

$$U(\phi) = -E_{\rm J}\,\cos(\phi) - E_{\rm I}\phi\,, \tag{6.130}$$

where $E_{\rm I} = (\hbar/2e)I_{\rm b}$ is the energy corresponding to the bias current $I_{\rm b}$ and the effective diffusion constant is found as

$$D(\phi) = [1 - \theta\cos(\phi)]^{-1}\,, \qquad \theta = \Lambda\beta E_{\rm J}\,. \tag{6.131}$$

From the Λ-function specified in (6.119) and reading here

$$\Lambda = 2\rho\left[C + \frac{2\pi^2\rho}{\beta E_{\rm c}} + \Psi\left(\frac{\beta E_{\rm c}}{2\pi^2\rho}\right)\right] \tag{6.132}$$

one sees immediately that $\beta E_{\rm c}/\pi\rho = \gamma\hbar\beta$ controls the changeover from classical to quantum Smoluchowski dynamics.

An important observable is the response of the JJ to an external bias current, namely, the average voltage $\langle V\rangle$. It is related to the steady state current via $\langle V\rangle = (\hbar/2\pi)\lim_{t\to\infty}\langle\dot{\phi}\rangle = 2\pi J_{\rm st}$. One then finds the current voltage–characteristics of a current biased junction to read

$$\langle V\rangle = \frac{\rho\,\pi}{\beta e}\frac{1 - {\rm e}^{-2\pi\beta E_{\rm I}}}{T_{\rm qm}}\,. \tag{6.133}$$

Here, the nominator $T_{\rm qm}$ results from normalizing the steady state phase distribution to 1 and can be written as

$$\begin{aligned} T_{\rm qm} = \frac{1}{2\pi}\int_0^{2\pi}{\rm d}\phi\int_0^{2\pi}{\rm d}\phi'\,{\rm e}^{-\beta E_{\rm I}\phi}\,{\rm e}^{-2\beta E_{\rm J}\cos(\phi')\sin(\phi/2)} \\ \times[1 - \theta\sin(\phi' - \phi/2)]\,{\rm e}^{2\beta\theta\xi(\phi,\phi')} \end{aligned} \tag{6.134}$$

with

$$\xi(\phi,\phi') = \sin(\phi')\sin(\phi/2)\left[E_{\rm I} + E_{\rm J}\cos(\phi')\cos(\phi/2)\right] . \tag{6.135}$$

The expression (6.133) together with (6.134) is the central result from which various known findings can be derived as limiting cases (see Fig. 6.9). (i) For $\beta E_{\rm c}/\rho \ll 1$ the function $T_{\rm qm}$ reduces to its classical form ($\theta \to 0$) and the classical Ivanchenko-Zil'berman Theory (IZT) [87] is recovered. (ii) In the low temperature domain $\beta E_{\rm c}/\rho \gg 1$, but for smaller couplings $\beta E_{\rm J} < 1$, terms with $\beta E_{\rm J}$ can be expanded. Due to the ϕ' integration only even powers of $\beta E_{\rm J}$ survive and one finds that quantum diffusion can be accounted for by a renormalized Josephson energy

$$E_{\rm J}^{\star} = E_{\rm J}(1 - \Lambda/2) . \tag{6.136}$$

This important extension of IZT has first been derived in [91] based on a direct evaluation of the real-time path integral expression. The corresponding supercurrent across the junction coincides with results from Coulomb blockade (CB) theory (cf. Fig. 6.9), thus describing an *incoherent* transfer of charges. (iii) For $\beta E_{\rm c}/\rho \gg 1$ and sufficiently larger couplings $\beta E_{\rm J} > 1$, coherent Cooper pair tunneling exists. Then, for $s = I/I_{\rm c} < 1$ occasional phase slips occur and lead to the voltage

$$\frac{\langle V\rangle}{RI_{\rm c}} = \frac{\sqrt{1-s^2}}{2\pi}\ {\rm e}^{-2\beta E_{\rm J}(1-s^2)^{3/2}/(3s^2)}\ {\rm e}^{\theta\sqrt{1-s^2}} , \tag{6.137}$$

which via θ is affected by diffusion related quantum fluctuations. As can be observed in Fig. 6.9, the result (6.137) tends for $\theta \to 0$ to classical thermal

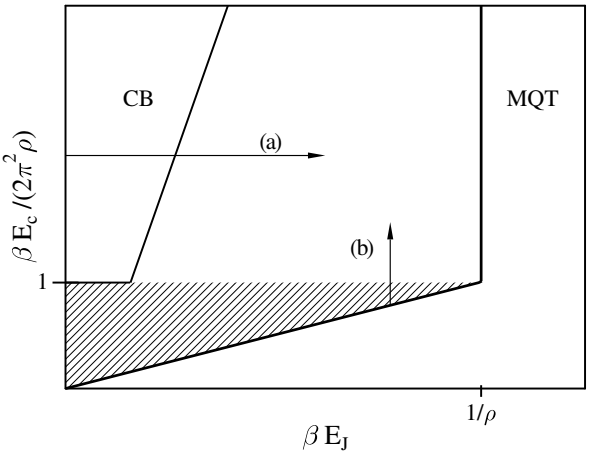

Fig. 6.9. Range of the QSE for a JJ with $\rho \ll 1$, $V/RI_{\rm c} < 1$. The classical IZT range (shaded) and the domains of Coulomb blockade (CB) and macroscopic quantum tunneling (MQT) are indicated. The QSE is applicable above the thick line, see (6.129), and the arrows illustrate various changeovers discussed in the text.

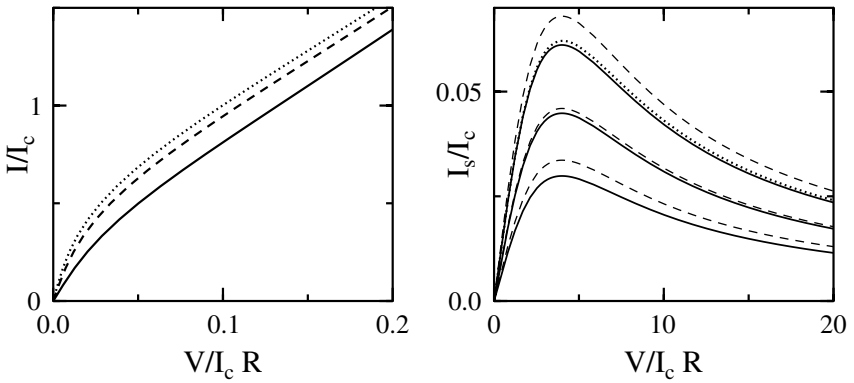

Fig. 6.10. Left: Current-voltage characteristics for $\beta E_\mathrm{J} = 2$, $\rho = 0.04$. The quantum results [$\beta E_\mathrm{c} = 1$ (dashed), $\beta E_\mathrm{c} = 20$ (solid)] are shown with the classical one ($\beta E_\mathrm{c} = 0$, dotted). Right: Supercurrent vs. voltage for $\beta E_\mathrm{J} = 0.25$, $\rho = 0.04$. The classical result (dotted, from [87]) and the CB expression [dashed, from [91]] are depicted together with the QSE result [solid, from [89]] for $\beta E_\mathrm{c} = 0.15$ (top), $\beta E_\mathrm{c} = 20$ (middle), $\beta E_\mathrm{c} = 1000$ (bottom).

activation over the barriers of the washboard potential $U(\phi)$, where quantum corrections are of the known damping independent form [92]. At lower temperatures, i.e. for finite θ, they show a complicated dependence on ρ and capture the precursors of macroscopic quantum tunneling (MQT) found at very low temperatures [93].

Thus, the central result (6.133) fills the gap between established results in different transport domains: On the one hand, for fixed $\beta E_\mathrm{c}/\rho > 1$ it leads with increasing βE_J from Coulomb blockade to coherent Cooper pair tunneling [Fig. 6.9, arrow (a)]. On the other hand, for fixed $\beta E_\mathrm{J} > 1$ it connects with varying $\beta E_\mathrm{c}/\rho$ classical thermal activation with MQT [Fig. 6.9, arrow (b)]. Apart from limiting cases, (6.133) is easily evaluated numerically; some results are shown in Fig. 6.10. Hence, the QSE approach allows to give, in a seemingly transparent manner, a complete description throughout a broad range in parameter space and must be supplemented only for very low temperatures ($T \to 0$) by more sophisticated techniques [94, 95].

6.6.2 Transport in Quantum Ratchets

Directed transport is supported in spatially periodic structures with broken reflection symmetry, so-called ratchet potentials, when they are driven far from equilibrium due to the presence of non-thermal noise sources [96, 97]. Realizations include asymmetric quantum dots [98, 99] and arrays of Josephson junctions [100]. Theoretically, this issue has been studied in the classical realm for a variety of designs [101]. Much less is known in the quantum realm though, where dissipation, quantum fluctuations, and driving may give rise to

new features [102, 103, 104, 105, 106]. While as we have seen above, a complete real-time description is extremely complicated, in the overdamped limit the QSE offers the basis to access low temperature phenomena.

For this purpose, a dimensionless ratchet potential has been considered in [82]

$$V(x) = V_0 \left\{\sin(2\pi x) + a\, \sin[4\pi(x-b)] + c\, \sin[6\pi(x-b)]\right\} \tag{6.138}$$

with numerical shape parameters a, b, c and a parameter V_0 chosen such that the dimensionless barrier height is 1. The additional nonthermal noise source is modeled by a Markovian two-state noise $\eta = \{\eta_0, -\eta_0\}$ that switches with a rate ϵ between the levels $\pm\eta_0$. In the adiabatic limit of a very small switching rate ϵ, the stationary averaged current can be obtained from the stationary solution of the QSE via $\bar{J} = [J(-\eta_0) + J(\eta_0)]/2$ where the stationary current in level η_0 reads

$$J(\eta_0) = \frac{1 - \exp[-\theta\eta_0]}{\int_0^1 \mathrm{d}y \theta D(y)^{-1} \exp[-\theta\psi(y,\eta_0)] \int_y^{y+1} \mathrm{d}x \exp[\theta\psi(x,\eta_0)]}\,. \tag{6.139}$$

Here, the dimensionless inverse temperature is denoted by θ and

$$\psi(y,\eta_0) = V(y) - \frac{1}{2}\lambda\theta[V'(y)]^2 + \eta_0\lambda\theta V'(y) - \eta_0\, y \tag{6.140}$$

is the dimensionless form of the effective thermodynamic potential $P_\beta(y) \propto \exp[-\theta\psi(y,\eta_0)]$ with λ the dimensionless fluctuation function (6.119).

A numerical analysis of the average velocity $\bar{J} \equiv \langle v \rangle$ shows, see Fig. 6.11, that the above ratchet potential with $a = 0.4, b = 0.45$, and $c = 0.3$ exhibits in

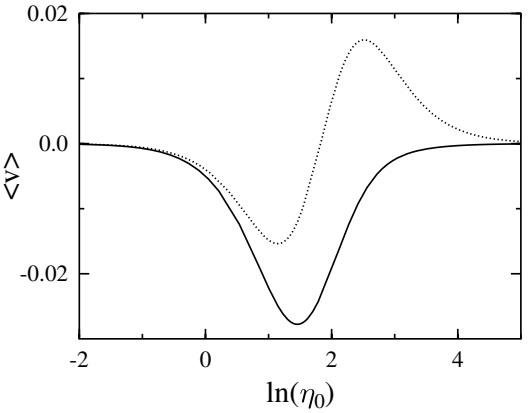

Fig. 6.11. Mean current in the ratchet potential (6.138) with $V_0 = 0.372, a = 0.4, b = 0.45, c = 0.3$ vs. the driving level. Depicted are the quantum Smoluchowski result (solid) with ($\lambda = 0.0025, \theta = 2$) and the corresponding classical one ($\lambda = 0$, dotted).

the classical case ($\lambda = 0$) a current reversal when the noise level η_0 is varied. While for weak noise the current flows in the negative direction, for larger η_0 it changes sign to approach a vanishing flux for very large η_0. However, in the quantum case ($\lambda = 0.0025$) fluctuations suppress this changeover completely. This effect can be attributed to the position and temperature dependent diffusion coefficient in (6.139) and illustrates that even small values of λ have substantial impact on the transport.

References

1. K. Blum. *Density Matrix Theory and Applications*. Plenum Press, 1981.
2. H.P. Breuer and F. Petruccione. *The Theory of Open Quantum Systems*. Oxford University Press, 2002.
3. R.K. Wangsness and F. Bloch. *Phys. Rev.*, 89:728, 1953.
4. A.G. Redfield. *IBM J. Res. Develop.*, 1:19, 1957.
5. C.W. Gardiner. *Quantum Noise*. Springer, 1991.
6. M.A. Nielsen and I.L. Chuang. *Quantum Computation and Quantum Information*. Cambridge University Press, 2000.
7. R.P. Feynman and F.L. Vernon. *Ann. Phys. (N.Y.)*, 243:118, 1963.
8. A.O. Caldeira and A.J. Leggett. *Phys. Rev. Lett.*, 46:211, 1981.
9. H. Grabert, P. Schramm, and G.-L. Ingold. *Phys. Rep.*, 168:115, 1988.
10. U. Weiss. *Quantum Dissipative Systems*. World Scientific, 1999.
11. J. Ankerhold and E. Pollak, editors. *Real-time Dynamics in Complex Quantum Systems*, volume 322 of *Chemical Physics*, 2006.
12. R. Karrlein and H. Grabert. *Phys. Rev. E*, 55:153, 1997.
13. P. Hänggi and G.L. Ingold. *Chaos*, 15:026105, 2005.
14. H. Grabert. *Chem. Phys.*, 322:160, 2006.
15. I.M. Gelfand and A.M. Yaglom. *J. Math. Phys.*, 1:48, 1959.
16. R. P. Feynman and A. P. Hibbs. *Quantum Mechanics and Path Integrals*. McGraw-Hill, 1965.
17. P. Hänggi. *Lect. Notes Phys.*, 484:15, 1997.
18. A. Schmid. *Ann. Phys. (NY)*, 170:333, 1986.
19. J. Ankerhold, H. Grabert, and G.L. Ingold. *Phys. Rev. E*, 51:4267, 1995.
20. J. Ankerhold and H. Grabert. *Chem. Phys.*, 204:27, 1996.
21. H. Hofmann and G.-L. Ingold. *Phys. Lett. B*, 264:2 53, 1991.
22. J. Ankerhold, F. Grossmann, and D.J. Tannor. *Phys. Chem. Chem. Phys.*, 1:1333, 1999.
23. Y. Tanimura and P.G. Wolynes. *J. Chem. Phys.*, 96:8485, 1992.
24. J. Ankerhold and H. Grabert. *Physica A*, 188:568, 1992.
25. J. Ankerhold and H. Grabert. *Phys. Rev. E*, 52:4704, 1995.
26. J. Ankerhold and H. Grabert. *Phys. Rev. E*, 55:1355, 1997.
27. J. Ankerhold and H. Grabert. *Europhys. Lett.*, 47:285, 1999.
28. G. Gamow. *Z. Phys.*, 51:204, 1928.
29. J.R. Oppenheimer. *Phys. Rev.*, 31:80, 1928.
30. R.W. Gurney and E.U. Condon. *Nature*, 122:439, 1928.
31. H. Hofmann. *The Physics of Warm Nuclei and of Mesocopic Systems*. Oxford University Press, 2005.

32. N. Bohr and J.A. Wheeler. *Phys. Rev.*, 56:426, 1939.
33. H.A. Kramers. *Physica*, 7:284, 1940.
34. H. Hofmann. *Phys. Rep.*, 284:137, 1997.
35. Y.A. Oganessian. *Nature*, 400:242, 1999.
36. S. Hofmann and G. Münzenberg. *Rev. Mod. Phys.*, 72:733, 2000.
37. Y.A. Oganessian. *Phys. Rev. C*, 63:011301, 2001.
38. H. Attias and Y. Alhassid. *Nucl. Phys. A*, 625:565, 1997.
39. P. Ring and P. Schuck. *The Nuclear Many Body.* Springer, 1980.
40. D. Bohm and D. Pines. *Phys. Rev.*, 92:609, 1953.
41. H. Hofmann and R. Sollacher. *Ann. Phys.*, 184:62, 1988.
42. R.L. Stratonovitch. *Sov. Phys. Dokl.*, 2:416, 1958.
43. J. Hubbard. *Phys. Rev. Lett.*, 3:77, 1959.
44. A. Bohr and B.R. Mottelson. *Nuclear Structure (vol. 1& 2).* Benjamin, 1975.
45. H. Hofmann and D. Kiderlen. *Int. J. Mod. Phys. E*, 7:243, 1998.
46. H. Hofmann, G.-L. Ingold, and M. Thoma. *Phys. Lett. B*, 317:489, 1993.
47. C. Rummel and H. Hofmann. *Phys. Rev. E*, 64:066126, 2001.
48. C. Rummel and J. Ankerhold. *Eur. Phys. J. B*, 29:105, 2002.
49. C. Rummel and H. Hofmann. *Nucl. Phys. A*, 727:24, 2003.
50. C. Rummel. *PhD thesis.* TU München, 2004.
51. W.H. Miller. *Adv. Chem. Phys.*, XXV:69, 1974.
52. F.J. Mc Lafferty and P. Pechukas. *Chem. Phys. Lett.*, 27:511, 1974.
53. W.H. Miller, S.D. Schwartz, and J.W. Tromp. *J. Chem. Phys.*, 70:4889, 1983.
54. E. Pollak. *J. Chem. Phys.*, 107:64, 1997.
55. M. Topaler and N. Makri. *Chem. Phys. Lett.*, 210:285, 1993.
56. M. Topaler and N. Makri. *Chem. Phys. Lett.*, 210:448, 1993.
57. D.E. Makarov and N. Makri. *Chem. Phys. Lett.*, 221:482, 1994.
58. M. Topaler and N. Makri. *J. Chem. Phys.*, 101:7500, 1994.
59. W.H. Miller. *Faraday. Discuss.*, 110:1, 1998.
60. H. Wang, X. Sun, and W.H. Miller. *J. Chem. Phys.*, 108:9726, 1998.
61. X. Sun, H. Wang, and W.H. Miller. *J. Chem. Phys.*, 109:4190, 1998.
62. J. Shao and N. Makri. *J. Phys. Chem. A*, 103:7753, 1999.
63. K. Thompson and N. Makri. *Phys. Rev. E*, 59:4729(R), 1999.
64. H. Wang, M. Thoss, and W.H. Miller. *J. Chem. Phys.*, 112:47, 2000.
65. Q. Shi and E. Gevan. *J. Chem. Phys.*, 121:3393, 2004.
66. T. Yamamoto. *J. Chem. Phys.*, 33:281, 1960.
67. E. Wigner. *Phys. Rev.*, 40:749, 1932.
68. E. Pollak and B. Eckhardt. *Phys. Rev. E*, 58:5436, 1998.
69. E. Pollak and J.L. Liao. *J. Chem. Phys.*, 108:2733, 1998.
70. J. Shao, J.L. Liao, and E. Pollak. *J. Chem. Phys.*, 108:9711, 1998.
71. E. Pollak. In S.D. Schwartz, editor, *Theoretical Methods in Condensed Phase Chemistry.* Kluwer Academic, Plenum, 2000.
72. E. Pollak and J. Shao. *J. Chem. Phys.*, 115:6876, 2001.
73. J. Ankerhold, M. Saltzer, and E. Pollak. *J. Chem. Phys.*, 116:5925, 2002.
74. C. Eckart. *Phys. Rev.*, 35:1303, 1930.
75. M. Smoluchowski. *Ann. Phys. (Leipzig)*, 21:772, 1906.
76. J. Ankerhold, P. Pechukas, and H. Grabert. *Phys. Rev. Lett.*, 87:086802, 2001.
77. J. Ankerhold. In F. Benatti and R. Floreani, editors, *Irreversible Quantum Dynamics*, volume 622 of *Lecture Notes in Physics.* Springer, 2003.
78. J. Ankerhold, H. Grabert, and P. Pechukas. *Chaos*, 15:026106, 2005. Focus issue "100 Years of Brownian motion".

79. H. Risken. *The Fokker Planck Equation*. Springer, 1984.
80. P. Pechukas, J. Ankerhold, and H. Grabert. *J. Phys. Chem. B*, 105:6638, 2001.
81. H. Grabert, U. Weiss, and P. Talkner. *Z. Phys. B*, 55:87, 1984.
82. L. Machura, M. Kostur, P. Hänggi, P. Talkner, and J. Łuczka. *Phys. Rev. E*, 70:031107, 2004.
83. J. Ankerhold. *Europhys. Lett.*, 61:301, 2003.
84. P. Pechukas, J. Ankerhold, and H. Grabert. *Ann. Phys. (Leipzig)*, 9:653, 2000.
85. P. Hänggi and H. Thomas. *Phys. Rep.*, 88:207, 1982.
86. P. Jung and P. Hänggi. *Adv. Chem. Phys.*, 89:239, 1995.
87. Yu.M. Ivanchenko and L.A. Zil'berman. *Sov. Phys. JETP*, 28:1272, 1969.
88. V. Ambegaokar and B.I. Halperin. *Phys. Rev. Lett.*, 25:1364, 1969.
89. J. Ankerhold. *Europhys. Lett.*, 67:280, 2004.
90. L. Machura, M. Kostur, P. Talkner, J. Łuczka, and P. Hänggi. *Phys. Rev. E*, 73:031105, 2005.
91. H. Grabert, G.-L. Ingold, and B. Paul. *Europhys. Lett.*, 44:360, 1998.
92. R. P. Feynman. *Statistical Mechanics*. Benjamin, 1972.
93. S.E. Korshunov. *Sov. Phys. JETP*, 65:1025, 1987.
94. G.-L. Ingold, H. Grabert, and U. Eberhardt. *Phys. Rev. B*, 50:395, 1994.
95. G.-L. Ingold and H. Grabert. *Phys. Rev. Lett.*, 83:786, 1999.
96. P. Hänggi and R. Bartussek. *Lect. Notes Phys.*, 476:294, 1996.
97. R.D. Astumian and P. Hänggi. *Physics Today*, 55:33, 2002.
98. H. Linke, T.E. Humphrey, and P.E. Lindelof. *Science*, 286:2314, 1999.
99. T.E. Humphrey, R. Newbury, R.P. Taylor, and H. Linke. *Phys. Rev. Lett.*, 89:116801, 2002.
100. J.B. Majer, J. Peguiron, M. Grifoni, M. Tusveld, and J.E. Mooij. *Phys. Rev. Lett.*, 90:056802, 2003.
101. P. Reimann. *Phys. Rep.*, 361:57, 2002.
102. P. Reimann, M. Grifoni, and P. Hänggi. *Phys. Rev. Lett.*, 79:10, 1997.
103. I. Goychuk, M. Grifoni, and P. Hänggi. *Phys. Rev. Lett.*, 81:649, 1998.
104. M. Grifoni, M.S. Ferreira, J. Peguiron, and J.B. Majer. *Phys. Rev. Lett.*, 89:146801, 2002.
105. S. Scheidl and V.M. Vinokur. *Phys. Rev. B*, 65:195305, 2002.
106. J. Lehmann, S. Kohler, P. Hänggi, and A. Nitzan. *Phys. Rev. Lett.*, 88:228305, 2002.

7

Unified Dynamical Theory –

From Thermal Activation to Coherent and Incoherent Tunneling

As has become clear in the previous Chapter, the most challenging domain for a dynamical theory of escape processes, i.e. a description in real-time, is the low temperature range. There, quantum mechanical non-locality renders any standard semiclassical approach to fail. Consequently, the quantum Kramers theory outlined in Sect. 6.2 applies only to temperatures slightly above the critical temperature T_c. Below T_c tunneling tends to play a prevailing role and for even lower temperatures qualitatively two different types of tunneling events may occur: One is tunneling through a barrier into a continuum supporting only outgoing states either coming from another continuum, typical for barrier scattering, or from a metastable state, typical for decay; another one is coherent tunneling typical for bi- and multistable potentials, where interferences generate a flux periodically oscillating in time. In previous Sections quantum decay rates and tunnel splittings have been calculated within thermodynamic methods based on imaginary time orbits. In this Chapter we generalize the findings for wave packet tunneling in real-time (Sect. 4) to the time evolution of ensembles and outline a unified semiclassical approach for density matrices [1, 2], which allows to calculate escape rates from high down to very low temperatures and to capture coherent as well as incoherent processes. In particular, the real-time description for barrier penetration developed in Chap. 6 for temperatures above T_c (quantum Kramers) will see its extension to the low temperature domain. While the theory will be formulated for the non-dissipative case, in principle, it can also be extended to include friction. However, analytical progress can be achieved only for vanishing friction, which then reveals the underlying structure of the semiclassical approximation and the changeover from classical escape to quantum tunneling. We remark that in the sequel we recall some theoretical foundations already specified in previous Chapters to allow for a certain degree of self-contained reading.

Joachim Ankerhold: *Quantum Tunneling in Complex Systems*
STMP **224**, 171–201 (2007)
DOI 10.1007/3-540-68076-4_7

7.1 Preliminaries

Let us consider a statistical ensemble of quantum mechanical particles of mass M moving in a barrier potential $V(q)$ separating two domains in coordinate space. The barrier top is located at $q = 0$ and energies are measured relative to the barrier energy by putting $V(0) = 0$. Initially this ensembles is prepared in a nonequilibrium state which is assumed to be of the form of an equilibrium state restricted to the left side of the barrier. We will invoke the semiclassical approximation which is appropriate provided the barrier height V_b is by far the largest energy scale in the system.

Then, the time evolution of the density matrix reads in coordinate representation

$$\rho(q_\mathrm{f}, q'_\mathrm{f}, t) = \int \mathrm{d}q_\mathrm{i}\mathrm{d}q'_\mathrm{i}\; G(q_\mathrm{f}, q_\mathrm{i}, t)\, \rho(q_\mathrm{i}, q'_\mathrm{i}, 0)\, G(q'_\mathrm{f}, q'_\mathrm{i}, t)^* \,, \tag{7.1}$$

where the real-time propagator is given by

$$G(q, q', t) = \langle q| \exp(-\mathrm{i}Ht/\hbar)|q'\rangle \tag{7.2}$$

and $\rho(q_\mathrm{i}, q'_\mathrm{i}, 0)$ describes the initial state. In principle, for our purpose any initial distribution that matches onto equilibrium on the left side and vanishes on the right side of the barrier top is appropriate. As long as the restricted equilibrium state gives vanishing probability to find the particle on the right side of the barrier top, different initial preparations lead to the same long time behavior of the density matrix. Here we put explicitly

$$\rho(q, q', 0) = Z^{-1}\, \rho_\beta(q, q')\, \Theta(-q)\, \Theta(-q') \tag{7.3}$$

for convenience with the proper normalization factor Z and the equilibrium density matrix

$$\rho_\beta(q, q') = \langle q| \exp(-\beta H)|q'\rangle \,. \tag{7.4}$$

Now, employing the path integral representation for the propagators in real and imaginary time, the above integrand in (7.1) can be written as a threefold path integral where two real time paths $q(u)$ and $q'(u)$ run in the interval $0 \le u \le t$ from q_i and q'_i to fixed endpoints q_f and q'_f, respectively, while those former coordinates are connected by an imaginary time path $\bar{q}(\sigma)$ in the interval $0 \le \sigma \le \hbar\beta$, see Fig. 7.1. The real time paths describe the time evolution of the system and the imaginary time path the initial state. Note that this formulation is the zero-friction limit of the general formulation outlined in Sect. 6.1.

The density matrix $\rho(q, q', t)$ contains all information about the nonequilibrium quantum process, in particular, the average of the operator $\hat{F} = [p\delta(q) + \delta(q)p]/2M$ gives the flux out of the metastable state, i.e., in coordinate representation

$$J(t) = (\hbar/2\mathrm{i}M)\, [\partial\rho(q_\mathrm{f}, -q_\mathrm{f}, t)/\partial q_\mathrm{f}]_{q_\mathrm{f}=0}. \tag{7.5}$$

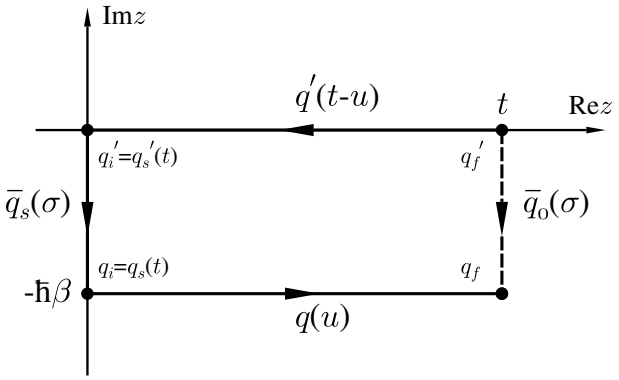

Fig. 7.1. Loop of stationary imaginary and real time paths in the complex time plane $z = u + \mathrm{i}\sigma$.

When the flux becomes quasi-stationary, $J(t) = J_{\rm st}$ within a certain *plateau region* of time, the escape rate follows from $\Gamma = J_{\rm st}$.

In the semiclassical limit (high barrier), the above path integrals are dominated by minimal action paths determined by Hamilton's equation of motion either in the potential $V(q)$ (for the real time propagators) or $-V(q)$ (for the equilibrium density matrix). Each path contributes with an exponential factor containing its minimal action and a prefactor arising from the Gaussian fluctuations about the minimal action paths. Specifically, the action in real time reads

$$S(q,q') = \int_0^t \mathrm{d}u \, [M\dot{q}^2/2 - V(q)] \,, \tag{7.6}$$

while its imaginary time version, the Euclidian action, is given by

$$\bar{S}(q,q') = \int_0^{\hbar\beta} \mathrm{d}\sigma \, [M\dot{\bar{q}}^2/2 + V(\bar{q})] \,. \tag{7.7}$$

Thus, as seen in Sect. 2.2, the propagator (7.2) is approximated as

$$G_t(q,q') = \sum_{\rm cl.paths} \sqrt{A(q,q')} \, \exp\left[\frac{\mathrm{i}}{\hbar} S(q,q') - \mathrm{i}\frac{\pi}{2}\nu\right] \,, \tag{7.8}$$

where $A(q,q') = [-\partial^2 S(q,q')/\partial q \partial q']/2\pi\mathrm{i}\hbar$ and ν is the Maslov index. An equivalent representation of the prefactor is given by

$$A(q,q') = \frac{\mathrm{i}M}{2\pi\hbar} \left[\dot{q}(0)\dot{q}(t)\frac{\partial^2 W(q,q')}{\partial E^2}\right]^{-1} \,, \tag{7.9}$$

where $W(q,q') = \int_q^{q'} \mathrm{d}q'' \, p = S(q,q') + Et$ is the short action. The corresponding approximation to the equilibrium density matrix (7.4) follows by

replacing $S(q,q')$ by $\mathrm{i}\bar{S}(q,q')$ in (7.8) with $\nu = 0$. As a result, the integrand in (7.1) is completely determined by classical mechanics in real and imaginary time, respectively, and dominated by an action factor $\exp[-\Sigma(q_\mathrm{f},q'_\mathrm{f}|q_\mathrm{i},q'_\mathrm{i})/\hbar - \mathrm{i}\pi(\nu-\nu')/2]$ with

$$\Sigma(q_\mathrm{f},q'_\mathrm{f}|q_\mathrm{i},q'_\mathrm{i}) = -iS(q_\mathrm{f},q_\mathrm{i}) + \bar{S}(q_\mathrm{i},q'_\mathrm{i}) + \mathrm{i}S(q'_\mathrm{f},q'_\mathrm{i})\,. \tag{7.10}$$

With the approximate integrand at hand, it is consistent to evaluate the ordinary integrations in (7.1) in stationary phase. The stationary phase points are determined by minimizing Σ with respect to the initial coordinates $q_\mathrm{i}, q'_\mathrm{i}$, i.e.,

$$\left.\frac{\partial\Sigma}{\partial q_\mathrm{i}}\right|_{(q_\mathrm{f},q'_\mathrm{f})} = 0, \qquad \left.\frac{\partial\Sigma}{\partial q'_\mathrm{i}}\right|_{(q_\mathrm{f},q'_\mathrm{f})} = 0\,. \tag{7.11}$$

Since the endpoints $q_\mathrm{f}, q'_\mathrm{f}$ are fixed, the resulting stationary phase points $q_\mathrm{s}(t)$ and $q'_\mathrm{s}(t)$ are functions of time with $q_\mathrm{s}(0) = q_\mathrm{f}$, $q'_\mathrm{s}(0) = q'_\mathrm{f}$. For finite t these roots are in general complex. The dominant imaginary time path $\bar{q}_\mathrm{s}(\sigma)$ connects $q'_\mathrm{s}(t)$ with $q_\mathrm{s}(t)$, and the two real time paths $q(u)$ and $q'(u)$ connect $q_\mathrm{s}(t)$ and $q'_\mathrm{s}(t)$ with q_f and q'_f, respectively. Hence, the steepest–descent approximation naturally provides a mapping from the integration contour in the complex time plane onto a loop in the complex coordinate space connecting the endpoints (Fig. 7.1). We emphasize that the appearance of complex paths has nothing to do with tunneling but rather is merely a consequence of the stationary phase approximation and holds also for systems with no barrier at all. In fact, it turns out that the complex semiclassical real-time trajectories used here never cross the barrier top, in contrast to paths emerging from *ad hoc* complexification procedures occasionally adopted to describe barrier penetration [3].

Starting from the steepest descent conditions (7.11) and exploiting Hamilton Jacobi mechanics, one immediately derives

$$p_\mathrm{s}(0) = \mathrm{i}\bar{p}_\mathrm{s}(\hbar\beta)\ ,\ p'_\mathrm{s}(0) = \mathrm{i}\bar{p}_\mathrm{s}(0)\ ,\ E = E' = \bar{E}\,. \tag{7.12}$$

Here, $p_\mathrm{s}(u)$ $[p'_\mathrm{s}(u)]$ is the momentum of the real time path $q(u)$ $[q'(u)]$ with energy E $[E']$ connecting q_s $[q'_\mathrm{s}]$ and q_f $[q'_\mathrm{f}]$; accordingly, $\bar{p}_\mathrm{s}(\sigma)$ denotes the momentum of the imaginary time path $\bar{q}_\mathrm{s}(\sigma)$ running from q'_s to q_s with Euclidian energy $\bar{E} = -\bar{p}_\mathrm{s}^2/2M + V(\bar{q})$, see Fig. 7.1. Equation (7.12) can also be expressed as $\mathrm{d}\Sigma/\mathrm{d}t = 0$ with the solution

$$\Sigma(q_\mathrm{f},q'_\mathrm{f}|q_\mathrm{s},q'_\mathrm{s}) = \bar{S}(q_\mathrm{f},q'_\mathrm{f})\,. \tag{7.13}$$

Hence along the loop of steepest descent paths the full action is just given by the equilibrium action and thus independent of time. Differentiating (7.13) with respect to $q_\mathrm{f}, q'_\mathrm{f}$, one finds

$$p_\mathrm{s}(t) = \mathrm{i}\bar{p}_0(\hbar\beta), \quad p'_\mathrm{s}(t) = \mathrm{i}\bar{p}_0(0)\,, \tag{7.14}$$

where $\bar{p}_0(\sigma)$ is now the momentum of the imaginary time path $\bar{q}_0(\sigma)$ connecting $q'_{\rm f}$ with $q_{\rm f}$ in imaginary time $\hbar\beta$. This path has Euclidean energy $\bar{E}_{\rm f}$ which depends on $q_{\rm f}, q'_{\rm f}$ and $\hbar\beta$ but not on t. Hence, we first deduce that the energies in (7.12) are given by $\bar{E}_{\rm f}$, which implies energy and momentum conservation throughout the loop in Fig. 7.1. Secondly, we arrive at the remarkable result that the sequence of time-dependent stationary phase points $q_{\rm s}(t)$ $[q'_{\rm s}(t)]$ is itself a minimal action path starting at $q_{\rm s}(0) = q_{\rm f}$ $[q'_{\rm s}(0) = q'_{\rm f}]$ with energy $\bar{E}_{\rm f}$.

To complete the ordinary integrations in (7.1) over the initial coordinates $q_{\rm i}, q'_{\rm i}$, we transform to fluctuations $y = q_{\rm i} - q_{\rm s}$ and $y' = q'_{\rm i} - q'_{\rm s}$ about the stationary phase points. An expansion of the full action (7.10) for fixed endpoints $q_{\rm f}, q'_{\rm f}$ around the stationary phase points up to second order leads to $\Sigma(q_{\rm f}, q'_{\rm f}|q_{\rm i}, q'_{\rm i}) = \bar{S}(q_{\rm f}, q'_{\rm f}) + \delta\Sigma^{(2)}(y, y')$ with

$$\delta^{(2)}\Sigma(y, y') = \frac{1}{2}\ (y, y')\ \Sigma^{(2)}\ \begin{pmatrix} y \\ y' \end{pmatrix}, \tag{7.15}$$

where

$$\Sigma^{(2)} = \begin{pmatrix} \Sigma_{\rm ss}\Sigma_{\rm ss'} \\ \Sigma_{\rm ss'}\Sigma_{\rm s's'} \end{pmatrix} \tag{7.16}$$

is the matrix of second order derivatives, $\Sigma_{\rm ss} = \partial^2\Sigma(q_{\rm i}, q'_{\rm i})/\partial q_{\rm i}^2$ etc., to be taken at $q_{\rm i} = q_{\rm s}, q'_{\rm i} = q'_{\rm s}$.

Upon inserting (7.3) into (7.1) the integrand reduces to a product of Gaussian weighting factors for deviations from the stationary phase points and an initial state factor $\theta(-q_{\rm s} - y)\theta(-q'_{\rm s} - y')$ describing deviations from thermal equilibrium at $t = 0$. Provided there is only one semiclassical path for each of the propagators, we obtain from (7.1) by virtue of (7.13) and (7.15) the semiclassical time dependent density matrix in the form

$$\rho(q_{\rm f}, q'_{\rm f}, t) = \frac{1}{Z}\rho_\beta(q_{\rm f}, q'_{\rm f})\, g(q_{\rm f}, q'_{\rm f}, t)\,. \tag{7.17}$$

Here, deviations from equilibrium are described by a *form factor*

$$g(q_{\rm f}, q'_{\rm f}, t) = \frac{1}{\pi}\int_{-\infty}^{u(q_{\rm s})} {\rm d}z \int_{-\infty}^{u'(z,q'_{\rm s})} {\rm d}z'\, {\rm e}^{-(z^2+z'^2)}\,, \tag{7.18}$$

where

$$u(q_{\rm s}) = -q_{\rm s}\sqrt{\frac{{\rm Det}[\Sigma^{(2)}]}{2\hbar\Sigma_{\rm s's'}}}, \qquad u'(q'_{\rm s}, z) = -q'_{\rm s}\sqrt{\frac{\Sigma_{\rm s's'}}{2\hbar}} + z\frac{\Sigma_{\rm ss'}}{\sqrt{{\rm Det}[\Sigma^{(2)}]}} \tag{7.19}$$

with ${\rm Det}[\Sigma^{(2)}] = \Sigma_{\rm ss}\Sigma_{\rm s's'} - (\Sigma_{\rm ss'})^2$. In deriving (7.17) we invoked that Hamilton Jacobi mechanics implies [4]

$$\left[\frac{A(q_{\rm f}, q_{\rm s})\bar{A}(q_{\rm s}, q'_{\rm s})A(q'_{\rm f}, q'_{\rm s})}{{\rm Det}[\Sigma^{(2)}]}\right]^{1/2} = \bar{A}(q_{\rm f}, q'_{\rm f})\,. \tag{7.20}$$

Note that for an initial equilibrium state, formally $\theta(\cdot) \to 1$ in (7.3) so that $u, u' \to \infty$ in (7.18), the form factor becomes 1 and the semiclassical density matrix is in fact stationary. When there is more than one classical path one has to sum in (7.17) over the contributions of all of them. Certainly, the above formulae (7.18) and (7.19) are only applicable as long as the Gaussian semiclassical and stationary phase approximations are valid, i.e. as fluctuations are sufficiently small. This will be seen to be no longer the case for low temperatures and/or very long times. How the classical paths in the complex plane can then be used as a skeleton for an extended semiclassical/stationary phase calculation will be shown below.

Since in the sequel we are particularly interested in the flux across a barrier, we restrict our analysis to non-diagonal end-coordinates q_f and $q'_\mathrm{f} = -q_\mathrm{f}$ of the density matrix close to the barrier top.

7.2 Parabolic Barrier

The semiclassical and the stationary phase approximations are always exact for quadratic potentials. In this Section we will thus first re-derive the findings gained in Sect. 6.2 within the methodology developed above and for vanishing dissipation. We consider a parabolic barrier

$$V(q) = -\frac{1}{2} M \omega_b^2 \, q^2 \tag{7.21}$$

so that the imaginary time dynamics runs in a harmonic oscillator potential. For the minimal action path $\bar{q}_0(\sigma)$ connecting $-q_\mathrm{f}$ with q_f in time $\hbar\beta$ one obtains

$$\bar{q}_0(\sigma) = \frac{q_\mathrm{f}}{\sin(\omega_\mathrm{b}\hbar\beta/2)} \, \sin\left[\omega_\mathrm{b}(\sigma - \hbar\beta/2)\right] . \tag{7.22}$$

This leads to the known equilibrium density matrix

$$\rho_\beta(q_\mathrm{f}, -q_\mathrm{f}) = \frac{1}{\sqrt{4\pi\delta_\mathrm{b}^2 \sin(\omega_\mathrm{b}\hbar\beta)}} \, \exp\left[-\cot(\omega_\mathrm{b}\hbar\beta/2)\, \frac{q_\mathrm{f}^2}{2\delta_\mathrm{b}^2}\right] \tag{7.23}$$

with the relevant length scale $\delta_\mathrm{b} = \sqrt{\hbar/2M\omega_\mathrm{b}}$.

The real-time dynamics simply follows. The classical real-time paths $q(u)$ and $q'(u)$ lead to the endpoints q_f and $-q_\mathrm{f}$, respectively, and hence obey $q(t) = q_\mathrm{f}$, $q'(t) = -q_\mathrm{f}$. On the other hand, the stationary phase condition (7.12) implies $\dot{q}(t) = \mathrm{i}\dot{\bar{q}}(\hbar\beta)$, $\dot{q}'(t) = \mathrm{i}\dot{\bar{q}}(0)$ and we readily find $q(u) = \bar{q}(\hbar\beta - \mathrm{i}t + \mathrm{i}u)$, i.e.,

$$\begin{aligned} q(u) &= \frac{q_\mathrm{f}}{\sin(\omega_\mathrm{b}\hbar\beta/2)} \, \sin\left[\omega_\mathrm{b}(\hbar\beta/2 - it + iu)\right], \\ q'(u) &= q(u + \mathrm{i}\hbar\beta), \quad 0 \le u \le t. \end{aligned} \tag{7.24}$$

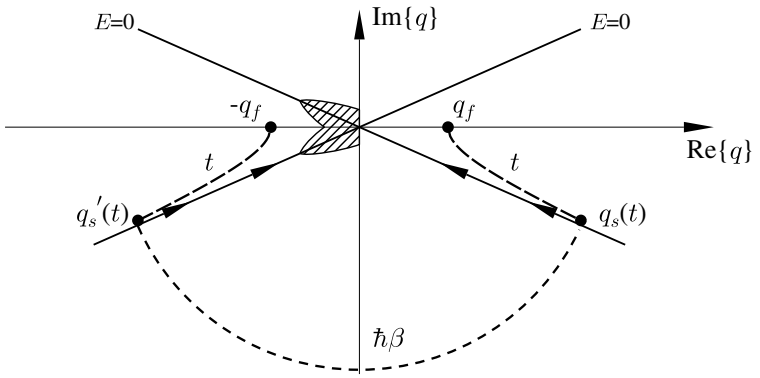

Fig. 7.2. Semiclassical paths (dashed lines) in the complex plane near the parabolic barrier top. Shaded area contains relevant intermediate coordinates $q_\mathrm{i}, q_\mathrm{i}'$ reached by fluctuations along arrows.

At time t the imaginary time path $\bar{q}_0(\sigma)$ from $-q_\mathrm{f}$ to q_f is mapped onto the path $\bar{q}_\mathrm{s}(\sigma) = q(\mathrm{i}\hbar\beta - \mathrm{i}\sigma), 0 \le \sigma \le \hbar\beta$ connecting $q_\mathrm{s}'(t) = q'(0)$ with $q_\mathrm{s}(t) = q(0)$ (Fig. 7.2). The stationary phase points

$$\begin{aligned} q_\mathrm{s}(t) &= \frac{q_\mathrm{f}}{\sin(\omega_\mathrm{b}\hbar\beta/2)} \sin\left[\omega_\mathrm{b}(\hbar\beta/2 - it)\right] \\ q_\mathrm{s}'(t) &= -q_\mathrm{s}(t)^* \end{aligned} \tag{7.25}$$

are as functions of t also classical paths moving away from the barrier top as t increases – $q_\mathrm{s}(t)$ to the right and $q_\mathrm{s}'(t)$ to the left for $q_\mathrm{f} > 0$. For longer times $\omega_\mathrm{b}t \gg 1$, the stationary phase points asymptotically tend towards the limiting trajectories starting from $q_\mathrm{f} = 0$ referred to as asymptotes henceforth. Similar to separatrices in classical phase space, these asymptotes divide the complex plane in regions of negative and positive Euclidian energy: in the sectors including the real axis classical real time motion has $\bar{E} < 0$ (but $E \le 0$ or $E > 0$) while in the remaining parts $\bar{E} > 0$. However, in contrast to simple classical separatrices the asymptotes are temperature dependent. The angle α of the q_s and q_s'-asymptotes with the positive and negative real axis, respectively, is found as

$$\alpha = \frac{\pi - \omega_\mathrm{b}\hbar\beta}{2}\,. \tag{7.26}$$

Now, for the nonequilibrium preparation (7.3) the initial coordinates $q_\mathrm{i}, q_\mathrm{i}'$ are constrained to $\mathrm{Re}\{q_\mathrm{i}\}$, $\mathrm{Re}\{q_\mathrm{i}'\} \le 0$. Since $q_\mathrm{s}(t)$ and $q_\mathrm{s}'(t)$ are on different sides of the barrier, $\rho(q_\mathrm{f}, -q_\mathrm{f}, t)$ gains nonvanishing values *only due to fluctuations* that effectively shift q_i away from q_s and across the barrier top [see (7.19)]. For the parabolic barrier potential the matrix elements in (7.16) take the simple form

$$\Sigma_{\rm ss} = M\omega_{\rm b}\left[\cot(\omega_{\rm b}\hbar\beta) - {\rm i}\coth(\omega_{\rm b}t)\right], \quad \Sigma_{\rm s's'} = \Sigma^*_{\rm ss},$$
$$\Sigma_{\rm ss'} = -\frac{M\omega_{\rm b}}{\sin(\omega_{\rm b}\hbar\beta)} \tag{7.27}$$

so that the matrix $\Sigma^{(2)}$ can easily be diagonalized. One finds for the eigenvalues

$$\frac{\lambda_\pm}{M\omega_{\rm b}} = \cot(\omega_{\rm b}\hbar\beta) \pm \left[\cot(\omega_{\rm b}\hbar\beta)^2 - \frac{1}{\sinh(\omega_{\rm b}t)^2}\right]^{1/2}. \tag{7.28}$$

While, in principle, with (7.18) we can now evaluate the complete dynamics of the density matrix, we will concentrate here on the long time asymptotics of the nonequilibrium state. Then, in the asymptotic region $\omega_{\rm b}t \gg 1$ the eigenvalue λ_- tends to zero as $\lambda_- \propto M\omega_{\rm b}\exp(-\omega_{\rm b}t)$, reflecting the instability of the parabolic barrier. Hence, fluctuations around the stationary phase points with the least action increase occur in the direction of the eigenvector with eigenvalue λ_-. These fluctuations are of the form $y_{\rm i} = |y_{\rm i}|\exp[{\rm i}(\alpha+\omega_{\rm b}\hbar\beta)]$ and $y'_{\rm i} = |y_{\rm i}|\exp({\rm i}\alpha)$ so that $q_{\rm i}$ and $q'_{\rm i}$ move simultaneously along their asymptotes meeting at the barrier top (see Fig. 7.2). Now, inserting the matrix elements (7.27) and the stationary phase points (7.25) into (7.19) and considering the limit $\omega_{\rm b}t \gg 1$, the relevant form factor turns out to be stationary

$$g_{\rm fl}(q,-q) = \frac{1}{\sqrt{\pi}}\int_{-\infty}^{{\rm i}2q\Omega} {\rm d}x\ {\rm e}^{-x^2} \tag{7.29}$$

with $\Omega = \sqrt{\cot(\omega_{\rm b}\hbar\beta/2)/(8\delta_{\rm b}^2)}$. The corresponding constant flux across the barrier is obtained from (7.5) and (7.17) as

$$J_{\rm st} = \frac{\hbar}{2ZM}\rho_\beta(0,0)\ \left.\frac{\partial g_{\rm fl}(q_{\rm f},-q_{\rm f})}{\partial q_{\rm f}}\right|_{q_{\rm f}=0}, \tag{7.30}$$

which leads to the known result

$$\Gamma = J_{\rm st} = \frac{\omega_b}{4\pi}\,\frac{1}{Z\sin(\omega_{\rm b}\hbar\beta/2)}\,. \tag{7.31}$$

Here, Z denotes an appropriate normalization constant, which may be taken as the relative normalization with respect to the minimum of the full anharmonic potential. We mention that the parabolic barrier approximation makes physically only sense for temperatures above the critical temperature $T_{\rm c}$ [see Sect. 6.3] and the specific form of the barrier potential must be considered for $T < T_{\rm c}$.

7.3 Double Well Potential

A model well-behaved for the entire range of temperatures is the bistable dynamics of a particle moving in a double well potential

$$V(q) = -\frac{M\omega_{\rm b}^2}{2}\, q^2 \left[1 - \frac{q^2}{2q_{\rm a}^2}\right]. \tag{7.32}$$

Here, the barrier is located at $q = 0$, the wells at $q = \pm q_{\rm a}$, and the barrier height is $V_{\rm b} = -V(q_{\rm a}) = (M\omega_{\rm b}^2/4)q_{\rm a}^2$. This potential exhibits rich quantum dynamics, namely, incoherent hopping between the wells over a broad range of temperatures that changes to coherent oscillations for $T \to 0$. Due to the complexity of the dynamics this is a highly nontrivial problem for the semiclassical approach where the ratio $\delta_{\rm b}/q_{\rm a}$ serves as the small parameter.

7.3.1 Thermal Equilibrium

The Euclidian mechanics in the inverted potential $-V(q)$ can be solved exactly using Jacobian elliptic functions [5]. For the general solution one obtains

$$\bar{q}_0(q_{\rm f}, \sigma) = B\,{\rm sn}\left[\omega(B)\sigma - \phi_f|m\right], \quad 0 \le \sigma \le \hbar\beta\,, \tag{7.33}$$

where the boundary conditions $\bar{q}_0(q_{\rm f}, 0) = -q_{\rm f}$ and $\bar{q}_0(q_{\rm f}, \hbar\beta) = q_{\rm f}$ fix the amplitude B and phase $\phi_{\rm f}$. Since the potential is no longer purely quadratic, depending on temperature there may be several solutions each of them with another amplitude. In (7.33) the frequency is given by

$$\omega(B) = \omega_{\rm b}\,\sqrt{1-\eta^2}, \quad \eta^2 = \frac{B^2}{2q_{\rm a}^2}, \tag{7.34}$$

and the phase can be represented as an incomplete elliptic integral

$$\phi_{\rm f} = F(q_{\rm f}/B|m) = \int_0^{q_{\rm f}/B} {\rm d}x \frac{1}{\sqrt{(1-x^2)(1-m\,x^2)}} \tag{7.35}$$

with the so-called modul $m = \eta^2/(1-\eta^2)$. From the boundary condition $\bar{q}_0(\hbar\beta) = -\bar{q}_0(0)$ and the periodicity of the Jacobian function, ${\rm sn}[z + 2rK(m)|m] = (-1)^r {\rm sn}[z|m], r = 1, 2, 3, \ldots$ with $K(m) = F(1, m)$, the amplitude B is determined by

$$\omega(B)\hbar\beta = 2rK(m) + \left[1 + (-1)^r\right]\phi_{\rm f}\,. \tag{7.36}$$

Since $K(m), \phi_{\rm f} > 0$, for fixed $\omega_{\rm b}\hbar\beta$ real solutions to this equation exist only for a finite number of integers $r \ge 0$.

Let us briefly discuss the trajectories $\bar{q}_0(q_{\rm f}, \sigma)$ as the temperature is lowered. For high temperatures only solutions of (7.36) with $r = 0$ exist corresponding to direct paths from $-q_{\rm f}$ to $q_{\rm f}$; particularly, $\bar{q}_0(0, \sigma) = 0$. As the temperature drops below the critical temperature

$$T_{\rm c} = \hbar\omega_{\rm b}/\pi k_{\rm B}, \tag{7.37}$$

i.e. $\omega_{\rm b}\hbar\beta > \pi$, solutions of (7.36) with $r = 1$ arise. Then, for $q_{\rm f} = 0$ the barrier top can be joined with itself also by two nonlocal paths denoted by

$\bar{q}_\pm(0,\sigma)$ oscillating in $-V(q)$ to the right and to the left with amplitudes $\pm q_1$, respectively, and energy $\bar{E}_1 = V(q_1)$. With further decreasing temperature q_1 grows and eventually saturates at q_a for $T \to 0$. For finite q_f the situation is rather similar: oscillating paths $\bar{q}_\pm(q_\mathrm{f},\sigma)$ exist for all $q_\mathrm{f} < q_1$. These paths connect $-q_\mathrm{f}$ with q_f via a turning point at $\pm q_1$, thus, differing from $\bar{q}_\pm(0,\sigma)$ only by a phase shift. The described scenario repeats in an analog way at all $T = T_\mathrm{c}/r, r = 2,3,4,\ldots$, where r counts the number of turning points. At zero temperature all these oscillating paths reach $\pm q_\mathrm{a}$ with the same energy $\bar{E}_\mathrm{a} = V(q_\mathrm{a})$ and are then called instantons.

Now that all proper Euclidian trajectories are identified, the semiclassical equilibrium state follows readily. For high temperatures $T > T_\mathrm{c}$ and end-coordinates q_f near the barrier top, $\rho_\beta(q_\mathrm{f},-q_\mathrm{f})$ basically coincides with the parabolic result (7.23) and anharmonic corrections are negligible. This situation changes drastically for temperatures near T_c. Then, the bifurcation of new classical paths leads to large quantum fluctuations and one has to go beyond the Gaussian approximation of the fluctuation integral. Slightly below T_c a caustic appears for $q_\mathrm{f} = q_1$. It turns out that the paths newly emerging near T_c are stable and dominate $\rho_\beta(q,q')$ for all $T_\mathrm{c} > T > 0$ while the unstable high temperature paths and those popping up at even lower T give negligible contributions. Since for $q_\mathrm{f} < q_1$ all paths $\bar{q}_\pm(q_\mathrm{f},\sigma)$ differ only by a phase shift, one has for the corresponding actions

$$\bar{S}_\pm(q_\mathrm{f},-q_\mathrm{f}) = \bar{S}_+(0,0) = \bar{S}_-(0,0) \tag{7.38}$$

so that

$$\rho_\beta(q_\mathrm{f},-q_\mathrm{f}) = 2[\bar{A}(q_\mathrm{f},-q_\mathrm{f})]^{1/2}\exp[-\bar{S}_+(0,0)/\hbar], \quad q_\mathrm{f} < q_1\,. \tag{7.39}$$

Accordingly, the matrix element $\rho_\beta(q_\mathrm{f},-q_\mathrm{f})$ changes to a non-Gaussian distribution with a local minimum at $q_\mathrm{f} = 0$ and two maxima at $q_\mathrm{f} = \pm q_1$. Thereby $\bar{S}_+(0,0) < 0$, so that the probability $\rho_\beta(0,0)$ to find the particle at $q = 0$ is substantially enhanced compared to its classical value.

For $T \to 0$ it is no longer sufficient to include only the trajectories with $r = 1$ in the semiclassical analysis but rather all other paths with $r > 1$ must also be taken into account. This is due to the fact that the smaller action factors of these latter paths are compensated for by zero mode phase factors from the corresponding fluctuation path integrals. Hence, all instanton contributions are summed up to yield e.g. for coordinates near the barrier top

$$\begin{aligned}\rho_\beta(q_\mathrm{f},-q_\mathrm{f}) = {} & \frac{8}{\delta_\mathrm{a}\sqrt{2\pi}}\,\mathrm{e}^{-\beta[V(q_\mathrm{a})+\hbar\omega_\mathrm{a}/2]-\bar{W}_\mathrm{a}/\hbar} \\ & \times\left[\cosh\left(\frac{\hbar\beta\Delta}{2}\right)+\cosh\left(\frac{q_\mathrm{f}q_\mathrm{a}}{2\delta_\mathrm{a}^2}\right)\sinh\left(\frac{\hbar\beta\Delta}{2}\right)\right]. \end{aligned}\tag{7.40}$$

Here, $\bar{W}_\mathrm{a} \equiv \bar{W}(-q_\mathrm{a},q_\mathrm{a}) = -\hbar\beta\bar{E} + \bar{S}(-q_\mathrm{a},q_\mathrm{a})$ is the short action for an instanton from $-q_\mathrm{a}$ to q_a. Further,

$$\Delta = \omega_{\rm a} \frac{4q_{\rm a}}{\sqrt{2\pi}\delta_{\rm a}} \exp(-\bar{W}_{\rm a}/\hbar) \tag{7.41}$$

denotes the WKB tunnel splitting with the well frequency $\omega_{\rm a} = \omega_{\rm b}\sqrt{2}$ and $\delta_{\rm a}^2 = \hbar/2M\omega_{\rm a}$.

7.3.2 Dynamics of Stationary Phase Points

As in case of the parabolic barrier, the stationary real-time paths can be directly inferred from the Euclidian dynamics at $t = 0$. From (7.33) and the stationary phase condition we have

$$q_{\rm s}(t) = B\,{\rm sn}[\phi_{\rm f} - {\rm i}\omega(B)t|m], \qquad q'_{\rm s}(t) = -q_{\rm s}[(-1)^{r+1}t] \tag{7.42}$$

and $\bar{q}_0(\sigma)$ is mapped at time t onto $\bar{q}_{\rm s}(\sigma) = \bar{q}_0[\sigma + {\rm i}(-1)^{r+1}t]$ where r follows from (7.36). In the sequel we always formulate the semiclassical theory in terms of the real time paths $q_{\rm s}, q'_{\rm s}$ that start at the endpoints $q_{\rm f}, -q_{\rm f}$, respectively, and reach the initial points $q_{\rm i}, q'_{\rm i}$ after time t. Since the endpoints $q_{\rm f}, -q_{\rm f}$ are fixed, while the most relevant initial coordinates depend on time, this backward view of the dynamics is in fact more transparent. The real time trajectories now start from the end coordinates we are interested in and lead to the relevant initial coordinates that need to be integrated over with an integrand weighted according to the initial deviations from equilibrium. The path $q_{\rm s}(t)$ runs in the complex coordinate plane as a periodic orbit with period $t_{\rm p}(q_{\rm f}) = 2K(1-m)/\omega(B)$ (Fig. 7.3). Within one period it connects $q_{\rm f}$ with $q_{\rm f}$ via a loop crossing the real axis also after time $t_{\rm p}(q_{\rm f})/2$ at the point $q_{\rm c}(q_{\rm f}) = q_{\rm s}[q_{\rm f}, t_{\rm p}(q_{\rm f})/2] \geq q_{\rm a}$. Thus $q_{\rm s}(t)$ stays always on the same side of the barrier top and likewise $q'_{\rm s}(t)$ on the other side so that the complex dynamics of the stationary phase points starting from $q_{\rm f}$ and $-q_{\rm f}$, respectively, reflects a bounded motion in either of the potential wells.

Let us consider the stationary orbits as the temperature decreases. For high temperatures $T > T_{\rm c}$, i.e. $r = 0$, each $q_{\rm f}$-dependent loop carries its own period $t_{\rm p}(q_{\rm f})$ and energy $E(q_{\rm f})$. If $q_{\rm f} \neq 0$, $t_{\rm p}$ is small for $T \gg T_{\rm c}$ and the real time dynamics corresponds to a fast bouncing back and forth in the well. As the temperature is lowered the period grows while simultaneously the width of the loop $q_{\rm c}(q_{\rm f})$ shrinks. In the special case $q_{\rm f} = 0$ the real time path reduces to a constant $q_{\rm s}(0,t) = 0$. For temperatures $T < T_{\rm c}$ the situation changes according to the appearance of new oscillating Euclidian paths $\bar{q}_{\pm}(q_{\rm f}, \sigma)$ for $q_{\rm f} < q_1$. In contrast to the high temperature case *all* stationary phase point paths with $q_{\rm f} < q_1$ have then the same period $t_{\rm p}(q_{\rm f}) = t_{\rm p}(q_1)$ and energy $E(q_{\rm f}) = \bar{E}_1$, and differ only in their respective phases. Special cases are $q_{\rm f} = 0$ and $q_{\rm f} = q_1$: The path $q_{\rm s}(q_{\rm f}, t), q_{\rm f} \to 0$ runs along the imaginary axis, while the orbit $q_{\rm s}(q_1, t)$ degenerates to a usual well oscillation along the real axis. These properties have a direct effect on the corresponding actions. One finds by employing Cauchy's theorem that after each period

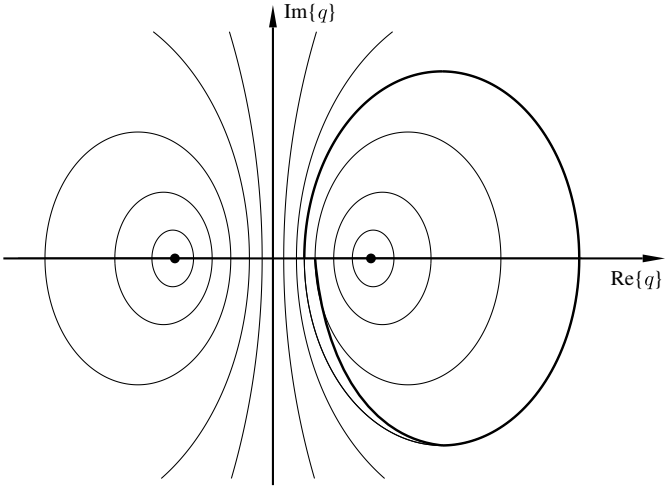

Fig. 7.3. Real time paths in the double well potential with wells at $\pm q_\mathrm{a}$ (dots) for various q_f and $T = 0$ (thin lines). The thick line shows a typical fluctuation connecting orbits with different q_f.

$$S[q_\mathrm{s}(q_\mathrm{f}, nt_\mathrm{p}), q_\mathrm{f}] = S[q_\mathrm{s}(q_1, nt_\mathrm{p}), q_1], \quad q_\mathrm{f} \leq q_1. \tag{7.43}$$

Hence, all $q_\mathrm{s}(q_\mathrm{f}, t)$ for $q_\mathrm{f} < q_1$ can be seen as phase shifted copies of the specific real path $q_\mathrm{s}(q_1, t)$ having the same energy, period, and action increase during one period. In particular, the period $t_\mathrm{p}(q_1)$ is large for $T \lesssim T_\mathrm{c}$ when q_1 is still small, $t_p(q_1) \approx \ln(q_\mathrm{a}/q_1)/\omega_b$, and drops down to $t_\mathrm{p}(q_\mathrm{a}) = 2\pi/\omega_\mathrm{a}$ in the limit $T \to 0$.

7.3.3 Dynamics for High and Moderate Low Temperatures

For $t = 0$ the density matrix is given by the initial state (7.3). The semiclassical time evolution of this state follows by inserting the proper classical paths into (7.17). In the sequel, we mainly focus on the long time dynamics and are especially interested in a plateau region where the time evolution becomes quasi-stationary.

We start by addressing the question when a plateau region does exist at all. Inserting the classical paths into $g(q_\mathrm{f}, -q_\mathrm{f}, t)$ in (7.19), the detailed analysis reveals that this function becomes stationary when the ratio $q_\mathrm{s}(t)/p_\mathrm{s}(t)$ reduces to a constant. Since this will only occur within the parabolic barrier region, a least upper bound for a plateau region follows from the time interval within which a particle starting at a typical point q_b near the barrier top continues to experience a nearly parabolic potential. This leads to $t \ll t_\mathrm{p}(q_\mathrm{b})$. The lower bound is obvious: it is given by the transient time near the top, i.e. by $1/\omega_\mathrm{b}$. Hence, a plateau region can be estimated to occur as long as there is clear separation of time scales between local barrier motion and global well

oscillations, i.e., $1 \ll \omega_b t \ll \omega_b t_p(q_b)$. Particularly, in the temperature domain where a plateau region exists, the Gaussian/stationary phase approximations are valid and we can actually calculate a rate. These approximations break down when the stationary phase points move far from the barrier top and times of order $t_p(q_b)$ become relevant for the barrier crossing.

For high temperatures $T > T_c$ the typical length scale q_b can be identified with $\delta_b = \sqrt{\hbar/2M\omega_b}$. Then, the separation of time scales fails for very high temperatures where $k_B T \gtrsim 8V_b$ meaning that the thermal energy is of the same order or larger than the barrier height. With decreasing temperature t_p grows so that for $\omega_b \hbar\beta$ of order 1 a wide plateau range appears with $t_p \approx \ln(q_a/\delta_b)/\omega_b$. In the corresponding density matrix anharmonic corrections are small, and we obtain approximately the parabolic result (7.29). To get the rate, here, the proper normalization constant Z is taken as the partition function of the harmonic well oscillator

$$Z = \frac{1}{2\sinh(\omega_a \hbar\beta/2)}\, \mathrm{e}^{\beta V_b}\,. \tag{7.44}$$

Hence, from (7.30) one regains the known result

$$\Gamma = \frac{\omega_b}{2\pi}\, \frac{\sinh(\omega_a \hbar\beta/2)}{\sin(\omega_b \hbar\beta/2)}\, \mathrm{e}^{-\beta V_b} \tag{7.45}$$

with the exponential Arrhenius factor and a characteristic $\hbar$-dependent prefactor that formally tends to ω_a/ω_b in the classical limit and describes the quantum enhancement of the rate as T_c is approached.

At this point we have to be very careful: the detailed analysis [6, 7] of the full density matrix $\rho(q_f, q_f', t)$ in Sect. 6.2.1, not only of its nondiagonal part, reveals that the nonequilibrium effects described by the flux state are restricted to the barrier region only in the presence of damping, consistent with the fact that finite temperature decay rates require coupling to a heat bath. In the absence of damping the full density matrix does not become quasi-stationary and the real time trajectories explore the strongly anharmonic range of the potential. Hence, an evaluation of the rate based upon a supposedly quasi-stationary flux state $\rho_{\mathrm{fl}}(q_f, -q_f)$ for the undamped case corresponds to the transition state theory result.

As the temperature reaches T_c large quantum fluctuations occur and the impact of anharmonicities becomes substantial. A detailed study of the bifurcation range around T_c is quite tedious and was already presented in [8, 9]. Thus, we omit explicit results here and proceed with temperatures $T \lesssim T_c$ where for coordinates close to the barrier top a Gaussian approximation – then around the newly emerging paths with amplitudes $\pm q_1$ – is again appropriate. As discussed above all real time paths with $q_f < q_1$ have now the same oscillation period $t_p(q_1) \approx \ln(q_a/q_1)/\omega_b$. One observes that even though they are influenced by the anharmonicity of the potential via the Euclidian amplitude q_1, their time evolution for $T \lesssim T_c$ is still dominated by parabolic

properties. A somewhat lengthy algebra leads to the quasi-stationary density matrix

$$\rho_{\rm fl}(q_{\rm f},-q_{\rm f}) = \frac{1}{2}\rho_\beta(q_{\rm f},-q_{\rm f})\left[g_{\rm fl}^{(+)}(q_{\rm f},-q_{\rm f}) + g_{\rm fl}^{(-)}(q_{\rm f},-q_{\rm f})\right], \tag{7.46}$$

where $g_{\rm fl}^{(\pm)}$ describe the contributions from each of the two oscillating Euclidian paths. Note that due to symmetry in $\rho_\beta(q_{\rm f},-q_{\rm f})$, these contributions are identical and just lead to a factor of 2. In the temperature domain studied here, q_1 can be gained analytically from (7.36) as

$$q_1 = \frac{2q_{\rm a}}{\sqrt{3}}\left(1-\frac{\pi^2}{\omega_{\rm b}^2\hbar^2\beta^2}\right)^{1/2}. \tag{7.47}$$

Accordingly, one finds with some algebra for the thermal distribution

$$\rho_\beta(0,0) = \frac{1}{\sqrt{2\pi\delta_{\rm b}^2|\sin(\omega_{\rm b}\hbar\beta)|}}\exp\left[\frac{\omega_{\rm b}\hbar\beta q_{\rm a}^2}{12\delta_{\rm b}^2}\left(1-\frac{\pi^2}{\omega_{\rm b}^2\hbar^2\beta^2}\right)^2\right]. \tag{7.48}$$

The form factor now has two contributions of the form (7.18) and for $\kappa_1 = \partial\ln(q_1)/\partial(\omega_{\rm b}\hbar\beta) \gg 1$ the corresponding integration boundaries read

$$u^{(\pm)}(q_{\rm f}) = \frac{\pm q_1 + {\rm i}q_{\rm f}}{4\delta_{\rm b}\sqrt{\kappa_1}}, \quad u'^{(\pm)}(q_{\rm f},z) = \kappa_1\left[u^{(\pm)}(q_{\rm f}) - z\right]. \tag{7.49}$$

Here, we employed that near $T_{\rm c}$ the derivative $\Sigma_{\rm ss}$ is dominated by $\partial^2\bar{S}/\partial q_{\rm i}^2$ which is proportional to $\partial E_1/\partial(\omega_{\rm b}\hbar\beta) \propto \kappa_1$. This way, using the normalization (7.44), the result for the rate is

$$\Gamma = \frac{\omega_{\rm b}}{2\pi}\frac{\sinh(\omega_{\rm a}\hbar\beta/2)}{\sqrt{2|\sin(\omega_{\rm b}\hbar\beta)|}}\sqrt{\omega_{\rm b}\hbar\beta - \frac{\pi^2}{\omega_{\rm b}\hbar\beta}}\;\,{\rm e}^{-\beta V_{\rm b}}. \tag{7.50}$$

This expression is valid for temperatures $T < T_{\rm c}$ where still $\kappa_1 \gg 1$, a region which can be estimated as T somewhat larger than $T_{\rm c}/2$. There are two interesting observations to mention: first, the exponentially large term in the thermal distribution (7.48) – a consequence of the new Euclidian paths – is exactly canceled by a corresponding term which arises from the derivative of the form factor. This way, the rate is still dominated by the characteristic Arrhenius factor. Second, in the limit $T \to T_{\rm c}$ the above-$T_{\rm c}$ formula (7.45) and the below-$T_{\rm c}$ result (7.50) both approach $\Gamma_{\rm c} = (\omega_b/2\pi)\sinh(\omega_{\rm a}\hbar\beta/2)\exp(-\beta V_{\rm b})$, however, the derivatives $\partial\Gamma/\partial T$ are different. This discontinuity in the slope of the temperature dependent rate is removed by a full semiclassical theory [9] which takes the non-Gaussian fluctuations near $T_{\rm c}$ into account and leads to a smooth changeover between the rate formulas (7.45) and (7.50).

With further decreasing temperature the amplitude q_1 tends to saturate at $q_{\rm a}$ so that $\kappa_1 \to 0$ and the above rate expression is no longer applicable.

Furthermore, the plateau region shrinks and eventually vanishes so that the assumption of a quasi-stationary flux state becomes inadequate even in the sense of a transition state theory limit of a weak damping theory. We note that in case of finite damping a meaningful rate can be found for much lower temperatures, then describing incoherent quantum tunneling (see Sect. 5.6). To investigate the time dependence of $\rho(q_\mathrm{f}, -q_\mathrm{f}, t)$ with no damping in the limit of deep tunneling, we consider the case $T = 0$ in the next Section.

7.3.4 Nonequilibrium Dynamics for Zero Temperature

In Chap. 4 we discussed tunneling processes for wave packet propagations. It turned out that any Gaussian semiclassics to the real time propagator is expected to break down, when deep tunneling prevails. Here, we extend these studies to the case of the time evolution of the density matrix describing the nonequilibrium dynamics of an ensemble.

The analysis is based upon the complex plane mechanics discussed above. Since this dynamics behaves as the usual classical real time mechanics, paths with $E < 0$ never cross the barrier. However, a full semiclassical treatment needs to account for the dominant fluctuations about the semiclassical paths. Now, for $T < T_\mathrm{c}$ there is a whole family of loop-like orbits in the complex plane; all with the same energy, period, and action increase after one period differing from each other only by their respective phases, i.e. by their crossing points $q_\mathrm{f} \leq q_1$ with the real axis. It turns out that each time these orbits pass their end-coordinate q_f there are other trajectories of this family arbitrarily close in phase space (see Fig. 7.4). The role of quantum mechanics then is to induce transitions between these orbits via small fluctuations. For sufficiently long times a path starting at a certain q_f near the barrier top may successively

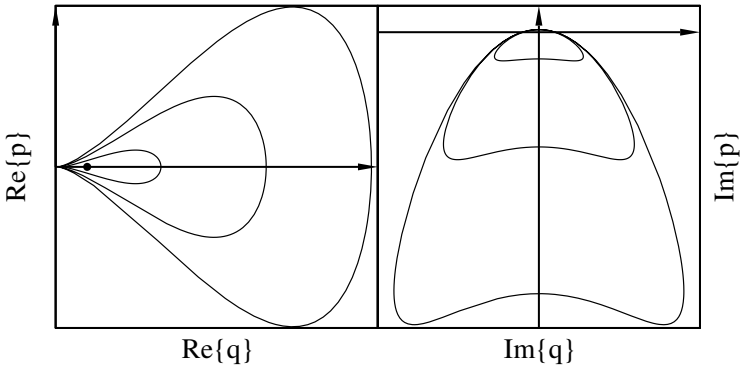

Fig. 7.4. Phase spaces orbits of complex real time paths in the double well potential at $T = 0$. In the left picture the real part of the orbits is shown for trajectories starting with $q_\mathrm{f} > 0$ near the barrier top; the dot indicates the well at q_a. In the right picture the corresponding imaginary parts are depicted.

slip down to an orbit with another phase $q'_{\rm f}$, eventually reach the stable regions around $\pm q_{\rm a}$, and fluctuate in the long time limit between these regions. That this scenario actually captures the low temperature coherent tunneling dynamics will be described in some detail in the sequel.

Fluctuation Paths

For $T = 0$ the amplitude of the Euclidian time paths is $q_1 = q_{\rm a}$. Thus, all stationary paths $q_{\rm s}(q_{\rm f}, t)$, $q'_{\rm s}(q_{\rm f}, t)$ have energy $E = V(q_{\rm a})$ and period $t_{\rm a} \equiv t_{\rm p}(q_{\rm a}) = 2\pi/\omega_{\rm a}$. Then, the Euclidian action $\bar{S}(q_{\rm i}, q'_{\rm i})$ suppresses energy fluctuations around $E = V(q_{\rm a})$ exponentially, so that classical paths running in time t from $q_{\rm i} \neq q_{\rm s}$ and $q'_{\rm i} \neq q'_{\rm s}$ to $q_{\rm f}$ and $-q_{\rm f}$, respectively, i.e. with $E \neq V(q_{\rm a})$, are negligible. Further, studying the short action, $W(q, q') = \int_q^{q'} {\rm d}q\, p \equiv S(q, q') + Et$, one finds according to (7.43) that after each period $W(q_{\rm f}, q_{\rm f}) = W(q_{\rm a}, q_{\rm a}) = 0$. This result combined with the fluctuation prefactor [see (7.9)] gives for the Gaussian propagator after multiple round trips and for coordinates $q_{\rm f} < q_{\rm a}$

$$|G(q_{\rm f}, q_{\rm f}, nt_{\rm a})|^2 \propto \frac{1}{nt_{\rm a}(q_{\rm a}^2 - q_{\rm f}^2)}, \quad n = 1, 2, 3, \ldots . \tag{7.51}$$

Hence, the probability to return to the starting point decreases as the number of periods increases. In contrast, in the vicinity of the wells the Gaussian propagator coincides with the harmonic propagator. To be more precise, due to caustics in the semiclassics of this simple propagator at all $nt_{\rm a}/2$, an extended semiclassical analysis must be invoked leading to an Airy function; details of the procedure are well-known [10] and of no interest here. The important point is that in the barrier region the simple semiclassical return probability decays to zero for large times while in the well regions it remains constant. Thus, we conclude that the dominant quantum fluctuations neglected in the Gaussian approximation to the real time propagators are those that connect stationary paths with the same energy but different phases, i.e. initial coordinates $q_{\rm f}$. Effectively, these relevant fluctuations shift q slightly away from the classical path $q_{\rm s}(q_{\rm f}, t)$ to reach another stationary path $q_{\rm s}(q'_{\rm f}, t)$ (cf. Fig 7.3). The corresponding change in action after a period and for small deviations is simply

$$W(q'_{\rm f}, q_{\rm f}) \approx p_{\rm s}(q_{\rm f}, 0)(q'_{\rm f} - q_{\rm f}). \tag{7.52}$$

This repeats at subsequent oscillations. Hence, a *fluctuation path* can be characterized by its sequence of crossing points with the real axis after each round trip, e.g. by $q^{(k)}, k = 1, \ldots, n$ for $t = nt_{\rm a}$ where $q^{(1)} = q_{\rm f}$. Accordingly, a fluctuation path is not a classical path, i.e. it does not fulfill Newton's equation of motion, but can be seen as almost classical since it stays always in the close vicinity of a classical path. In the sequel we first explain the general structure of the extended semiclassical approximation and later on turn to details of the calculation. As an example let us consider a fluctuation path starting at $q_{\rm f}$

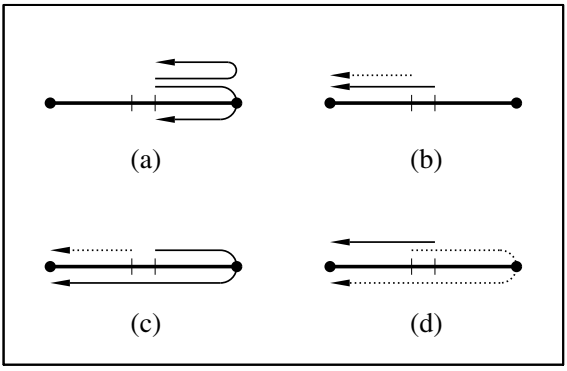

Fig. 7.5. Diffusion of the crossing point $q^{(n)}$ of a fluctuation path along the real axis (thick lines) for various cases discussed in the text. Dots indicate the wells at $\pm q_{\rm a}$ that are branch points for the momenta, thin vertical lines the end-coordinates at $\pm q_{\rm f}$. Solid lines refer to the forward, dotted ones to the backward propagator, a crossing of a dot a TP.

that spirals around $q_{\rm a}$ while the crossing point $q^{(n)}$ with the real axis diffuses close to $q_{\rm a}$ and returns to $q_{\rm f}$ in $t \gg t_{\rm a}$ (see Fig. 7.5a). According to (7.52) on the way to $q_{\rm a}$ a particular path gathers an additional action $W^+(q_{\rm a}, q_{\rm f})$ which is imaginary due to imaginary $p_s(q, 0)$ [see (7.12)] where

$$|W^+(q_{\rm a}, q_{\rm f})| = \int_{q_{\rm f}}^{q_{\rm a}} {\rm d}q \, \{2M[V(q) - V(q_{\rm a})]\}^{1/2} \tag{7.53}$$

and the $+$ $[-]$ sign stands for clockwise [anti-clockwise] rotation of the path in the complex plane. As long as the crossing point $q_{\rm f}$ does not diffuse the imaginary time path connecting the endpoints of the two real time paths coincides at $t = nt_{\rm a}$ with the imaginary time orbit connecting $-q_{\rm f}$ with $q_{\rm f}$ at $t = 0$. Taking into account the phase fluctuations, however, forces the endpoint of the imaginary time path to move with the endpoint $q^{(n)}$ of the real time path also towards $q_{\rm a}$. The mapped imaginary time path after $t \gg t_{\rm a}$ therefore runs from $-q_{\rm f}$ to $q_{\rm a}$. According to (7.12) the additional amount of Euclidian action required for this deformation of the imaginary time path exactly counterbalances $W(q_{\rm a}, q_{\rm f})$ so that the total action Σ remains constant which reflects the stationarity of Σ along stationary paths. From close to $q_{\rm a}$ the fluctuation path spirals back to $q_{\rm f}$. However, since $q_{\rm a}$ is a branching point of the momentum there are two channels: the real time fluctuation path can maintain the direction of rotation or pass the turning point (TP) $q_{\rm a}$, thus changing the sense of rotation (cf. Fig. 7.5a). In the former case on the way back from $q_{\rm a}$ to $q_{\rm f}$ the fluctuation path crosses the real axis with the same direction of momentum as on the way to $q_{\rm a}$, so that due to $W^+(q, q') = -W^+(q', q)$ the path looses the action $W^+(q_{\rm a}, q_{\rm f})$ again and returns to $q_{\rm f}$ with $W(q_{\rm f}, q_{\rm f}) = 0$. In the latter case, momenta on the way back have opposite

direction to those on the way forth so that the path arrives at q_f with action $W(q_\mathrm{f}, q_\mathrm{f}) = W^+(q_\mathrm{a}, q_\mathrm{f}) + W^-(q_\mathrm{f}, q_\mathrm{a}) = 2W^+(q_\mathrm{a}, q_\mathrm{f})$ and momentum $-p_\mathrm{s}(q_\mathrm{f}, 0)$.

Moreover, a fluctuation path starting at $q_\mathrm{f} > 0$ can either move along the real axis to the right to reach q_a or move to the left to arrive at $-q_\mathrm{a}$. In the latter case, the crossing point $q^{(n)}$ diffuses across the barrier top so that the path initially spiraling around q_a finally orbits around $-q_\mathrm{a}$ with opposite sense of rotation. Accordingly, due to $W^+(q_\mathrm{a}, 0) = -W^-(-q_\mathrm{a}, 0)$ the real time action factor $\exp[\mathrm{i}W(\pm q_\mathrm{a}, 0)/\hbar]$ grows or decreases exponentially for diffusion to the right or to the left, respectively. In any case, near $\pm q_\mathrm{a}$ the semiclassical propagator has to match onto the propagators in the harmonic wells. For the two lowest lying eigenstates which are relevant here, the matching procedure was discussed in detail by Coleman [11]. Correspondingly, these two states determine the relevant propagator in its spectral representation. Then, it turns out that a TP may only occur if $iW(q_\mathrm{f}, \pm q_\mathrm{a}) < 0$. This has profound consequences on the extended semiclassical approximation: (i) A relevant fluctuation path from q_f to q_f must reach $\pm q_\mathrm{a}$ rotating clockwise to have a TP. Then $W^+(q_\mathrm{a}, q_\mathrm{f}) + W^-(q_\mathrm{f}, q_\mathrm{a}) = 2\mathrm{i}|W(q_\mathrm{a}, q_\mathrm{f})|$ and the corresponding contribution to the propagator has an exponentially small factor $\exp[-2|W(q_\mathrm{a}, q_\mathrm{f})|]$. (ii) A fluctuation path with more than one TP has to alternately visit TPs at $\pm q_\mathrm{a}$ thereby changing its sense of rotation repeatedly. In passing from one TP to the next the path gathers the action $W^-(0, -q_\mathrm{a}) + W^+(q_\mathrm{a}, 0) = W^-(0, q_\mathrm{a}) + W^+(-q_\mathrm{a}, 0) = \mathrm{i}|W(q_\mathrm{a}, -q_\mathrm{a})| \equiv \mathrm{i}\bar{W}_\mathrm{a}$ which coincides with the instanton action in Δ introduced in (7.41). Hence, according to (i) contributions from fluctuation paths with TPs do not play any role for short times. For longer times, however, they become increasingly important, particularly, since a fluctuation path may spend an arbitrary period of time at the TPs $\pm q_\mathrm{a}$ where $V'(q_\mathrm{a}) = 0$ before leaving them. The detailed analysis shows (see below) that for $t \gg t_\mathrm{a}$ the phase space of equivalent fluctuations with one TP is therefore $\propto t$ which compensates for the exponentially small action factor. Moreover, at each TP a path gathers an additional Maslov index $\nu \to \nu + 1$. Then, according to (ii) the full density matrix is given by a sum over ν, ν' taking into account the proper order of TPs, i.e.

$$\rho(q_\mathrm{f}, -q_\mathrm{f}, t) = \sum_{\nu,\nu' \geq 0} \rho_{\nu,\nu'}(q_\mathrm{f}, -q_\mathrm{f}, t)\,, \tag{7.54}$$

where $\rho_{\nu,\nu'}$ denotes the contribution from relevant fluctuation paths with ν TPs in the forward and ν' TPs in the backward propagator. Note that ν, ν' only label the TPs of the two real time paths. For each ν, ν' one has also to sum over all imaginary time paths connecting the endpoints of the real time orbits.

Nonequilibrium Density Matrix

To evaluate the sum in (7.54) we start by analysing the term with $\nu = \nu' = 0$. As discussed above the diffusion of the real time orbits is then irrelevant and

the imaginary time path has to run form $-q_\mathrm{f}$ to q_f. To lowest order in Δ [see (7.40)] we have the two imaginary time paths $\bar{q}_\pm(q_\mathrm{f},\sigma)$ emerging at T_c that connect $-q_\mathrm{f}$ with q_f via TPs at $\pm q_\mathrm{a}$, respectively. At $T=0$ other solutions of the imaginary time dynamics with $r>1$ [cf. (7.36)] just contain additional intermediate instantons, i.e. imaginary time trajectories connecting q_a with $-q_\mathrm{a}$ or vice versa. For an equilibrium initial preparation (small) fluctuations about the stationary paths towards $\pm q_\mathrm{a}$, respectively, give identical contributions and we thus recover $\rho_\beta(q_\mathrm{f},-q_\mathrm{f})/Z$ (7.40) in the limit $T\to 0$ with the partition function

$$Z = 2\exp[-\beta V(q_\mathrm{a}) - \beta\hbar\omega_\mathrm{a}/2]\,\cosh(\hbar\beta\Delta/2)\,. \tag{7.55}$$

For the nonequilibrium preparation, however, only fluctuations towards $-q_\mathrm{a}$ contribute (Fig. 7.5b). This way, one obtains for coordinates q_f near the barrier top

$$\begin{aligned}\rho_{0,0}(q_\mathrm{f},-q_\mathrm{f},t) &= \frac{1}{2}\lim_{\beta\to\infty}\frac{1}{Z}\rho_\beta(q_\mathrm{f},-q_\mathrm{f})\\ &= \frac{4}{\sqrt{2\pi}\delta_\mathrm{a}}\,\exp[-\bar{W}_\mathrm{a}/\hbar]\,\cosh\left(q_\mathrm{f}q_\mathrm{a}/4\delta_\mathrm{a}^2\right)^2\\ &\equiv \frac{1}{2}\,\psi_0(q_\mathrm{f})^2\,,\end{aligned} \tag{7.56}$$

where we used the short action of an instanton $\bar{W}_\mathrm{a}=\bar{W}(q_\mathrm{a},-q_\mathrm{a})$ with $\bar{W}_\mathrm{a}=|W(q_\mathrm{a},-q_\mathrm{a})|$ and $\psi_0(q_\mathrm{f})$ denotes the semiclassical ground state wave function in the double well.

The next order real time paths are those with one TP, i.e. $\nu=1,\nu'=0$ and $\nu=0,\nu'=1$ in (7.54). Thereby, the real time path $q_\mathrm{s}(t)$ makes an excursion from q_f via a TP at q_a to $-q_\mathrm{a}$ in case where at $t=0$ the endpoints $-q_\mathrm{f}$ and q_f are connected by an imaginary time path $\bar{q}_-$, while it diffuses from q_f via a TP at $-q_\mathrm{a}$ to q_a in case of $\bar{q}_+$. Accordingly, one observes that for an equilibrium initial preparation all contributions cancel, e.g. the contribution corresponding to $\bar{q}_-$ with $\nu=1,\nu'=0$ cancels that corresponding to $\bar{q}_+$ with $\nu=0,\nu'=1$. In fact, it can be shown in the same way that for an equilibrium initial state *all* terms in the sum (7.54) with $\nu,\nu'>0$ vanish. However, for the initial preparation (7.3) a finite result follows due to the projection onto the left side of the complex plane. Hence, both real time orbits have to end near $-q_\mathrm{a}$ whereby one trajectory has a TP at q_a. According to the above discussion we gain the following action factors: for $\nu=1,\nu'=0$ one has $\exp[-3|W(q_\mathrm{a},0)|/\hbar + q_\mathrm{a}q_\mathrm{f}/(4\delta_\mathrm{a}^2)]$ from the forward and $\exp[-|W(q_\mathrm{a},0)|/\hbar + q_\mathrm{a}q_\mathrm{f}/(4\delta_\mathrm{a}^2)]$ from the backward propagator (cf. Fig. 7.5c) while $\nu=0,\nu'=1$ gives $\exp[-|W(q_\mathrm{a},0)|/\hbar - q_\mathrm{a}q_\mathrm{f}/(4\delta_\mathrm{a}^2)]$ and $\exp[-3|W(q_\mathrm{a},0)|/\hbar - q_\mathrm{a}q_\mathrm{f}/(4\delta_\mathrm{a}^2)]$ (cf. Fig. 7.5d), respectively. After expanding the integrand in (7.1) around $-q_\mathrm{a}$ up to second order, the ordinary integrations over the initial coordinates are seen to be restricted to the harmonic range around $-q_\mathrm{a}$ so that the θ functions can be put to 1. Then, the integrals effectively describe the stationary real

time motion of the equilibrium well distribution $\rho_\beta(-q_\mathrm{a}, -q_\mathrm{a})$. Combining these findings yields

$$\begin{aligned}\rho_1(q_\mathrm{f}, -q_\mathrm{f}, t) &\equiv \rho_{1,0}(q_\mathrm{f}, -q_\mathrm{f}, t) + \rho_{0,1}(q_\mathrm{f}, -q_\mathrm{f}, t) \\ &= \mathrm{i}8\,\Phi(t)\,\exp[-\frac{2}{\hbar}|W(q_\mathrm{a}, -q_\mathrm{a})|] \\ &\qquad \times \sinh\left(\frac{q_\mathrm{f} q_\mathrm{a}}{2\delta_\mathrm{a}^2}\right)\,\frac{1}{Z}\,\rho_\beta(-q_\mathrm{a}, -q_\mathrm{a})\,. \quad (7.57)\end{aligned}$$

Here $\rho_\beta(-q_\mathrm{a}, -q_\mathrm{a})$ includes a sum over multi-instanton contributions of the imaginary time paths, resulting for $T \to 0$ in $\rho_\beta(-q_\mathrm{a}, -q_\mathrm{a})/Z = \sqrt{M\omega_\mathrm{a}/4\pi\hbar}$. Further, $\Phi(t) \propto t$ takes into account the phase space contribution from equivalent fluctuation paths connecting q_f via a TP at q_a with $-q_\mathrm{a}$. These paths differ only in their *sojourn times* at the TP q_a. To evaluate Φ we adopt the method outlined in [12] to which we also refer for further details and write

$$G(q_\mathrm{a}, -q_\mathrm{a}, t) = \int_0^t \mathrm{d}u\, G(q_\mathrm{a}, t-u)\,\dot{q}_s(0,u)\,G(0, -q_\mathrm{a}, u)\,. \quad (7.58)$$

Since for $t \gg t_\mathrm{a}$ the sojourn time is exponentially large, one can actually sum the intermediate time step u over the entire time interval up to negligible corrections. To calculate the semiclassical propagators in the integrand of (7.58) one exploits that a fluctuation path moving from $q = 0$ to q_a in time $t \gg t_\mathrm{a}$ spends almost all time by orbiting in the vicinity of q_a thereby diffusing along the classical stationary paths (7.42) with $q_\mathrm{f} \lesssim q_\mathrm{a}$ towards the TP. Hence, the time dependence of the propagators is determined only by the asymptotic behavior of the fluctuation paths. Then, as already derived in the previous paragraph, the actions turn out to be independent of time up to exponentially small corrections and their sum gives rise to the action factor $\exp[-|W(q_\mathrm{a}, -q_\mathrm{a})|/\hbar]$ in $G(q_\mathrm{a}, -q_\mathrm{a}, t)$. For the prefactors one uses the representation (7.9), and exploits the fact that $\dot{q}_\mathrm{s}(0,u)\sqrt{A_{t-u}(q_\mathrm{a},0)A_u(0,-q_\mathrm{a})}$ depends for $t \gg t_\mathrm{a}$ on time and temperature only through $\exp[-(\hbar\beta + it)\omega_\mathrm{a}/2]$ while its dependence on the intermediate time step u is exponentially small. This way, since both exponential factors are already accounted for in (7.57), we arrive at

$$\Phi(t) = G(q_\mathrm{a}, -q_\mathrm{a}, t)\exp[|W(q_\mathrm{a}, -q_\mathrm{a})|/\hbar + (\hbar\beta + it)\omega_\mathrm{a}/2]\,, \quad (7.59)$$

which leads to

$$\Phi(t) = t\,\frac{4\omega_\mathrm{a} q_\mathrm{a}}{\sqrt{2\pi}\delta_\mathrm{a}}\,. \quad (7.60)$$

Combining this result with (7.57) we derive the one-TP contribution to (7.54) as

$$\rho_1(q_\mathrm{f}, -q_\mathrm{f}, t) = \mathrm{i}t\Delta^2\,\frac{\sinh(q_\mathrm{a} q_\mathrm{f}/2\delta_\mathrm{a}^2)}{\omega_\mathrm{a} q_\mathrm{a}}\,, \quad (7.61)$$

where the tunnel splitting is specified in (7.41). Likewise, contributions from real time paths with more than one TP can be calculated where the proper order of TPs must be taken into account. Eventually, only contributions with $\mathrm{i}^{2k-1}\Delta^{2k}, k = 1, 2, \ldots$ survive and the time dependent density matrix (7.54) for coordinates near barrier top reads

$$\rho(q_\mathrm{f}, -q_\mathrm{f}, t) = \frac{1}{2}\psi_0(q_\mathrm{f}, -q_\mathrm{f})^2 + \mathrm{i}\Delta\,\sin(\Delta t)\,\sinh(q_\mathrm{a}q_\mathrm{f}/2\delta_\mathrm{a}^2)/(\omega_\mathrm{a}q_\mathrm{a})\,. \tag{7.62}$$

Hence, the initial state (7.3) develops an imaginary, time dependent part from which the tunneling current (7.5) is gained as

$$J(t) = \Delta\sin(\Delta t) \tag{7.63}$$

describing coherent tunneling between the wells. This shows that a systematic semiclassical analysis of the real time dynamics of the system covers also low temperature tunneling. We note that the tunnel splitting coincides exactly with the result of the instanton approach [see (7.41)] where Δ is related to the action of an *imaginary* time path. Within the real time description the instanton dynamics is replaced by the above-mentioned diffusion along the real axis in the complex coordinate plane.

Before we conclude this Section let us briefly sketch how the changeover from coherent decay to incoherent tunneling occurs within the present formalism as the temperature is raised. For finite temperatures $T > 0$ the energy of the stationary paths is $|\bar{E}_1| = |V(q_1)| < |V(q_\mathrm{a})|$ so that the TPs of the fluctuation paths $q_1 < q_\mathrm{a}$ are shifted towards the barrier top. Accordingly, $V'(q_1) \neq 0$ and the corresponding actions in (7.58) are no longer independent of time. Thus, the time interval $t \gg t_\mathrm{a}$ may eventually exceed the region where the integrand gives a contribution so that $\Phi(t) \to \Phi_\mathrm{fl}$ saturates. We note that for a system with dissipation basically the same mechanism, namely, an effective action depending on time via damping induced correlations, may cause incoherent tunneling even at $T = 0$.

7.4 Eckart Barrier

As another instructive example we analyse the transport across a genuine scattering potential, namely, the Eckart barrier [13] addressed in previous Sections

$$V(q) = \frac{V_0}{\cosh(q/L_0)^2}\,. \tag{7.64}$$

Here, V_0 is the barrier height and L_0 the typical interaction range. We drop the condition $V(q = 0) = 0$ in this Section so that energies are shifted by V_0. In fact, the real time dynamics in this potential is much simpler as in the double well: particles steadily injected from a thermal reservoir to the left of the barrier built up a flux across the barrier that is stationary for all times

after a certain transient time has elapsed. Thus, the corresponding quantum dynamics is described by a barrier transmission rate for all temperatures (incoherent tunneling). In a semiclassical expansion we use $\hbar/\sqrt{2ML_0^2V_0}$ as the small parameter which demands high and broad barriers.

7.4.1 Thermal Equilibrium and Stationary Phase Points

The solution of Newton's equation of motion for the Eckart barrier in imaginary time reads [14]

$$\bar{q}_0(q_\mathrm{f},\sigma) = L_0 \,\mathrm{arsinh}\left\{\sqrt{\frac{V_0-\bar{E}}{\bar{E}}}\sin\left[\omega(\bar{E})\sigma-\phi_\mathrm{f}\right]\right\}, \tag{7.65}$$

where we introduced the energy dependent frequency

$$\omega(\bar{E}) = \omega_\mathrm{b}\sqrt{\frac{\bar{E}}{V_0}} \tag{7.66}$$

with the barrier frequency $\omega_\mathrm{b} = \sqrt{2V_0/ML_0^2}$. Energy $\bar{E}$ and phase ϕ_f are determined by the boundary conditions $\bar{q}_0(q_\mathrm{f},0) = -q_\mathrm{f}$ and $\bar{q}_0(q_\mathrm{f},\hbar\beta) = q_\mathrm{f}$. Accordingly, employing one of these conditions to fix ϕ_f, the energy can be evaluated from

$$\omega(\bar{E})\hbar\beta = r\pi + [1+(-1)^r]\phi_\mathrm{f}\,, \tag{7.67}$$

where for given temperature real solutions exist only for a finite number of integers $r \geq 0$. Accordingly, this nonlinear equation gives the amplitude of the semiclassical path. As a function of temperature the solutions (7.65) and (7.67) resemble those in the inverted double well potential (cf. Sect. 7.3.2). Particularly, for $T < T_\mathrm{c}$ again all paths with $r = 1$ have the same energy independent of q_f

$$\bar{E}_1 \equiv V(q_1) = \frac{\pi^2 V_0}{\omega_\mathrm{b}^2\hbar^2\beta^2} \tag{7.68}$$

with amplitudes $\pm q_1$ and the same frequency $\omega_1 = \omega(\bar{E}_1)$. An important difference to the double well case, however, is that the amplitude q_1 of the paths here grows without any limit as $T \to 0$, i.e. $\bar{E}_1 \to 0$. Hence, the equilibrium density matrices $\rho_\beta(q_\mathrm{f},-q_\mathrm{f})$ differ qualitatively in the deep tunneling regime. While for the double well potential near $T = 0$ contributions from all multi-instanton paths must be summed up [see (7.40)], here, the density matrix is dominated by the oscillating paths newly emerging around $T_\mathrm{c} = \omega_\mathrm{b}\hbar/k_\mathrm{B}\pi$ for *all* $T < T_\mathrm{c}$. For further details of the Euclidian semiclassics we refer to [14].

Now, for the stationary phase points one has

$$\begin{aligned} q_\mathrm{s}(t) &= L_0 \,\mathrm{arsinh}\left\{\sqrt{\frac{V_0-\bar{E}}{\bar{E}}}\sin\left[\phi_\mathrm{f}-\mathrm{i}\omega(\bar{E})t\right]\right\} \\ q_\mathrm{s}'(t) &= -q_\mathrm{s}[(-1)^{r+1}t]\,, \end{aligned} \tag{7.69}$$

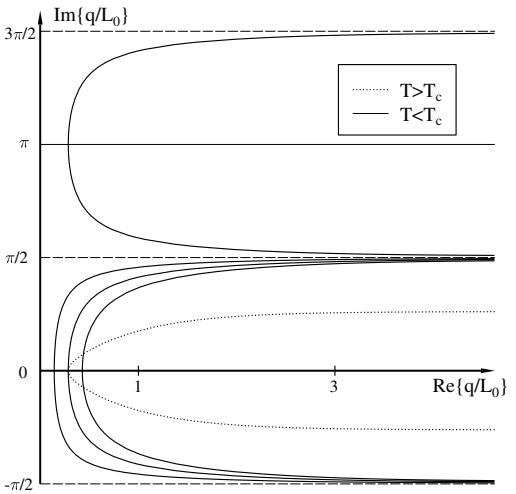

Fig. 7.6. Real time paths in the complex plane for the Eckart barrier. Solid lines show orbits for $T < T_c$, dotted lines orbits for $T > T_c$.

which are connected by the Euclidian path $\bar{q}_s(\sigma) = \bar{q}_0[\sigma + i(-1)^{r+1}t]$. Starting at q_f $[-q_f]$ the path $q_s(t)$ $[q_s'(t)]$ describes for large times an almost free motion parallel to the real axis in accordance with the asymptotically vanishing interaction $V(q) \to 0$ as $q \to \pm\infty$. The energy of $q_s(t)$ is controlled by temperature where qualitatively the two ranges $T > T_c$ and $T \leq T_c$ must be distinguished. In the first case, $\bar{E}$ depends on q_f and for $q_f > 0$ we find asymptotically, i.e. for $\omega(\bar{E})t \gg 1$,

$$q_s(q_f, t) \approx L_0 \,\mathrm{arsinh}\left[\frac{\sinh(q_f/L_0)}{2\sin(\omega_b\hbar\beta/2)}\,\mathrm{e}^{\omega(\bar{E})t}\right] - iL_0\left(\frac{\pi}{2} - \frac{\omega_b\hbar\beta}{2}\right) \tag{7.70}$$

so that for $T > T_c$ all stationary paths are restricted to the strip $i(L_0/2)[-(\pi - \omega_b\hbar\beta), (\pi - \omega_b\hbar\beta)]$ (cf. Fig. 7.6). In the range $T < T_c$ and for end-coordinates $q_f < q_1$ the oscillating Euclidian paths determine the energy independent of q_f as $E = \bar{E}_1$ [see (7.68)] with the frequency $\omega_1 = \omega(\bar{E}_1)$. Hence, in $T \ll T_c$ *all* path starting in the barrier range ($q_f \lesssim L_0$) nearly coincide asymptotically (see also Fig. 7.6) for $\omega_b t \gg 1$

$$q_s(q_f, t) \approx q_1 + L_0 \,\ln\left[\sinh(\omega_1 t)\right] + iL_0\pi/2\,. \tag{7.71}$$

Orbits with $q_f > L_0$ come also close to $iL_0\pi/2$ but on a larger time scale, e.g. for q_f close to $q_1 \gg L_0$ on the scale $1/\omega_1$. Since $\mathrm{Im}\{q_s'\} \to -iL_0\pi/2$ for large t we conclude that the real time stationary phase dynamics for $T < T_c$ is restricted to the strip $[-iL_0\pi/2, iL_0\pi/2]$ in the complex plane (Fig. 7.6). To complete this discussion we address the special cases $q_f = q_1$ and $q_f = 0$, respectively. In the former case the motion starts with zero momentum and takes place along the real axis, asymptotically ($\omega_1 t \gg 1$) as

$$q_{\rm s}(t,q_1) \approx q_1 + L_0\omega_1 t\,. \tag{7.72}$$

In the latter case the orbit can only be defined as the limiting trajectory of $q_{\rm s}(t,q_{\rm f})$ for $q_{\rm f} \to 0$, thus, running along the imaginary axis from $q = 0$ to $q = iL_0\pi/2$ and afterwards parallel to the real axis.

The described complex plane dynamics depends essentially on the analytic properties of the potential $V(q)$. Interestingly, in case of the Eckart barrier one has for complex q the periodicity

$$V(q) = V(q + {\rm i}L_0 n\pi), \quad n \text{ integer}. \tag{7.73}$$

Hence, the complex plane falls into strips $[(2n-1){\rm i}L_0\pi/2, (2n+1){\rm i}L_0\pi/2]$, n integer, parallel to the real axis each of which with identical classical mechanics and corresponding stationary phase paths $q_{\rm s}(q_f + iL_0 n\pi, t)$. As shown above, for $T < T_{\rm c}$ the real time dynamics starting from the real axis at $t = 0$ reaches asymptotically the boundaries of the strip $n = 0$, while in the range $T > T_{\rm c}$ it does not. This has crucial impact on the semiclassical analysis for lower temperatures as we will see below.

7.4.2 Flux for High and Moderate Low Temperatures

The systems starts from an initial state where the thermal equilibrium is restricted to the left of the barrier, thus extending to $q \to -\infty$. Accordingly, after a certain transient time has elapsed the flux across the barrier remains stationary forever. Since with increasing time the stationary phase points move away from the barrier top, for large times fluctuations of the order of L_0 or larger are needed to shift $q_{\rm i}$ into the region ${\rm Re}\{q_{\rm i}\} \le 0$, then rendering the Gaussian stationary phase approximation insufficient. Yet, we can use (7.17) to gain $J_{\rm st}$ as long as the flux becomes stationary on a time scale within which $q_{\rm s}$ remains smaller than L_0.

In the range $T > T_{\rm c}$ and for $q_{\rm f}$ near the barrier top one has $\bar{E} \approx V_0$ so that $\omega(\bar{E}) \approx \omega_{\rm b}$. Then, the density matrix $\rho(q_{\rm f}, -q_{\rm f}, t)$ tends to stationarity on the scale $1/\omega_{\rm b}$ while $q_{\rm s}(t)$ reaches L_0 on the much longer time scale $\ln[V_0/(\bar{E}-V_0)]$ only. We thus regain within this time window approximately the parabolic result (7.29) in the semiclassical limit – large V_0 and L_0 – where anharmonicities are negligibly small. Correspondingly, the rate reads as specified in (7.31) with $\omega_{\rm b} = \sqrt{2V_0/ML_0^2}$.

For temperatures $T < T_{\rm c}$ the transient time range grows according to $1/\omega_1 = \hbar\beta/\pi$, while the upper bound for the validity of the Gaussian approximation eventually shrinks to $1/\omega_{\rm b}$. Hence, while one can no longer use the local barrier dynamics for temperatures $T \ll T_{\rm c}$, in a region sufficiently close to $T_{\rm c}$ a rate calculation along the lines described in Sect. 7.3.3 still makes sense. Accordingly, for $T \lesssim T_{\rm c}$ the density matrix is obtained as in (7.46) with the amplitude q_1 derived from (7.67) for $r = 1$ as

$$q_1 = L_0\,{\rm arsinh}\left[\frac{\sqrt{(\omega_{\rm b}\hbar\beta)^2 - \pi^2}}{\pi}\right]. \tag{7.74}$$

This way, one gets the rate

$$\Gamma = \frac{\omega_\mathrm{b}}{4\pi^2 Z} \frac{\sqrt{(\omega_\mathrm{b}\hbar\beta)^2 - \pi^2}}{\mathrm{arsinh}\left[\sqrt{(\omega_\mathrm{b}\hbar\beta/\pi)^2 - 1}\right]} \exp\left(-\beta V_0\right) \tag{7.75}$$

for temperatures below T_c but still above $T_\mathrm{c}/2$. For even lower temperatures higher order terms in the expansion around the stationary phase points $q_\mathrm{s}, q'_\mathrm{s}$ must be taken into account. In the following Section we show that for T below $T_\mathrm{c}/2$ the rate is dominated by quantum tunneling which requires an extended semiclassical analysis. Thus, a higher order expansion is needed only in the close vicinity of $T_\mathrm{c}/2$ where the changeover from the thermal to the quantum rate occurs.

7.4.3 Transmission for Low Temperatures

As in case of the double well potential, at very low temperatures a semiclassical approximation needs to based upon a careful analysis of the quantum fluctuations around the classical paths. This program will be now carried out for the Eckart barrier.

We begin by recalling that in the range $T \ll T_\mathrm{c}$ and for coordinates $q_\mathrm{f} < q_1$ the classical mechanics in the complex plane takes place in strips $[(2n-1)\mathrm{i}L_0\pi/2, (2n+1)\mathrm{i}L_0\pi/2], n$ integer, parallel to the real axis. One thus has families of classical paths (cf. Fig. 7.6) all with the same energy $\bar{E}_1$ that start at $t \to -\infty$ to the far right on the lines $(2n-1)\mathrm{i}L_0\pi/2$, run close together with almost vanishing momentum $-ML_0\omega_1$ towards the barrier top, pass at $t = 0$ the coordinates $q_\mathrm{f} + \mathrm{i}nL_0\pi$ and then leave again to the far right moving close together with momentum $ML_0\omega_1$ asymptotically along the lines $(2n+1)iL_0\pi/2$. Accordingly, for $T \to 0$ in classical phase space, see Fig. 7.7, orbits with different phases ϕ_f, i.e. different q_f, but from the same or from adjacent strips lie arbitrarily close to each other in the asymptotic range where $|V(q)| \to 0$. The effort of quantum fluctuations then is to link these paths which reflects the asymptotically free particle diffusion in the Eckart potential. In simple semiclassical approximation one has asymptotically the propagator

$$G(q, q', t) = \left(\frac{M}{2\pi\mathrm{i}\hbar t}\right)^{1/2} \exp\left[iM\frac{(q-q')^2}{2\hbar t}\right] \tag{7.76}$$

so that for fixed $q - q'$ and large times the transition probability decreases as $|G(q, q', t)|^2 \propto 1/t$ [cf. (7.51)]. Correspondingly, two different types of fluctuations can be identified: one type of fluctuations connects paths $q_\mathrm{s}(q_\mathrm{f} + \mathrm{i}L_0 n\pi, t)$ and $q_\mathrm{s}(q'_\mathrm{f} + \mathrm{i}L_0 n\pi, t)$ within the same strip, while the other type of fluctuations switches between paths $q_\mathrm{s}(q_\mathrm{f} + iL_0 n\pi, t)$ and $q_\mathrm{s}(q'_\mathrm{f} + \mathrm{i}L_0(n+1)\pi, t)$ in adjacent strips. The first type is already accounted for in the simple semiclassical approximation to the real time propagator since these fluctuations never leave strip $n = 0$ and stay in the close vicinity to the asymptotic $q_\mathrm{s}(q_\mathrm{f}, t)$. In

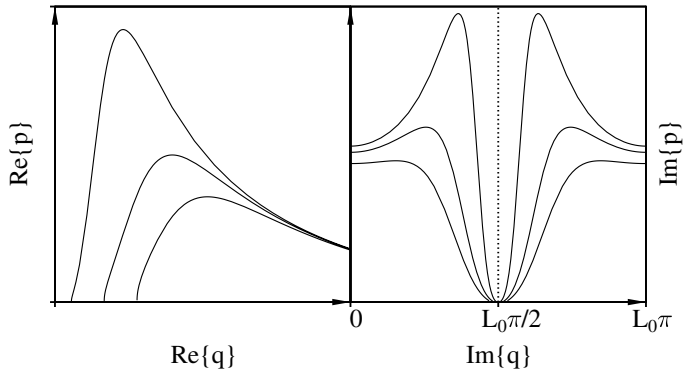

Fig. 7.7. Phase space orbits of complex real time paths in the Eckart barrier potential at $T \ll T_c$. In the left picture the real part of the orbits is shown for trajectories starting with $q_f > 0$ near the barrier top. In the right picture the corresponding imaginary parts are depicted; the dotted line separates the strips $n = 0$ and $n = 1$.

contrast, the second type is relevant beyond the Gaussian semiclassics since it causes large deviations and allows a path $q_s(q_f, t)$ by subsequently diffusing to another strip to reach a path $q_s(q'_f + iL_0 n\pi, t)$ with q'_f far from q_f and n large. Interestingly, this second kind of fluctuations does not exist for $T > T_c$ where asymptotically there is always a gap $i\omega_b\hbar\beta$ between paths in adjacent strips (see Fig. 7.6).

As an example let us consider a trajectory $q_s(q_f, t)$ with q_f close to the barrier top for $T \ll T_c$ and times $t \gg 1/\omega_1 \gg 1/\omega_b$. In this limit the orbit runs for $\omega_b t \gg 1$ along the boundary $iL_0\pi/2$ of the strip $n = 0$ where fluctuations of the second class bridge the tiny gap to an orbit $q_s(q'_f + iL_0\pi, t)$ with a different q'_f in the strip $n = 1$. This trajectory passes $q'_f + iL_0\pi$, and exploiting the periodicity of $V(q)$ the corresponding change in action $W(q_f, q'_f)$ is shown to read as in (7.52). Obviously, the described fluctuations always lead from an outgoing to an in-going orbit thereby increasing the strip number which in turn requires a momentum fluctuation of order $2|\dot{q}_s(t)| = 2ML_0\omega_1$. Estimating typical momentum fluctuations by $\hbar/L_0$ one re-derives from $\hbar/L_0 \gg ML_0\omega_1$ the condition $T \ll T_c$ so that at low temperatures these fluctuations will indeed occur. By the same procedure the path $q_s(q'_f + iL_0\pi, t)$ can be linked to a path $q_s(q''_f + iL_0 2\pi, t)$ and so forth. Similar as in case of the double well potential a fluctuation path is characterized by its sequence of crossing points $q^{(k)} + iL_0 k\pi$, $k = 0, 1, 2, \ldots, n$ $[q^{(0)} = q_f]$, with the lines $iL_0 k\pi$, i.e. the copies of the real axis in the strips k. Accordingly, for very large times $t \gg 1/\omega_1$ the point $q^{(n)} + iL_0 n\pi$ moves with increasing n along the positive imaginary axis while simultaneously $q^{(n)}$ can slide down the real axis and away from the barrier top to reach the proximity of q_1. From close to q_1 relevant fluctuation paths traverse q_1 as a turning point (TP) – q_1 is a branch

point for the momentum – and return via the described scenario to q_f in the strip $k = 0$, however, crossing the lines $\mathrm{i}L_0 k\pi$ with opposite direction of momentum as on the way forth. The total change in action is imaginary and given by $W(q_\mathrm{f}, q_\mathrm{f}) = W(q_1, q_\mathrm{f}) - W(q_\mathrm{f}, q_1) = 2W(q_1, q_\mathrm{f})$, n arbitrary but large, where for q_f close to the top

$$\begin{aligned} |W(q_1, q_\mathrm{f})| &= \int_{q_\mathrm{f}}^{q_1} \mathrm{d}q \, [2M(V(q) - V(q_1))]^{1/2} \\ &= \frac{\pi V_0}{\omega_\mathrm{b}} \left(1 - \frac{\pi}{\omega_\mathrm{b}\hbar\beta}\right) - \omega_\mathrm{b} M L_0 q_\mathrm{f} \,. \end{aligned} \tag{7.77}$$

In a similar way, the sequence of $q^{(n)}$ of a fluctuation path starting at q_f can move directly towards the barrier top, diffuse across the barrier to enter the left half-plane of the complex plane, and end up in the asymptotic region $\mathrm{Re}\{q\} \to -\infty$. Since in leading order the semiclassical propagator has asymptotically to match onto the free propagator (7.76), a TP may only occur if $iW(q_\mathrm{f}, \pm q_1) < 0$. Hence, what we discussed in Sect. 7.3.4 [see paragraph above (7.54)] can directly be transferred to the situation here and the density matrix can be cast into the same form as in (7.54). In a notable difference to the double well potential, however, the TP q_1 here is not an isolated extremum of the potential meaning that each TP – for Euclidian and real time fluctuation paths as well – is *not* related to an additional phase factor for equivalent paths.

After having elucidated the general structure of the semiclassical density matrix we now turn to the explicit calculation of the sum (7.54) and begin with the term $\rho_{0,0}(q_\mathrm{f}, -q_\mathrm{f}, t)$. This matrix element follows by the same arguments as given in Sect. 7.3.4. Since the equilibrium density matrix for the Eckart barrier is dominated by the oscillating paths newly emerging around T_c for all lower temperatures, all further contributions from Euclidian trajectories with $r \neq 1$ in (7.67) are negligible. Accordingly, we find for coordinates around the barrier top

$$\begin{aligned} \rho_{0,0}(q_\mathrm{f}, -q_\mathrm{f}) &= \frac{1}{2} \lim_{T \ll T_\mathrm{c}} \frac{1}{Z} \rho_\beta(q_\mathrm{f}, -q_\mathrm{f}) \\ &= \frac{1}{ZL_0} \left\{ \frac{\pi V_0}{\omega_\mathrm{b}^2 \hbar^2 \beta [(\omega_\mathrm{b}\hbar\beta)^2 (1 - q_\mathrm{f}^2/L_0^2) - \pi^2]} \right\}^{1/2} \\ &\qquad \times \exp\left[-\frac{\pi V_0}{\omega_\mathrm{b}\hbar} \left(2 - \frac{\pi}{\omega_\mathrm{b}\hbar\beta}\right) \right] . \end{aligned} \tag{7.78}$$

Note that in contrast to bounded systems the above density matrix remains temperature dependent even for $T \ll T_\mathrm{c}$.

To next order real time paths with $\nu = 1, \nu' = 0$ and $\nu = 0, \nu' = 1$, respectively, contribute (cf. Figs. 7.5c,d). For $t \gg 1/\omega_1$ a relevant real time fluctuation path with $\nu = 1$ starting at q_f moves via a TP at $q_1 + \mathrm{i}L_0 n'\pi$, n' large, to the left half-plane where it eventually crosses $-q_1 + \mathrm{i}L_0 n\pi$, n

large, to run along the line $\mathrm{i}L_0 n\pi$ and reach $q_\mathrm{i} + \mathrm{i}L_0 n\pi$ in the far left. For the segment of the fluctuation path from q_f via a TP to $-q_1 + iL_0 n\pi$ the corresponding action factor is $\exp[-3|W(q_1,0)|/\hbar + \omega_\mathrm{b} M L_0 q_\mathrm{f}/\hbar]$. Due to the periodicity (7.73) of the potential the segment from $-q_1 + iL_0 n\pi$ to $q_\mathrm{i} + iL_0 n\pi$, $q_\mathrm{i} < -q_1$, can just be treated as the corresponding one along the real axis; for very large times $\omega_1 t \gg 1$, i.e. $|q_\mathrm{i}| \gg q_1$ according to (7.72), we then get the action factor $\exp[-iMq^2/2\hbar t]$. Hence, the corresponding relevant real time propagator reads

$$G_t(q_\mathrm{f}, q_\mathrm{i}) = -\mathrm{i}\sqrt{A(q_\mathrm{f}, q_\mathrm{i})}\, \exp\left[-\frac{3|W(q_1,0)|}{\hbar} + \frac{\omega_\mathrm{b} M L_0 q_\mathrm{f}}{\hbar} + iM\frac{q_\mathrm{i}^2}{2\hbar t}\right]. \quad (7.79)$$

Likewise, the propagator from $-q_\mathrm{f}$ directly to $q_\mathrm{i}' + \mathrm{i}L_0 n\pi$ is gained. The crucial point is now that for the integral in (7.1) there are no longer isolated stationary phase points but rather *all* $q_\mathrm{i}, q_\mathrm{i}'$ on the line $\mathrm{i}L_0 n\pi$ and to the far left of the barrier top make the integrand for very large times stationary. The ordinary integrals in (7.1) can thus be seen as sums over stationary phase points $q_\mathrm{i}, q_\mathrm{i}'$ whereby their distance is weighted by the asymptotic thermal distribution, i.e. in leading order the free particle equilibrium density matrix

$$\rho_\beta(q, q') = \left(\frac{M}{2\pi\hbar^2\beta}\right)^{1/2} \exp\left[-\frac{M(q-q')^2}{2\hbar^2\beta}\right]. \quad (7.80)$$

Accordingly, for $T \to 0$ one has $\rho_\beta(q_\mathrm{i}, q_\mathrm{i}') \to \delta(q_\mathrm{i} - q_\mathrm{i}')$ so that contributions from $q_\mathrm{i} \neq q_\mathrm{i}'$ are caused by thermal fluctuations at elevated temperatures. Further, for large $q_\mathrm{i}, q_\mathrm{i}'$ and large times the prefactors $A(q_\mathrm{f}, q_\mathrm{i})$ and $A'(-q_\mathrm{f}, q_\mathrm{i}')$, respectively, are independent of $q_\mathrm{i}, q_\mathrm{i}'$, thus allowing us to carry out the $q_\mathrm{i}, q_\mathrm{i}'$ integrals over the exponentials only. Then, using $-q_1$ as an upper bound for the asymptotic coordinate range it turns out that for $\omega_1 t \gg 1$ the result for the integrals in leading order is $\pi\hbar t/M$. Now, combining all factors we finally obtain the time independent density

$$\begin{aligned}\rho_1(q_\mathrm{f}, -q_\mathrm{f}) &= \lim_{\omega_1 t \gg 1} [\rho_{1,0}(q_\mathrm{f}, -q_\mathrm{f}, t) + \rho_{0,1}(q_\mathrm{f}, -q_\mathrm{f}, t)] \\ &= \frac{\mathrm{i}}{ZL_0}\left[\frac{4\pi V_0}{\hbar\omega_\mathrm{b}(\omega_\mathrm{b}\hbar\beta)^3}\right]^{1/2} \sinh\left(\frac{2\omega_\mathrm{b} M L_0 q_\mathrm{f}}{\hbar}\right) \mathrm{e}^{-4|W(q_1,0)|/\hbar}, \quad (7.81)\end{aligned}$$

where $|W(q_1,0)|$ follows from (7.77). Employing the same procedure, contributions in the sum (7.54) from real time paths with more than one TP can be derived, however, they contain additional action factors and are thus exponentially small compared to ρ_1. Hence, the stationary semiclassical density matrix for low temperatures and very large times is found as

$$\rho_\mathrm{fl}(q_\mathrm{f}, -q_\mathrm{f}) = \frac{1}{2Z}\rho_\beta(q_\mathrm{f}, -q_\mathrm{f}) + \rho_1(q_\mathrm{f}, -q_\mathrm{f}) \quad (7.82)$$

with ρ_β as specified in (7.78). Finally, from (7.5) we gain the thermal tunneling rate

$$\Gamma = \frac{1}{Z}\left[\frac{4\pi V_0\omega_\mathrm{b}}{\hbar(\omega_\mathrm{b}\hbar\beta)^3}\right]^{1/2} \mathrm{e}^{-4|W(q_1,0)|/\hbar}\,. \tag{7.83}$$

This simple formula is applicable as long as $q_1 > L_0$, a temperature range which can be estimated by T below $T_\mathrm{c}/2$, or equivalently $\omega_\mathrm{b}\hbar\beta > 2\pi$. To be precise, there is also a lower bound for the temperature. Namely, for $T \to 0$ any semiclassics in the Eckart barrier breaks down due to the fact that then tunneling takes place in the low energy range near the base of the barrier where the wave length of a wave function tends to exceed the width of the barrier. From the known exact transition probability (see e.g. [14]) one derives that this scenario becomes relevant for $\omega_\mathrm{b}\hbar\beta \gg 2\pi^4(V_0/\hbar\omega_\mathrm{b})$ corresponding in the semiclassical limit $V_0/\hbar\omega_\mathrm{b} \gg 1$ to extremely low temperatures. In the broad temperature range between these bounds, i.e. $2\pi < \omega_\mathrm{b}\hbar\beta \lesssim 2\pi^4(V_0/\hbar\omega_\mathrm{b})$, the above rate expression describes the decay rate with remarkable accuracy when compared to the exact result even for moderate barrier heights (see Fig. 7.8).

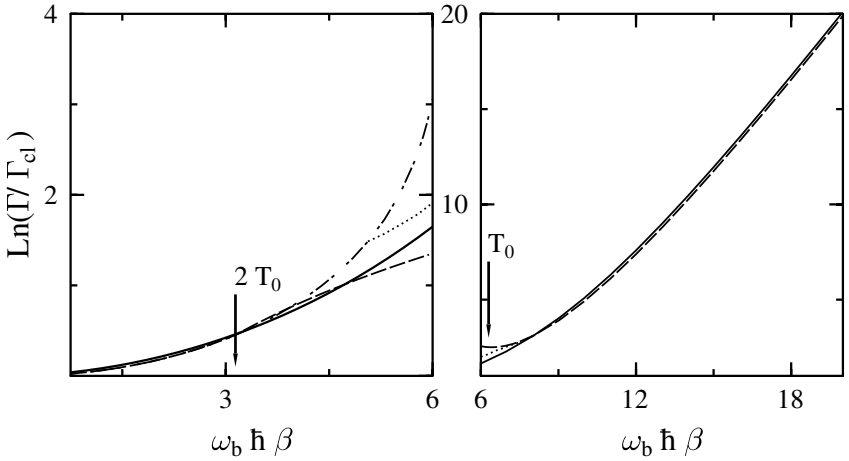

Fig. 7.8. Transmission factor P as a function of inverse temperature for an Eckart barrier with $\alpha = 12$, $\alpha = 2\pi V_0/\hbar\omega_\mathrm{b}$. P is defined by $P = \Gamma/\Gamma_\mathrm{cl}$ with Γ_cl the classical rate, i.e. the high temperature limit to (7.31). The solid line is the exact result. In the left picture the dotted-dashed line shows the parabolic result (7.31), the dashed line represents (7.75), and the arrow indicates the inverse temperature corresponding to T_c. In the right picture the dashed line depicts the result (7.83) and the arrow refers to the crossover temperature $T_0 = T_\mathrm{c}/2$. The ImF result beyond the Gaussian approximation around T_0 is represented by the dotted lines.

Table I presents a numerical comparison with the exact transmission factor. For temperatures above $T_\mathrm{c}/2$ the real-time semiclassical rate is slightly too small and coincides for $T > T_\mathrm{c}$ with the well-known unified semiclassical rate formula gained by the thermal average over the transmission

Table 7.1. Transmission factor $P = \Gamma/\Gamma_{\rm cl}$ for the symmetric Eckart barrier. $\Gamma_{\rm cl}$ is the classical rate and parameters are the same as in Fig. 7.8.

$\omega_b\hbar\beta$	$P^{\rm a}_{\rm rsemi}$	$P^{\rm b}_{\rm uni}$	$P^{\rm c}_{\rm QTST}$	$P^{d}_{\rm SQTST}$	$P^{\rm e}_{ex}$
1.5	1.10	1.10	1.13	1.13	1.13
3	1.50	1.50	1.54	1.52	1.52
5	2.98	3.84	3.18	–	3.11
6	3.86	8.92	5.74	2.2	5.2
8	21.99	17.97	29.3	11.9	21.8
10	136.2	132.2	248	149	162
12	1613	1606	3058	3006	1970
16	$6.03 \cdot 10^5$	$6.03 \cdot 10^5$	–	$2.56 \cdot 10^6$	$7.41 \cdot 10^5$
18	$1.54 \cdot 10^7$	$1.54 \cdot 10^7$	–	$9.1 \cdot 10^7$	$1.88 \cdot 10^7$

[a] $P_{\rm rsemi}$ is the transmission factor as derived by the real-time semiclassical approach presented here
[b] $P_{\rm uni}$ is the transmission factor of the semiclassical approach based on the uniform WKB expression
[c] $P_{\rm QTST}$ is the transmission factor according to the simplest version of Pollak's QTST, from [15]
[d] $P_{\rm SQTST}$ is the transmission factor according to the full semiclassical version of Pollak's QTST, from [15]
[e] $P_{\rm ex}$ is the exact transmission factor

$T(E) = 1/\{1+\exp[S_{\rm B}(E)/\hbar]\}$, where $S_{\rm B}(E)$ is the bounce action for $T < T_{\rm c}/2$ [see Sect. 2.1]. The small deviations from the exact rate are due to the fact that in the simple version of the theory presented here anharmonicities of the potential are neglected for $T > T_{\rm c}$ and taken into account only in leading order in $T_{\rm c} > T > T_{\rm c}/2$. A perturbative expansion in an anharmonicity parameter allows for a systematic improvement. For the same reason, the temperature region around $T_{\rm c}/2$ is not well described. In the deep tunneling region $T < T_{\rm c}/2$, which is notoriously problematic for real-time rate theories, the theory performs quite accurately. In fact, the low temperature formula (7.83) turns out to be identical to the result derived within the instanton/bounce approach [see Sect. 5.2.4]. The bounce is an oscillating Euclidian orbit, periodic in phase space, which connects $q_{\rm f} = 0$ with itself, thus emerging as a solution of (7.67) at $T = T_{\rm c}/2$ $(r = 2)$. While in imaginary time methods the bounce trajectory describes barrier penetration, here, effectively the same tunneling rate arises from *fluctuations around real time paths* the energy of which is fixed by oscillating Euclidian orbits, closed in phase space, emerging at $T_{\rm c}$ $(r = 1)$. These latter minimal action paths solely determine the semiclassical thermal equilibrium for lower temperatures $T < T_{\rm c}$, thus establishing within a semiclassical real time approach the relation between the thermal density matrix and the thermal tunneling rate.

Let us also compare with results obtained within other approaches, also partially described in previous Sections. The phase space formulation presented in Sect. 6.4.2 suffers from a standard semiclassical approximation to the real time propagators so that only half of the bounce action appears in the for temperatures below $T_c/2$; the corresponding tunneling rates are too large (see Table I). The centroid method, see Sect. 5.7, [16, 17] gives the correct action factor, however, its semi-empirical factorization of thermal and dynamical contributions leads to a prefactor which is too small for lower temperatures.

References

1. J. Ankerhold and H. Grabert. *Europhys. Lett.*, 47:285, 1999.
2. J. Ankerhold and H. Grabert. *Phys. Rev. E*, 61:3450, 2000.
3. W.H. Miller. *Adv. Chem. Phys.*, XXV:69, 1974.
4. M.V. Berry and K.E. Mount. *Rep. Prog. Phys.*, 35:315, 1972.
5. M. Abramowitz and J.E. Stegun (eds.). *Handbook of Mathematical Functions.* National Bureau of Standards, 1972.
6. J. Ankerhold, H. Grabert, and G.L. Ingold. *Phys. Rev. E*, 51:4267, 1995.
7. J. Ankerhold and H. Grabert. *Chem. Phys.*, 204:27, 1996.
8. J. Ankerhold and H. Grabert. *Physica A*, 188:568, 1992.
9. J. Ankerhold and H. Grabert. *Phys. Rev. E*, 52:4704, 1995.
10. L.S. Schulman. *Techniques and Applications of Path Integrals.* Wiley, 1981.
11. S. Coleman. In A. Zichichi, editor, *The Whys of Subnuclear Physics*, Plenum, 1979.
12. U. Weiss and W. Haeffner. *Phys. Rev. D*, 27:2916, 1983.
13. C. Eckart. *Phys. Rev.*, 35:1303, 1930.
14. F.J. Weiper, J. Ankerhold, and H. Grabert. *J. Chem. Phys.*, 104:7526, 1996.
15. E. Pollak and B. Eckhardt. *Phys. Rev. E*, 58:5436, 1998.
16. G.A. Voth, D. Chandler, and W.H. Miller. *J. Chem. Phys.*, 91:7749, 1989.
17. G.A. Voth, D. Chandler, and W.H. Miller. *J. Phys. Chem.*, 93:7009, 1989.

8

Final Remarks and Outlook

This book presents an overview over semiclassical methods to describe processes of quantum tunneling. The picture that emerges is that few theoretical concepts are able to capture an astonishingly variety of systems with completely different physical realizations. Semiclassical approximations are well-developed for undriven one-dimensional tunneling degrees of freedom; when the corresponding anharmonic barriers are high, they are often, particularly for dissipative tunneling, the only efficient means to determine exponentially small transmission probabilities or rates. Direct numerical evaluations based on the Schrödinger equation or path integrals may complement these results, but usually require an (exponentially) increasing amount of simulation time at lower temperatures, stronger friction, or higher barriers, especially in dynamical treatments. In this direction approaches based e.g. on basis set methods and Monte Carlo techniques have been pushed forward in the last years. In contrast, for driven tunneling and/or tunneling in higher dimensions much less progress has been achieved and a deeper understanding how semiclassical methods can be applied efficiently is still needed. We will close this presentation by briefly touching some of these questions: Where do we go? Which problems wait for a solution?

- *Tunneling in higher dimensions:* Even for systems with regular classical dynamics has been a semiclassical calculation of transmission rates through higher dimensional anharmonic barrier potentials elusive so far. Attempts have been made, with restricted success though. The problem can be traced back to the WKB approximation in higher dimensions, particularly, to the WKB wave function. In principle, dynamical formulations in terms of extended HK propagators or IVR series provide a tool to attack these situations, but the proliferation of orbits certainly requires a better efficiency in numerical calculations (see below).
- *Tunneling in systems with classically chaotic dynamics:* In conservative systems with classically mixed dynamics (regular and chaotic) semiclassical approaches for tunneling encounter a similar problem as above: the

Joachim Ankerhold: *Quantum Tunneling in Complex Systems*
STMP **224**, 203–205 (2007)
DOI 10.1007/3-540-68076-4_8

lack of a consistent theory for a WKB type of wave function, from which tunneling rates could be gained. These systems belong certainly to one of the most exciting ones, because of their complexity on the one hand and their ubiquitous appearance in nature on the other hand. Specific systems have been studied, a general semiclassical scheme still needs to be formulated.

- *Tunneling in presence of external driving:* In presence of external driving forces real-time approaches for tunneling are required. While the limit of slow driving can be treated by means of adiabatic approximations, the regime of fast frequencies/strong driving is the most challenging. Here, we have reported on a semiclassical formulation (extended HK), which even described the intimate relation between resonant excitations in a well of a metastable potential and tunneling through its barrier. Processes including photon absorption *during* tunneling, i.e. *under* the barrier, have not been addressed so far. For time periodic forces the Floquet theory may provide a framework for further developments (semiclassical Floquet theory). Apart from that, stochastic driving forces are of relevance as well, e.g. for tunneling through fluctuating barriers.
- *Extended HK propagator and the IVR series:* The extended HK propagator has already led to promising results; the same holds for the more rigorous IVR series expansion. While the former approach works efficiently at least in one-dimensional systems, its extension to higher dimensions is not straightforward. On the other hand, the latter formulation is conceptually well founded, but an increasing number of phase space integrations combined with an increasing dimension of the fluctuation matrix renders a treatment of higher dimensional tunneling presently prohibitive. One way to soothe these problems could be to work with prefactor free representations. From a more fundamental point of view it would be interesting to explore the relation between the extended HK scheme and the IVR series representation.
- *Dynamical rate theory for very weak friction:* In the classical domain the escape over the barrier occurs for weak friction via energy diffusion. In the quantum regime this limit has been studied on the basis of the general expression (3.1), where the steady state energy distribution must be gained from an integral equation to account for deviations from the thermal distributions for energies near the barrier top [1, 2, 3]. Even a turnover theory has been put forward along the lines discussed for the classical regime [4]. How the regime of weak damping can be captured within a dynamical theory has not been explored yet. In particular, such an investigation should provide detailed insight in how the energy diffusion regime shrinks towards lower temperatures such that sufficiently below the crossover it basically ceases to exist.
- *Real-time theory for dissipative tunneling below the crossover:* This is certainly one the most demanding problems. In Sect. 7 we have laid out the foundations for a full real-time theory of the density matrix from high to

low temperatures and for coherent and incoherent tunneling. In the domain above the crossover temperature, a dynamical description including dissipation has been obtained by the quantum Kramers theory in Sect. 6. What remains to do is to extend the frictionless theory below the crossover accordingly. A major problem then is the fluctuations prefactor, which cannot be determined from the minimal effective action since irreversibility does not allow to exploit the Gelfand-Yaglom prescription. Moreover, explicit results certainly necessitate the development of proper numerical techniques. In particular, the diffusion of minimal action paths in the complex configuration space may then be described by a Langevin-type of dynamics.

References

1. P. Hänggi. *J. Stat. Phys.*, 42:105, 1986.
2. M. Büttiker. In F. Moss and P.V.E. McClintock, editors, *Noise in Nonlinear Dynamical Systems*, Cambridge University Press, 1989.
3. U. Griff, H. Grabert, P. Hänggi, and P. Riseborough. *Phys. Rev. B*, 40:7295, 1989.
4. I. Rips and E. Pollak. *Phys. Rev. A*, 41:5366, 1990.

Index

Springer Tracts in Modern Physics

181 **Emulsion Science**
Basic Principles. An Overview
By J. Bibette, F. Leal-Calderon, V. Schmitt, and P. Poulin 2002. 50 figs., IX, 140 pages

182 **Transmission Electron Microscopy of Semiconductor Nanostructures**
An Analysis of Composition and Strain State
By A. Rosenauer 2003. 136 figs., XII, 238 pages

183 **Transverse Patterns in Nonlinear Optical Resonators**
By K. Staliūnas, V. J. Sánchez-Morcillo 2003. 132 figs., XII, 226 pages

184 **Statistical Physics and Economics**
Concepts, Tools and Applications
By M. Schulz 2003. 54 figs., XII, 244 pages

185 **Electronic Defect States in Alkali Halides**
Effects of Interaction with Molecular Ions
By V. Dierolf 2003. 80 figs., XII, 196 pages

186 **Electron-Beam Interactions with Solids**
Application of the Monte Carlo Method to Electron Scattering Problems
By M. Dapor 2003. 27 figs., X, 110 pages

187 **High-Field Transport in Semiconductor Superlattices**
By K. Leo 2003. 164 figs.,XIV, 240 pages

188 **Transverse Pattern Formation in Photorefractive Optics**
By C. Denz, M. Schwab, and C. Weilnau 2003. 143 figs., XVIII, 331 pages

189 **Spatio-Temporal Dynamics and Quantum Fluctuations in Semiconductor Lasers**
By O. Hess, E. Gehrig 2003. 91 figs., XIV, 232 pages

190 **Neutrino Mass**
Edited by G. Altarelli, K. Winter 2003. 118 figs., XII, 248 pages

191 **Spin-orbit Coupling Effects in Two-dimensional Electron and Hole Systems**
By R. Winkler 2003. 66 figs., XII, 224 pages

192 **Electronic Quantum Transport in Mesoscopic Semiconductor Structures**
By T. Ihn 2003. 90 figs., XII, 280 pages

193 **Spinning Particles – Semiclassics and Spectral Statistics**
By S. Keppeler 2003. 15 figs., X, 190 pages

194 **Light Emitting Silicon for Microphotonics**
By S. Ossicini, L. Pavesi, and F. Priolo 2003. 206 figs., XII, 284 pages

195 **Uncovering *CP* Violation**
Experimental Clarification in the Neutral K Meson and B Meson Systems
By K. Kleinknecht 2003. 67 figs., XII, 144 pages

196 **Ising-type Antiferromagnets**
Model Systems in Statistical Physics and in the Magnetism of Exchange Bias
By C. Binek 2003. 52 figs., X, 120 pages

197 **Electroweak Processes in External Electromagnetic Fields**
By A. Kuznetsov and N. Mikheev 2003. 24 figs., XII, 136 pages

198 **Electroweak Symmetry Breaking**
The Bottom-Up Approach
By W. Kilian 2003. 25 figs., X, 128 pages

199 **X-Ray Diffuse Scattering from Self-Organized Mesoscopic Semiconductor Structures**
By M. Schmidbauer 2003. 102 figs., X, 204 pages

200 **Compton Scattering**
Investigating the Structure of the Nucleon with Real Photons
By F. Wissmann 2003. 68 figs., VIII, 142 pages

201 **Heavy Quark Effective Theory**
By A. Grozin 2004. 72 figs., X, 213 pages

Springer Tracts in Modern Physics

202 **Theory of Unconventional Superconductors**
By D. Manske 2004. 84 figs., XII, 228 pages

203 **Effective Field Theories in Flavour Physics**
By T. Mannel 2004. 29 figs., VIII, 175 pages

204 **Stopping of Heavy Ions**
By P. Sigmund 2004. 43 figs., XIV, 157 pages

205 **Three-Dimensional X-Ray Diffraction Microscopy**
Mapping Polycrystals and Their Dynamics
By H. Poulsen 2004. 49 figs., XI, 154 pages

206 **Ultrathin Metal Films**
Magnetic and Structural Properties
By M. Wuttig and X. Liu 2004. 234 figs., XII, 375 pages

207 **Dynamics of Spatio-Temporal Cellular Structures**
Henri Benard Centenary Review
Edited by I. Mutabazi, J.E. Wesfreid, and E. Guyon 2005. approx. 50 figs., 150 pages

208 **Nuclear Condensed Matter Physics with Synchrotron Radiation**
Basic Principles, Methodology and Applications
By R. Röhlsberger 2004. 152 figs., XVI, 318 pages

209 **Infrared Ellipsometry on Semiconductor Layer Structures**
Phonons, Plasmons, and Polaritons
By M. Schubert 2004. 77 figs., XI, 193 pages

210 **Cosmology**
By D.-E. Liebscher 2005. Approx. 100 figs., 300 pages

211 **Evaluating Feynman Integrals**
By V.A. Smirnov 2004. 48 figs., IX, 247 pages

213 **Parametric X-ray Radiation in Crystals**
By V.G. Baryshevsky, I.D. Feranchuk, and A.P. Ulyanenkov 2006. 63 figs., IX, 172 pages

214 **Unconventional Superconductors**
Experimental Investigation of the Order-Parameter Symmetry
By G. Goll 2006. 67 figs., XII, 172 pages

215 **Control Theory in Physics and other Fields of Science**
Concepts, Tools, and Applications
By M. Schulz 2006. 46 figs., X, 294 pages

216 **Theory of the Muon Anomalous Magnetic Moment**
By K. Melnikov, A. Vainshtein 2006. 33 figs., XII, 176 pages

217 **The Flow Equation Approach to Many-Particle Systems**
By S. Kehrein 2006. 24 figs., XII, 170 pages

219 **Inelastic Light Scattering of Semiconductor Nanostructures**
By C. Schüller 2007. 105 figs., XII, 178 pages

220 **Precision Electroweak Physics at Electron-Positron Colliders**
By S. Roth 2007. 107 figs., X, 174 pages

221 **Free Surface Flows under Compensated Gravity Conditions**
By M. Dreyer 2007. 128 figs., X, 272 pages

222 **Theory of Light Hydrogenic Bound States**
By M.I. Eides, H. Grotch, and V.A. Shelyuto 2007. 108 figs., XVI, 260 pages

223 **Electrical Resistivity of Thin Metal Films**
By P. Wißmann, H.-U. Finzel 2007. 110 figs., VII, 150 pages

224 **Quantum Tunneling in Complex Systems**
By J. Ankerhold 2007. 62 figs., XII, 210 pages